AN ION SELECTIVE MICROGRIPPER SENSOR DEVICE

DAUNTON, RACHAEL,HANNAH

AN ION SELECTIVE MICROGRIPPER SENSOR DEVICE

A thesis submitted for the degree of Doctor of Philosophy

By

Rachael H. Daunton

Department of Chemistry

School of Engineering and Computing Sciences

Durham University

2013

ABSTRACT

This thesis presents the design, fabrication, characterisation and testing of a chemically modified electrothermally actuated microgripper. The chemical modification involves the integration of a potentiometric ion selective electrode (ISE) onto a bare electrode fabricated within the tip of the microgripper. This microgripper sensor device is intended for use in the application of detecting, in real time, the movement of key ions that are involved in intercellular communication from a mechanically stressed cell.

An optimised fabrication route for the specifically designed microgrippers, which have tip dimensions of 10 – 60 μm, is described in detail. The fabrication route delivers a high yield (95%) of operational unmodified devices. An 1800 ± 20 μm^2 bare gold electrode that is fabricated at the tip of the microgripper is modified into an all solid state ISE that uses PEDOT as the ion-to-electron solid contact. Suitable ionophores that selectively detect K^+, Na^+ and Ca^{2+} are used to fabricate potassium, sodium and calcium ion selective microgripper sensor devices.

The quality control and testing characteristics that follow the guidelines defined by IUPAC are performed to ascertain the sensitivity, selectivity and stability of the microgripper sensor devices. Good selectivity is achieved, with limits of detection of 2.4×10^{-4} M, 1.8×10^{-4} M and 2.0×10^{-5} M for the K^+, Na^+ and Ca^{2+} devices respectively. Proof of concept experiments of the real life testing of the K^+ ISE device used to mechanically stress mouse oocytes gave preliminary measurements that indicate that stress signalling occurs via a switch on mechanism, and that there is a small increase in K^+ concentration as applied stress increases. Due to the high systematic error within the calibration process the magnitude of this concentration increase is unknown. The Na^+ and Ca^{2+} ISE devices suffer from interference and sensitivity restrictions respectively so a signal response vs. applied cell stress relationship of these ions is currently unobtainable.

DECLARATION

This work was carried out in the School of Engineering and Computing Sciences and in the Department of Chemistry at Durham University. The work described within is all my own work and contains no material that has been previously submitted for a degree at this or any other university.

STATEMENT OF COPYRIGHT

DEDICATION

I dedicate this work in memory of Mark Ashton, as a reminder that life's greatest tragedies can take you on a journey that you would never have imagined.

ACKNOWLEDGEMENTS

I would like to thank both my supervisors Dr. Ritu Kataky and Prof. David Wood for all their supervision and the support they have given me over the years. Additionally, I would like to thank Dr. Andrew Gallant, the other member of my supervision team, for his helpful input and friendship.

I would like to acknowledge the contribution from MMI for the loan of the CellEctor macromanipulator system and for their input and interest in the development of the microgripper for use in biological system manipulation.

Additionally, I would like to thank Prof. Mary Herbert at the Centre for Life in Newcastle for her generous supply of mouse oocytes. I would specifically like to thank Lisa Lister for extracting the cells and preparing them for use in this project.

Late night technical discussions with Dr. Mark Rosamond, as well as his unending support and understanding, were instrumental in sustaining motivation and confidence throughout this work. His help and close friendship is thoroughly appreciated, I could not have done it without him.

I would like to thank Dr. Fred Hamlin for his contribution and advice in the design of the microgripper integration system. Additionally, his help in learning to use several drawing packages to create 3D images of the microgripper device was invaluable.

I would also like to thank the numerous friends who have kept me (relatively) sane throughout the whole process. Specifically Dr. Paula Lopes, Dr. Alice Delcourt-Lancon and Dr. Rui Campos for their support in the chemistry lab and wine filled dinner parties; Dr. Aruna Prakash, Dr. Louise Gildea (previously Parkes), Dr. Marie-Helene Thibault and Laura Mackay for girly chat over cocktails, cinema trips and even a wedding; and Linzi Dodd and the boys in the

office (you know who you are!) for copious Friday pub, or more accurately Zen, lunches and (sometimes long) games of Killer Bunnies, Munchkin, Monopoly Deal or Flux.

I would also like to thank my friends outside of the University for helping me see the wider perspective of life. Specifically I would like to thank Tony and Jemma Maslen for bringing me back to Earth in moments of complete frustration and exhaustion, and generally being available to chat through out the day.

Finally, but by no means least, I would like to thank my family. My parents, Captain Paul and Pam Daunton and my not so little brother, Peter Daunton, for just being there when I needed them, no matter what.

I have dedicated this thesis to Mark Ashton, who was tragically killed in a car accident in 2008. He is a huge reason why I am here today; my determination to better myself and to always try to see the good in people is inspired by his faith in me and how he chose to live his life. Although he is no longer here to hear it, I owe him so much for that, thank you.

PUBLICATIONS

R. Daunton, A. J. Gallant, D. Wood and R. Kataky, "A thermally actuated microgripper as an electrochemical sensor with the ability to manipulate single cells," *Chemical Communications,* vol. 47, pp. 6446-6448, 2011.

R. Daunton, A. J. Gallant and D. Wood, "Manipulation of exposure dose parameters to improve production of high aspect ratio structures using SU-8," *Journal of Micromechanics and Microengineering,* vol. 22, pp. 075016-075024, 2012.

R. Daunton, A. J. Gallant, R. Kataky and D. Wood, "A multifunctional microgripper capable of simultaneous single cell manipulation and associated ion sensing," *Proceedings of the Materials Research Society Meeting Spring Conference (San Francisco, USA)*, vol. 1463, 2012.

R. Daunton, A. J. Gallant and D. Wood. "Manipulation of 10-40 µm diameter cells using a thermally actuated microgripper," *Proceedings of the Materials Research Society Meeting Spring Conference (San Francisco, USA)*, vol. 1463, 2012.

CONFERENCES

Electrochem 2010: Electrochemistry and Sustainability, University of Wolverhampton, Telford Campus, 14-15 September 2010 – poster presentation.

2012 MRS Spring Meeting and Exhibit, San Francisco, California, USA, 9-13 April 2012 – poster and oral presentation.

Analytical Research Forum 2012, Durham University, Durham 2-4 July 2012 – poster presentation (2nd place prize).

Electrochem 2012: Electrochemical Horizons, Trinity College, Dublin, 2-4 September 2012 – poster presentation (1st place prize).

Forensic Science Society: Forensic Intelligence and New Product Design, University of Warwick, Coventry 10 November 2012 – invited to give an oral presentation.

BSI meetings, Durham University, Durham – several posters and oral presentations.

Engineering Research Day, Durham University, Durham – several oral presentations (2nd place IET oral presentation prize).

Chemistry Research Day, Durham University, Durham – several poster and oral presentations.

TABLE OF CONTENTS

TABLE OF FIGURES

TABLE OF TABLES

TABLE OF ABBREVIATIONS

Abbreviation	Meaning
AC	Alternating current
AFM	Atomic force microscopy
Ag	Silver
Ag^+	Silver ion
AgCl	Silver Chloride
AOC	Agnostic-gated channel
Aq	Aqueous
ASSISE	All solid state ion selective electrode
ATP	Adenosine triphosphate
CA	Chronoamperometry
Ca^{2+}	Calcium ion
$CaCl_2$	Calcium chloride
CE	Counter electrode
$Ce(NH_4)_2(NO_3)_6$	Ammonium cerium (IV) nitrate
Cl^-	Chloride ion
CMOS	Complementary metal oxide conductor
CO_2	Carbon dioxide
[CP]	Cyclopentanone (concentration of)
CP	Conducting polymer
CTE	Coefficient of thermal expansion
CV	Cyclic voltammetry
CWE	Coated wire electrode
DC	Direct current
DI	Deionised water
DNA	Deoxyribonucleic acid
DNQ	Diazonaptho quinone sulphonate
DRIE	Deep reactive ion etcher
EC	Electrical conductor
EC solvent	Ethyl lactate based solvent
EDOT	3,4-ethylenedioxythiophene
EMF	Electromotive force
EPR	Electron paramagnetic resonance
ESR	Electron spin resonance
EuF_6	Europium (III) fluoride
Ex	Exposure
g	Gaseous
GDP	Guanosine diphosphate
GIRK	G protein coupled inwardly rectifying potassium channel
GTP	Guanosine triphosphate
H^+	Hydrogen ion
H_2O	Water
H_2O_2	Hydrogen peroxide
H_2SO_4	Sulphuric acid
HAR	High aspect ratio
HF	Hydrofluoric acid
HNO_3	Nitric acid
$HSbF_6$	Fluoroantimonic acid

Abbreviation	Meaning
I	Iodine
I^-	Iodide ion
IC	Integrated circuit
IHP	Inner Helmholtz plane
IPA	Isopropyl alcohol
IR_s	Ohmic drop
ISE	Ion selective electrode
ISM	Ion selective membrane
IUPAC	International union of pure and applied chemistry
IVF	In vitro fertilisation
K	Potassium
K^+	Potassium ion
$K_3Fe(CN)_6$	Potassium ferricyanide
KCl	Potassium chloride
KI	Potassium iodide
KNO_3	Potassium nitrate
KOH	Potassium hydroxide
KTpClPB	Potassium tetrakis (4-chloro phenyl) borate
Li^+	Lithium ion
$LiClO_4$	Lithium perchlorate
LOD	Limit of detection
$\log K_{i,j}$	Selectivity coefficient
MEMS	Microelectromechanical systems
Mg^{2+}	Magnesium ion
$MgCl_2$	Magnesium chloride
MMI	Molecular Machines and Industries
N_2	Nitrogen
Na^+	Sodium ion
NaCl	Sodium chloride
NaH_2PO_4	Monosodium phosphate
$NaHCO_3$	Sodium bicarbonate
NaPSS	Poly(sodium 4-styrenesulfonate)
NH_3	Ammonia
NH_3F	Ammonium fluoride
NH_4^+	Ammonium ion
O_2	Oxygen
OHP	Outer Helmholtz layer
oNPOE	o – Nitro phenyl octyl ether
PA	Polyaniline
PAA	Poly(acrylic acid)
Pb^{2+}	Lead ion
PCB	Printed circuit board
PDMS	Poly(dimethylsiloxane)
PEB	Post exposure bake
PEDOT	Poly(3,4-ethylenedioxythiophene)
PI	Polyimide
PMMA	Poly(methyl methacrylate)
POT	Poly(3-ocylthiophene)
PPy	Poly(pyrrole)
PSS	Poly(styrene sulfonate)

Abbreviation	Meaning
PT	Poly(thiophene)
PU	Polyurethane
PVC	Poly(vinyl chloride)
Rb^+	Rubdium ion
RE	Reference electrode
Ref_{in}	Internal reference solution
RIE	Reactive ion etcher
RP	Rapid prototype
RPM	Rotations per minute
RT	Room temperature
s	Solid
SB	Soft bake
SEM	Scanning electron microscope
Si	Silicon
SiF_4	Silicon tetrafluoride
SiO_2	Silicon oxide
SPISE	Single piece ion selective electrode
tArSbF	Triarylsulfonium hexafluoroantimonate
TBAP	Tetrabutylammonium perchlorate
$TBAPF_6$	Tetrabutylammonium hexafluorophosphate
T_g	Glass transition temperature
THF	Tetrahydrofuran
Tl^+	Thalium ion
TPB^-	Tetraphenylborate ion
$TpClPB^-$	Tetrkis(4-chloro phenyl) borate ion
UV	Ultraviolet
VOC	Voltage-gated channel
WE	Working electrode
Xe	Xenon
XeF_2	Xenon difluoride

1.0 INTRODUCTION

This thesis presents the novel approach of including a potentiometric ion selective electrode (ISE) at the tip of a specially designed microgripper for the application of detecting the intercellular movement of potassium, sodium and calcium ions from a single cell. This is a further development into the thermally actuated microgripper technology initially designed by Dr Belen Solano [1]. The advantage of this microgripper sensor device is that not only can it be used to isolate a single cell, but it can also be used to mechanically stress the cell and the ionic response can be investigated.

The overall aim of the microgripper sensor device fabricated in this project was to produce a sensor that could monitor, in real time, the evolution of key ions involved in intercellular communication due to mechanical and/or electrical external stresses. This device also needed to be able to manipulate the cell under investigation. The idea is that these two technologies, once combined, will enable the user to monitor cell stress while under manipulation; for example in cell transport during *in vitro* fertilisation (IVF) treatments. This thesis concentrates on the design, fabrication, characterisation, calibration and testing of this microgripper sensor device. Mouse oocytes were used as the testing cell. However, the microgripper has been designed to manipulate many different cell types, both plant and animal.

There has always been great interest in the ability to study inter- and intracellular events using diverse chemical sensing applications. Cells generally communicate via influxes and effluxes of electroactive species, prompting a need to develop sensors with greater sensitivity and a reduction in the electrode to substrate contact, essentially miniaturising the sensor. Since the proposal of micro-total analysis in the 1980s [2], there has been a boom in the development of miniaturised biological sensors that have been used in a large range of

biological areas, including immunoassays, proteomics and cell biology [3] [4] [5] [6] [7]. The ability to miniaturise biological sensors is desirable as it enables investigation into small sample volumes and reduces the amount of material used to fabricate each device [8] [9].

Electrochemical techniques are very versatile with respect to quantitative biochemical sensing as many biological processes involve movement of ions or electrons. They also have advantages over other methods, such as measurement simplicity, response time, sensitivity and specificity, power requirements, ease of microfabrication and good compatibility with biological media [10]. Microanalytical devices, when combined with electrochemical techniques, generally fall under one of the following categories: electrodes used for electrochemical detection [11]; electrophoresis microchips [12]; or electrode as the base layer in electrochemical sensing [13].

Ion selective electrodes (ISEs) fall into the category of electrochemical sensors where the electrode acts as the base layer. The field of ISE based sensors is of great interest as these devices are advantageous in sensing many different ions found in bodily fluids due to their ease of use, relatively low cost and small power consumption [14]. Initial development into ISEs involved devices that contained a liquid inner filling solution, used to maintain ionic equilibrium within the system. Although this type of ISE has been shown to have excellent long term stability and the ability to detect analyte concentrations down to picomolar levels [8], they do, however, have many drawbacks when it comes to maintenance and miniaturisation. Liquid ISEs need frequent recalibration and rejuvenation of the inner filling solution, and upon miniaturisation they often leak. This led to the development of all solid state ion selective electrodes (ASSISEs), which are compatible with microfabrication techniques and are much more readily miniaturised, though usually at the cost of the excellent stability seen in liquid ISEs [9] [15]. ASSISEs do suffer from leakage of membrane components into the sample solution, which can cause biocompatibility issues, as well as delamination of the membrane

completely, meaning that there is a trade off between the size of the electrode and its characterisation.

Many sensor techniques retrieve information from a collection of cells, meaning that single cell response is often an approximation at best [16]. However, separating cells before sensing without causing damage can be complex, time consuming and involve expensive equipment [17]. There is, therefore, a need for a manipulation device that can also act as a biological sensor. Lab-on-chip systems are the closest to achieving this; however, they are restricted in how they manipulate objects. An additional disadvantage of these lab-on-chip systems is that they often contain an array of micro-ISEs that require multi-calibration, which can be complicated and time consuming [8] [18].

Due to the diversity of cells the microgripper sensor device can manipulate, this device has the potential to also be used to detect cell signalling in plants. While the main focus of this thesis is the manipulation and sensing of animal cells, by modifying the ionophore (the sensing element) in the ion selective membrane (ISM) deposited onto the electrode, other ions can be sensed, further widening the potential applications to include, for example, heavy metal sensing in soil particulates.

The sensor device must be produced via a cost effective manufacturing methodology, and should be capable of use in the analysis of minute volumes, i.e. it should be fabricated in the micron scale. To be capable of in vivo monitoring it must be possible to sterilise the device, and so it must be relatively robust, as well as it being essential that all parts of the sensor are biocompatible. The sensor must operate with excellent stability, in that there must be negligible potential drift within the experimental time frame of several minutes. The sensing element of the device must be able to detect small changes in concentration that relates to the movement of ions, as well as being able to reasonably respond to the influx or efflux of the

ions of interest, which occurs over several seconds. The development of single use planar ISEs should be used to ensure that the device should work without, or with minimal, calibration.

1.1 Overview of Thesis

CHAPTER 1 – INTRODUCTION. This chapter looks at the background and motivation of the device and states the general aims of the thesis.

CHAPTER 2 – MICROGRIPPER DEVICE. This chapter outlines the different manipulation techniques, gives an overview of the microelectromechanical system (MEMS) techniques and materials used in the microgripper fabrication process, explains the need to miniaturise the device and the methods of reducing thin layer stress to achieve this, and finally details the microgripper fabrication processes.

CHAPTER 3 – ELECTROCHEMICAL SENSORS. This chapter gives an overview into the background of electrochemistry, looking at the thermodynamic and kinetic effects of the different analytical techniques used. It delves into the background and the current literature surrounding ions selective electrodes (ISEs), including all solid state ion selective electrodes (ASSISEs), and gives a breakdown into the different components used in ASSISEs, concentrating on why they are used and how they affect the sensors response. Finally it looks at the characterisation of the electrode fabricated at the microgripper tip and details the fabrication process of the ASSISE element onto the microgripper device.

CHAPTER 4 – CALIBRATION AND CHARACTERISATION OF THE MICROGRIPPER SENSOR DEVICE. This chapter looks at the calibration response and characterisation of the microgripper sensor device in controlled solutions. The characterisation section includes investigations into the detection limit, response time, selectivity coefficients and drift and hysteresis of the device.

CHAPTER 5 – CELL TESTING. This chapter investigated the operation of the microgripper sensor device in a real life environment study, specifically looking at the manipulation of mouse

oocytes and sensing their excretion of potassium, sodium and calcium ions upon mechanical stressing.

CHAPTER 6 – CONCLUSION. This chapter summarises all the findings in this thesis and looks at further developments into the microgripper sensor device.

1.2 References

[1] B. Solano, A microgripper for single cell manipulation, PhD thesis, Durham Unversity, 2008.

[2] D. R. Reyes, D. Iossifidis, P.-A. Auroux and A. Manz, "Micro total analysis systems. 1. Introduction, theory and technology," *Analytical Chemistry,* vol. 74, pp. 2623-2636, 2002.

[3] P. S. Dittrich, K. Tachikawa and A. Manz, "Micro total analysis systems. Latest advancements and trends," *Analytical Chemistry,* vol. 78, no. 12, pp. 3887-3907, 2006.

[4] J. West, M. Becker, S. Tombrink and A. Manz, "Micro total analysis systems: Latest achievements," *Analytical Chemistry,* vol. 80, no. 12, pp. 4403-4419, 2008.

[5] M. L. Kovarik, D. M. Ornoff, A. T. Melvin, N. C. Dobes, Y. Wang, A. J. Dickinson, P. C. Gach, P. K. Shah and N. L. Allbritton, "Micro total analysis systems: Fundamental advances and applications in the laboratory, clinic and field," *Analytical Chemistry,* vol. 85, pp. 451-472, 2013.

[6] S. Hong, Q. Pan and L. P. Lee, "Single-cell level co-culture platform for intercellular communication," *Integrative Biology,* vol. 4, pp. 374-380, 2012.

[7] S. S. Rubakhin, E. V. Romanova, P. Nemes and J. V. Sweedler, "Profiling metabolites and peptides in single cells," *Nature Methods,* vol. 8, no. 4, pp. 520-529, 2011.

[8] S. Makarychev-Mikhailov, A. Shvarev and E. Bakker, "Chapter 4 - New trends in ion selective electrodes," in *Electrochemical Sensors, Biosensors and their Biomedical Applications*, USA, Academic Press, 2008, pp. 71-114.

[9] J. Bobacka, A. Ivaska and A. Lewenstam, "Potentiometric ion sensors," *Chemical Reviews,* vol. 108, no. 2, pp. 329-351, 2008.

[10] X. Xu, S. Zhang, H. Chen and J. Kong, "Integration of electrochemistry in micro-total analysis systems for biochemical assays: Recent developments," *Talanta,* vol. 80, pp. 8-18, 2009.

[11] J. Wang, "Electrochemical detection for microscale detection for microscale analytical systems: A review," *Talanta,* vol. 56, no. 2, pp. 223-231, 2002.

[12] J. Wang, "Electrochemical detection for capillary electrophoresis microchips: A review," *Electroanalysis,* vol. 17, no. 13, pp. 1133-1140, 2005.

[13] J. J. Gooding, “Electrochemical DNA hybridization biosensors,” *Electroanalysis,* vol. 14, no. 17, pp. 1149-1156, 2002.

[14] A. J. Bard and L. R. Faulkner, Electrochemical Methods: Fundamentals and Applications, New York: Wiley and Sons, 2000.

[15] J. Bobacka, “Conducting polymer based solid state ion selective electrodes,” *Electroanalysis,* vol. 18, no. 1, pp. 7-18, 2006.

[16] S. Lindstrom and H. Andersson-Svahn, “Miniaturization of biological assays - Overview on microwell devices for single-cell analysis,” *Biochimica et Biophysica Acta,* vol. 1810, no. 3, pp. 308-316, 2011.

[17] J. Castillo, M. Dimaki and W. E. Svendsen, “Manipulation of biological samples using micro and nano techniques,” *Integrative Biology,* vol. 1, pp. 30-42, 2009.

[18] M. Hartnett and D. Diamond, “Potentiometric nonlinear multivariate calibration with genetic algorithm and simplex optimization,” *Analytical Chemistry,* vol. 69, no. 10, pp. 1909-1918, 1997.

2.0 MICROGRIPPER DEVICE

This chapter is split into three main sections: a brief background outlining the different manipulation techniques that are possible; an overview of the microelectromechanical systems (MEMS) techniques and materials that are used in the fabrication process; and a detailed explanation of the main fabrication improvements made to the electrothermally actuated microgripper first proposed by Belen Solano [1]. This last section focusses on the need to miniaturise the original design to allow single cell analysis of a much greater range of cell types.

2.1 Overview of Manipulation Techniques

This thesis concentrates on a microgripper that is used for biological manipulation. This area of manipulation includes the transportation, positioning and orientating of biological materials, as well as material injection. This is a major area of research, as the ability to perform the above mentioned tasks allows significant development in the areas of genomics and proteomics [2] [3] [4], human reproduction [5] [6] [7], medicine [8] and cancer research [9]. In areas such as assisted medicine, for example in-vitro fertilisation (IVF) (one application of interest for a microgripper), the manipulation of small cells in liquid environments is a necessity to ensure that the samples are protected. It is important, therefore, to choose the method of manipulation carefully as some methods cannot be used in liquids, or may cause damage to the object being manipulated. Positioning and transportation can be split into two main techniques: contact and non-contact manipulation methods.

Non-contact manipulation techniques are ones where the device does not come into contact with the object under investigations. These techniques include systems based on optical forces [10] [11] [12], electrical fields [13] [14] [15] [16] [17] [18] [19] [20] [21] [22] [23]

[24], an electroactive polymer [2] [25] [26] and magnetic fields [27] [28] [29] [30] [31] [32] [33] [34].

Contact manipulation techniques are where the device is in contact with the object of interest. These techniques include systems which rely on vacuum suction [35], adhesive forces [36] [37], acoustic traps [38] [39] and cryogenics [40].

Non-contact methods often have a higher accuracy in cell positioning than contact methods. However, there are several reports indicating that cell damage [41] and the potential for inducing abnormalities into the genetic material of the cell are possible [42] via several of these methods. Additionally, due to optimal field strengths for these techniques being limited spatially, the distances moved and the size of the samples are restricted. This confinement also means that only one technique can be used within the working area, otherwise the techniques will interfere with each other. All this, coupled with the high cost of these systems ($10k-100k), has made contact techniques more desirable, especially for this project. A few of these will be described in more detail below.

2.1.1 Vacuum Contact

Vacuum contact is a relatively common technique in biological fields and has been around for over a century [35]. It is used extensively in the field of in vitro fertilisation (IVF) mainly due to its relatively low cost (for example, around £25 start-up cost, then £5 per replaced pipette unit) and diversity. However, this technique requires a skilled operator and it can easily damage the cell membrane as the vacuum force is applied on a small area of the cell causing it to deform during manipulation. To avoid this, capillary suction techniques have been introduced where vacuum or oil pumps are used to suck the cell into the tip of a micro capillary for transport between liquid media. This is the main competitive technique used in industry and is often the comparison standard in the effectiveness of operation. The technique

is also used quite successfully on lab-on-chip type devices that can direct, separate and hold cells in position for analysis.

This is the main competitive technique for the device in this thesis, as most cell handling is done using capillary suction vacuum pipettes, with many companies providing slightly different connotations on denudation (where the cell is taken into the glass capillary) and holding (where the cell is held on the outside of the glass capillary) pipettes. While no one, to the author's knowledge, has created a fully incorporated sensor/manipulation device using a vacuum capillary as the manipulation element, the electrothermal actuation manipulation element used in the device in this project still needs to operate to the same positioning and cell damage specifications as the vacuum capillary.

2.1.2 Electrostatic

Electrostatic actuation relies on the electric field that is created around any electrically charged surface, and its ability to apply a force to a charged particle. There is great interest in using electrostatic actuators in microelectromechanical systems (MEMS) devices, mainly because the electrostatic effect decreases with the square of the distance between two charged species. When using electrostatic MEMS structures to manipulate objects via a tweezer like actuation, the devices often have low aspect ratios. This makes the fast drop off in force a desirable factor, as the electrostatic actuation elements in each arm will not interfere with each other. The main disadvantage of electrostatic actuation is that large actuation voltages are required to achieve large displacements, which can be quite challenging on a microscale device, especially in liquids as this often results in electrolysis.

Electrostatic actuation is successfully used in microswitches where two plates are attracted to each other to form an electrical contact (Figure 2.1(a)). Tweezer like actuation can be achieved with comb-drive actuators; however, due to the fact that the displacement direction is different to the electrical field, very high voltages are often required [43] (Figure

2.1(b)). There has been interest in improving the displacement for a given voltage via exploiting the Young's modulus of polymer based actuators (such as poly(methylmethacrylate) (PMMA)) to reduce these high voltages [44].

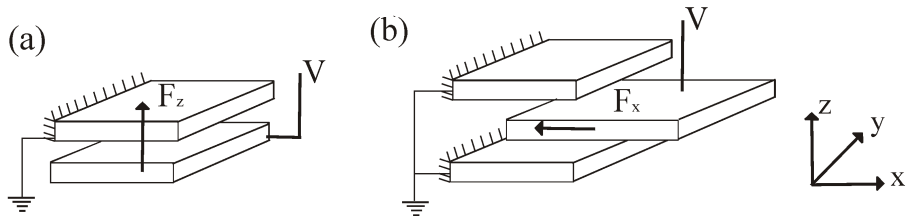

Figure 2.1 – Schematic representation of electrostatic actuation of (a) Perpendicular forces (F_z) of parallel plates and (b) Lateral forces (F_x) of comb drive actuators.

2.1.3 Thermally Actuated

There are two main types of thermal actuation: one that relies of the deformation of materials due to their changing structure on temperature changes, for example shape memory alloys; and one that relies on material deformation due to thermal expansion, for example electrothermal.

2.1.3.1 Shape Memory Alloys

The shape memory effect occurs either via one-way or two-way. In a one-way memory effect only one shape is remembered while the temperature is maintained. On a change in temperature the material re-sets its shape allowing it to be reshaped at that temperature. A two-way memory effect remembers two shapes, one at a low temperature and one at a higher temperature. As the temperature is changed the material switches between these two shapes [45] [46] [47] [48].

Shape memory alloy actuators are able to give large displacements with relatively low operating voltages. However, they suffer from slow responses and high processing temperatures, making them unsuitable for working in aqueous environments and with biological material.

2.1.3.2 Electrothermal Actuation

Electrothermal actuation operates by using a metal element that, when a current is passed through, it heats (due to the energy loss due to resistance) and expands. The small deflection can then be mechanical amplified [49] [50] [51]. Electrothermal actuators generally use more power than others as power is proportional to the product of the square of the current and the resistance; however, given that the microgripper design is not limited by the conduction path of the heating element, devices where small deflections are mechanically amplified can be fabricated. There are three main types of electrothermal actuators, and these are described below.

2.1.3.3 Bimorph

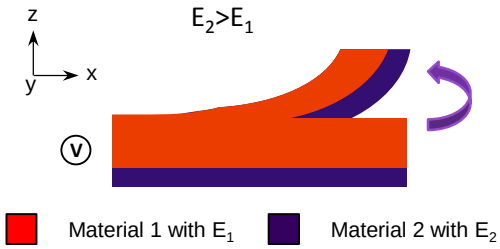

Figure 2.2 – Schematic representation of a C shaped thermal actuator (E = expansion coefficient).

A bimorph actuator (shown in Figure 2.2) relies on two materials with different coefficients of expansion. On an induced change in temperature asymmetric expansion occurs producing out of plane bending [52]. They are often orientated into cage like structures to capture particles, which is ideal for lab-on-chip type systems, but can be quite restrictive if, once held, the particle is required to be moved around.

2.1.3.4 Chevron

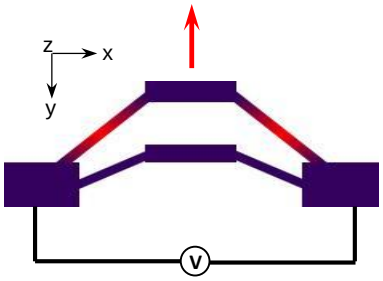

Figure 2.3 – Schematic representation of a V shaped thermal actuator.

A chevron actuator (shown in Figure 2.3) relies on the asymmetric heating of a homogeneous structure where two beams are fixed at a support forming a V shape. Upon heating the beams expand causing in plane bending [53] [54]. While this design often requires quite low voltages to operate, high temperatures have also been reported making it unsuitable for biological manipulation.

2.1.3.5 Pseudo-bimorph

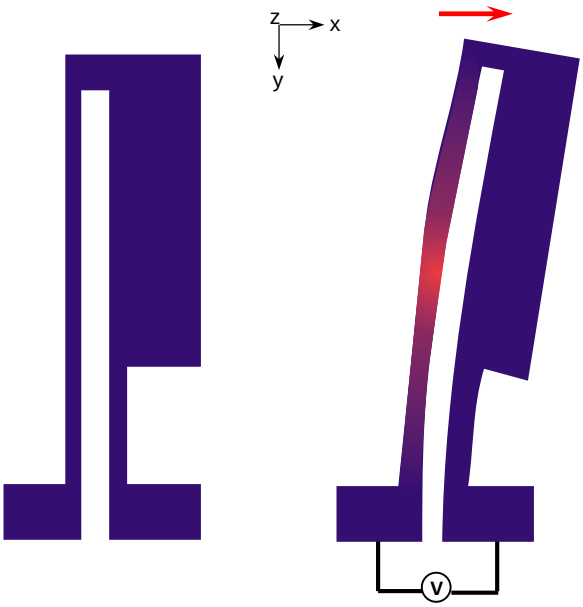

Figure 2.4 – Schematic representation of a U shaped thermal actuator.

This actuator design (shown in Figure 2.4) also relies on the asymmetric heating of a homogeneous structure, but is U shaped. Generally, the actuator consists of metal tracks running through a polymer microbeam. As an electric current is applied, the power dissipated

in the resistance of the metal tracks causes them to heat up; this in turn heats the surrounding polymer. This increase in temperature causes the polymer to expand. The temperature differential is established due to the difference in resistance of the metal. As a cooler beam is mechanically coupled to a hotter one, an in plane bend is observed. To enable large displacements, however, large temperature differences are required, making this design inappropriate for manipulating biological particles [51]. Previous work on a U-shaped actuator [55] determined a novel approach. Using expansion materials to form the U-shape, but only placing the metal in one beam, allows large displacements for significant lower temperatures. In this case the expanding polymer is connected via a flexure to an unheated (non-expanding) section of polymer, causing the in plane bend of the actuator; as shown in Figure 2.5.

Given that this design of electrothermal actuator allows large displacements for the manipulation of cells in a liquid environment without affecting the external media (via temperature change or passage of current), coupled with flexibility and cost effectiveness, this is the method by which the microgripper developed in the project operates.

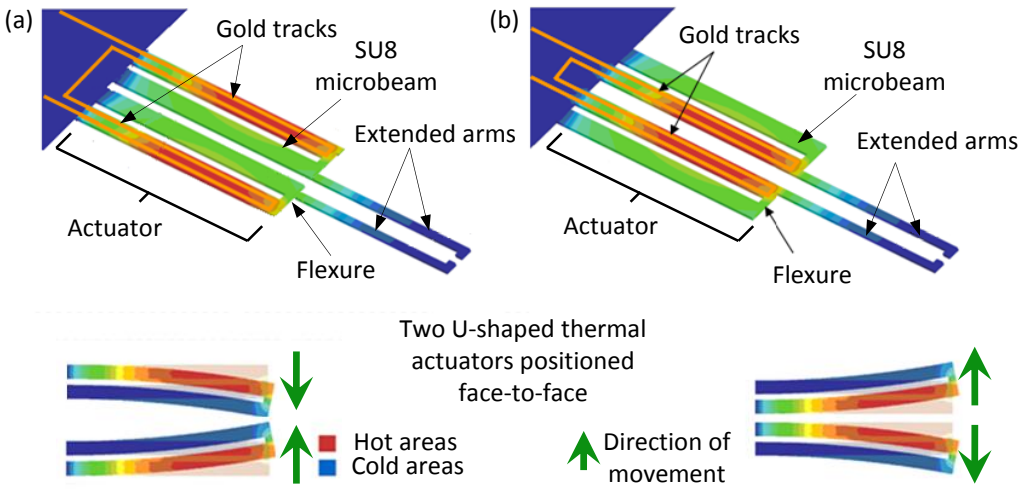

Figure 2.5 – Schematic representation of the electrothermal actuation of the microgripper designed to (a) close from open and (b) open from close.

2.2 Device Operation

The microgripper used in this work falls into the class of electrothermal actuators, which, given the need for the manipulation of biological media in an aqueous environment, are more suitable for the manipulation of cells (that is required for this project) compared to other actuation types, as this type of microgripper has lower actuation voltages and is able to be immersed in fluidic media.

The actuator consists of gold tracks running through an SU8 microbeam, as depicted in Figure 2.5. When the gold tracks lie on the outside of the actuator, Figure 2.5(a), the net effect on the microgripper tips is for them to close. The opposite effect is seen when the gold tracks lie on the inside of the actuator, Figure 2.5(b). The microgripper can also be designed to have gold tracks encapsulated within both sides of the actuator, allowing the tips to be either opened or closed.

Figure 2.6 shows the dimensioned layout of the lower polymeric and metal sections of the microgripper, including the electrode fabricated down to the microgripper tip. The arms of the microgripper are 3.54 mm in length; 1.95 mm of which is the actuator section that contains the gold tracks. In this design a continuous circuit is formed from one bond pad; down and back the SU8 microbeam on one arm of the microgripper; then around the bond pad of the electrode; down and back up the SU8 microbeam of the other arm to the remaining bond pad. The resistance of this gold track (at a thickness of 100 nm) is between 138 – 141 Ω depending on the tolerances of the fabrication process. To fully close the microgripper tips (the largest distance being 100 μm) up to 2.1 V is required. The actuation, and therefore tweezer like action of the microgripper tips, occurs almost instantaneously, and can be done in graduations; though the deflection does not increase linearly with input voltage (Figure 5 from reference [55]).

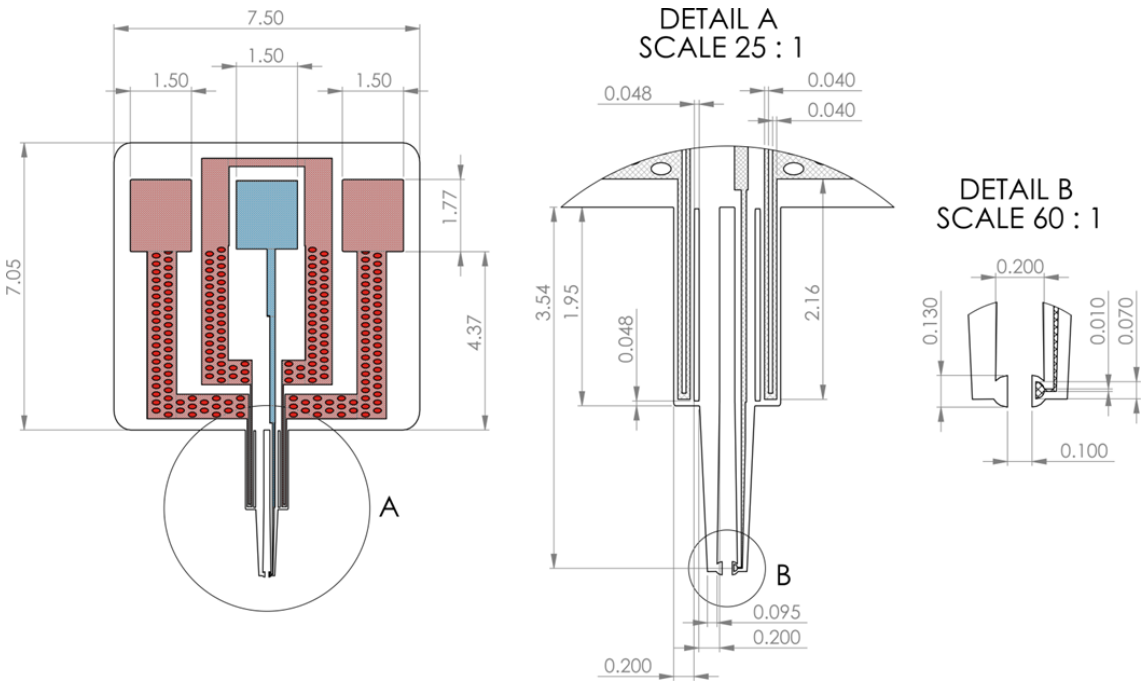

Figure 2.6 – Technical drawing of the microgripper including the metal tracks (actuators are in red, electrode is in blue). All dimensions are in millimetres.

The tips of the microgripper were fabricated with a separation gap that depends on the size of the cell being manipulated. A range of sizes have been fabricated within a 10 – 100 µm tip separation gap. The current tapered nature of the extended arm design means that separations below 10 µm would be quite challenging.

Another design consideration is the shape of the cell being manipulated. Figure 2.7 shows images of several different size and shape connotations of the microgripper tips that have been successfully fabricated during this project using the same fabrication process but with different mask designs. Certain shape designs will allow smaller tip separation gaps to be achieved, though there are still limitations due to the fabrication method used.

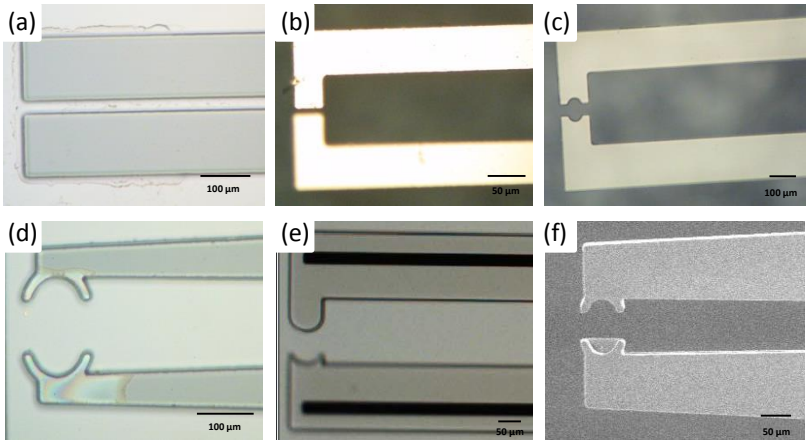

Figure 2.7 – Optical microscope and SEM images of different tip shapes: (a) 30 µm gap, flat tips; (b) 10 µm gap, square tips; (c) 40 µm gap, recessed curve tips; (d) 100 µm gap, curved tips; (e) 50 µm gap, pestle and mortar tips; and (f) 50 µm gap, scoop tip.

The bottom layer of polymer must extend underneath the bond pads (as shown in Figure 2.6) to ensure that the electrode (the central bond pad) and the actuator circuit (the outside bond pads) are isolated. Without this layer of SU8 the gold bond pads are deposited directly onto the silicon dioxide. Due to defects in this layer, occurring at the silicon dioxide etch step of the fabrication process, the isolation of the two circuits is incomplete. Leakage occurs through the silicon, between the bond pads of the actuation circuit and the bond pad of the electrode.

2.3 Microelectromechanical Systems (MEMS) Fabrication Techniques

Microelectromechanical systems (MEMS) is an area of engineering that focusses on the fabrication of electronic and mechanical devices that are made up of components in the micro scale or lower. Microsized devices have the advantage over regular ones as the integrated circuit (IC) techniques used to fabricate them allow bulk processing, which means each device is produced at a relatively low cost. There is also a greater flexibility in their design, meaning that miniaturised devices have been applied to many concepts, including immunassays, biosensors, clinical diagnostics, environmental monitoring, biochemistry and cell biology [56].

MEMS devices can be fabricated using IC processes. Besides IC techniques, modified semiconductor device fabrication process, such as moulding, wet etching (isotropic, for example HF, and crystallographic, for example KOH) and dry etching (plasma etching; reactive ion etching (RIE), deep reactive ion etching (DRIE) and vapour phase etching, such as XeF_2), ion- and electron-beam machining, and drop delivery systems, can also be used [57].

The basic processing involved in micromanufacturing is the deposition of thin films of material, patterning of that material, then etching away any material not wanted in the final device.

Deposition can occur via many routes that are dependent on the type of material being deposited. For example, metal deposition can be achieved via metal evaporation or sputtering, and polymeric support layers can be deposited via spin coating.

Patterning is generally achieved by lithography techniques. There are several different types of lithography techniques, including photolithography, electron beam lithography, ion beam lithography and x-ray lithography. In this work only photolithography is used.

2.3.1 Photolithography

The photolithographic process involves using light (near-UV) to transfer a pattern onto a photo-reactive polymer known as a photoresist. This is then often followed by an etching process to remove the material under the photoresist layer that is not protected by that photoresist, thus transferring the pattern to the material. Photoresists are generally separated into two classes, positive and negative; however by manipulating the chemical processes involved [58], or using specially designed masks [59] their behaviour can be altered to achieve a wider range of fabrication routes.

Masks are usually used in photolithography, and these can either be used in contact or proximity with the wafer. Both methods need uniform substrate UV illumination and the

ability to precisely align the features on the wafer with the features on the mask. Contact methods put the mask in direct contact with the wafer, achieving high optical resolution; however the forces used to ensure homogeneous contact can damage both the mask and wafer. In particular, particles of dust can scratch a mask, leading to permanent defects on all subsequent devices. For this reason, this method is not as widely used in industry for small features, although it is often seen in research and prototyping due to its relatively inexpensive hardware, and is the method used in this work.

Proximity methods put a small gap between the mask and wafer to reduce the potential for damage. This is done with a sacrifice in resolution, as the resolution is roughly the square root of the product of the wavelength and the gap distance. This method is fine for larger features (μm range) but not for small features (nm range).

Masks do not have to be used in physical contact with the substrate; projection or shadow mask systems can be used instead. Rather than using a physical mask, these systems project a mask image onto the substrate. The image is focussed and sized using lenses. The advantage of this system is that it produces more consistent devices when processing in bulk as one mask image can be used to fabricate many devices without the loss in resolution that proximity masks suffer from, or the risk of damage, as for contact masks; this system can achieve resolutions of tens of nm. Projection systems are more common in industry, but are seen in some research applications, where good resolution is required.

There is growing interest for printing feature sizes of tens of nm and smaller. Common photolithographic methods are unable to achieve this effectively; however, modern research is exploring alternatives to using UV light, such as electron beam lithography, x-ray lithography, extreme UV lithography, ion projection lithography and immersion lithography, as well as techniques such as nano imprint lithography. Features in the 10^{-8} to 10^{-7} m range are now routine, but much smaller sizes are still somewhat of a challenge.

2.4 Materials

The microgripper fabrication was done in layers, shown schematically in Figure 2.8.

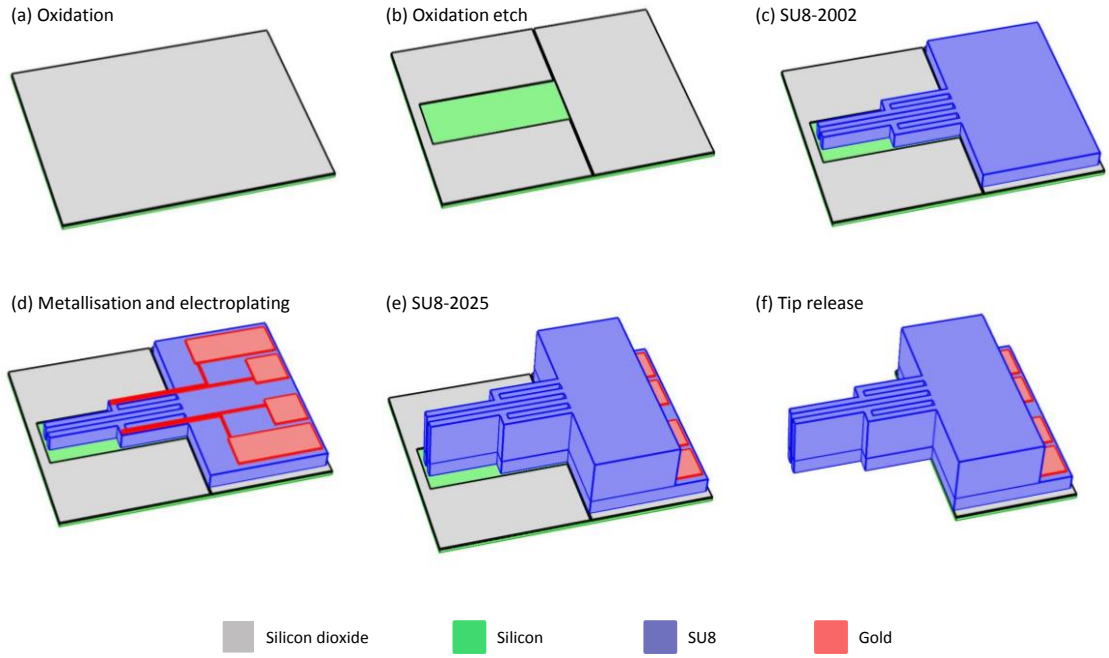

Figure 2.8 – Schematic of the microgripper fabrication (not to scale).

Firstly a thin oxide layer was grown onto a 2 inch silicon wafer (a). This was then patterned to expose the silicon around the microgripper tips (b); this aids the tip release at a later stage. A 1.7 μm layer of SU8 was patterned into the shape of the microgripper device and acts as a structural layer (c). A 25 nm layer of chromium followed by 0.25 μm of gold was e-beam evaporated and patterned into the actuation tracks (d). A 60 μm SU8 layer was patterned into the shape of the microgripper device which encapsulates the metal and acts as a structural layer (e). Finally the exposed silicon was etched away, releasing the tips from the wafer (f).

2.4.1 Silicon

For the fabrication of the microgripper a substrate that is highly stable is needed; but one that can selectively be removed from around the microgripper tips to free them. Silicon can be etched using xenon difluoride gas which is highly selective over silicon dioxide. By

oxidising a substrate and etching using hydrofluoric acid, a hard mask can be formed for the microgripper to be fabricated onto meaning that, once completed, the exposed silicon around the microgripper tips can be easily removed.

Silicon is a major material used in many MEMS processing fabrications due to its excellent physical (mechanical and electrical) properties [60]. It has a highly hydrophobic surface, which can be readily and controllably oxidised to yield a hydrophilic surface, meaning that it has good adhesion with many different materials. The excellent thermal conductivity means that polymer layers can be readily processed and the considerable chemical resistance of silicon means that it is compatible with many MEMS fabrication etchants.

2.4.1.1 Silicon Etching

Silicon and its oxide are etched either via wet or dry etching.

Wet etching involves the use of chemical liquids as etchants, for example, the use of hydrofluoric acid for preferential etching of silicon dioxide over silicon. Wet etchants are generally isotropic, which can cause problems when etching thick films. Another problem associated with this type of etching is that of having to dispose of large amounts of hazardous waste. For thin films (such as removal of silicon dioxide and metal patterning), wet etching is perfectly suitable. However, for situations such as selective etching of silicon where near vertical sidewall profiles are important, dry etching, or crystallographic wet etches, are often more suitable.

Dry etching involves the removal of specific material via the bombardment of, and/or reaction with, ions, usually a plasma of reactive gases. Unlike most wet etches, dry etching can also occur directionally or anisotropically (for example in RIE). For the selective etching of silicon, xenon difluoride etching (which does not involve plasmas) is faster, with a more isotropic etch rate. It is also very selective towards silicon in the presence of polymers, silicon dioxide and various metals [61].

Xenon difluoride etching occurs via vapourising solid xenon difluoride at reduced pressure (3 Torr), which then reacts with the silicon via the following scheme:

$$2XeF_2\ (g) + Si\ (s) \longrightarrow 2Xe\ (g) + SiF_4\ (g)$$

The only drawback with this type of etching is that xenon difluoride reacts with water to form hydrofluoric acid, which then attacks most other materials used in microfabrication. This means great care has to be taken to ensure that the equipment is not contaminated by water vapour. To help to reduce this problem an inert gas, usually nitrogen, is also mixed with the xenon difluoride gas.

2.4.2 Photoresists and Building Polymers

For the device in this project photoresists were needed for two reasons, to pattern inorganic materials and to provide rigidity to the structure. Given the complex patterns required to form each device layer, as shown in Figure 2.8, photoreactive polymers are very desirable.

Photoresist are light sensitive polymers that can be controllably spin deposited to a wide range of thicknesses, depending on the viscosity of the solution being spun. Other non-light sensitive polymers can also be used in fabrication processes; these include poly(methylmethacrylate) (PMMA) and poly(dimethylsiloxane) (PDMS).

PMMA behaves similarly to a positive photoresist, however it cannot be patterned using UV lithography. Instead x-ray, e-beam or ion exposures are used. PDMS is an elastomeric polymer that has good biocompatibility with living species. Unfortunately it has poor chemical stability against most of the organic solvents used in MEMS fabrication, and so is not a suitable building material if additional layers need to be added [62]. The two categories of photoresists are described below.

2.4.2.1 Positive Photoresists

Positive photoresists are generally used for patterning non-photoreactive layers such as inorganics or metals. One method by which they are processed (known as etch back) is shown in the schematic in Figure 2.9. On exposure to UV radiation through a patterned mask (b) the polymer chains decompose making them more soluble in alkaline developers (c). This means that the exposed regions are removed (d). The underlying layer can then also be patterned (e) and the photoresist removed (f). The pattern transferred is a direct replica of that of the mask, leading to the term positive photoresists.

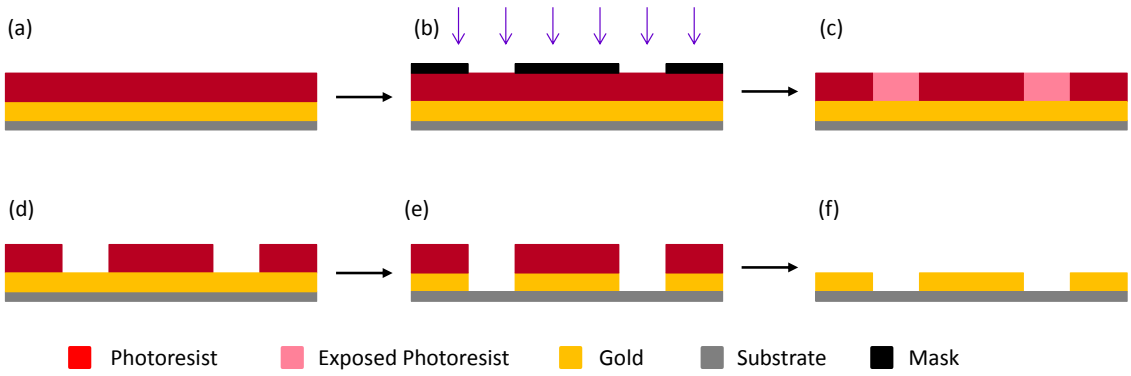

Figure 2.9 – Schematic of the etch back patterning process for positive photoresists.

The main polymer that makes up most positive resists belongs to the group of diazonapthoquinone sulphonates (DNQs). Their presence significantly reduces (by an order of magnitude) the alkaline solubility of the resist [63] making it resistant to alkaline based developers. Upon exposure, the DNQ undergoes a photodecomposition reaction to form a carboxylic acid. This is shown in Figure 2.10(a). The presence of the carboxylic acid increases the solubility of the photoresist towards alkaline developers, meaning that the exposed regions are dissolved away, successfully patterning the layer.

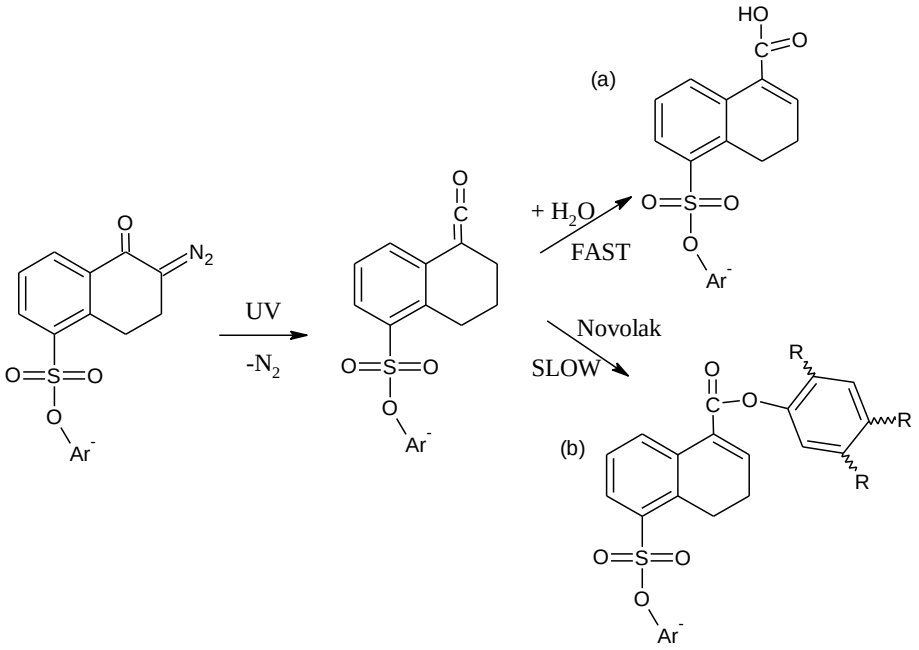

Figure 2.10 – Photodecompostion of DNQ (a) in the presence and (b) absence of water.

This, however, requires the presence of water within the photoresist layer. Without the presence of water a competitive reaction occurs where the novolak resin within the photoresist layer react with the DNQ molecule to form a highly chemical resistant polymer, shown in Figure 2.10(b). This is a problem for the thicker positive resists, such as the AZ series. The thicker layers require longer baking times, which drives off more water, increasing the chance of the competitive reaction happening on exposure. To avoid this, an additional process step is often included to rehydrate the layer [64].

2.4.2.2 Negative Photoresists

Negative photoresist are often used for building in MEMS as once they are exposed they form more stable structures. They are generally processed as shown schematically in Figure 2.11. Upon exposure though a mask pattern (b) they undergo a complex series of chemical reactions that cross-link the polymer resins, forming a very chemically stable layer (c). On treatment with solvent developers, the non-exposed regions are removed (d), leaving behind a structure that is the inverse of the mask pattern.

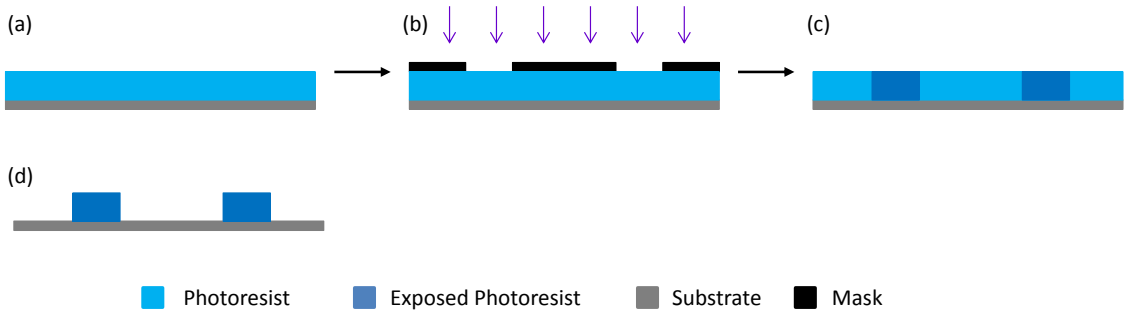

Figure 2.11 – Schematic of the pattering process for negative photoresists.

There are several widely used negative photoresists, the main ones being SU8 and polyimide (PI).

PI is more limited with respect to SU8 as, although some are photodefinable, they are often limited with respect to high aspect ratios and layer thicknesses. SU8, however, has good resolution in terms of aspect ratio as well as having excellent mechanical properties and chemically stability. It has also been shown to be biocompatible, which is important for the microgripper application [56].

Table 2.1 compares the material properties of the polymeric building materials that are commonly used in MEMS fabrication.

Table 2.1 – Some material properties of the commonly used polymers in MEMS fabrication.

Material	**T_g / °C**	**Melting / degradation temp. / °C**	**CTE / ppm °C^{-1}**	**Thermal conductivity / W mK^{-1}**	**UV transparency**	**Visible light transparency**	**Organic solvent effect**
PMMA	106	205	70	0.19	Opaque	Good	Soluble in many
PDMS	-125	400	310	0.15	> 230 nm	Good	Swelling with many
SU8	240	> 340	50-102	0.2	> 350 nm	Good	Mostly no effect
PI	400	620	3	0.2	Opaque	Good	Mostly no effect

2.4.3 Metals

Metals can be relatively easily deposited to a controllable thickness via a number of MEMS techniques; the most simple of which is via e-beam or thermal evaporation. Here a crucible of metal is placed in a vacuum and heated (by an electron beam or heating element respectively) to evaporate the metal onto a substrate. Sputtering and electroplating can also be used to deposit metals, although electroplating usually requires a seed layer of metal to be deposited beforehand, meaning it is more generally used to thicken already existing layers.

For the functionalisation of the microgripper for use with electrochemical techniques, gold and platinum are the preferred metals to use. Given the relative costs, gold was more desirable. It has also been shown previously that microgrippers fabricated using SU8 and gold could achieve displacements of 12 μm with a relatively low voltage (1.8 V) [51], whereas one using a titanium/platinum heating element used much higher voltages (10 V) for only slightly greater displacements [50].

2.5 Miniaturisation and Functionalisation

Previously, the microgripper dimensions were designed for manipulation of large cells, typically 100 – 150 μm in diameter [1]. However, given most eukaryotic plant and animal cells have diameters within the 10 – 100 μm and 10 – 30 μm range respectively, significant miniaturisation was needed before the device could be functionalised.

The main challenges in miniaturising the device were in the adhesion between the layers and the feature definition of the device, both of which are related to the thin film stress of each individual layer deposited during fabrication. It was also important to maintain good vertical sidewall profiles, which is increasingly challenging as the aspect ratio becomes greater (i.e. the feature line width is smaller than the layer thickness). The lack of homogeneity across the wafer, due to their uniformity, is a large factor in thin film stress. All silicon wafers vary in thickness, flatness (variation in thickness across a single wafer) and bow as a result of their

production. Typically wafers used for this project have specifications of thickness ± 10 µm, flatness < 2 µm and bow < 20 µm. In the fabrication process, described in detail in Section 2.6.2, the oxide and metal film thicknesses are sufficiently thin that their effect on the stress on the system are negligible and can be ignored. This meant that the SU8 processing was the main contributor towards stress within the device. If the adhesion between the wafer and SU8 is good, then the extent of bowing will increase as the solvent is evaporated and the layer begins to shrink (tensile stress). This can cause issues at the release stage with cantilever bending. If the adhesion between the wafer and SU8 is poor, then the layer will delaminate from the surface. Both the increased bowing and the delamination are undesirable when fabricating cantilevers, so the thin layer stress needed to be reduced significantly in order to achieve the miniaturised dimensions required.

2.5.1 SU8 Development

SU8 is processed via the following basic scheme:

Spin deposition → Soft bake (SB) → Exposure → Post exposure bake (PEB) → Development

Del Campo *et al.* [65] determined that the SB parameters contribute up to 50 % to the internal stress of the film, followed by 10, 15 and 5 % for the exposure dose, PEB and development respectively.

Molecular mobility after baking has a serious impact on the film stress within the device. If the SU8 polymers are unable to flow, the layer shrinks to a greater extent upon cross-linking (during exposure and PEB), increasing the level of tensile stress within the device causing cantilever bending (as shown in Figure 2.12), as well as catastrophic delamination between the layers due to adhesion failure.

Additionally, the thicker the SU8 is, the more difficult it is to process. Viscous SU8 solutions are notoriously difficult to spin evenly and often result in edge beading. Also, uneven

coatings can occur when SU8 is spun over existing features, which can have a great effect on the baking consistency. All trials described in Section 2.5.1 were therefore undertaken using SU8 2025 as this was the more difficult layer to process.

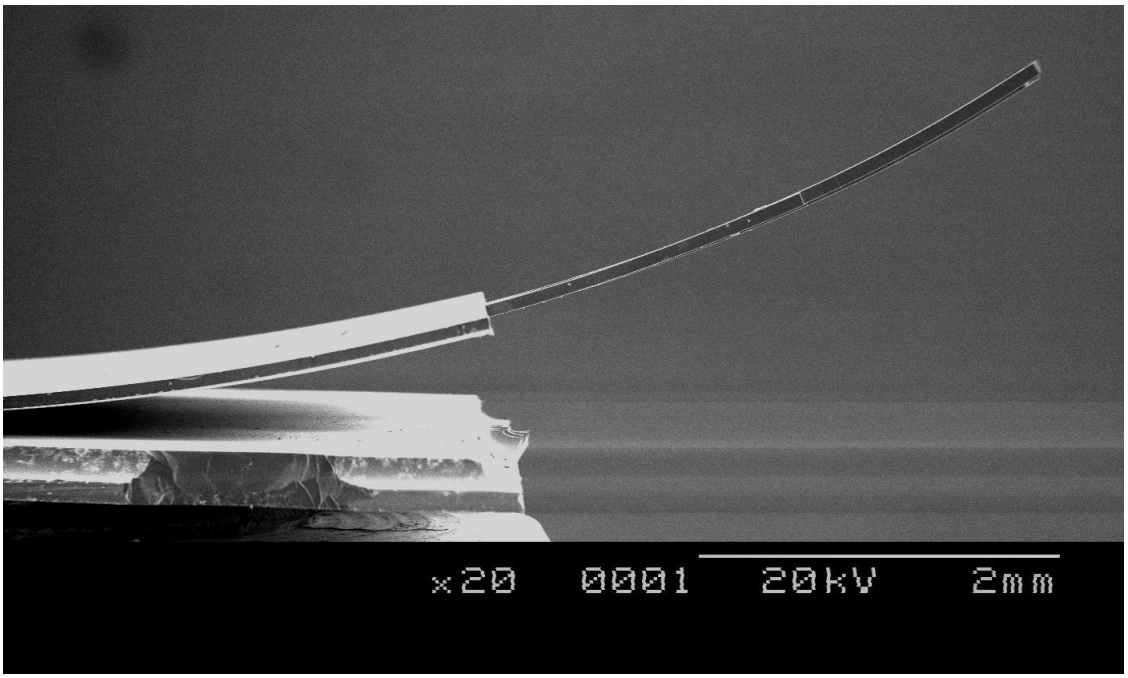

Figure 2.12 – An extreme example of the effect of thin film stress on cantilever bending.

There are several studies that have focussed on the optimal processing details for producing high aspect ratio features with SU8 [66] [67] [68] [69]. While these give important information on baking regimes [67] and how this affects feature definition and device performance, not many publications consider what is happening from a chemical perspective within the SU8 layer. For this reason, modelling of the exposure parameter is often skipped in discussions; when mentioned, it is usually in the context of controlling exposure for replication reliability [68]. For this reason, modelling of the exposure parameter was completed to fully utilise SU8 processing for miniaturisation.

SU8 is a multi-branched epoxy resin (structure shown in Figure 2.13) which is classed as a negative photoresist (on exposure to UV radiation the epoxide rings cross-link forming a very chemical resistant layer, which remains as a building layer). The resin is usually dissolved

in cyclopentanone and also contains a photo acid generator (triaryl sulfonium hexafluoroantimonate salt) that is needed to initiate the cross-linking.

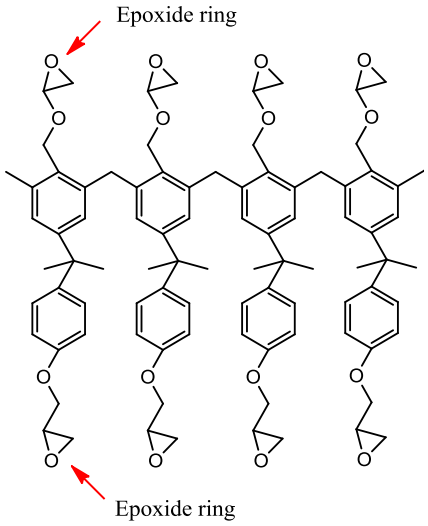

Figure 2.13 – Chemical structure of SU8, indicating the epoxide rings.

2.5.1.1 Spin Parameter

The spin step of the fabrication process is designed to spread the SU8 evenly across the wafer to a desired layer thickness. The layer thickness is dependent on the viscosity (and therefore the temperature) of the SU8 and the spin speed and/or duration. It was observed that the centrifugal forces applied to the wafer during spinning caused tensile stress within the SU8 layer, which, if not reduced, causes significant cantilever bending at the release stage (Figure 2.12). To overcome all these challenges a 10 min rest period was introduced after the spin and before the baking stage. This allowed the shear forces applied to the polymers to relax, letting the SU8 flow and back fill any potential air pockets caused by spinning over step heights, and to level the film thickness, reducing edge beading effects.

2.5.1.2 Soft Bake Parameter

The soft bake step is designed to evaporate the excess solvent and 'set' the layer. If the layer is under baked then there is not enough rigidity in the SU8 layer, so on development the features can collapse. However, if the layer is over baked, feature definition is lost due to a

restriction in the rate of polymerisation of the cross-linking required to cure the SU8 layer. This, coupled with the issues related to molecular mobility that increases tensile stress, can significantly affect the processing of the SU8 film. Process trails were conducted to determine the optimum soft bake time and a temperature ramp profile was introduced to replace the generally used 2-step process.

Figure 2.14 compares the features fabricated from a 2-step process with those from several temperature ramp profiles and shows some of the effects of changing the baking regime.

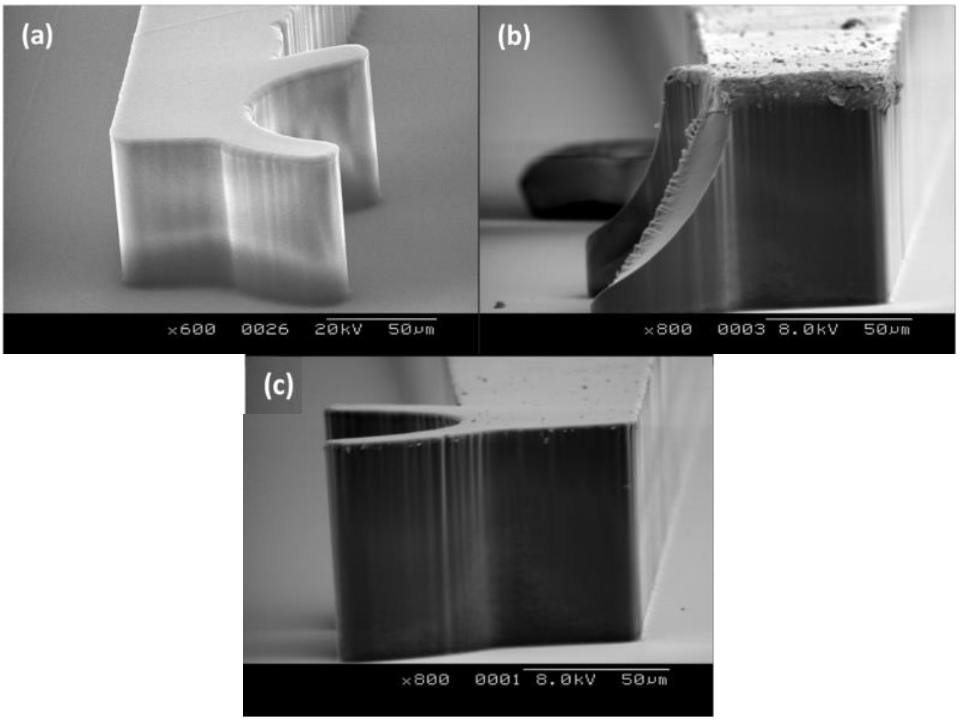

Figure 2.14 – Comparison of different baking regimes (a) 2-step process, (b) short temperature ramp, and (c) optimised temperature ramp.

Figure 2.14(a) shows the features fabricated via a 2-step process and poor sidewall definition can be seen (slight T-topping profile); poor adhesion to the substrate was also observed indicating a high level of internal stress. Figure 2.14(b) shows the result from a temperature ramp profile that was too short, so under baking occurred, resulting in feature

collapse; a similar effect would be seen for over baking. Figure 2.14(c) shows the result from a more optimised ramp profile. All ramp profiles had better adhesion to the substrate.

Table 2.2 – Summary of the processing parameters of the different baking regimes.

	Spin	Soft bake	Exposure	PEB	Development
(a)	10 s at 500 RPM[a] + 50 s at 2000 RPM[b] + 10 min rest.	6 min at 65 °C + 19 min at 95 °C + 1 min at 65 °C, cool at room temperature (RT)	800 $mJcm^{-2}$	1 min at 65 °C + 4 min at 95 °C + 1 min at 65 °C	6 min with agitation in EC solvent
(b)	10 s at 500 RPM[a] + 50 s at 2000 RPM[b] + 10 min rest	2 min at 65 °C, 3 min ramp to 95 °C, 4 min at 95 °C + 1 min at 65 °C, cool at RT	800 $mJcm^{-2}$	1 min at 65 °C + 4 min at 95 °C + 1 min at 65 °C	6 min with agitation in EC solvent
(c)	10 s at 500 RPM[a] + 50 s at 2000 RPM[b] + 10 min rest	2 min at 65 °C, 3 min ramp to 95 °C, 9 min at 95 °C, 7 min cool ramp to 65 °C, cool at RT	800 $mJcm^{-2}$	1 min at 65 °C + 4 min at 95 °C + 1 min at 65 °C	6 min with agitation in EC solvent

[a] 164 RPM s^{-1} acceleration
[b] 246 RPM s^{-1} acceleration

Ramping the temperature implemented a gradual change which evaporated the solvent much more slowly, maintaining a more uniform bake (helping to reduce the tensile stress). A cool down period was also included, which helped to reduce the chance of adhesion failure due to fast layer shrinkage.

2.5.1.3 Exposure Parameter

The exposure dose dictates the quantity of the catalytic acid generated in the irradiated areas of SU8. As the SU8 layer is irradiated with UV radiation, the triaryl sulfonium hexafluoroantimonate (tArSbF) salt is broken down to form a strong lewis acid ($HSbF_6$) and bi-products (Figure 2.15).

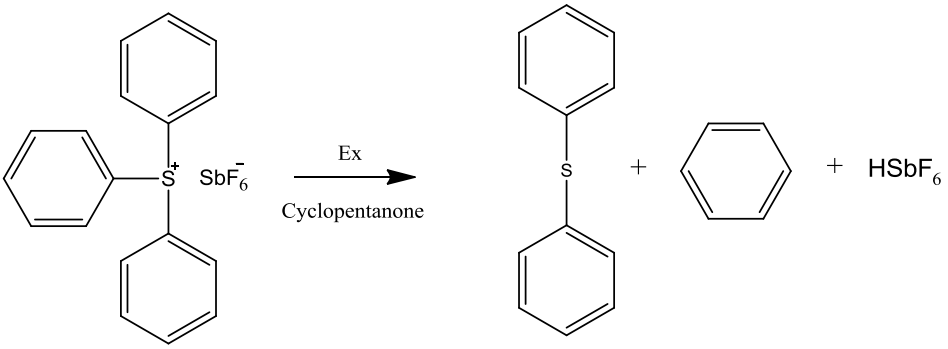

Figure 2.15 – Photolysis of the triaryl sulfonium hexafluoroantimonate salt.

The rate of production of lewis acid is directly reliant on the energy of the irradiation, i.e. the exposure dose, as shown in Equation 2.1.

$$R_{Ph} = k_{Ph}[Ar_3S^+SbF_6^-][CP][Ex]$$

Equation 2.1

where R_{Ph} is the rate of photolysis (M s^{-1});

k_{Ph} is the rate constant of photolysis (s M^{-1} Kg^{-1});

[$Ar_3S^+SbF_6^-$] is the concentration of the tArSbF salt (M);

[*CP*] is the concentration of cyclopentanone solvent (M);

[*Ex*] is the exposure dose (mJ cm^{-2}).

It was observed that the device dimensions could be fine tuned by controlling the chemistry occurring within the layer simply by varying the exposure dose due to the linear relationship between the quantity of acid available (dictated by the exposure dose) and the dark field gap distance (dictated by the rate of cross-linking). This requires precise control over the volume of SU8 (i.e. the concentration of tArSbF salt) and soft bake regime (i.e. solvent concentration), so is by no means trivial.

Low exposure doses do not saturate the whole layer, so not enough acid is generated to cross-link the SU8 at the bottom of the feature. This leads to undercutting, which is shown in Figure 2.16.

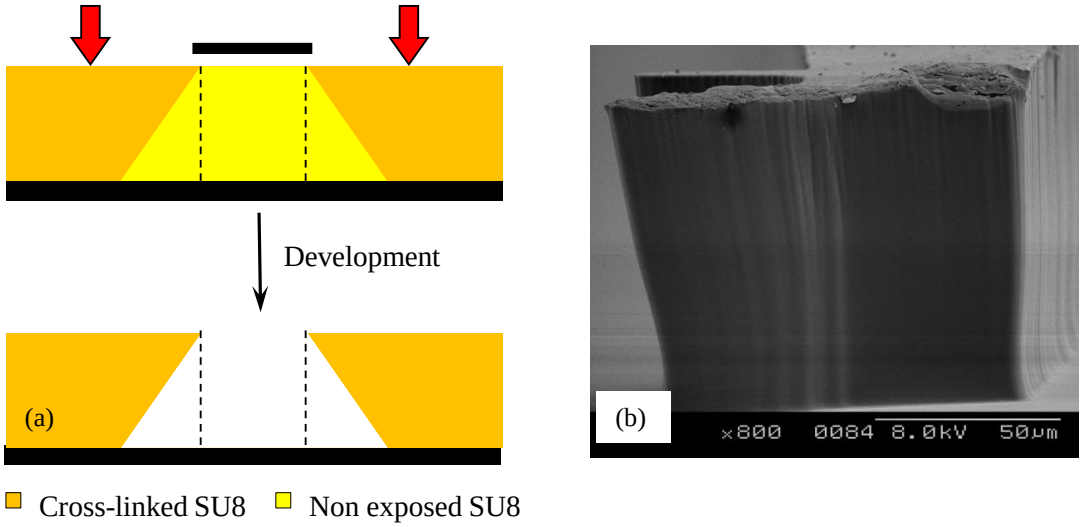

Figure 2.16 – (a) Schematic representation of the undercutting effect after underexposure, (b) SEM image of undercutting and feature collapse due to underexposure.

At high exposures the top of the SU8 layer, which readily absorbs the shorter wavelengths, forms an area of greater cross-link density after the post exposure bake regime. This results in a t-topping sidewall profile as seen in Figure 2.17.

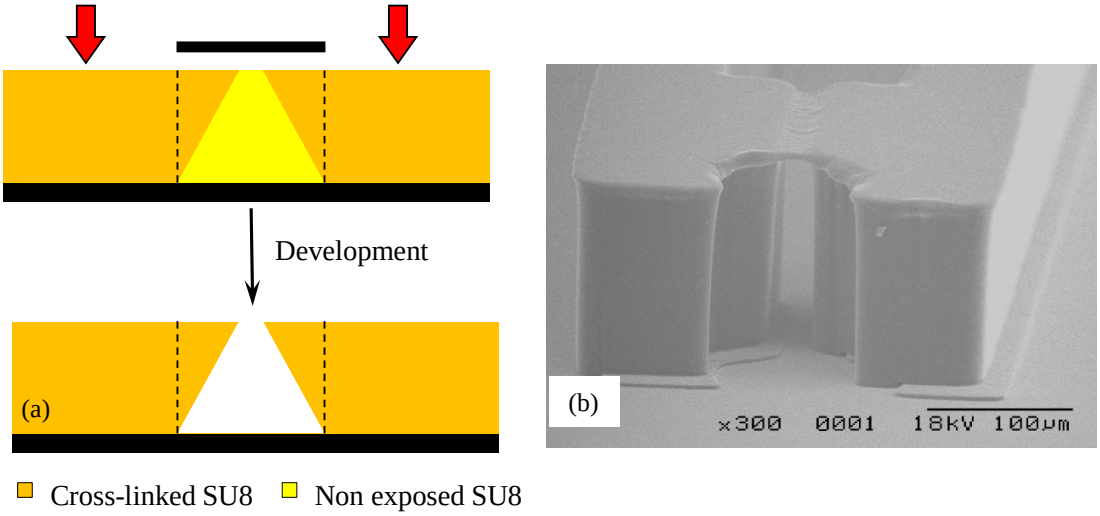

Figure 2.17 – (a) Schematic representation of the t-topping effect after overexposure, (b) SEM image of fused features due to overexposure.

The use of a 360 nm filter removes the shorter wavelengths from a broadband UV source and only allows the passage of the dominant 365, 405 and 436 nm wavelengths. SU8 is highly absorbing for wavelengths less than 350 nm but is almost transparent for wavelengths above 400 nm [70]. Therefore, at the wavelengths that pass through the filter, the absorption

coefficient of SU8 will be much lower, and so t-topping does not occur as readily. It is important to note that comparatively higher exposure doses are required to achieve the same rate of lewis acid generation within the SU8 layer when the filter is used.

As the radiation passes through the layer the intensity decays due to absorption by SU8.

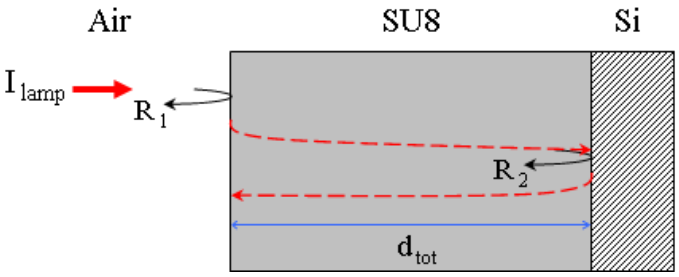

Figure 2.18 – Schematic representation of the three material model.

Using a simple three material model [71] (Figure 2.18) it can be determined that, if no reflection from the silicon substrate is assumed (R_1 only), then the relative exposure at the bottom of the layer can be calculated, using Equation 2.2, to be 25% less than at the top (assuming a layer thickness of 60 μm).

$$D(d) = I_{lamp}t(1 - R_1)e^{-\alpha d}$$

Equation 2.2 [71]

where D is the exposure dose (mJ cm^{-2});

d is the distance through the layer (cm);

I_{lamp} is the intensity of the lamp (mW cm^{-2});

t is the time of the exposure (s);

R_1 is the reflection coefficient at the air|SU8 interface;

α is the absorption coefficient of SU8 (cm^{-1}).

If we take into account light passing through the complete SU8 layer, and reflecting from the silicon substrate (R_1 and R_2), the exposure non-uniformity through the layer can be calculated to still be within 15% using Equation 2.3.

$$D(d) = I_{lamp}t(1 - R_1)e^{-\alpha d}\left(1 + R_2 e^{-2\alpha d_{tot} - d}\right)$$

Equation 2.3 [71]

where R_2 is the reflection coefficient at the SU8|substrate interface;

d_{tot} is the total thickness of the layer (cm).

This model does not take into account the change in the absorption coefficient of SU8 as it is exposed [71]. Despite this simplification, the three material model is a good representation of our system given the lower absorption coefficients when using the optical filter. Therefore it can be said that for the layer thicknesses of the device used in this study (i.e. less than 60 μm), the exposure dose is very similar at the top and bottom of the layer, and so near vertical walls would be expected once the optimal exposure dose has been reached. However, one would expect a slight angle to the sidewalls to begin to show when the exposure non-uniformity is greater than 25%.

2.5.1.4 Post Exposure Bake Parameter

The main purpose of the PEB regime is to kinetically improve the rate of cross-linking to ensure good feature definition. Figure 2.19 shows the chemistry of the cross-linking. A temperature ramp was again used during this step to ensure a more uniform bake and to reduce the internal layer stress. A cool down ramp was not used in the PEB regime as it results in loss of feature definition.

The lewis acid generated via photolysis initiates the polymerisation of the epoxide groups in SU8 as shown in Figure 2.19(a). The initiated species then goes on to propagate the polymerisation which is shown in Figure 2.19(b).

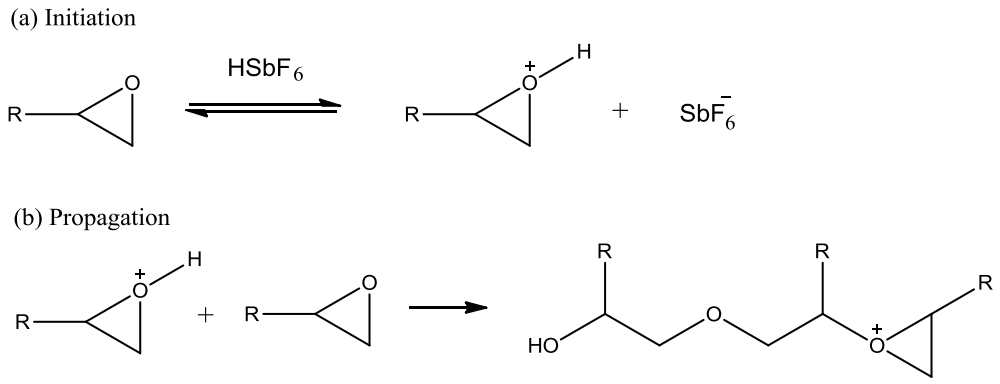

Figure 2.19 – Reaction scheme for (a) the initiation and (b) propagation of SU8.

The rates of initiation, propagation and termination are shown below.

$$R_i = k_i[SU8][HSbF_6]$$

Equation 2.4

$$R_p = k_p[SU8][SU8^+ - H]$$

Equation 2.5

$$R_t = k_t[SU8^+ - H]$$

Equation 2.6

where R_i, R_p and R_t are the rates of initiation, propagation and termination respectively (M s^{-1});

k_i, k_p and k_t are the rate constants for the initiation, propagation and termination respectively (M^{-1} s^{-1});

[*SU8*] is the concentration of SU8 monomer (M);

[$HSbF_6$] is the concentration of lewis acid generated by the photolysis reaction (M);

[$SU8^+$-*H*] is the concentration of initiated SU8 monomer (M).

Assuming steady state behaviour (when R_i = R_t), it can be shown that the rate of propagation is directly proportional to the concentration of the lewis acid.

$$R_p = \frac{k_i k_p [SU8]^2 [HSbF_6]}{k_t}$$

Equation 2.7

Given that the rate of production of lewis acid is directly reliant on the energy of the irradiation, i.e. the exposure dose, as shown in Equation 2.1, it would then be expected that, as the exposure dose is increased linearly, there would be an equivalent linear increase in the rate of polymerisation. So over a fixed time, the distance within which the cross-linking of the SU8 occurs would also increase linearly. This was confirmed experimentally by the relationship between the gap distance and exposure dose in Figure 2.20 (error bars were calculated from the standard deviation of repeated data sets).

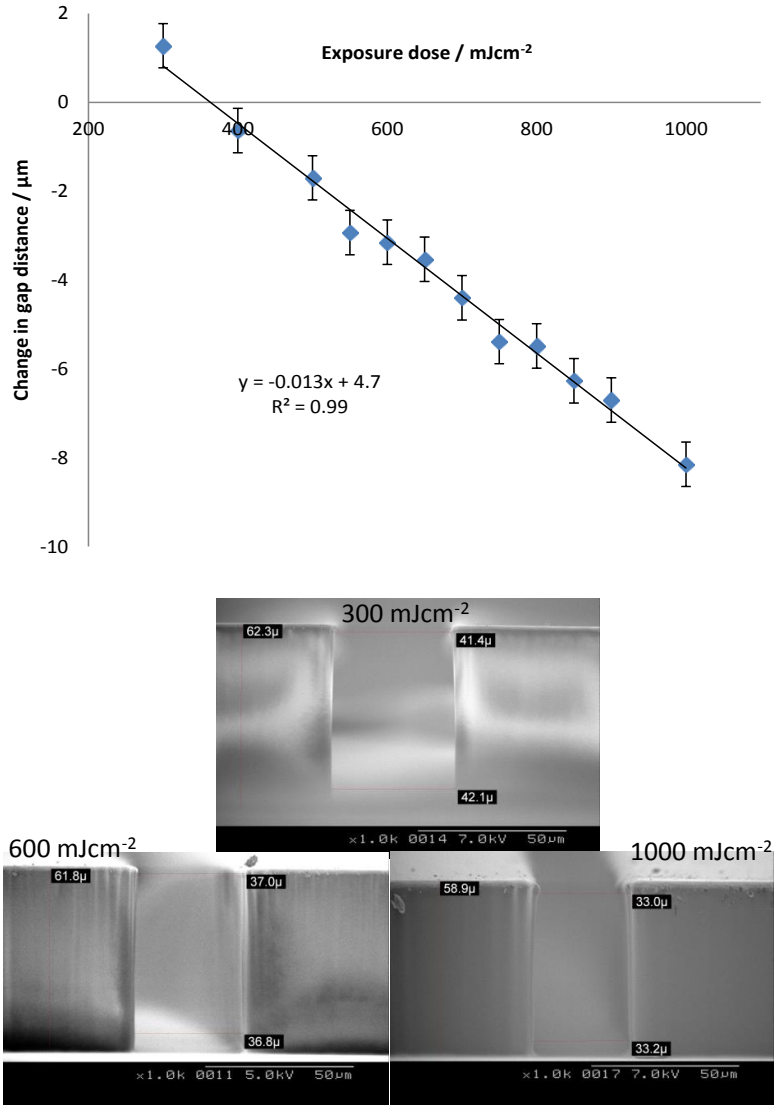

Figure 2.20 – The change in tip distance against exposure dose relationship and SEM images of the sidewall profiles at three exposure doses for a layer thickness of 60 µm.

2.5.1.5 Development Parameter

The development step removes the non cross-linked material by dissolving it into a solvent. Cheng and Chen [72] have published details of how the orientation of the wafer during development affects the ease of production of high aspect ratio (HAR) features with good feature definition with PMMA. Given the similarities in the chemistry between PMMA curing and development and that of SU8, some of these procedures were applied to the device fabrication, with successful results. Figure 2.21 shows this schematically.

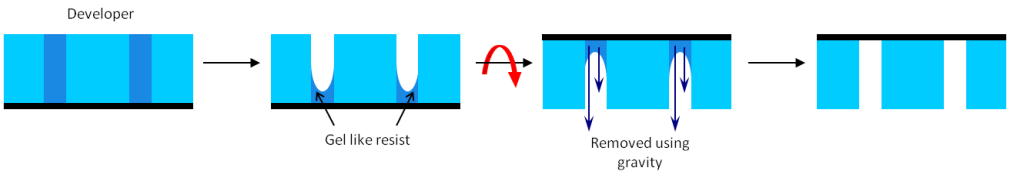

Figure 2.21 – Schematic representation of the development regime.

The non cross-linked material absorbs the solvent and forms a gel like matrix. This has a higher density than the surrounding solvent, so when the wafer is inverted, the gel is removed cleanly, leaving behind well resolved features.

2.5.2 Electrode Incorporation

There is much research interest in many different methods of functionalising the microgripper, including the addition of force sensors, piezoelectric agitators to remove sticky cells from the tips, electromagnetic pulses to break up clumps of cells, as well as electrode incorporation. Fabricating an electrode at the microgripper tips can allow cytolysis and electroporation experiments to be carried out as well as opening up the potential use in electrochemical sensors; for example ion or DNA sensors. Many of these applications involve the modification of this electrode, and therefore controllable fabrication is important.

Photolithography can be used to pattern an electrode down one or both of the microgripper arms to tip(s). Thick positive photoresist can be used to pattern a template onto

a seed layer of metal and more metal is then deposited into the voids, via electroplating, to give the electrode shape. A schematic of the electroplating process is shown in Figure 2.22.

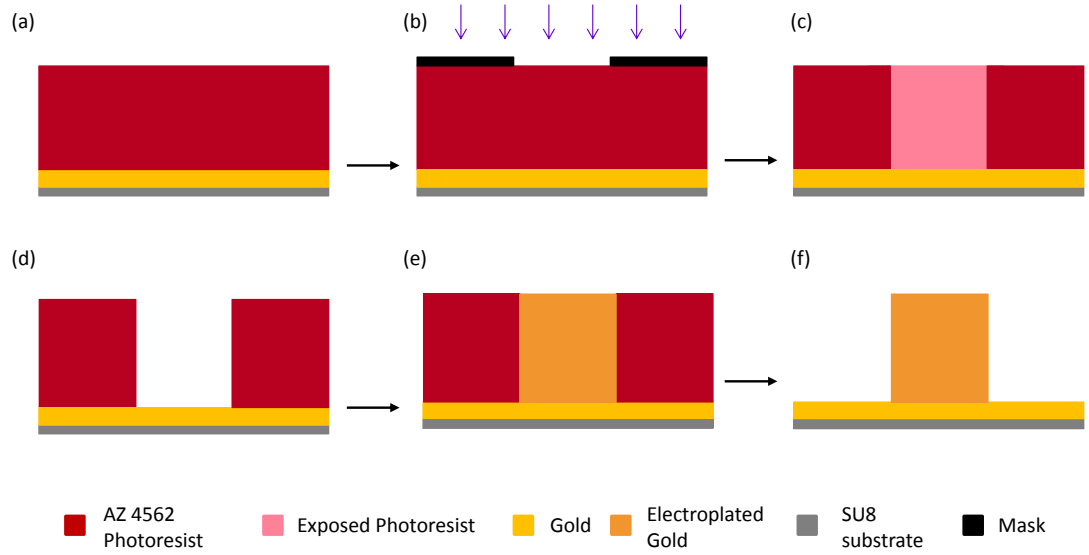

Figure 2.22 – Schematic of the patterned electroplating process.

The successful fabrication of this is shown in Figure 2.23.

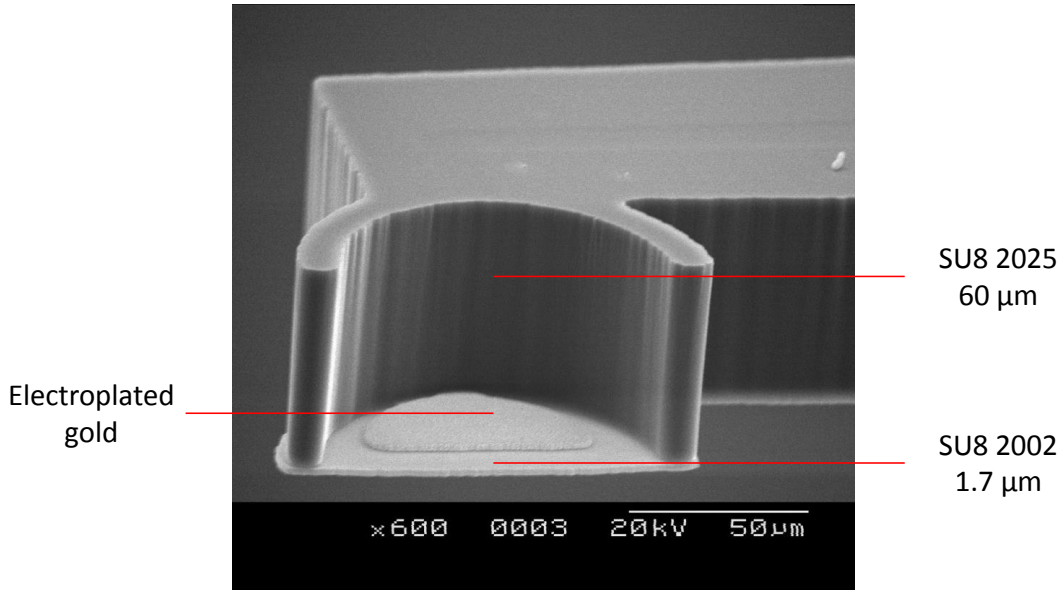

Figure 2.23 – SEM image of the electrode at the microgripper tip.

For the application of ion selective electrodes the surface morphology of the electrode needs to be fairly rough (rms roughness (R_q) of the microgripper electrode is 150 nm) to ensure good adhesion of the poly(3,4-ethylenedioxythiophene) (PEDOT) layer to the electrode,

so careful optimisation of the electroplating parameters are not needed. The only consideration is the current density and the plating time.

The current density needs to be low enough for pattern fidelity to be maintained for a given thickness. In this case, due to the mask design, there are large areas and small areas to be plated, so pulse plating is used to allow effective diffusion of the ions in and out of the photoresist template, which ensures that the local solution concentration stays constant.

The plating time also needs to be carefully considered to limit the thickness of the metal being deposited. If the thickness exceeds that of the photoresist template a mushroom effect occurs as the metal is deposited without any constraints. This is shown in Figure 2.24.

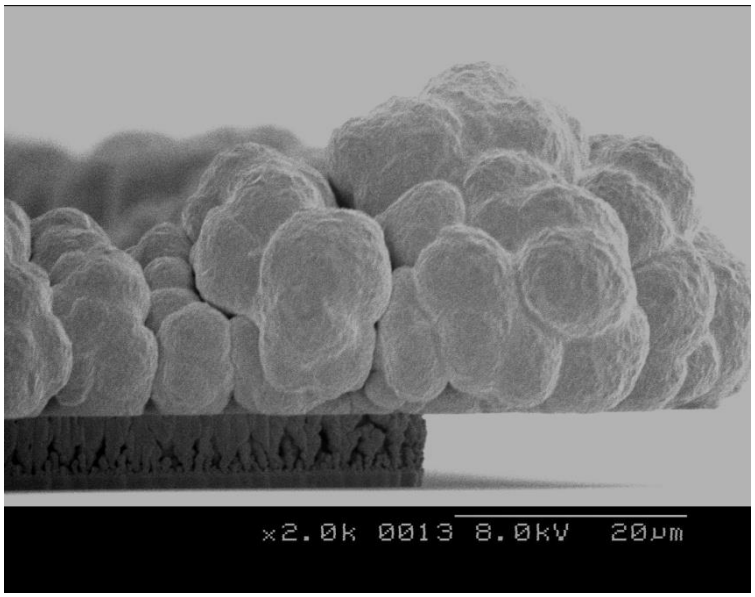

Figure 2.24 – SEM image of the 'mushrooming effect' seen after over plating through a photoresist mask.

The processing parameters described in Section 2.6.2.3 gave appropriate surface roughness for the subsequent deposition and with excellent pattern reproducibility, which ensures that the electrode dimensions remain consistent between devices. This is important to ensure consistent electrochemical modification later on in the fabrication of ion selective electrodes.

2.6 Device Fabrication

2.6.1 Chemicals and Reagents

The positive resists were purchased from Chestech and all SU8 photoresists from MicroChem; these were used as instructed for their respective data sheets and without any modification. The solvent developers relating to the photoresists were purchased from Microposit.

1.2 SPR 350 was spin coated using a Laurell spinner at 700 RPM for 10 s, then 3700 RPM for 30 s, to yield a 1.2 µm thick layer. This was baked at 110 °C for 3 minutes and exposed through a chromium mask using an EVG 620 mask aligner for 3.2 s. The resulting pattern was then developed in MF-319 developer for 1 minute.

AZ 4562 was spin coated using a Laurell spinner at 700 RPM for 10 s, then 3700 RPM for 30 s, to yield a 10 µm thick layer. This was baked at 95 °C for 20 minutes then left submerged beneath deionised water (DI) water for 40 minutes. The layer was then exposed through a chromium mask using an EVG 620 mask aligner for 30 s and the resulting pattern was then developed in 1:3 351 developer:H_2O for 4 minutes.

The chemicals used to make up the gold and chromium etches, the acid cleaning/etches and the solvents were purchased from Fischer Scientific and were used without further purification.

2.6.2 Fabrication Overview

The microgripper is fabricated via the scheme shown in Figure 2.25.

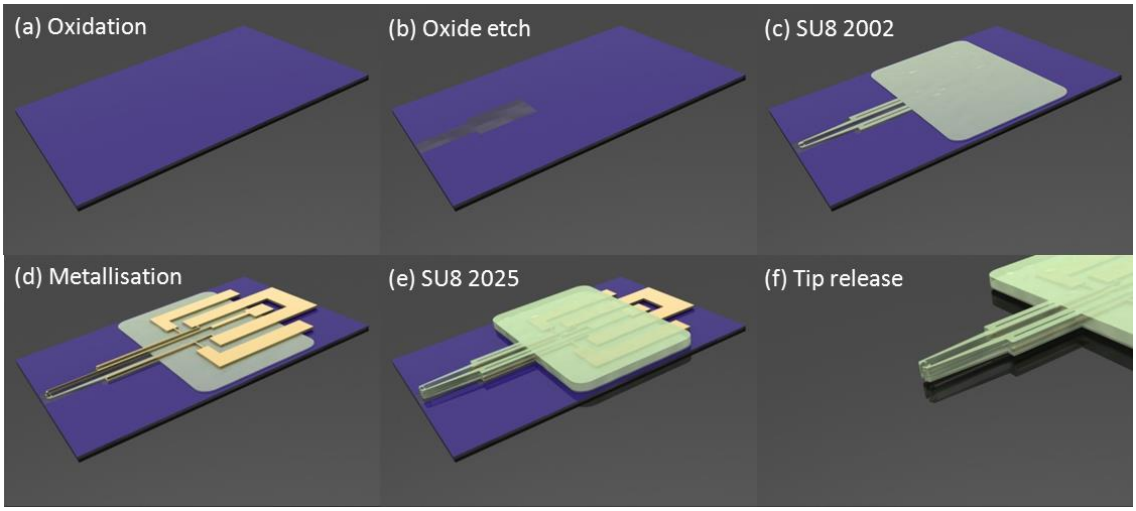

Figure 2.25 – Schematic of the microgripper fabrication.

2.6.2.1 Oxidation

2 inch <100> silicon wafers were first cleaned in a solution of 1:1 H_2SO_4:H_2O_2 for 20 minutes and then rinsed with sonication. Any residual oxide was removed by etching using 10% HF for 2 minutes. The wafers were then placed into an oxidation furnace at 1100 °C with 3 litres min^{-1} dry O_2 flow for 100 minutes. This resulted in a 0.1 µm thick oxide grown on the surface (checked with a Rudolph Auto ELIII elipsometer).

The oxide layer was removed to leave an area around where the microgripper tip will be; this is important for the release stage at the end of the process. This was achieved using 1.2 SRP 350 photoresist patterned as described in Section 2.6.1. The exposed silicon dioxide was etched using buffered HF (1:4 HF:NH_3F) for 2 minutes. The SPR 350 photoresist was then removed using acetone to leave the patterned silicon dioxide.

2.6.2.2 SU8-2002

The bottom layer of the microgripper device was patterned using SU8-2002 negative photoresist.

1 ml of SU8-2002 was spin coated onto the patterned silicon wafer using a Laurell spinner at 500 RPM for 10 s (acceleration of 164 RPM s^{-1}) followed by 1500 RPM for 15 s

(acceleration of 246 RPM s^{-1}) to give a 1.7 µm layer. This was soft baked at 65 °C for 1 minute, then 95 °C for 1 minute and finally 65 °C for 1 minute. The layer was then exposed through a PL-360LP Omega optical filter and a chromium mask using an EVG 620 mask aligner at a dose of 200 mJ cm^{-2}. The wafer was then baked via a 3 minute temperature ramp from 65 °C to 95 °C, held at 95 °C for 2 minutes and then placed at 65 °C for 1 minute. The resulting pattern was then developed in EC solvent for 1 minute and rinsed with EC solvent then iso-propyl alcohol (IPA) for 10 s each. Finally the layer underwent a hard bake for 5 minutes at 115 °C to fully cure the polymer.

2.6.2.3 Metallisation and Electroplating

During this step 25 nm of chromium then 100 nm of gold was e-beam evaporated. Typically chromium and gold are deposited at a rate of 6 and 4 Å s^{-1} respectively. The gold layer was then patterned using AZ 4562 into the design of the electrode as described in Section 2.6.1. The layer was then pulse electroplated (3 ms at 40 mA then 7 ms at 1 µA for 90 minutes), using a Neutronex 309 A gold electroplating solution from Enthone, to yield a 5 µm thick patterned gold layer. The AZ 4562 layer was then removed using acetone and the wafer rinsed with IPA.

The wafer was then patterned using SPR-350 into the design of the electrode and actuators as described in Section 2.6.1. The exposed gold was then etched using a gold etch (4:1:8 by weight of $KI:I:H_2O$) for 10 s and then the exposed chromium was etched using a chromium etch (7:34:1 by weight of $Ce(NH_4)_2(NO_3)_6:HNO_3:H_2O$) for 20 s. The SPR 350 photoresist was then removed using acetone leaving the patterned metal tracks for the electrode and actuators.

2.6.2.4 SU8-2025

The metal tracks were then encapsulated in a top layer of SU8-2025 negative photoresist.

3 ml of SU8-2025 was spin coated onto the patterned silicon wafer using a Laurell spinner at 500 RPM for 10 s (acceleration of 164 RPM s^{-1}) followed by 2000 RPM for 20 s (acceleration of 246 RPM s^{-1}) followed by a 10 minute rest which resulted in a 60 µm layer. This was soft baked via a 3 minute temperature ramp from room temperature (RT) to 65 °C and held for 1 minute then followed by a 3 minute temperature ramp to 95 °C and held for 3 minutes. The wafer was then cooled on the hotplate until at RT (approximately 40 minutes). The layer was then exposed through a PL-360LP Omega Optical filter and a chromium mask using an EVG 620 mask aligner at a dose of 300 mJ cm^{-2}. The wafer was then baked during a 3 minute temperature ramp from RT to 65 °C and held for 1 minute, then followed by a 3 minute temperature ramp to 95 °C and held for 4 minutes and then placed at 65 °C for 1 minute. The resulting pattern was then developed in EC solvent for 6 minutes and rinsed with EC solvent then and IPA for 10 s each. Finally the layer underwent a hard bake for 5 minutes at 110 °C to fully cure the polymer.

2.6.2.5 Tip Release

The final stage is the release of the microgripper tips from the silicon wafer. This was done using a XeF_2 vapour phase etch in a XACTIX etcher. A mixture of 3 T XeF_2 and 3 T N_2 was cycled every 60 s for 160 cycles to etch any exposed silicon (patterned in the first stage). The wafer was then broken along the grooves etched into the wafer releasing the microgripper tips from the silicon and allowing them space to move.

2.7 Integration into External Handling System

The microgripper devices are batch processed with 10 devices arranged on a 2 inch wafer as shown in Figure 2.26.

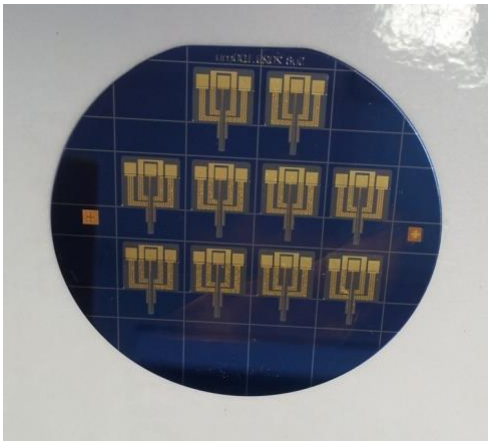

Figure 2.26 – Orientation of devices on a 2 inch wafer.

At the XeF_2 tip release stage score lines are also etched so that the wafer can be broken into individual chips. The device then needed to be connected to an external circuit for operation. This was achieved initially using a custom made printed circuit board (PCB) with the bond pad on the device chip wire bonded to pads on the PCB (as shown in Figure 2.27). Output from the PCB was taken, via a ribbon cable from the pin connector.

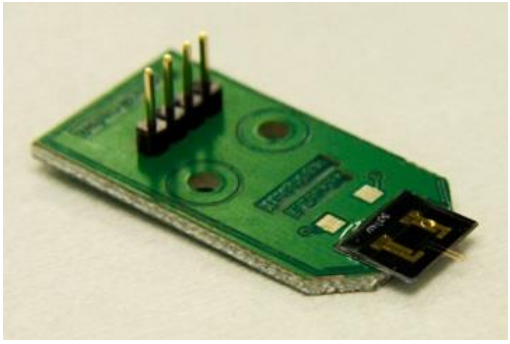

Figure 2.27 – PCB design for device integration.

The PCBs, however, were not waterproof, and so were not feasible for use with the electrochemical analysis, which was carried out in electrolyte solutions. The copper contacts on the PCB oxidised and broke the gold wire bond contacts, as well as contaminating the electrode tip.

To overcome this, an L shaped piece containing pogo pins in the upright to contact to the bond pads on the chip was designed. This was manufactured using rapid prototyping (RP) and is shown in Figure 2.28.

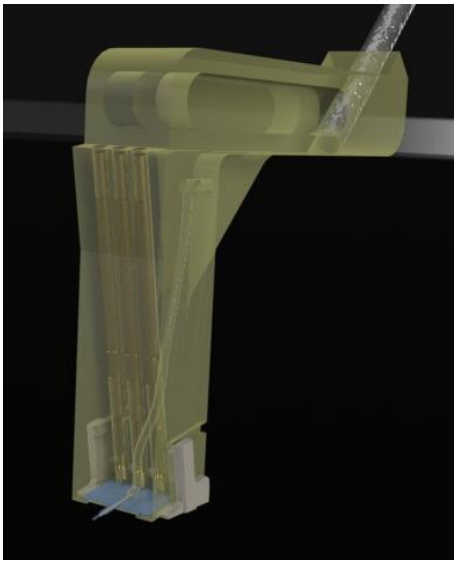

Figure 2.28 – Schematic representation of the RP holder design.

The RP holder was designed for use with the CellEctor that was used as the external handling system for the ISM deposition and cell handling work done in this project (Section 3.3.3 and 5.5 respectively); as well as with the flow cell that was used in the characterisation of the ion selective electrode behaviour (Section 4.1.1). The vertical section of the RP holder needed to be long enough to allow the device to be used in the flow cell, in that it was submerged up to a depth of 2 cm. To connect the RP holder to the CellEctor a steel bar was used (Figure 2.29). To ensure that the microgripper tip was in the beam of the microscope, a horizontal section was added; this needed to be 4.5 cm long. These dimensions resulted in the L-shape design of the RP holder.

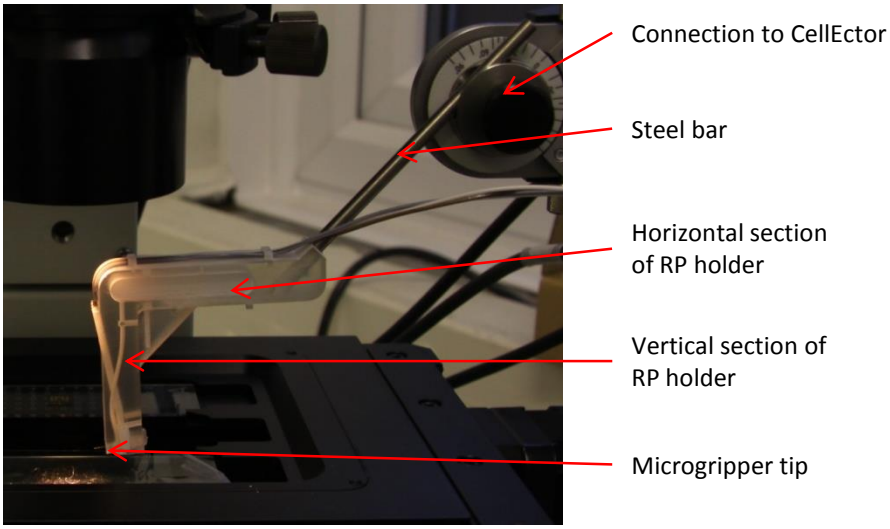

Figure 2.29 – Image of the microgripper in the RP holder within the CellEctor external handling system.

The microgripper chip was simply glued into a holder clip (Figure 2.30) which slotted onto the bottom of the RP holder, making contact through the pogo pins to the external circuit. A small quantity of silicon grease was applied to the microgripper chip so once the holder clip was slotted onto the RP holder the contact pads and pogo pins were insulated from the external solution.

The inside width of the holder clip was exactly the same width of the chip of the microgripper to ensure that the bond pads and the pogo pins lined up directly. This was important as there was only 250 μm between the bond pads and the gold track going around the electrode bond pad, even though a 1 mm gap existed between the bond pads (and hence the pogo pins). A slight misalignment would cause a short and the microgripper would not actuate effectively. The bottom of the holder clip is set at a 10° angle to ensure that while manipulating cells, the microgripper tips are in contact with the surface of the cell container.

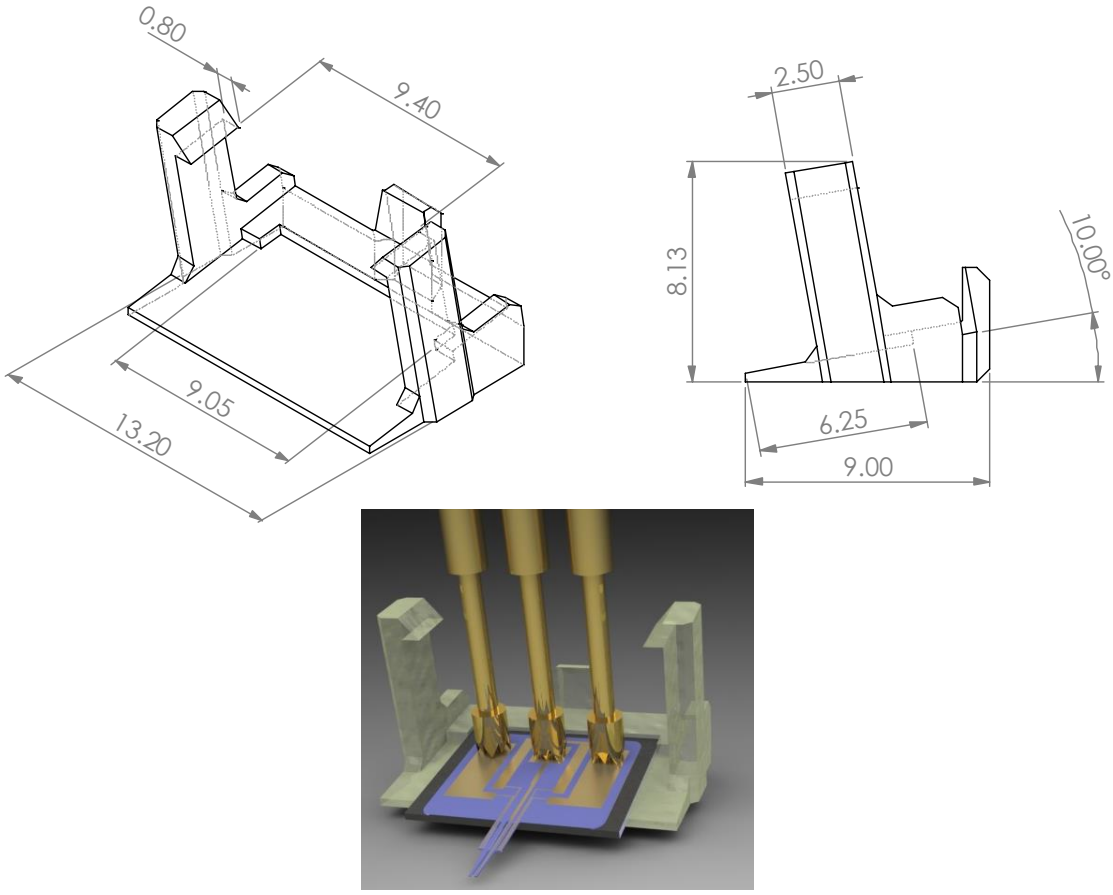

Figure 2.30 – Dimensions of the RP holder clip and a schematic representation of the released tip device in the RP holder clip.

2.8 Chapter Summary

The beginning of this chapter detailed the three main competitive actuation techniques commonly used for cell (or biological particle) sorting, positioning and transporting. Manipulation devices based on electrostatic actuation were shown to be limited spatially and generally required much higher voltages to achieve similar displacements compared to other techniques. Using vacuum holding pipettes and denudation capillaries to position and transport cells is a widely used technique, although a skilled user is required. The simplicity of their design meant that the unit costs are very low, making them very popular for use in a wide range of industries. Glass capillaries are, however, difficult to modify. This meant that to include additional elements for sensing applications, separate, alternative devices must be used. Manipulation via thermal actuation was initially disregarded by researchers due to the high temperatures required to achieve suitable deflections. However, investigation into their

design has significantly reduced working temperatures (actuator temperature not exceeding 80 °C, tip temperature never rising over ambient), allowing them to be considered as a competitive technique. Their low operating voltages and working temperatures, coupled with the fact that fabricated devices can readily be modified to increase functionality means that electrothermal actuation was used as the actuation technique in the microgripper device fabricated in this work.

The next section of this chapter focussed on the materials used in the fabrication process and how the manipulation of the building polymer used (SU8) enabled improvements to be made to the initial microgripper design. Silicon was used as the fabrication substrate as it could be selectively etched using xenon difluoride vapours to release the cantilever tips; this, coupled with the fact that its oxide could be readily patterned, meant it was a very desirable substrate material. Photodefinable polymer resists were used for both patterning and building. SU8 was the building resist of choice as its mechanical properties meant that the tweezer like action of the microgripper was realised. This, coupled with its high biocompatibility, an important parameter when the finished device was to be used for biological applications, meant this material was an excellent choice.

The final section dealt with the modification of the device so that the function of biological ion sensing could be realised. The microgripper device was miniaturised and the tip effectors were shown to be readily tailored to the cell (or biological particle) of interest. A gold electrode was introduced at the tip of the microgripper that could be modified into the ion sensing element. Additional work was also done in designing an external handling system for the microgripper that would allow both manipulation of cells and electrochemical analysis to be achieved. A rapid prototype L-shaped holder was the final design used in this project, with the microgripper chip placed into a specially designed clip that was easily attached to the holder.

2.9 References

[1] B. Solano, A microgripper for single cell manipulation, PhD Thesis: Durham University, 2008.

[2] E. W. H. Jager, O. Inganas and I. Lundstrom, "Microbots for micrometer-size objects in aqueous media: Potential tools for single-cell manipulation," *Science,* vol. 288, pp. 2335-2338, 2000.

[3] M. E. Chicurel, C. S. Chen and D. E. Ingber, "Cellular control lies in the balance of forces," *Current opinion in Cell Biology,* vol. 10, pp. 35-53, 2007.

[4] G. Bao, "Molecular biomechanics," in *Advances in Biomechanics*, Beijing, China, 2001.

[5] K. Yanagida, H. Katayose, H. Yazawa, Y. Kimura, K. Konnai and A. Sato, "The usefulness of a piezomanipulator in intracytoplasmic sperm injections in humans," *Human reproduction,* vol. 14, pp. 448-453, 1998.

[6] Y. Sun, K. T. Wan, K. P. Roberts, J. C. Bischof and B. J. Nelson, "Mechanical property characterization of mouse zona pellucida," *IEEE Transactions on Nanobioscience,* vol. 2, pp. 279-286, 2003.

[7] Y. Murayama, J. Mizumo, H. Kamaruka, Y. Fueta, H. Nakamura, K. Akaishi, K. Anazai, A. Watanabe, H. Inui and S. Omata, "Mouse zona pellucida dynamically changes its elasticity during oocyte maturation, fertilization and early embryo development," *Human Cell,* vol. 19, pp. 119-125, 2006.

[8] K. Nagayama, S. Yanagihara and T. Matsumoto, "A novel micro tensile tester with feed-back control for viscoelastic analysis of single isolated smooth muscle cells," *Medical Engineering and Physics,* vol. 29, pp. 620-628, 2007.

[9] S. Suresh, "Biomechanics and biophysics of cancer cells," *Acta Biomaterialia,* vol. 3, pp. 413-438, 2007.

[10] M. Lang and S. Block, "Resource Letter: LBOT-1 laser based optical tweezers," *American Journal of Physics,* vol. 71, pp. 201-215, 2003.

[11] M. L. Juan, M. Righini and R. Quidant, "Plasmon nano-optical tweezers," *Nature photonics,* vol. 5, no. 6, pp. 349-356, 2011.

[12] S. E. Skelton, M. Sergides, R. Saija, M. A. Lati, O. M. Marago and P. H. Jones, "Trapping volume control in optical tweezers using cylindrical vector beams," *Optics Letters,* vol. 38, no. 1, pp. 28-30, 2013.

[13] J. Desai, A. Pillarisetti and A. Brooks, "Engineering approaches to biomanipulation," *Annual Review in Biomedical Engineering,* vol. 9, pp. 35-53, 2007.

[14] L. Yao, A. Pandit, S. Yao and C. D. McCaid, "Electrical field-guided neuron migration: A novel approach in neurogenesis," *Tissue Engineering Part B - Reviews,* vol. 17, no. 3, pp. 143-153, 2011.

[15] B. Edwards and N. Engheta, “Electric tweezers: Negative dielectrophoretic multiple particle positioning,” *New Journal of Physics,* vol. 14, p. 063012, 2012.

[16] C. Kim, A. Pisano and R. Muller, “Silicon processed overhanging microgripper,” *Journal of Microelectromechanical Systems,* vol. 1, pp. 31-36, 1992.

[17] P. B. Chu and K. S. J. Pister, “Analysis of closed loop control of parallel plate electrostatic microgrippers,” in *IEEE International Conference on Robotics and Automation*, San Diego, Califonia, USA, 1994.

[18] B. E. Volland, H. Heerlein and I. W. Rangelow, “Electrostatically driven microgripper,” *Microelectronic Engineering,* vol. 61, pp. 1015-1023, 2002.

[19] K. Molhave, T. Wich, A. Kortschack and P. Boggild, “Pick and place nanomanipulation using microfabricated grippers,” *Nanotechnology,* vol. 17, pp. 2434-2441, 2006.

[20] O. Millet, P. Bernardoni, S. Regnier, P. Bidaud, E. Tsitsiris, D. Collard and L. Buchaillot, “Electrostatic actuated microgripper using an amplification mechanism,” *Sensors and Actuators A-Physical,* vol. 114, pp. 371-378, 2004.

[21] R. Salim, H. Wurmus, A. Harnish and D. Hulsenberg, “Microgrippers created in microstructurable glass,” *Microsystems Technology,* vol. 4, pp. 32-34, 1997.

[22] J. Park and W. Moon, “The systematic design and fabrication of a three chopstick microgripper,” *International Journal of Advanced Manuacturing Technology,* vol. 26, pp. 251-261, 2005.

[23] R. Perez, N. Chaillet, K. Domanski, P. Janus and P. Grabiec, “Fabrication, modeling and integration of a silicon technology force sensor in a piezoelectric micro-manipulator,” *Sensors and Actuators A-Physical,* vol. 128, pp. 367-375, 2006.

[24] C. S. Jeon, J. S. Park, S. Y. Lee and C. W. Moon, “Fabrication and characteristics of out of plane piezoelectric microgrippers using MEMS processes,” *Thin Solid Films,* vol. 515, pp. 4901-4904, 2007.

[25] W. L. Zhou and W. J. Li, “Micro ICPF actuators for aqueous sensing and manipulation,” *Sensors and Actuators A-Physical,* vol. 114, pp. 406-412, 2004.

[26] K. Yun and W. J. Kim, “System identification and microposition control of ionic polymer metal composite for three finger gripper manipulation,” *IEEE-ASME Transactions on Mechatronics,* vol. 9, pp. 334-342, 2004.

[27] D. H. Kim, M. G. Lee, B. Kim and Y. Sun, “A superelastic alloy microgripper with embedded electromagnetic actuators and piezoelectric force sensors: a numerical and experimental study,” *Smart Materials and Stuctures,* vol. 14, pp. 1265-1272, 2005.

[28] T. Petit, L. Zhang, K. E. Peyer, B. E. Kratochvil and B. J. Nelson, “Selective trapping and manipulation of microscale objects using mobile microvortices,” *Nano Letters,* vol. 12, no. 1, pp. 156-160, 2012.

[29] S. J. Phillips, K. Thorton, L. Barker, M. Mina, M. Aris, N. Bedore, S. Grant and R. H. Zeff, “Using magnostrictive metal as a pump for biomedical application,” *American Society for*

Artificial Internal Organs, vol. 37, no. 3, pp. M509-M510, 1991.

[30] S. Selimovic, W. L. Sim, S. B. Kirn, Y. H. Jang, W. G. Lee, M. Khabiry, H. Bae, S. Jambovane, J. W. Hong and A. Khademhosseini, "Generating non linear concentration gradient in microfluidic devices for cell studies," *Analytical Chemistry,* vol. 83, no. 6, pp. 2020-2028, 2011.

[31] H. W. Bang, C. N. Chung, J. K. Kim, S. H. Kim, S. Chung, J. Park, W. G. Lee, H. Jun, J. Lee, K. C. Cho, D. C. Han and J. K. Chang, "Microfabricated fluorescence activated cell sorter through hydrodynamic flow manipulation," *Microsystem Technologies Micro- and Nanosystems Information Storage and Processing Systems,* vol. 12, no. 8, pp. 746-753, 2006.

[32] S. H. Cho, C. H. Chen, F. S. Tsai, J. M. Godin and Y. H. Lo, "Human mammalian cell sorting using a highly integrated micro-fabricated fluorescence activated cell sorter," *Lab on Chip,* vol. 10, no. 12, pp. 1567-1573, 2010.

[33] S. Hesse and C. Schaffel, "Nano positioning over large travel ranges," *TM-Technisces Messen,* vol. 73, no. 9, pp. 493-499, 2006.

[34] M. Heyne, T. Erbe and R. Theska, "Concept of high precision ball guideways with three DOFs," in *Mechanika 15th International Conference*, 2010.

[35] V. A. Nikitin and E. E. Fesenko, "Biophysical aspects of recontruction of a single cell by the methods of cell engineering," *Biofizika,* vol. 51, pp. 673-678, 2006.

[36] M. Yu, Q. S. He, D. S. Yu, X. Q. Zhang, A. H. Ji, H. Zhang, C. Guo and Z. D. Dai, "Efficient active actuation to imitate locomotion of gecko's toes using an ionic polymer-metal composite actuator enhanced by carbon nanotubes," *Applied Physics Letters,* vol. 101, no. 16, p. 163701, 2012.

[37] M. Ali, T. Ueki, D. Tsurumi and T. Hirai, "Influence of plastizicer content on the transition of electromechanical behaviour of PVC gel actuator," *Langmuir,* vol. 27, no. 12, pp. 7902-7908, 2011.

[38] J. D. Whitehill, I. Gralinski, D. Joiner and A. Neild, "Nanoparticle manipulation within a microscale acousofluidic droplet," *Journal of Nanoparticle Research,* vol. 14, no. 11, p. 1223, 2012.

[39] M. Wiklund and B. Onfelt, "Ultrasonic manipulation of single cells," *Methods in Molecular Biology,* vol. 853, pp. 177-196, 2012.

[40] D. Martins, L. Riibeiro, D. Lopes, I. Catarino, I. A. A. C. Esteves, J. P. B. Mota and G. Bonfait, "Sorption characterization and actuation of a gas-gap heat switch," *Sensors and Actuators A-Physical,* vol. 171, no. 2, pp. 324-331, 2011.

[41] A. Ashkin, "History of optical trapping and manipulation of small neutral particles, atoms and molecules," *IEEE Journal of Selective Topics in Quantum Electronics,* vol. 6, pp. 841-856, 2000.

[42] K. C. Neuman and S. M. Block, "Optical Trapping," *Review of Scientific Instruments,* vol. 75,

pp. 2787-2809, 2004.

[43] W. C. Tang, T. C. H. Nguyen and R. T. Howe, “Laterally driven polysilicon resonant microstructures,” *Sensors and Actuators,* vol. 20, pp. 25-32, 1989.

[44] Y. J. Zhao and T. H. Cui, “Fabrication of high aspect ratio polymer based electrostatic comb drives using the hot embossing technique,” *Journal of Micromechanics and Microengineering,* vol. 13, pp. 430-435, 2003.

[45] A. Menciassi, A. Moglia, S. Gorini, G. Pernorio, C. Stefanini and P. Dario, “Shape memory alloy clamping devices of a capsule for monitoring tasks in the gastrointestinal tract,” *Journal of Micromechanics and Microengineering ,* vol. 15, pp. 2045-2055, 2005.

[46] M. Kohl, B. Krevet and E. Just, “SMA microgripper system,” *Sensors and Actuators A-Physical,* vol. 97, no. 8, pp. 646-652, 2002.

[47] Z. W. Zhong and C. K. Yeong, “Development of a gripper using SMA wire,” *Sensors and Actuators A-Physical,* vol. 126, pp. 375-381, 2006.

[48] J. S. Leng, X. Lan, Y. J. Liu and S. Y. Du, “Shape memory polymers and their composites: Stimulus methods and applications,” *Progress in Materials Science,* vol. 56, no. 7, pp. 1077-1135, 2011.

[49] C. S. Pan and W. Hsu, “An electro-thermally and laterally driven polysilicon microactuator,” *Journal of Micromechanics and Microengineering,* vol. 7, pp. 7-13, 1997.

[50] N. Nguyen, S. Ho and C. Low, “A polymeric microgripper with integrated thermal actuators,” *Journal of Micromechanics and Microengineering,* vol. 14, pp. 969-974, 2004.

[51] N. Chronis and L. Lee, “Electrothermally activated SU8 microgripper for single cell manipulation in solution,” *Journal of Microelectromechanical Systems,* vol. 14, pp. 857-863, 2005.

[52] J. K. Luo, R. Huang, J. H. He, Y. Q. Fu, A. J. Flewitt, S. M. Spearing, N. A. Fleck and W. I. Milne, “Modelling and fabrication of low operation temperature microcages with a polymer/metal/DLC trilayer structure,” *Sensors and Actuators A-Physical,* vol. 132, pp. 346-353, 2006.

[53] M. J. F. Zeman, E. V. Bordatchev and G. K. Knopf, “Design, kinematic modelling and performance testing of an electro-thermally driven microgripper for micromanipulation applications,” *Journal of Micromechanics and Microengineering,* vol. 16, pp. 1540-1549, 2006.

[54] Y.-S. Choi, Y. Zhang and D.-W. Lee, “A thermal-driven silicon micro xy-stage integrated with piezoresistive sensors for nano-positioning,” *Journal of Micromechanical and Microengineering,* vol. 22, p. 055002, 2012.

[55] B. Solano and D. Wood, “Design and testing of a polymeric microgripper for cell manipulation,” *Microelectronic Engineering,* vol. 84, pp. 1219-1222, 2007.

[56] X. Xu, S. Zhang, H. Chen and J. Kong, “Integration of electrochemistry in micro-total analysis systems for biochemical assays: Recent developments,” *Talanta,* vol. 80, no. 1,

pp. 8-18, 2009.

[57] M. J. Madou, Fundamentals of Microfabrication: The Science of Miniaturization, New York: CRC Press, 2001.

[58] R. Daunton, A. J. Gallant and D. Wood, “Manipulation of exposure dose parameters to improve production of high aspect ratio structures using SU-8,” *Journal of Micromechanics and Microengineering,* vol. 22, no. 7, p. 075016, 2012.

[59] J. A. Rogers, K. E. Paul, R. J. Jackman and G. M. Whitesides, “Using an elastomeric phase mask for sub-100 nm photolithography in the optical near field,” *Applied Physics Letters,* vol. 70, no. 20, pp. 2658-2660, 1997.

[60] K. E. Petersen, “Silicon as a mechanical material,” *Proceedings of IEEE,* vol. 70, pp. 420-457, 1982.

[61] J. F. Veyan, M. D. Halls, S. Rangan, D. Aureau, X. M. Yan and Y. J. Chabal, “XeF2-induced removal of SiO2 near Si surfaces at 300 K: An unexpected proximity effect,” *Journal of Applied Physics,* vol. 108, p. 114914, 2010.

[62] I. Klammer, M. C. Hofmann, A. Buchenauer, W. Mokwa and U. Schnakenberg, “Long term stability of PDMS based microfluidic systems used for biocatalytic reactions,” *Journal of Micromechanics and Microengineering,* vol. 16, pp. 2425-2425, 2006.

[63] “Thick Resist Processing,” MicroChemicals, 11 11 2009. [Online]. Available: www.microchemicals.eu/technical_information.

[64] O. P. Lehar, M. Spak, S. Meyer, R. R. Dammel, C. J. Brodsky and C. G. Willson, “Resist re-hydration during thick film processing,” in *Advances in Resist Technology and Processing XVIII*, Santa Clara, California, USA, 2001.

[65] A. del Campo and C. Greiner, “SU-8: A photoresist for high aspect ratio and 3D submicron lithography,” *Journal of Micromechanic and Microengineering,* vol. 17, pp. R81 - R95, 2007.

[66] R. Feng and R. J. Farris, “Influence of processing conditions on the thermal and mechanical properties of SU8 negative photoresist coatings,” *Journal of Micromechanics and Microengineering,* vol. 13, pp. 80-88, 2003.

[67] T. A. Anhoi, A. M. Jorgensen and D. A. Zauner, “The effect of soft bake temperature on the polymerization of SU-8 photoresist,” *Journal of Micromechanics and Microengineering,* vol. 16, pp. 1819-1824, 2006.

[68] J. Zhang, M. B. Chan-Park and S. R. Conner, “Effect of exposure dose on the replication fidelity and profile of very high aspect ratio microchannels in SU-8,” *Lab on Chip,* vol. 4, pp. 646-653, 2004.

[69] L. Matejka, K. Dusek, P. Chabanne and J. P. Pascault, “Cationic polymerization of diglycidyl ether of bisphenol A 3. Comparison of the theory with experiment,” *Journal of Polymer Science A Polymer Chemistry,* vol. 35, no. 4, pp. 665-672, 1997.

[70] W. Wang and S. A. Soper, Bio-MEMS:Technologies and Application, CRC Press, 2007.

[71] M. Gaudet, J.-C. Camart, L. Buchaillot and S. Arscott, “Variation of absorption coefficient and determination of critical dose of SU-8 at 365 nm,” *Applied Physics Letters,* vol. 88, pp. 024107-024107-3, 2006.

[72] C. M. Cheng and R. H. Chen, “Development behaviours and microstructure quality of downward development in deep x-ray lithography,” *Journal of Micromechanics and Microengineering,* vol. 80, p. 8, 2001.

3.0 ELECTROCHEMICAL SENSORS

This chapter concentrates on the electrochemical sensing element of the device. It covers the background of electrochemistry, including the mass transport effects of the analytical voltammetric and amperometric techniques used in the analysis of the bare gold electrode, and the ion selective electrode potentiometry; the background of ion selective electrodes (the ionic sensor used in this project), including all solid state ion selective electrodes and their components; and finally the characterisation of the bare gold electrode at the microgripper tip and the fabrication of the all solid state ion selective sensor onto the microgripper device.

3.1 Fundamentals of Electrochemistry

Electrochemistry is an area of chemistry that focusses on the relation between electrical and chemical effects. Generally, chemical changes are caused by the passage of current or change in potential and the corresponding potential or current, released from the chemical reactions, is measured. The process is used to investigate a wide range of phenomena (such as electrophoresis), technologies (such as electroplating metals), and in devices (for example batteries, fuel cells and sensors) [1]. Electrochemical devices are used in a large range of applications, such as environmental monitoring, industrial quality control, batteries, chemical sensors (both in their use and in their development) and biomedical analysis [2] [3]. The area of electrochemistry covered in this chapter concentrates on the application of the electrochemical methods, specifically amperometry and voltammetry, which are used in the characterisation of the bare gold electrode, and potentiometry that is used for extracellular ion sensing.

Recently there has been an interest in using electrochemical sensors to monitor medical conditions [4] [5]. This has involved the miniaturisation of many of these sensors, with

interesting developments about their technologies being realised. This project uses a miniaturised ion selective membrane based sensor to gather information about cell communication via potassium, sodium and calcium ions.

3.1.1 Voltammetry and Amperometry

In voltammetry (or amperometry) a potential (or current) is applied and a resulting current (or potential) is measured [6]. Voltammetric methods are concerned with electroactive species in solution which, when in contact with an electrode, undergo an oxidation or reduction reaction at that electrode's surface. This reaction produces a current, which is then measured. This method is used to study oxidative and reductive processes in various media; adsorption processes on surfaces; and electron transfer mechanisms at chemically modified electrode surfaces.

3.1.1.1 Mass Transport and Kinetics

There are two main processes that occur at an electrode. One process is faradaic, where electrons are transferred across the metal|solution interface causing an oxidation or reduction to occur. The other process is non-faradaic; this covers the processes where the structure of the metal|solution interface is changed, such as adsorption or desorption and capacitive charging. Generally it is the faradaic process that is of greatest interest, but the non-faradaic processes need to be considered as they can swamp the faradaic signals.

The rate of reaction of an electroactive species at an electrode is governed by: mass transfer; electron transfer at the electrode surface; chemical reactions before or after electron transfer (homogeneous ones such as protonation, or heterogeneous ones like catalytic decomposition); and surface reactions (absorption, desorption or crystallisation).

Mass transfer can be separated into the following effects:

- Diffusion. This is the effect seen when a species is under the influence of a chemical potential gradient. They follow a concentration gradient.
- Migration. This is the effect seen when charged species are under the influence of an electric field and so they follow an electrical potential gradient.
- Convection. This is the effect seen when the system is under the influence of stirring or hydrodynamic transport. Species can follow a density gradient (natural), stagnant regions and turbulent flow (forced).

One dimensional mass transfer (along the x-axis) to an electrode is governed by the Nernst-Planck equation; the three terms represent the contributions of diffusion, migration and convection respectively, to the flux.

$$J_i(x) = -D_i \frac{\partial C_i(x)}{\partial x} - \frac{z_i F}{RT} D_i C_i \frac{\partial \phi(x)}{\partial x} + C_i \nu(x)$$

Equation 3.1

where $J_i(x)$ is the flux of species i (mol cm^{-2} s^{-1});

D_i is the diffusion coefficient (cm^2 s^{-1});

$\delta C_i(x)/\delta x$ is the concentration gradient at distance x (M m^{-1});

$\delta \phi(x)/\delta x$ is the potential gradient (V m^{-1});

z_i and C_i are the charge and concentration (M) respectively of species i;

v(x) is the velocity with which a volume element in solution moves (cm s^{-1});

R is the gas constant (J mol^{-1} K^{-1});

T is the temperature (K);

F is Faraday's constant (C mol^{-1}).

Electrochemical techniques have been designed with the reduction of mass transfer effects in mind. For example migration effects are reduced by adding an inert electrolyte at a concentration much greater than the electroactive species; convection effects are reduced by preventing stirring and vibrations.

3.1.2 Voltammetric Methods

Voltammetric methods can be classified into two main categories: potential step and sweep methods.

In potential step methods, for example chronoamperometry, the applied voltage is instantaneously stepped from one value (V_1) to another (V_2) as shown in Figure 3.1.

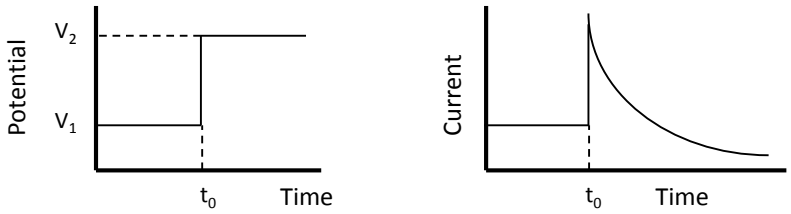

Figure 3.1 – The potential model and current response for potential step voltammetry.

The voltage range is usually such that at V_1 it is thermodynamically unfavourable to reduce the electroactive species and at V_2 the electroactive species that is in close proximity to the electrode is reduced. This yields the current response that is shown in Figure 3.1. The current rises instantaneously after the change in voltage due to the surface of the electrode being completely covered in reactant. This then drops as a function of time as the reactant is depleted.

In a diffusion controlled reaction, a plot of current, i, against 1/√t should yield a straight line, enabling the diffusion coefficient to be calculated using the Cottrell equation.

$$|i| = \frac{nFAC_{bulk}\sqrt{D}}{\sqrt{\pi}\sqrt{t}}$$

Equation 3.2

where n is the number of electrons in the half equation;

F is Faraday's constant (C mol^{-1});

A is the electrode surface area (cm^2);

C_{bulk} is the bulk reactant concentration (M);

D is the diffusion coefficient (cm^2 s^{-1});

t is the time (s).

In linear sweep voltammetry, for example cyclic voltammetry, the potential applied to the working electrode (WE) is varied linearly with respect to time. This is shown schematically in Figure 3.2.

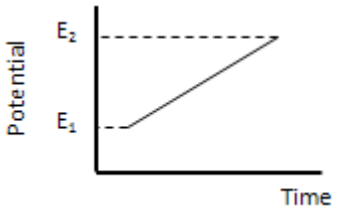

Figure 3.2 – The potential model for linear sweep voltammetry.

The voltage range is set such that the potential at which oxidation or reduction occurs lies between E_2 and E_1.

In a diffusion controlled reaction a plot of current, i, against √v should yield a straight line, according to the Randles-Sevcik equation.

$$i_p = 0.4463nFAC_{bulk}\left(\frac{nF\upsilon D}{RT}\right)^{1/2}$$

Equation 3.3

where i_p is the peak current (A);

n is the number of electrons in the half equation;

v is the scan rate (V s^{-1});

D is the diffusion coefficient (cm^2 s^{-1});

A is the surface area (cm^2);

C_{bulk} is the bulk concentration (M).

At room temperature, Equation 3.3 simplifies to:

$$i_p = 2.687x10^5\sqrt[3]{n}\sqrt{v}\sqrt{D}AC_{bulk}$$

Equation 3.4

In general, a voltammetric response depends on the reactivity of the solute through the potential of oxidation or reduction for an electroactive species, and the rate of mass transfer of the species from the solution to the electrode.

Voltammetric methods generally use a 3 electrode system as this helps to reduce both the unwanted polarisation effects on the reference electrode (RE) and to reduce iR drop. However, 2 and 4 electrode systems are also used.

3.1.2.1 Chronoamperometry

Chronoamperometry (an amperometric technique) is a potential step/pulse technique where the faradaic current, arising after capacitive current has dissipated, is measured; usually in a three electrode system. A potential is applied in a step from a value when analyte is not oxidised or reduced, to one where it is. The current is diffusion controlled and is plotted with respect to time.

The behaviour of the current with time is determined by:

$$i = \frac{E}{R_S} e^{-t/R_S C_d}$$

Equation 3.5

where i is the current (A);

E is the applied potential (V);

R_S is the solution resistance (Ω);

t is the time (s);

C_d is the double layer capacitance (F).

For each potential step there is an exponentially decaying current that has the time constant (τ /s) given by Equation 3.6, which determines the minimum step time required for the capacitive current to dissipate.

$$\tau = R_S C_d$$

Equation 3.6

Experimental parameters need to be carefully chosen as, if the step time is too short ($t < 3\tau$), the current measured is dominated by the capacitive, charging current. If the step time is too long, over 100 s, then convection develops (due to the density gradients), which results in positive deviations from the signal.

This technique is mass transport limiting: the current-time curve denotes the change in concentration gradient at the electrode surface during the gradual expansion of the diffusion layer (i.e. diminution of analyte), so the response plot's shape is defined by the Cottrell equation. This means that this technique requires a static system to ensure it is mass transport limiting.

3.1.2.2 Cyclic Voltammetry

Cyclic voltammetry (a voltammetric technique) provides a wealth of information on both the redox process (thermodynamic consideration) and electron transfer reaction (kinetics effects) for many chemical systems [7].

Cyclic voltammetry has the added advantage of being able to provide specific information about individual electroactive species in chemical systems containing more than one electroactive species.

Cyclic voltammetry is accomplished by performing a linear scan of the potential of the WE using the triangular waveform shown in Figure 3.3.

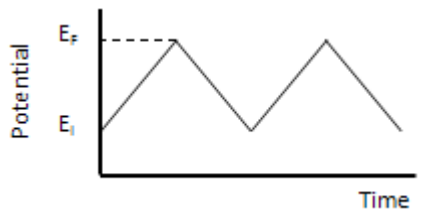

Figure 3.3 – Potential model for cyclic voltammetry.

The potential is ramped from E_I to E_F then back to E_I, with the oxidation or reduction potential lying between E_I and E_F (the potential window). The potentiostat measures the current resulting from the applied voltage. The current magnitude is due to the oxidation or reduction of the electroactive species (faradaic current) or the double layer charging (capacitive current).

3.1.2.3 Micro vs Macro Electrode

A macro electrode has a linear diffusion layer, which is shown schematically in Figure 3.4(a). This yields a Nernstian relationship in a potential difference against current plot as shown in Figure 3.4(b).

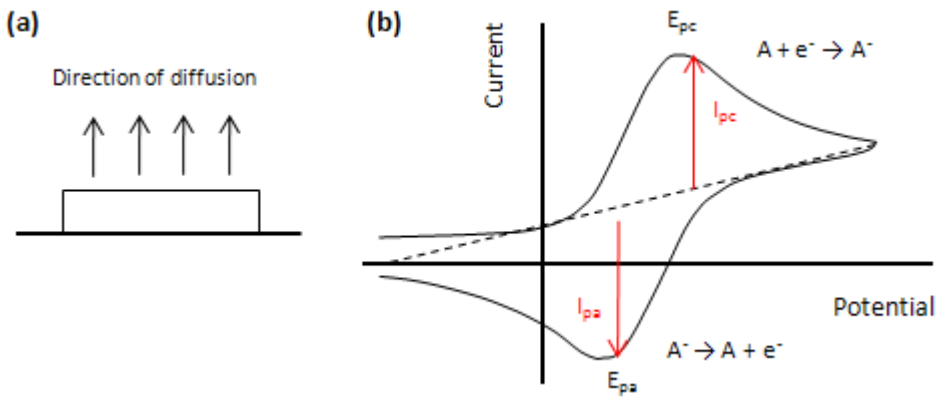

Figure 3.4 – (a) Schematic representation of a linear diffusion layer, (b) graph of typical Nernstian behaviour.

The characteristic features in a Nernstian relationship are that the current peak heights for the cathodic and anodic peak are equal in magnitude ($I_{pa} = I_{pc}$); and that the position of the peak potentials for oxidation (E_{pa}) and reduction (E_{pc}) are independent of scan rate. The current peak height must also be proportional to the square root of the scan rate according to the Randles-Sevcik equation (Equation 3.4). This occurs because the size of the diffusion layer depends on the scan rate. A slow scan rate therefore yields a larger diffusion layer; therefore, this means that the flux to the electrode surface is smaller. As the current is proportional to the flux, the magnitude of the current will be lower. Additionally the

separation between the two peak potentials should be equal to 59 mV/n, where n is the electron couple.

A micro electrode (which is defined as one whose surface is smaller than the scale of diffusion layer and/or there is one dimension in the micron scale [8]) has a radial diffusion layer; this leads to a Sigmoidal relationship in a potential difference against current plot, as shown in Figure 3.5.

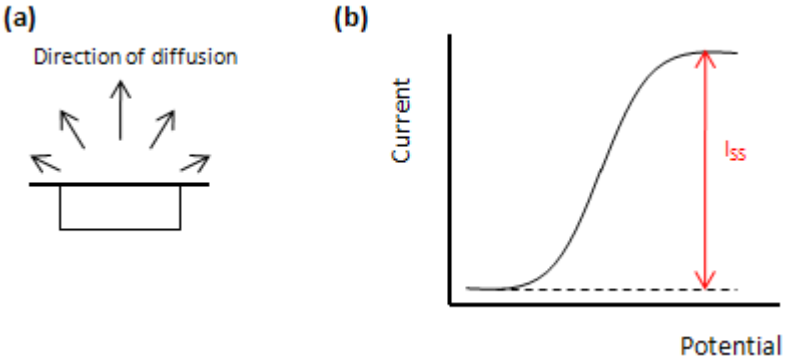

Figure 3.5 – (a) Schematic representation of a radial diffusion layer, (b) graph of typical Sigmoidal behaviour.

The characteristic features in a Sigmoidal relationship are that the mass transport is dominated by radial diffusion, so the current is independent of scan rate. The current is however dependent on the following relationship:

$$i_{ss} = 4nzFDC_{bulk}r$$

Equation 3.7

where i_{ss} is the steady state current (A);

n is the number of microelectrodes;

F is Faraday's constant (C mol^{-1});

D is the diffusion coefficient (cm^2 s^{-1});

C_{bulk} is the bulk concentration (M);

z is the ion valency;

r is the electrode radius (cm).

In a micro electrode there is a reduction in the capacitive current (as the capacitive current is proportional to the electrode area); therefore the current measured is mostly faradaic. This minimises the magnitude of the current measured, with an associated reduction in ohmic drop; however, micro electrodes are more sensitive to noise, so the signal-to-noise ratio is lower. To overcome this, microelectrodes are often used in arrays to increase the current magnitude.

3.1.3 Potentiometry

In potentiometry there is no applied potential and it is assumed that no current flows through the system. The voltage is passively measured between two electrodes and occurs due to the difference in Gibbs free energy of the electrons in equilibrium between two half cells. This technique is most commonly used to measure the transfer of ions across a selective membrane and is attractive in research due to the possibility of miniaturisation.

For potentiometric measurements a two electrode system is used. The potential of a solution is recorded, using a potentiometer, between an ion selective electrode (ISE) and a RE. The RE is required for the same reasons as in a voltammetric system (described in Section 3.1.1.1). The ISE is sensitive to changes in activity of a specific cation or anion, depending on the ionophore (sensing element) used.

Additionally to minimising the solution resistance, supporting electrolytes used in a potentiometric system helps to maintain a constant ionic strength. This is important as ISEs are used to relate changes in solution potential to changes in ion activity of ions within that solution.

The activity of an ion (a) is related to its concentration (C / M) via an activity coefficient (γ / M^{-1}) (Equation 3.8), which in turn is related to the ionic strength (I / M) of the solution (Equation 3.9).

$$a = \gamma C$$

Equation 3.8

The activity coefficient can be defined by the extended Debye-Huckel equation, shown in Equation 3.9.

$$log\gamma_{\pm} = \frac{-A|z_+ z_-|\sqrt{I}}{1 + B\sqrt{I}} + CI$$

Equation 3.9

where $|z_+z_-|$ is the absolute product of ion valencies;

A is a constant (0.5108 at 298 K);

B and C are empirical parameters for a given ionic species.

The ionic strength of a solution is related to the sum of the product of concentration (C_i / M) and charge (z_i) of all the ions present in that solution (Equation 3.10). If a large portion of the ionic strength of a solution comes from the supporting electrolyte (i.e. there is a low concentration of the analyte of interest), the activity coefficient of the solution in question comes from the supporting electrolyte, and is said to be constant; therefore Equation 3.8 can be reduced to the concentration of the analyte being directly equal to its activity.

$$I = \frac{1}{2}\sum C_i z_i^2$$

Equation 3.10

3.1.3.1 Thermodynamics: The Nernst Equation

The Nernst equation demonstrates how the potential difference depends upon the concentration or activity of the analytes concerned. For a cell reaction $wH_2 + xO \rightarrow yR + zH^+$ where w, x, y and z are the stoichiometric coefficients, and O and R are the oxidised and reduced species; the free energy (ΔG / kJ mol^{-1}) can be determined from basic thermodynamics to be [1]:

$$\Delta G = \Delta G^0 + RT ln \frac{a_R^y a_{H^+}^z}{a_O^x a_{H_2}^w}$$

Equation 3.11

where ΔG^0 is the standard Gibbs free energy (kJ mol^{-1});

R is the gas constant (J K^{-1} mol^{-1}) ;

T is the temperature (K);

a_i is the activity of species i.

Given that $\Delta G = -nFE$ (and therefore $\Delta G^0 = -nFE^0$), Equation 3.11 becomes:

$$E = E^0 - \frac{RT}{nF} ln \frac{a_R^y a_{H^+}^z}{a_O^x a_{H_2}^w}$$

Equation 3.12

where E is the potential (V);

E^0 is the standard electrode potential (V);

n is the number of electrons in the cell reaction;

F is Faraday's constant (C mol^{-1}).

Given that $a_{H^+} = a_{H_2} = 1$, Equation 3.12 reduces to the Nernst equation:

$$E = E^0 - \frac{RT}{nF} ln \left(\frac{a_R^y}{a_O^x} \right) = E^0 - \frac{RT}{nF} ln \left(\frac{[R]^y}{[O]^x} \right)$$

Equation 3.13

where [R] and [O] are the concentrations (M) of the reduced and oxidised species respectively.

This holds true as long as the solution contains only inert electrolytes. This means that the activity coefficients (γ) will be constant. Using the relationship, a = cγ, where c is the concentration of the analyte, the activity terms in the Nernst equation can be exchanged with concentration terms (Equation 3.13), illustrating the direct relationship between the observed potential and the concentration of the analytes.

3.2 Electrochemical Sensors

The IUPAC definition of a chemical sensor is when there is a device that transforms chemical information (such as the concentration of specific sample component or even total composition analysis) into a useful analytical signal [9].

Chemical sensors are divided into different classes depending on their transducing process: these include optical, electrochemical, electrical, mass sensitive, magnetic, and thermometric, to name a few. Electrochemical sensors are a well established group and these involve measuring potential or current via potentiometric (for example ISE) and amperometric techniques. This project deals only with potentiometric sensors so amperometric ones will not be considered here.

3.2.1 Ion Selective Electrodes

The area of ion selective electrodes (ISEs) has grown rapidly in a few decades due to the benefits of relative low cost, portability and fast readout signal that are associated with this technology. More than 60 different ions have been detected using the principle of ISEs [10].

ISEs are used to measure the concentration of specific ions in aqueous solutions. They work by selectively passing a single charged species from one phase to another to yield a potential difference that can be specifically related to the activity of that species via the Nernst equation. They are used in a large range of applications such as the monitoring of heavy metals in the environment and examining corrosion effects, as well as determining ion activities in biological systems.

The potential difference of the cell is usually measured via potentiometry, using two electrodes, the ISE and an external reference. Figure 3.6 shows the general cell arrangement.

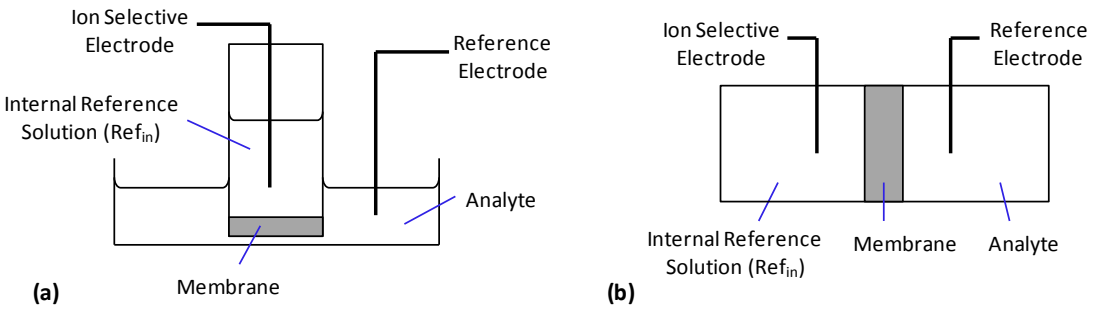

Figure 3.6 – (a) General arrangement of an ISE sensor, and (b) schematic representation of an ISE sensor.

A potential difference (historically known as electromotive force, EMF) is generated between the sample solution and internal filling solution as primary ions are transferred from the sample solution to the membrane phase. Under equilibrium conditions (zero current) the transfer of primary ions from the solution to the membrane is equal to the transfer of ions from the membrane to the solution.

3.2.1.1 Classical Phase Boundary Potential Model

The response functions, including non-Nernstian behaviour, and selectivity of an ISE can be fully described by the phase boundary potentials [11].

The general setup of the electrochemical cell of an ISE is:

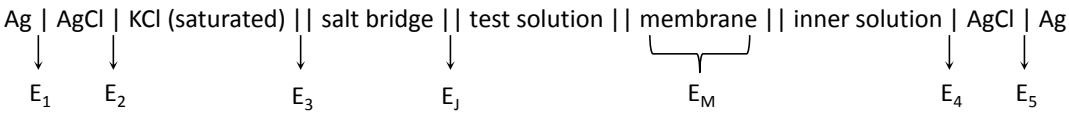

The potential of the whole cell is the sum of the different potentials at all interfaces.

$$EMF = E_1 + E_2 + E_3 + E_J + E_M + E_4 + E_5$$

Equation 3.14

As it is not possible to measure the individual absolute potentials for every system it is assumed that, under ideal conditions, E_1 to E_5 are constant. Therefore the total potential of the cell is given by [10]:

$$E = E^o_{Const} + E_J + E_M$$

Equation 3.15

Meyer and Sievers [12] approximated that the membrane potential (E_M) was the sum of the two phase boundary potentials (E_{PB}) of the sample|membrane interfaces, and the diffusion potential within the membrane (E_D). This concept is most relevant to thick (greater than biological membranes, around 10 nm), ion exchanging membranes, such as those generally seen in ISE constructions. The liquid junction potential (E_J) is that at the sample|bridge electrolyte interface and originated from the separation of charge created on the interface due to the differing ion mobilities.

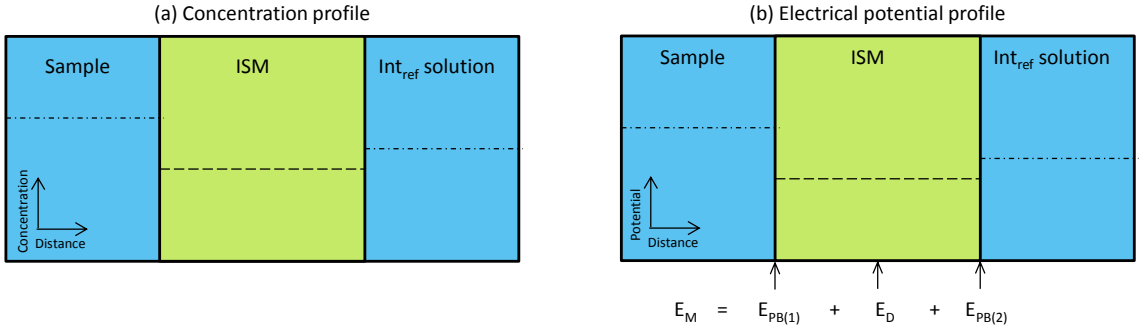

Figure 3.7 – Classical total equilibrium model showing the (a) concentration profile and (b) electrical potential profile.

In the classical model (Figure 3.7), where the system is in total equilibrium, migration of species is ignored. This means that it can be assumed that the phase boundary potential at the solution|membrane interface governs the membrane response and hence the diffusion potential, again related to the migration of the species involved, is negligible, i.e. E_J is negligible, and can be ignored; and that the membrane|solution interface is in chemical equilibrium (hence there is no ionic concentration gradient), i.e. E_D is zero. Therefore, the phase boundary potential (E_{PB}), which describes the response of an ion selective membrane based electrode of diverse composition exposed to any type of sample, is given by:

$$E_{PB} = \frac{RT}{z_i F} lnk_i + \frac{RT}{z_i F} \ln \frac{a_{sol}}{a_M}$$

Equation 3.16

where R is the gas constant (J K^{-1} mol^{-1});

T is the temperature (K);

z_i is the valency of ion i;

F is Faraday's constant (C mol^{-1});

a_{sol} and a_M are the activities of the uncomplexed ions in the solution and membrane phase respectively;

k_i is a function of the relative free energies of solvation (Equation 3.17).

$$k_i = \exp\left[\frac{\mu_i^0(sol) - \mu_i^0(mem)}{RT}\right]$$

Equation 3.17

where $\mu_i^0(sol)$ is the free energy of solvation of ion i into the solution phase (kJ mol^{-1});

$\mu_i^0(mem)$ is the free energy of solvation of ion i into the membrane phase (kJ mol^{-1}).

With all the assumptions holding true, and assuming fast local equilibria across the phase boundary, the electrode potential is only dependent on the E_{PB} part of the membrane potential [10].

The first part of Equation 3.16 is known as the standard potential, and is constant for a given ion (though varies from ion to ion), therefore the total potential of the cell can be described by:

$$E = const + \frac{RT}{z_i F} lna_i$$

Equation 3.18

With the similarities between Equation 3.18 and the Nernst equation, ISEs with a behaviour that is described by Equation 3.18 are said to have a Nernstian response. This is usually verified by calculating whether or not there is a variation of $59/z_i$ mV per decade in activity at 298 K; for example, for a monovalent ion such as sodium, a variation of 59 mV per decade would be observed.

The main failing with this model is that it interprets the sensor response, such as sensitivity and detection limits, as being time independent. This is contrary to that seen

experimentally in the field of potentiometric sensors [13] [14]. This has led to the development of the more advanced local equilibrium model.

3.2.1.2 Advanced Phase Boundary Potential Model

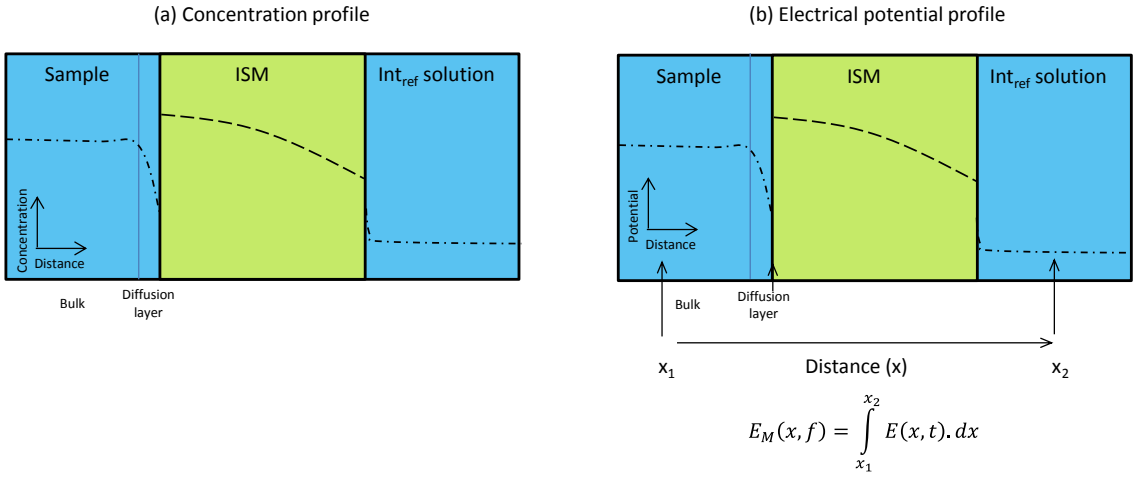

Figure 3.8 – Advanced local equilibrium model showing the (a) concentration profile and (b) electrical potential profile.

This model is also known as diffusion layer model [15] and was first introduced by Lewenstam. It assumes that there is a local equilibrium at all the interfaces of the sensor and that the concentration of the ions in all phases is dependent on their distance from the interface. The system is assumed to be at steady state so the equilibration rate is dependent on the diffusion of ions to and from the interfaces. The time dependent response that characterises the distance of the system under local equilibrium from total equilibrium is modelled using the surface coverage (or site filling) factor (s(t)), defined in Equation 3.19.

$$s(t) = \frac{\overline{c_{j0}}(t)}{\overline{c_{i0}}(t) + \overline{c_{j0}}(t)} = \frac{K_{ij} c_{j0}(t)}{c_{i0}(t) + K_{ij} c_{j0}(t)}$$

Equation 3.19

where $\overline{c_{i0}}(t)$ and $\overline{c_{j0}}(t)$ are the concentrations of the solution ions within the membrane at time t (M);

$c_{i0}(t)$ and $c_{j0}(t)$ are the concentrations of the solution ions at the membrane surface at time t (M);

K_{ij} is the selectivity coefficient.

Assuming a constant diffusion layer thickness and using mass conservation to couple the ion fluxes (J_iJ_j) to and from the interface:

$$E_M(t) = const + \frac{RT}{F} ln \frac{[1 - s(t)]K_{ij} + s(t)\frac{\overline{u_j}}{\overline{u_i}}K_{ij}}{K_{ij}[1 - s(t)] + \frac{D_j}{D_i}s(t)} \frac{\left(c_i + \frac{D_j}{D_i}c_j\right)}{\overline{c_{ib}}}$$

Equation 3.20

where D_i and D_j are the diffusion coefficients of the primary and interfering ions respectively ($m^2\ s^{-1}$);

$\overline{u_\iota}$ and $\overline{u_J}$ are the ionic mobilities of the primary and interfering ions respectively ($m^2\ V^{-1}\ s^{-1}$);

$\overline{c_{\iota b}}$ is the bulk concentration of the primary ion (M).

While the changes in this model only have a small impact on E_M, so the model is generally not used when trying to determine how changes in ion activity affect the sensor potential, it has been successfully used to demonstrate that the poor selectivities and detection limits have a common origin in the increased surface concentration of the primary ion (in relation to the bulk concentration) [16]. This concept can be manipulated to produce ISEs with much lower detection limits, while still maintaining true selectivity coefficients [17].

3.2.1.3 Glass Membrane Ion Selective Electrodes

Glass ISEs have been around since the early 20th century [18]. They are most commonly used for measurements of pH, as well as to determine the activities of alkali ions [19] [20]. The bulk of the membrane is about 50 µm thick dry glass; charge transfer occurs exclusively by mobile cations (usually Na^+ and Li^+ ions) in the glass. The faces of the glass membrane contain a hydrated silicate layer (Figure 3.9) that causes the interfaces to swell; this kinetically helps the interactions between the glass and the adjacent solution. This hydrated

silicate network has an affinity for certain cations (generally Na^+, Li^+, K^+, Ag^+ and NH_4^+) that are adsorbed within the structure, creating a charge separation that alters the potential at the interface.

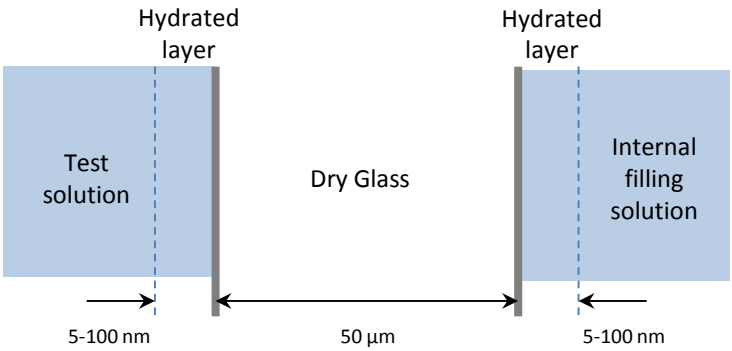

Figure 3.9 – Schematic representation of a glass electrode profile.

Glass membranes differ from others in that in some cases they are not permeable to the ion of interest, with the non-permeability of H^+ ions in the pH probes being the best example.

3.2.1.4 Crystalline Membrane Ion Selective Electrodes

Crystalline ISE membranes are classed as solid ISEs that contain fixed active sites. They function due to the fact that one of the ions in the crystal structure is more conductive with respect to the others. They can be either homogeneous or heterogeneous. A well-known crystalline sensor is the fluoride sensor that comprises of lanthanum fluoride pellets doped with a small quantity (0.5 wt%) of europium (III) fluoride. The lanthanum fluoride crystal has very low conductivity due to its ordered structure, but the inclusion of EuF_3 increases the conductivity as the crystal is sufficiently disordered [21]. Other crystalline membranes are commonly used for environmental monitoring of heavy metal ions, for example, copper, cadmium and silver.

3.2.1.5 Polymeric Membrane Ion Selective Electrodes

In polymeric membrane ISEs, chelating agents (either charged or uncharged) are immobilised into a hydrophobic membrane, known as an ion selective membrane (ISM). These chelating agents have a high selectivity towards the ion of interest and so provide the mechanism by which charge is transferred from a test solution and the inner filling solution. However, they also require a complex mixture of ion exchange equilibria compounds (such as ionic sites) to stabilise the ISE. Once optimised, electrodes based on this design generally offer superior performance over the other two membrane types [1]. Given the stability of polymeric membranes and the relative ease to miniaturise them, they are the best membrane type for the microgripper sensor device.

3.2.2 Liquid and All Solid State Polymeric Ion Selective Electrodes

James Ross and Martin Frant of Orion Research were the first to develop calcium and fluoride ISEs in the mid 1960s; they are known as the founding fathers of ISEs as this sparked a huge boom in potentiometric analysis [22].

In the late 1960s, research into the structure-selectivity relationship of many synthetic ionophores, plasticisers and additives by Wilhelm Simon, who worked at ETH in Zurich, allowed the development into many novel ISEs, allowing ionophore based liquid membrane sensors to quickly become the most successful class of ISE [22] [23].

Adam Shatkay [24] was the first to use polymers as a homogenous membrane matrix in 1967. They were made up of neutral carriers prepared in silicon rubber or poly(vinylchloride) (PVC) [25] without lipophilic ionic sites. It was realised, however, that a Nernstian response was only realised with the presences of ionic impurities [26] [27] [28] and other membrane components [29].

The procedure for compounding, casting, drying and mounting PVC sensor membranes, to produce solvent polymeric membrane electrodes, was first developed by John

D. R. Thomas and Gwylm Moody in the early 1970s [30]. Thomas and co-workers were instrumental in the further practical developments of ISE technologies.

In 1953 the theory of membrane potentials for thick, practical membranes was developed by George Scatchard, which was applied to the theory of corresponding ISEs by Richard Buck in 1968 [22]. In the subsequent years to the early 1990s Buck [31], alongside Adam Hulanicki, Andzej Lewenstam [32] and Thomas Sokalski [33], went on to develop many theories to explain membrane behaviour and responses in ISEs, including detection limits and selectivity coefficients.

3.2.2.1 Liquid Ion Selective Electrodes

A conventional liquid ISE is shown in Figure 3.10. An ion selective membrane is fixed at one end of a glass tube; the membrane is a plastic/rubber film that is impregnated by a complex organic molecule (ionophore). The glass tube is then filled with an internal reference solution. The membrane acts as a barrier between the external and internal solutions, only allowing specific ions to pass through it. When the ISE is immersed in an external solution the specific ions diffuse through the membrane until an electrical equilibrium between the two solutions is reached. This causes a build-up of a charge at the membrane|internal reference solution interface, which is proportional to the number of ions in the external solution. At equilibrium conditions there is little current (assumed zero), so the potential difference needs to be measured relative to a RE.

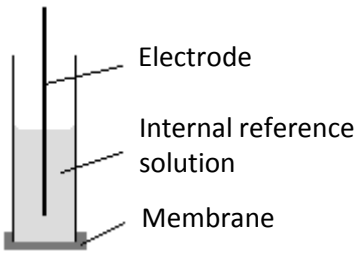

Figure 3.10 – Schematic of a conventional ISE.

In general, ISEs at equilibrium balance the increase or decrease of charge at the membrane|solution interface (which depends on the selectivity of the membrane) with an equal and opposite charge at the reference solution|membrane interface, causing a positive or negative deviation from the original stable reference voltage, which is registered on a potentiometer.

Liquid ISEs have many advantages, including the ability to measure ions in relatively dilute solutions and the ability to measure both positive and negative ions. They also have many advantages over other methods of ion analysis (such as ion amperometry). These include the speed of sample analysis, portability, large measuring range and the ability to analyse samples without destroying them.

They do, however, have one major drawback, in that the membrane is perishable. Over time the membrane components dissolute into the analyte; this changes the composition and surface structure of the membrane and therefore the potential response. This has a detrimental effect on the reproducibility of results and the portability of the device due to the constant 'in lab' (re-) calibration that is necessary. The lifetime for a conventional liquid-membrane ISE is approximately one year.

There is still much development work devoted to liquid ISEs, mainly concentrating on significantly reducing the detection limits, for example, to picomolar levels [33] by controlling the activity of the inner filling solution. However, due to the difficulty in their miniaturisation because of a leakage of the inner filling solution, another group of ISEs was formed; there were known as all solid state ion selective electrodes (ASSISEs).

3.2.2.2 All Solid State Ion Selective Electrodes

In the 1970s Cattrall and Freiser developed coated wire electrodes (CWE). While these had linear responses and selectivities comparable with liquid ISEs [34], they had poor stability

due to a blocking of the interface between the pure electron conductor (metal) and pure ionic conductor (membrane) [35].

Liquid ISEs have a symmetrical ionic charge transfer arrangement due to the membrane being in contact with two solutions. However, in ASSISE, the charge transfer from the membrane to the electrical conductor (EC) is electronic, giving an asymmetrical charge transfer arrangement. This is shown schematically in Figure 3.11. For ISEs to function effectively, a well-defined pathway across the membrane is required, which is in the form of a carefully designed solid contact mediator between the ISM and EC [36].

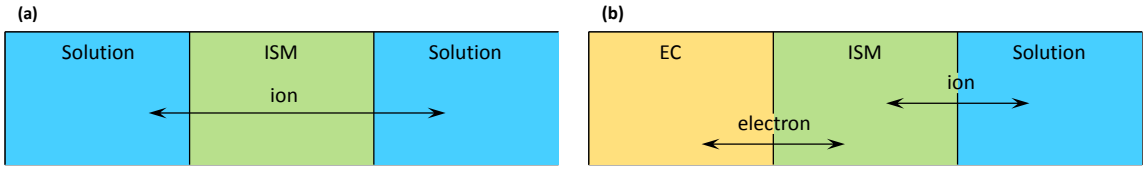

Figure 3.11 – Schematic representation of the (a) symmetrical (liquid ISE) and (b) asymmetrical (ASSISE) charge transfer.

Many different mediators have been used. These include: hydrogels [37], self assembled monolayers [38], and conducting polymers [39].

Hydrogel contacts had limitations due to water uptake of the gel causing volume changes within the mediator layer [40]. Self assembled monolayers were limited due to their inherently low redox capacitance (that needs to be high to minimise the polarisability of the solid contact [41]). The redox capacitance (C_{redox} / F) is inversely proportional to the potential drift ($\Delta E/\Delta t$ / V s^{-1}) as shown below (where i is the current / A):

$$\frac{\Delta E}{\Delta t} = \frac{i}{C_{redox}}$$

Equation 3.21

Conducting polymers were promising as a mediator due to the electronic and ionic conductivity of the material [10], which enabled them to act as an ion to electron transducer. Conducting polymers were first reported for use as a chemical sensor by Dong *et al.* in 1988

[42]. At first conducting polymers were used instead of an ISM [43] but these devices were found to be unsuitable due to the interference caused by redox reactants in solutions [44] and pH changes [45], as well as having poor ionic selectivity [46].

Since then, several other variations of conducting polymer (CP) and ISM have been tried, these are shown schematically in Figure 3.12.

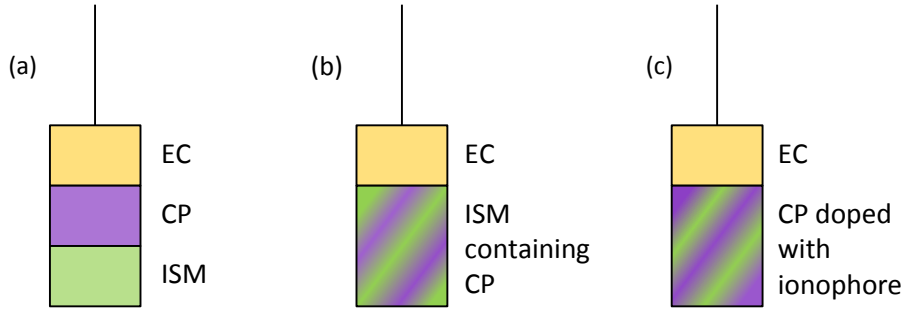

Figure 3.12 – Schematic representation of ASSISEs designs: (a) CP as transducer; (b) CP incorporated into ISM; and (c) CP doped with ionophore.

When the conducting polymer is placed between the electrical conductor (EC) and the ISM, as in Figure 3.12(a), the conducting polymer acts as a transducer and the selectivity is determined by the ISM. Ion transfer occurs reversibly at the ISM|solution and CP|ISM interfaces. The ionic signal is converted to electronic by the conducting polymer, and electron transfer occurs at the EC|CP interface.

Ion to electron transduction has a similar mechanism to that of the process at the internal reference electrode of liquid ISEs. Under equilibrium conditions, the charge transfer of primary ions from the solution to the membrane is at electrochemical equilibrium with the charge transfer of electrons from the membrane to the conducting polymer. In this system, ion transfer occurs reversibly at the ISM|solution (S) and CP|ISM interfaces. The ionic signal is transduced into an electrical signal in the CP layer and electron transfer occurs at the EC|CP interface. This is shown schematically in Figure 3.13. Many conducting polymers have been used: including poly(pyrrole) (PPy) [47]; poly(3-octylthiophene) (POT) [48] and poly(3,4-ethylenedioxythiophene) (PEDOT) [49].

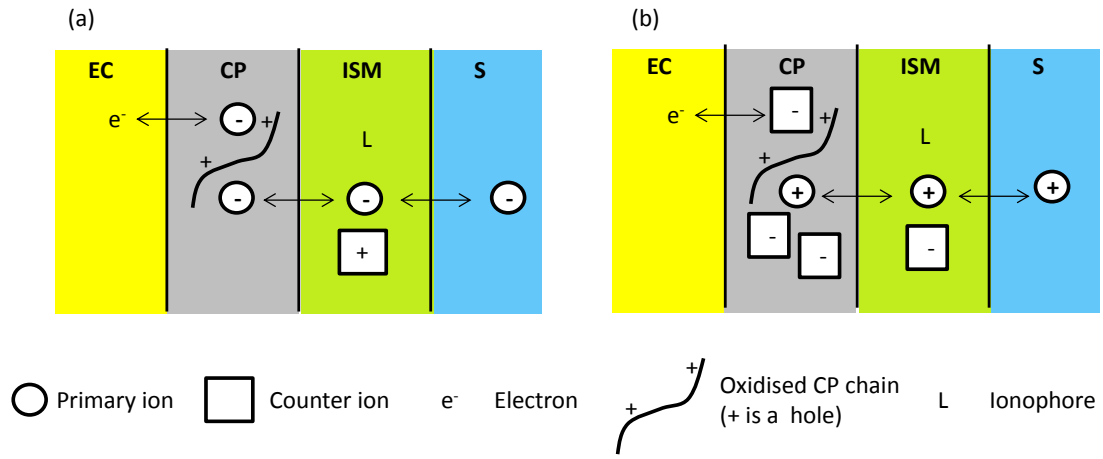

Figure 3.13 – Principle of ASSISEs based on CPs of (a) an anion and (b) a cation selective electrode.

The conducting polymer can also be either incorporated into the membrane or doped with an ionophore (Figure 3.12(b) and (c) respectively), these are known as single piece ion selective electrode (SPISE). The former relies on the conducting polymer to be soluble in tetrahydrofuran (THF), or another solvent, used to dissolve the membrane components. In this case the fabrication is simplified as it is better for mass production in industry, such as by solution casting, dip coating or spin coating. While near-Nernstian responses can be achieved, it was observed that the conducting polymer can affect the selectivity of the ISE [50] [51]. The latter can be achieved via doping the conducting polymer with metal complexing ligands [52] or via covalent binding of ion recognition sites [53] [54]. The main challenge in this orientation is in enhancing the selectivity, while suppressing the redox response of the conducting polymer. This orientation is still a long way from being used as a successful chemical sensor.

All-plastic ISEs were developed by Michalska and Maksymiuk [55]; here they solution cast poly(3,4-ethylenedioxythiophene)/poly(styrene sulfonate) (PEDOT/PSS) onto insulating plastic substrates. PEDOT/PSS acted as an electronic contact as well as an ion to electron transducer. However, there were problems with delamination of the PEDOT/PSS layer, which led to a loss of electrical contact.

Solid state ISEs still have several problems, with the main concerns being the lack of stability of the potential response over a wide pH range, low tolerance of other ions (poor detection limits), and the inability to maintain long term reproducibility (membrane ageing) [56].

Given the wide range of literature development into ASSISE with an arrangement similar to that of Figure 3.12(a), where the conducting polymer acts as the transducer, this is the arrangement that was used to fabricate the microgripper sensor device.

3.2.3 Arrangements of All Solid State Ion Selective Electrodes

ASSISEs, where the conducting polymer acts as a transducer, are usually fabricated via two steps: deposition of the conducting polymer transducer onto an electrical conductor, followed by deposition of the ISM onto the conducting polymer transducer.

3.2.4 Components

The components that make up the ISE must be carefully considered with the application and the environment in mind. For example, given that (i) the ISM is permeable to oxygen and carbon dioxide dissolved in the solution [57]; (ii) conducting polymers can be influenced by the O_2/H_2O redox couple [58] and (iii) CO_2 interferes with the ISE behaviour by changing the pH [59] [60], a conducting polymer that has a low sensitivity to both O_2 and CO_2 is required.

The application for the microgripper sensor device in this project is to detect the presence of ions that are used in cell signalling; of which the three most common are potassium, sodium and calcium ions. This will be undertaken in an aqueous environment, so the conditions mentioned above must be realised. PEDOT has low sensitivity to O_2 and CO_2, as well as being shown to be one of the most interesting and versatile conducting polymers as a solid contact in ASSISE [41] [61] [62].

3.2.4.1 Conducting Polymers

Conducting polymers were discovered about 36 years ago [63]. They are described as organic polymer semiconductors, or organic semiconductors, that can conduct electricity. Many of those used in ISEs are based on polyaniline (PA), polypyrrole (PPy), polythiophene (PT) and their derivatives.

Conducting polymers are synthesised by either chemical or electrochemical techniques [64]. Electropolymerisation has better control of the film thickness and can achieve high purities. However, via this method only small quantities can be produced, and it can be difficult to remove the polymer from the electrode. While this means that electropolymerisation is not the choice for bulk industrial production, it is perfect for the application of ISE fabrication.

Table 3.1 – Comparison of chemical and electrochemical polymerisation of conducting polymers.

Polymerisation Technique	Advantages	Disadvantages
Chemical Polymerisation	Large scale production Post covalent modification possible Modify CP backbone	Cannot make thin films Complicated synthesis Un-doped only Poor quality/impurities Over oxidation and/or decomposition problems
Electrochemical Polymerisation	Thin films possible More simplistic to synthesis Doping, via entrapment, occurs simultaneously Controllable thickness High purity	Difficult to remove from electrode Post covalent modification difficult Small quantities

There have been several mechanisms proposed for the electrochemical polymerisation of conducting polymers: these are Kim's [65]; Diaz' [66]; Pletcher's [67]; and Reynold's [68]. Diaz is the most common due to evidence supporting this mechanism, such as electron paramagnetic resonance (EPR) or electron spin resonance (ESR), pH and chronoabsorption studies [69] [66]. The mechanism of electrochemical polymerisation proceeds via the charged

species being produced by oxidation of the monomer at the anode. Polymerisation then proceeds via a complex combination of electrochemical and chemical reaction that depends on the conducting polymer.

In general, during monomer oxidisation, electron transfer is much faster than diffusion of the monomer, so there is a high concentration of radicals formed at the electrode surface. Two radicals couple to form a dimer after re-aromatisation. The dimer can then go on to form a radical cation, the radical combination reaction is repeated and the chain grows until the polymer becomes insoluble in the electrolytic solution and precipitates onto the electrode surface. This is shown in more detail in Figure 3.17 in Section 3.2.4.2.

PEDOT, the conducting polymer of choice, has a very high conductivity (~ 300 Sm^{-1}), a very high stability in its oxidised form, good environmental stability, high transparency [70], low oxidation potential, relatively low band gap [71] [72], and good chemical and electrochemical properties [73]. Mixed electronic and ionic conductivity means that it can be successfully used as an ion-to-electron transducer [41].

The substitution of H by O-electron donor on position 3 and 4 significantly lowers the oxidation of EDOT compared to thiophene [73], making it more suitable for use in aqueous environments where the potential window is defined by the redox potential of water.

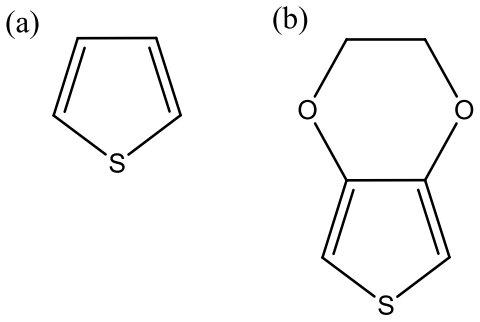

Figure 3.14 – Chemical structure of (a) Thiophene and (b) EDOT.

Bobacka [41] studied the influence of PEDOT as a solid contact on the potential stability of ISEs and found that the high redox capacitance of the ion-to-electron transducer stabilised the electrode potential. It was also observed that the potentials recorded for ISEs based on PEDOT were less sensitive to O_2 and CO_2 (pH changes) compared to PPy [74]. PEDOT doped with PSS was used to successfully fabricate ISEs sensitive to K^+ [41] [74], Na^+ [75] and Ca^{2+} [55]; as well as for other non-biological ions such as aromatic cations and silver.

3.2.4.2 Synthesis and Growth Mechanism of PEDOT

PEDOT can be synthesised via three methods: oxidative chemical polymerisation, electrochemical polymerisation and transition metal-mediated coupling of EDOT derivatives. Only electrochemical polymerisation will be considered here given that the dimensions of the microgripper tip, where the electrode is situated, make the other two methods incompatible.

Different electrochemical techniques can be used; for example, cyclic voltammetry (CV), chronoamperometry (CA) and chronopotentiometry [76], all of which use small amounts of monomer and take relatively short times for polymerisation, making them very cost effective.

Electrochemical deposition of PEDOT in organic media (usually acetronitrile) is more common due to the sparing solubility of PEDOT in aqueous solutions. In this case, solutions containing $LiClO_4$ [77], tetrabutylammonium perchlorate (TBAP) [78], or tetrabutylammonium hexafluorophosphate ($TBAPF_6$) [79] are used as dopants. However, due to the biological application of the microgripper sensor device, aqueous deposition is more suitable. Additionally, Yang et al [80] synthesised PEDOT galvanostatically from an aqueous solution containing poly(acrylic acid) (PAA) and found that the resulting nanofibril structure had lower electrical impedance due to the high surface area, which is better for the operation of ISEs.

EDOT/PEDOT is water insoluble/partially soluble (2.1 gL^{-1} at 20 ^0C) and infusible in neutral and doped forms [81]. The insolubility is overcome by including PSS during

polymerisation, which is a water soluble polyelectrolyte that acts as a charge-balance dopant [70] [73]. The chemical structure of the resulting film is shown in Figure 3.15.

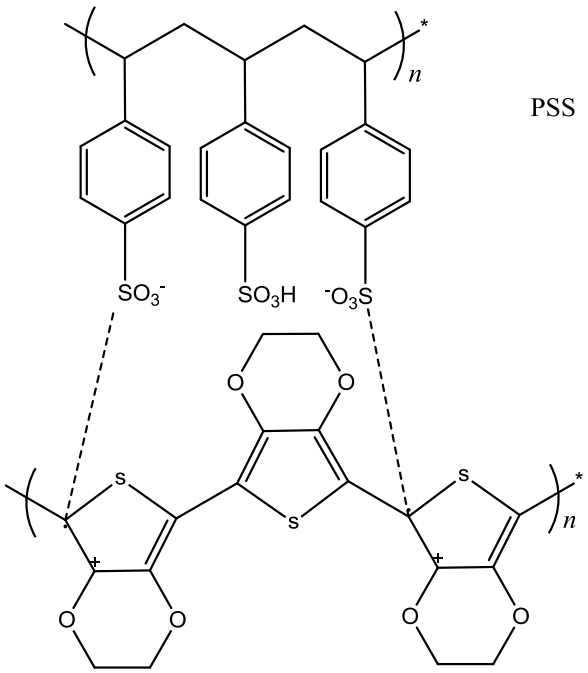

Figure 3.15 – Chemical structure of PEDOT doped with PSS.

The experimental parameters of the electropolymerisation of PEDOT greatly affect the surface morphology and detailed studies have been undertaken to assess these [82]. Aprotic solvents tend to yield smooth surfaces, while with aqueous solvents the opposite is true. It was observed however, that a rough PEDOT surface produced ISE devices with a more stable response. This, coupled with the fact that the fabrication route of the electrode formation at the microgripper tip yielded a rough surface of gold, made depositing a smooth PEDOT surface unrealistic, as well as undesirable, hence aqueous solution polymerisation was carried out. Figure 3.16 shows the CV of the electropolymerisation of PEDOT doped with NaPSS.

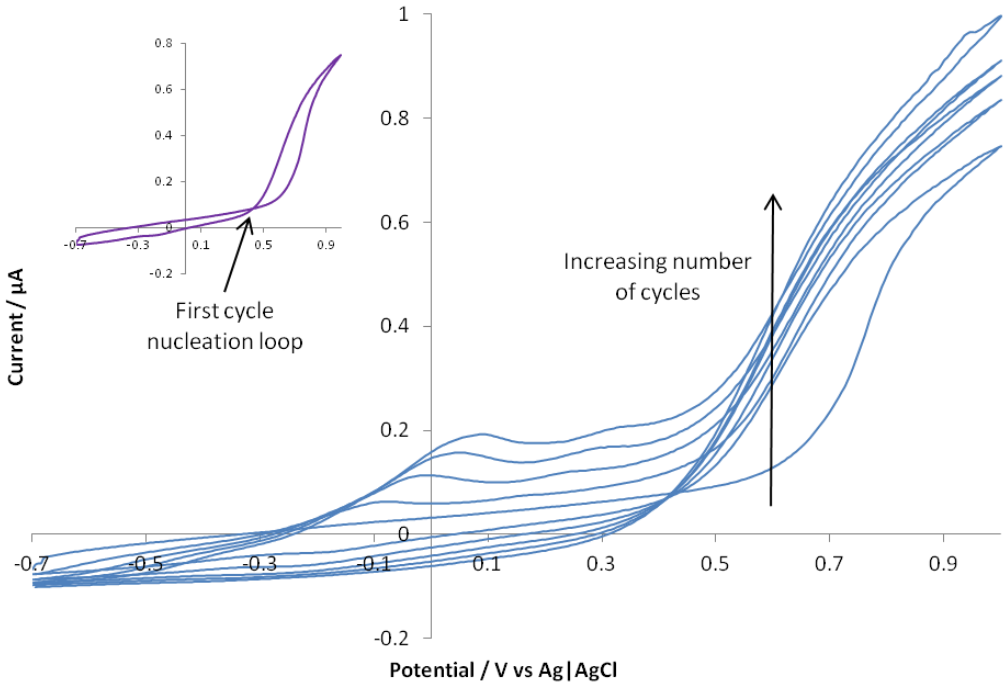

Figure 3.16 – CV of the electropolymerisation of EDOT showing the first cycle's nucleation loop.

In the first cycle there is a peak at 0.6 V, which is the oxidation of the EDOT monomer. At this point EDOT loses an electron and forms a reactive radical intermediate (Figure 3.17, step 1). This then reacts immediately with an available EDOT monomer to form a dimer species (Figure 3.17, step 2). As the potential is swept to -0.7 V, the dimer structure is reduced to give the charge stable form (Figure 3.17, step 3). As the cycles progress, more and more EDOT monomers are added to the polymer chain resulting in the formation of PEDOT (Figure 3.17, step 4). As the number of cycles increases an additional peak is seen around -0.2 V which is the oxidation of PEDOT (a redox active analyte in its own right). As the PEDOT layer gets thicker (hence the PEDOT concentration increases), the peak current increases.

As the chain grows, the polymer becomes insoluble in the electrolytic solution and deposits onto the electrode: this is known as nucleation. The occurrence of this can be seen in the CV trace where it crosses itself on the return scan, known as the nucleation loop, and is shown more clearly in the insert of Figure 3.16.

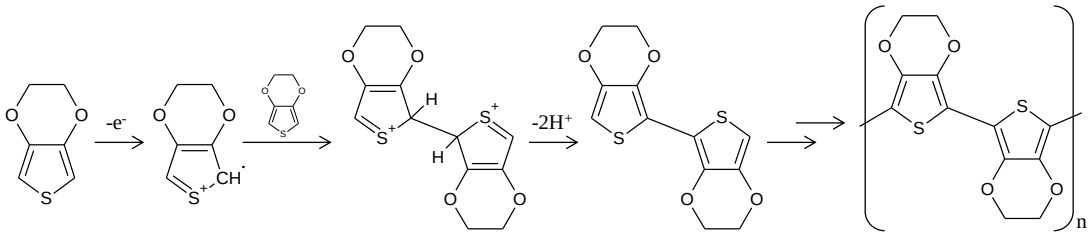

Figure 3.17 – Reaction scheme of the polymerization of EDOT to PEDOT.

3.2.4.3 Ion Selective Membrane Components

There are four main components in the ISM, and the nature and concentration of these components have a great effect on the characteristics of the sensor. An ISM generally contains: a polymer matrix; an ionophore (active recognition/sensing element that can be charged or neutral); a plasticiser (also known as the membrane solvent: it sets the membrane), and a lipophilic additive salt (also known as an ionic site: this has the opposite charge to the measured ion to ensure charge neutrality).

The most common membrane composition for an ion selective membrane where there is a PVC polymer type base containing an ionophore is, 33 wt% PVC, 66 wt% plasticiser, 1 wt% ionophore and a small amount of membrane additives [10] [30].

PVC is a common material for the polymer matrix as it gives the membrane mechanical strength and structural integrity. Polyurethane (PU) is also common due to its enhanced biocompatibility and adhesive property [83]: however, the detection limits tend to be poor [84].

The ionophore is an electron rich complexing compound that carries a specific ion; it can be an ion exchanger (charged) or neutral macrocycle with cavities to surround the target ions. The ionophore is considered the most important component as it is responsible for the selectivity and sensitivity (which is dependent on the binding constants of the ionophore and target ion) of the ISE. If the ionophore has a higher affinity for the target ion, then it will have a

higher selectivity towards that ion, as long as the complexation is reversible. Ions are transferred through the membrane via carrier translocation [85]. Natural and synthetic ionophores have been used extensively. Natural ones include valinomycin (K^+) [86], nonactin (which complexes with alkyl actions; the highest affinity is for K^+, Na^+ and Rb^+, and then for NH_4^+ and Tl^+) [87] [88], ionomycin (Ca^{2+}) [89], nigericin (H^+, K^+ and Pb^{2+}) [90] and monensin (Li^+, Na^+, K^+, Rb^+, Ag^+ and Tl^+) [91]. These are shown in Figure 3.18.

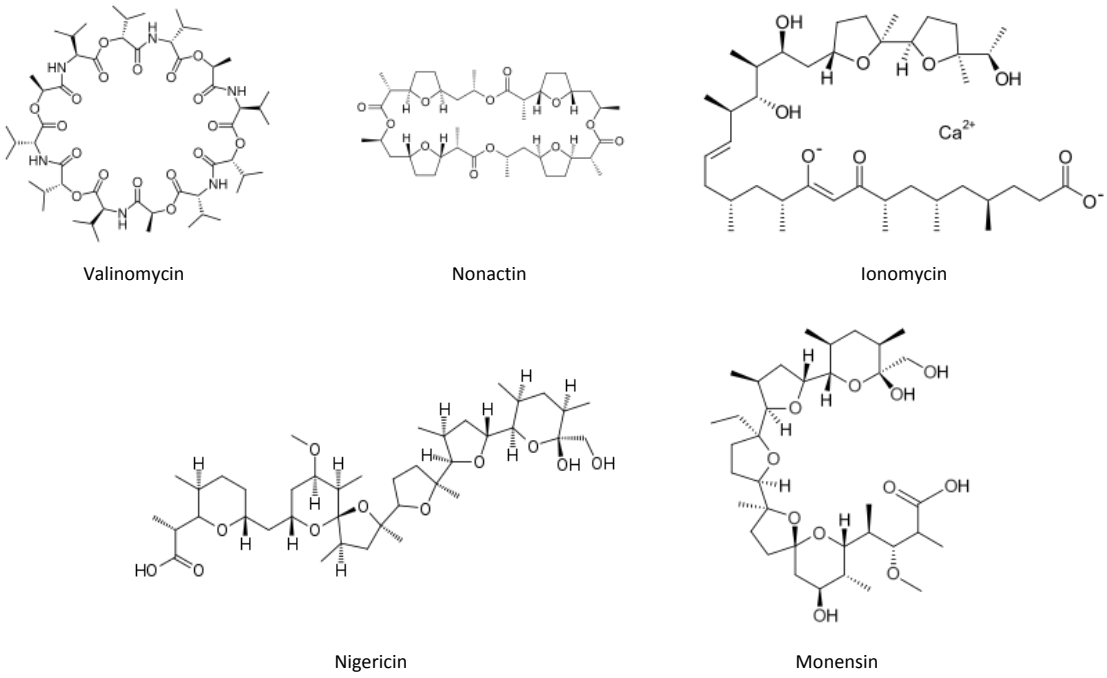

Figure 3.18 – Chemical structures of the more common naturally occurring ionophores **[92]**.

However, natural ionophores often have limited selectivity, and so specifically designed synthetic ones are occasionally used instead [93]. Valinomycin is the exception to this, and is still one of the more common ion selective ionophores used for the selective sensing of potassium. Figure 3.19 shows the more commonly used synthetic calcium and sodium ionophores.

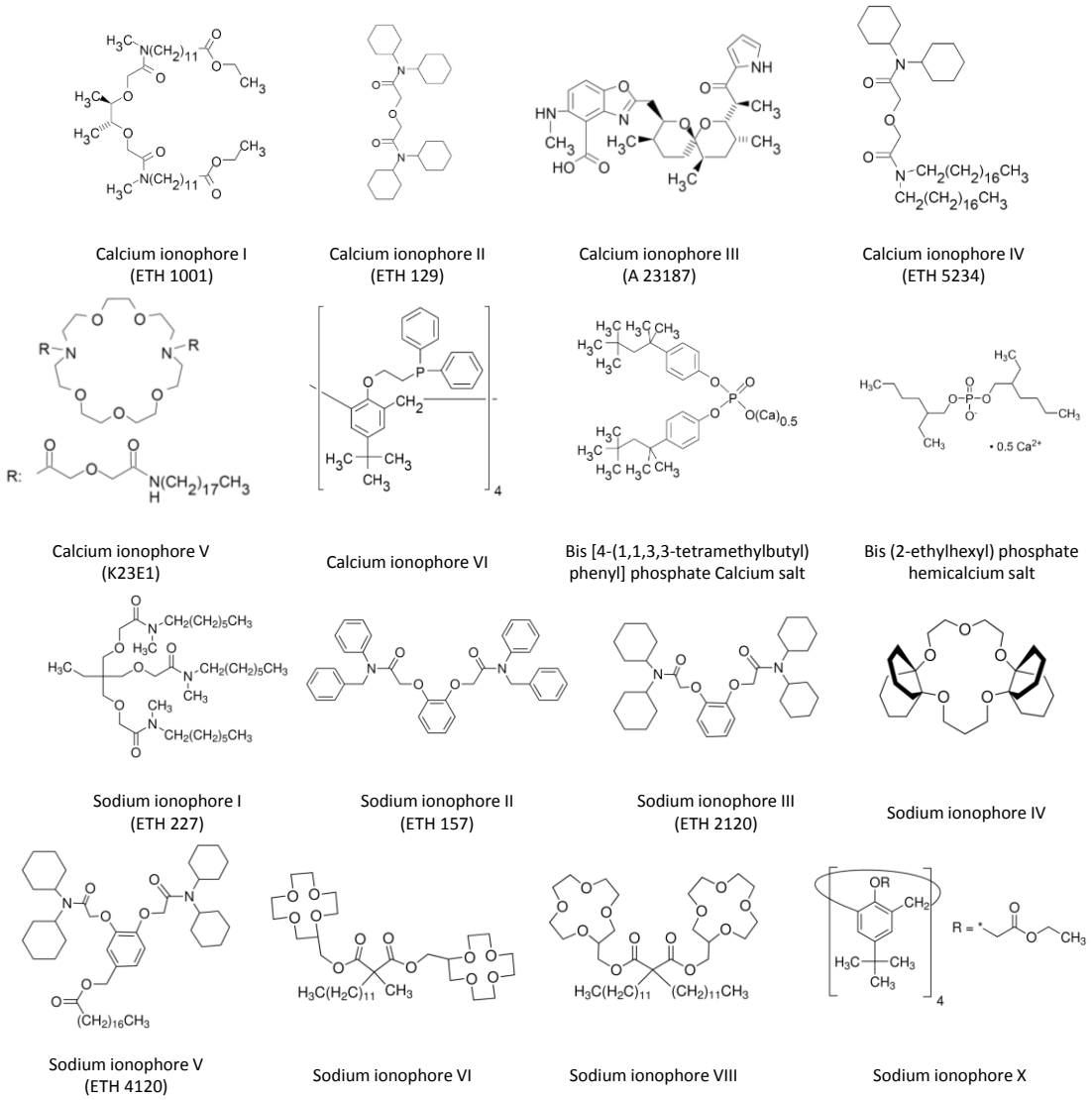

Figure 3.19 – Chemical structures of the more common synthetic calcium and sodium ionophores **[92]**.

The plasticiser is used to increase the plasticity of the membrane by reducing the glass transition temperature, T_g, of the polymer to below room temperature (i.e. it converts a brittle polymer into a soft flexible elastomer). The plasticiser also increases the dielectric constant of the polymer membrane, although no definitive correlation has been made between this membrane dielectric constant and its performance [94]. Ideally the plasticiser should be inert, in that it does not form complexes with the ions. It also needs to be able to dissolve the ionophore and ionic sites to ensure homogeneity within the polymer matrix. The main issue with plasticised membranes is that leaching is a problem; careful choice of plasticiser is

therefore important as leaching affects the ISE performance. Common plasticisers include adipates, phthalates, sebacates and phenyl ethers [94].

The lipophilic active sites are used as ion exchangers. They greatly improve the ISE response time, stability, reproducibility and selectivity, as well as lowering the electrical resistance of the membrane (which is very important for microelectrodes) [95] and controlling potentioselectivity [96]. Without lipophilic active sites, membranes do not respond to the changes in concentration of the ion of interest [97]. Initially, cationic salts (such as tetraphenyl borate) were added to cationic ISE to reduce the anionic interference from lipophilic anions [98]. However, it was realised that they were also needed for counter ion primary ion responses in ionophore based potentiometric sensors. The most commonly used active sites are tetraphenyl borate salts for cation ISEs and tetraalkyl ammonium salts for anion ISEs [94].

The mole ratio of ionophore to active site in the ISM is an important parameter to control as it significantly influences the selectivity of the ISE [99]. It is also important that the membranes do not contaminate their boundary layers. However, realistically, membranes with less than perfect ion selectivity and perma-selectively do introduce contamination.

It is also important to consider chemical interactions of the individual ISM components with each other, for example, ETH 5294 (usually used in mixed ionophore systems to detect potassium and calcium ions) decays photochemically, which initiates a singlet oxygen; in this case decomposition is facilitated by the presence of tetrakis(4-chloro phenyl) borate ($TpClPB^-$) and tetraphenylborate (TPB^-) ionic sites.

Furthermore, the method of ISM deposition is also important as it has been observed that smooth films result in better ISE potentiometric characteristics [100].

3.3 Device Fabrication

The WE fabricated at the tip of the microelectrode was made into an ISE via two steps: firstly a layer of PEDOT was deposited, via electropolymerisation, onto the gold surface, and then a layer of PVC based ISM was drop cast to encapsulate the PEDOT.

Cyclic voltammetry (CV) and chronoamperometry (CA) were undertaken using a potentiostat (Ivium CompactStat). A solid Silver|Silver Chloride electrode was used as the reference electrode (RE) and a platinum flag electrode was used as the counter electrode (CE). The gold electrode fabricated into the microgripper design was used as the working electrode (WE). All measurements were carried out in a 3-electrode cell arrangement with the RE fed through the upright of the RP holder to maintain a constant distance between the RE and WE. All chemicals, purchased from SigmaAldrich, were of analytical grade and were used without further purification.

3.3.1 Analysis of Bare Gold Electrode

Although the geometric area of the electrode was accurately known from the fabrication process (1400 μm^2), the roughness of the surface due to the electroplating process was not considered. The electroactive working area of the electrode was determined using chronoamperometry.

Potassium ferricyanide was used as it has a well-documented stable potential. 0.05 M $K_3Fe(CN)_6$ + 0.25 M KNO_3 (aq) was the electrochemical solution, the potential was stepped between -0.2 and 0.28 V (above and below the redox potential of the ferricyanide ion). The potentials were held for 30 s and the resulting current was measured; this is shown in Figure 3.20.

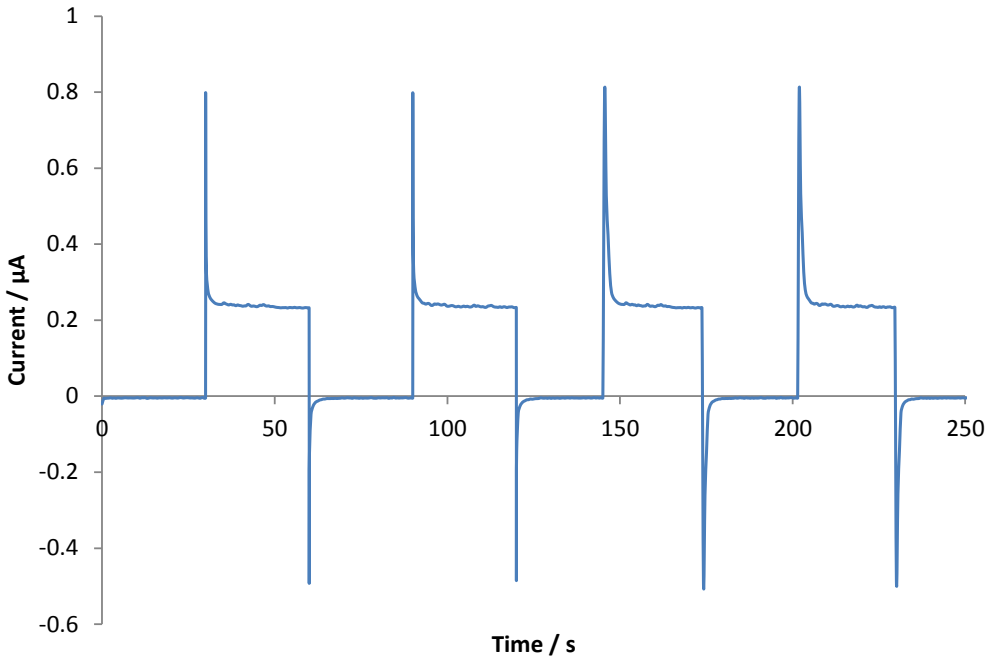

Figure 3.20 – Chronoamperometry plot in a solution of 0.05 M $K_3Fe(CN)_6$ + 0.25 M KNO_3 (aq) used to determine the electrode surface area.

The resulting steady state currents above the redox potential were averaged, yielding value of 0.240 ± 0.003 µA. Using the Cottrell equation (Equation 3.22),

$$|i| = \frac{nFAC_{bulk}\sqrt{D}}{\sqrt{\pi}\sqrt{t}}$$

Equation 3.22

where n = 1; F = 96485 C mol^{-1}; C_{bulk} = 0.050 ± 0.001 M; t = 30 s; and D = 0.073 ± 0.011 m^2 s^{-1} [101]; the value for the electroactive surface area of the WE at the microgripper tip was calculated as 1800 ± 20 μm^2. It should be noted that the Cottrell equation is generally used to analyse electrodes with strictly planar geometries with a well-defined boundary, for example atomically smooth metal discs [1]. Real electrode surfaces are rarely smooth, as is the case of the bare gold electrode at the tip of the microgripper device, and many electrochemical techniques can only determine the geometric surface area, sometimes known as the projected area, which does not take the surface roughness into account. However, in the case of the electroactive surface area of the microgripper electrode determined using chronoamperometry, there is a difference of 23 % from the known geometric surface area.

The surface area determined by the Cottrell equation is more accurately defined as the cross-sectional area of the diffusion field, which in most cases is the planar, unrestricted, projected area where the electronically conducting phase is in contact with the solution. However, in the case of the microgripper electrode, it is the SU8 walls that make up the scoop of the microgripper tip that define the shape and size of the diffusion layer, not the electrode itself. This would explain the overestimation of the electrochemical working area of the electrode using chronoamperometry as the projected surface area would be much greater.

AFM data collected on the surface area difference between the geometric surface area and the predicted surface area taking the surface roughness into consideration was 15 %. This is lower than that determined by electrochemical analysis, further indicating that the electrochemically defined electroactive area is determined by the shape of the tip (confinement by the SU8 sidewalls). However, it should be noted that the AFM data does not take the surface roughness of the electrode sidewalls into account. Figure 3.21(b) shows the effect that etching the gold electrode has on both the top surface and the sidewall. It can clearly be seen that there is pitting of the sidewall, which would not be included in the AFM calculations. Therefore, the actual surface area of the WE at the microgripper tip will likely reside somewhere within the range of 1610 – 1800 μm^2, though more likely closer to the bottom end of that range, but the electroactive area (which will define the electrode behaviour) is 1800 ± 20 μm^2.

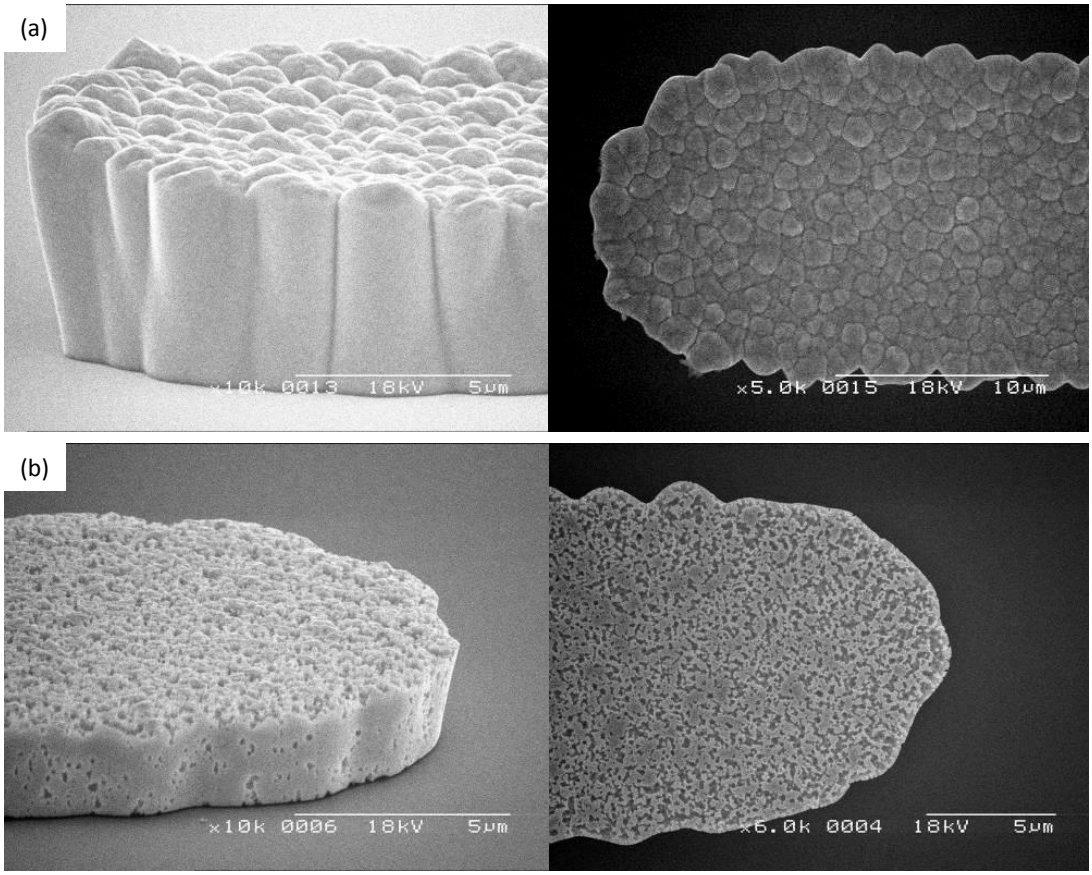

Figure 3.21 – SEM images showing the sidewall and top of the electrode (a) before and (b) after etching.[1]

As mentioned previously, the definition of a microelectrode is one whose surface is smaller than the scale of the diffusion layer and/or there is one dimension in the micron scale. With all the dimensions of the WE at the microgripper tip, and those of the microgripper tip itself, being in the micron scale, one would expect this electrode to behave as a microelectrode. Additionally, the fact that the microgripper tip scoop dimensions ensure that the diffusion layer is greater than the surface area also indicates that this electrode should behave as a microelectrode. Cyclic voltammetry was used to verify this, the resulting voltammogram in a solution of 0.05 M $K_3Fe(CN)_6$ + 0.25 M KNO_3 (aq) showing the plots at different scan rates is shown in Figure 3.22.

[1] Thanks to Dr. Mark Rosamond for the use of this figure.

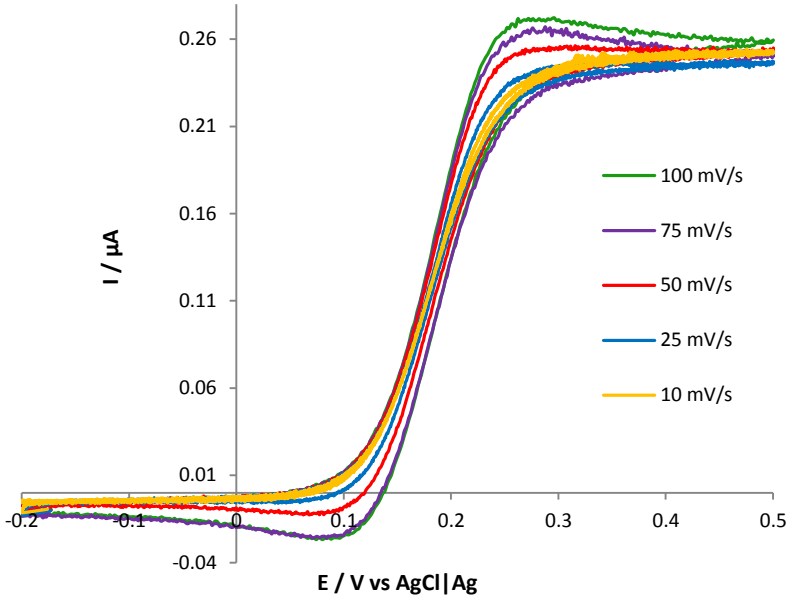

Figure 3.22 – CV of electrode in 0.05 M $K_3Fe(CN)_6$ + 0.25 M KNO_3 to determine electrode response.

The Sigmoidal shape that is characteristic of a microelectrode can clearly be seen. Additionally, the steady state current is independent of scan rate, again indicative of a microelectrode. At faster scan rates, slight capacitive peaking is observed; this is due to the fact that at faster scan rates the diffusion layer has more linear characteristics than radial ones, so mixed zone behaviour is observed, where the electrode behaves as both a micro and a macro electrode.

3.3.2 Preparation of PEDOT Film

The sodium poly(styrene sulfonate) (NaPSS) doped PEDOT layer was deposited via electropolymerisation onto the gold WE following the set up described below.

0.01 M EDOT + 5 mg/mL NaPSS (aq) (mixed by sonicating for 15 min, followed by 3 hours stirring) was deaerated with argon for 5 min. A 3 electrode set up was used to apply a cycling potential between -0.7 – 1.0 V at a scan rate of 50 mVs^{-1} for 10 cycles. The layer was then rinsed with deionised (DI) water and left to dry for at least 5 hours.

The resulting film had a fibril texture as shown in Figure 3.23.

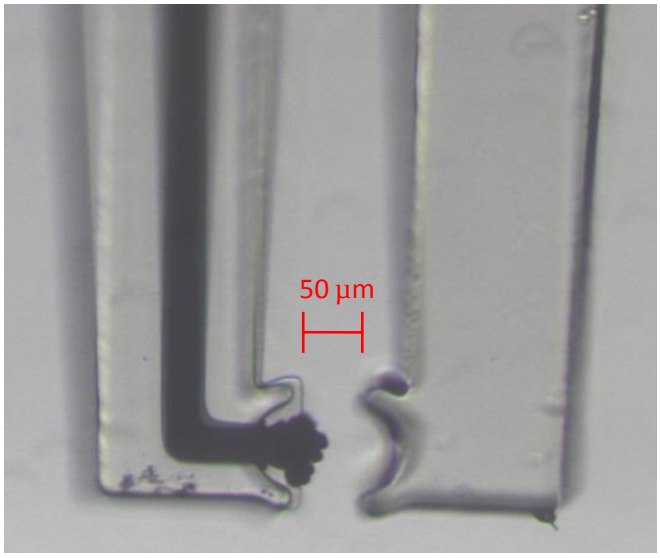

Figure 3.23 – Image of the microgripper tips showing the fibril texture of the PEDOT deposition onto the electrode.

The concentration of EDOT in solution affects the structure of the deposition of PEDOT; for example, higher concentrations of EDOT at the electrode cause a faster rate of polymerisation, so an over deposition can occur (seen in Figure 3.24(c)). However, the shape of the microgripper scoop counteracts this effect slightly, as the diffusion of EDOT to the electrode surface is limited spatially, slowing down the rate of polymerisation. Another consideration is the scan rate; if too slow, diffusion of the radical EDOT from the gold electrode means this EDOT radical can react with the uncapped SU8 chains, depositing on the microgripper scoop (seen in Figure 3.24(b)) instead of the electrode.

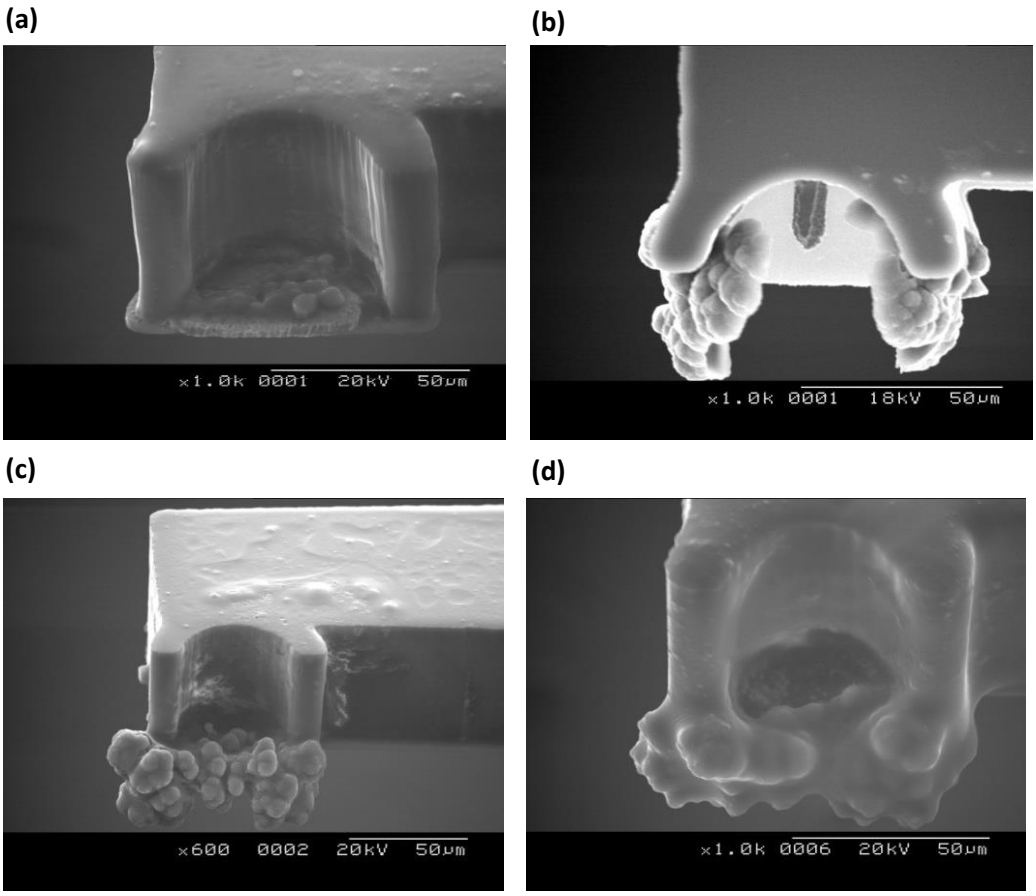

Figure 3.24 – SEM images of PEDOT at microgripper tip showing (a) the correct deposition of PEDOT onto the electrode; (b) deposition of PEDOT onto SU8 and not the electrode; (c) over deposition of PEDOT and (d) the over deposition of PEDOT after ISM deposition showing a burst air bubble.

It is more difficult to deposit the ISM properly on devices where PEDOT has been over deposited, as air bubbles can be trapped, causing an instable interface (due to lack of direct contact between the electrode and PEDOT) and/or membrane rupture on submerging into a solution (Figure 3.24(d)).

3.3.3 Ion Selective Membrane Deposition onto the Microgripper Electrode

The ion selective membranes for the various ion selective electrodes were made up with compositions as shown in Table 3.2. Three different ionophores, which are tailored to be most selective towards the ion of interest in the cell media environment, were used for the three different ion sensors.

A total weight of 200 mg of ISM components were measured and dissolved in no more than 3 ml of THF. The mixture was then stirred for 1 hour and the solution stored at 5 ^{0}C when not being used.

Table 3.2 – Ion selective membrane components made up to a total of 200 mg in 3 ml of tetrahydrofuran (THF).

Membrane component	Chemical		Quantity / % wt
Base membrane	Poly(vinyl chloride) (PVC)		32.6
Plasticiser	o-Nitro phenyl octyl ether (o-NPOE)		65.6
Ionophore	ETH 1001 (Calcium ionophore I)	Ca^{2+} ISE	1.3
	Sodium ionophore X	Na^{+} ISE	
	Valinomycin	K^{+} ISE	
Ionic Site	Potassium tetrakis (4-chlorophenyl) borate (KTpClPB)		0.5

The ISM solution was drop cast onto the electrode at the microgripper tip using the CellEctor on loan from MMI[2]. The CellEctor was equipped with a 30 µm capillary that was capable of precise deposition of small volumes of solutions. The CellEctor is shown in Figure 3.25.

Figure 3.25 – Image of the Cellector Plus **[102]**.

[2] MMI is a company based in Zurich which supplies innovative cell finding and sorting systems for ultra-precise preparation of biological samples from tissue, cell cultures or cell suspensions to a target market of life and material science related fields; mainly molecular pathology, drug discovery, medical diagnostics, food and environmental analytics.

Using the CellEctor in the reverse method that it has been built for, it was possible to deposit small volumes (0.5 - 1 µl) very accurately onto a substrate. The Cellector was therefore utilised to drop cast the ISM dissolved in THF into the SU8 'scoop' at the microgripper tip.

To reduce the evaporation rate of the THF from the ISM solution while it was within the deposition capillary, a saturated atmosphere of THF was maintained around the ISM solution. This was achieved by placing 2-3 µl of THF above and below the ISM solution in the capillary. This is shown schematically in Figure 3.26. This THF atmosphere ensures that the ISM does not set within the capillary. The top layer of THF is required as the residual pump oil left on the walls of the capillary contaminates the ISM layer.

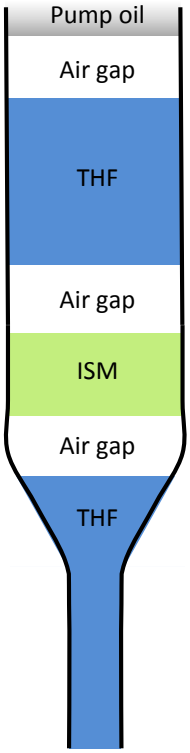

Figure 3.26 – Schematic representation of the deposition capillary.

During deposition the capillary was placed within the scoop at the microgripper tip, taking care that once in touch with the electrode surface the capillary was not moved laterally as this scrapes away the PEDOT layer. The THF solution at the tip of the deposition capillary was expelled first, wetting the electrode. This dried almost instantaneously under the heat of

the microscope. The ISM solution was then deposited and the capillary immediately removed. This needed to be be done rapidly otherwise the ISM layer would be removed on retraction of the capillary, as with time the ISM would set onto the tip of the capillary. The microgripper tip was left on the microscope for several minutes to ensure the membrane had set. It was then left to dry overnight to ensure all the THF had evaporated from the layer.

The ISM layer was checked optically to ensure that the microgripper tips were not fused (as in Figure 3.27(e)). However, occasionally the scoop at the microgripper tip was completely filled (as in Figure 3.27(d)). This not only affected how well the microgripper manipulates the cell, but also thick membrane depositions have a poor Nernstian response, as well as having poor detection limits [103]. Unfortunately this could not be observed using an optical microscope before use and SEM imaging was found to be destructive. Early prototypes suffered greatly from this type of membrane deposition; however, with the refined process described above this effect was very rare. Membranes that were deposited successfully (acceptable tolerances are shown in Figure 3.27 (a-c)) all showed similar Nernstian responses, detection limits and response times even though the surface morphology differed slightly. This is shown in more detail in Section 4.3.2.1.

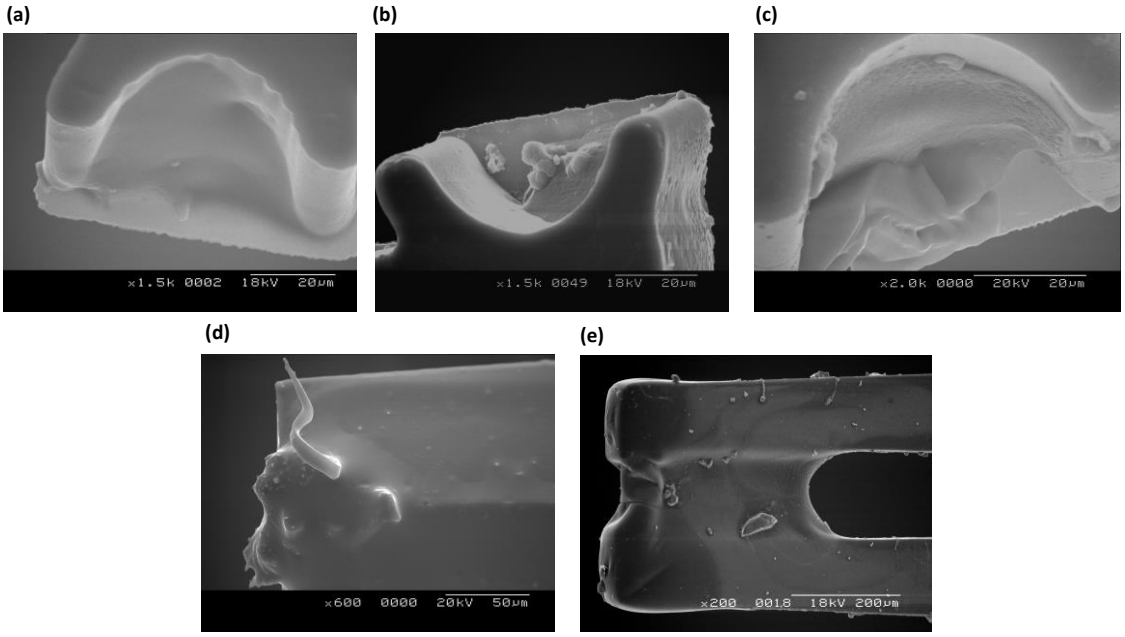

Figure 3.27 – SEM images of ISE devices with different ISM depositions: (a)-(c) Acceptable ISM deposition; (d) one tip coated and (e) both tips fused together.

3.3.4 Conditioning

Initial conditioning of an ISE is very important, though there is a lack in intensive research in how differing conditions affect the electrode response. Freshly prepared electrodes are generally conditioned in a relative concentrated primary ion solution (≥ 10^{-3} M), most often in an open circuit arrangement overnight.

Some more recent work [104] suggests conditioning in solutions containing the main interfering ions helps to lower the detection limits of the ISE in mixed solutions by avoiding the ion exchange effects seen when there is a high concentration of interfering ions in the sample solution. However some reports have observed poisoning effects of the ISM when exposed to these interfering ions for extended periods of time, especially for ASSISE type arrangements.

Planar sensors are very sensitive to transmembrane fluxes of H_2O, CO_2 and O_2 and require longer conditioning times, however these planar sensors are also very susceptible to leaching of membrane components and formation of a water layer at the conducting polymer|ISM interface when overconditioning occurs [105].

The devices used in this work were conditioned in 0.1 M solutions of the primary ion in an open circuit arrangement overnight.

3.4 Chapter Summary

The first section of this chapter covered the thermodynamics and kinetics for the voltammetric and amperometric techniques used as analysis tools in the characterisation of the bare gold electrode, specifically cyclic voltammetry and chronoamperometry. Additionally, the thermodynamics of ion selective electrode potentiometry were considered.

The second section of this chapter discussed the electrochemical sensor technology used in this project; specifically the development of conventional liquid ISEs and ASSISEs, and their components. Conventional liquid ISEs in clinical applications account for more than a billion of blood electrolyte analysis systems in the *in vitro* diagnostic sensor market. These macro-sized ISEs have sensing surface areas around 3 – 100 mm^2. With the success of these conventional liquid ISEs in many applications the motivation behind the development into ASSISEs is sometimes unclear, especially as literature indicates that currently their response behaviour, stability, life time and reproducibility is not yet comparable with conventional ISEs [106]. The major advantages of ASSISEs is that they are relatively maintenance free, easy to miniaturise, robust and cost-effect to manufacture. Many ASSISEs are compatible with MEMS fabrication techniques, which has the additional advantage of providing mass-produced sensors and sensors arrays that can be integrated with the measuring, data acquisition and control electronics [107] [108].

The main challenge in the design of ASSISEs was in interfacing the electrical conductor with the ion-conducting ISM. PEDOT was used as the ion-to-electron transducer as conducting polymers have been shown to behave well in this role due to their electronic and ionic properties. Additionally, PEDOT has a low sensitivity to O_2 and CO_2, which is important due to the aqueous environment the microgripper sensor devices must operate in. The ISM, made up

of four components, determines the sensitivity and selectivity of the ISE. The choice of components was important as each one had a different role, which should not interfere with that of any of the other components. The choice of ionophore was particularly important as it alone determined the selectivity of the device. The components of the ISM are given in Table 3.2.

The final section of this chapter presented the characterisation of the bare gold electrode fabricated at the tip of the microgripper, and detailed the fabrication process by which it was made into an ASSISE. The characterisation of the electrode was important as it defines the diffusion layer associated with it, and therefore determines the response behaviour. An electrode is classed as a microelectrode if that electrode either has one dimension in the micron range and/or is smaller than the diffusion layer. The gold electrode fabricated at the microgripper tip had an active surface area of $1800 \pm 20\ \mu m^2$, inferring that it should be classed as a microelectrode. This conclusion was confirmed by the plot shape of a cyclic voltammogram, which showed sigmoidal behaviour.

The concentration of EDOT and the scan rate that the CV technique was run at were both carefully controlled to ensure that a fibril PEDOT film was produced, that had not reacted with the SU8 polymer of the microgripper. The thickness of the film could be monitored by observing the steady state current at the redox potential of PEDOT to ensure that each device was fabricated identically. The ISM was drop cast onto the PEDOT layer using a CellEctor. Using this technique the volume of the ISM could be controlled. However, it was difficult to identically reproduce the surface morphology and thickness between devices.

3.5 References

[1] A. J. Bard and L. R. Faulkner, Electrochemical Methods: Fundamentals and Applications 2nd Ed., New York: J. Wiley and Sons, 2000.

[2] L. Adler-Abramovich, M. Badihi-Mossberg, E. Gazit and J. Rishpon, “Characterization of peptide-nanostructure-modified electrodes and their application for ultrasensitive

environmental monitoring," *Nanotechnology: Small,* vol. 6, no. 7, pp. 825-831, 2010.

[3] J. Wang, Analytical Electrochemistry 3rd Ed., Hoboken, New Jersey: Wiley and Sons, 2006.

[4] N. J. Ronkainen, H. B. Halsall and W. R. Heineman, "Electrochemical biosensors," *Chemical Society Reviews,* vol. 39, pp. 1747-1763, 2010.

[5] S. Carrara, S. Ghoreishizadeh, J. Olivo, I. Taurino, C. Baj-Rossi, A. Cavallini, M. Op de Beeck, C. Dehollain, W. Burleson, F. G. Moussy, A. Guiseppi-Elie and G. De Micheli, "Fully integrated biochip platforms for advanced healthcare," *Sensors,* vol. 12, pp. 11013-11060, 2012.

[6] P. Protti, Introduction to Modern Voltammetry and Polarographic Analysis Techniques 4th Ed., Amel Electrochemistry, 2001.

[7] R. G. Compton and C. E. Banks, Understanding Voltammetry 2nd Ed., Imperial College Press, 2011.

[8] M. I. Montenegro, M. A. Queiros and J. L. Daschbach, Microelectrodes: Theory and Application, Alvo, Portugal: Kluwer Academic, 1990.

[9] A. Hulanicki, S. Glab and F. Ingman, "Chemical sensors definitions and classifications," *Pure and Applied Chemistry,* vol. 63, pp. 1247-1250, 1991.

[10] E. Bakker, P. Buhlmann and E. Pretsch, "Carrier based ion selective electrodes and bulk optodes 1. General characteristics," *Chemical Reviews,* vol. 97, pp. 3083-3132, 1997.

[11] E. Bakker, P. Buhlmann and E. Pretsch, "The phase-boundary potential model," *Talanta,* vol. 63, pp. 3-20, 2004.

[12] K. H. Meyer and I. F. Sievers, "The permeability of membranes I - The theory of ionic permeability," *Helvetica Chimica Acta,* vol. 19, pp. 649-664, 1936.

[13] G. J. Moody and J. D. Thomas, "Selectivity ratios/coefficients of selective ion sensitive electrodes," *Talanta,* vol. 18, no. 12, pp. 1251-1252, 1971.

[14] A. Hulanicki and A. Lewenstam, "Interpretation of selectivity coefficients of solid state ion selectivite electrodes by means of diffusion layer model," *Talanta,* vol. 24, no. 3, pp. 171-175, 1977.

[15] J. Bobacka, A. Ivaska and A. Lewenstam, "Potentiometric ion sensors," *Chemical Reviews,* vol. 108, no. 2, pp. 329-531, 2008.

[16] T. Sokalski, M. Maj-Zurawska and A. Hulanicki, "Determination of true selectivity coefficients of neutral carrier calcium selective electrode," *Mikrochimica Acta,* vol. 1, no. 5-6, pp. 285-291, 1991.

[17] A. Hulanicki, T. Sokalski and A. Lewenstam, "Side-effects in measurements of selectivity coefficients of solid state ion selective electrodes," *Mikrochimica Acta,* vol. 3, no. 1-6, pp. 119-129, 1988.

[18] M. Dole, The Glass Electrode, New York: Wiley, 1941.

[19] M. Dole, "The theory of the glass electrode," *Journal of the American Chemical Society,* vol. 53, pp. 4260-4280, 1931.

[20] M. Dole, "The theory of the glass electrode III Statistical explanation of the alkaline solution behaviour," *Journal of Chemical Physics,* vol. 2, no. 12, p. 862, 1934.

[21] W. R. Fawcett, Liquids, Solutions, and Interfaces: From Classical Macroscopic Descriptions to Modern Microscopic Details, New York: Oxford University Press, 2004.

[22] R. P. Buck and E. Lindner, "Peer review: Tracing the history of selective ion sensors," *Analytical Chemistry,* vol. 73, no. 3, pp. 88-97, 2001.

[23] D. Ammann, W. E. Morf, P. Anker, P. C. Meier, E. Pretsch and W. Simon, "Neutral carrier based ion-selective electrodes," *Ion-Selective Electrode Reviews,* vol. 5, no. 1, pp. 3-92, 1983.

[24] A. Shatkay, "Ion specific membranes as electrodes in determination of activity of calcium," *Analytical Chemistry,* vol. 39, pp. 1056-1065, 1967.

[25] J. Pick, E. Pungor, M. Vasak and W. Simon, "Potassium selective silicone rubber membrane electrode based on a neutral carrier," *Analytica Chimica Acta,* vol. 64, pp. 477-480, 1973.

[26] G. Horvai, E. Graf, K. Toth, E. Pungor and R. P. Buck, "Plasticized poly(vinyl chloride) properties and characteristics of valinomycin electrodes 1. High frequency resistances and dielectric properties," *Analytical Chemistry,* vol. 58, pp. 2735-2740, 1986.

[27] E. Lindner, E. Graf, Z. Niegreisz, K. Toth, E. Pungor and R. P. Buck, "Responses of site controlled, plasticized membrane electrodes," *Analytical Chemistry,* vol. 60, pp. 295-301, 1988.

[28] A. Vandenberg, P. D. Vanderwal, M. Skowronskaptasinska, E. J. R. Sudholter and D. N. Reinhoudt, "Nature of anionic sites in plastized poly(vinyl chloride) membranes," *Analytical Chemistry,* vol. 59, pp. 2827-2829, 1987.

[29] P. Buhlmann, S. Yajima, K. Tohda, K. Umezawa, S. Nishizawa and Y. Umezawa, "Studies on the phase boundaries and the significance of ionic sites of liquid membrane ion selective electrodes," *Electroanalysis,* vol. 7, pp. 811-816, 1995.

[30] G. J. Moody, R. B. Oke and J. D. R. Thomas, "A calcium sensitive electrode based on a liquid ion exchanger in a poly (vinyl chloride) matrix," *Analyst,* vol. 95, pp. 910-918, 1970.

[31] R. P. Buck and P. Vanysek, "Interfacial potential differences at mixed conductor interfaces - Nernst, Nernst-Donnan, Nernst distribution and generalizations," *Journal of Electroanalytical Chemistry,* vol. 292, no. 1-2, pp. 73-91, 1990.

[32] A. Hulanicki and A. Lewenstam, "Diffusion-layer model for copper solid-state chalcocite membrane electrode - sensitivity to copper(II) ions," *Talanta,* vol. 23, no. 9, pp. 661-665, 1976.

[33] T. Sokalski, A. Ceresa, T. Zeickl and E. Pretsch, “Large improvement of the lower detection limit of ion selective polymer membrane electrodes,” *Journal of the American Chemical Society,* vol. 119, pp. 11347-11348, 1997.

[34] R. W. Cattrall and I. C. Hamilton, “Coated wire ion selective electrodes,” *Ion Selective Electrode Reviews,* vol. 6, pp. 125-172, 1984.

[35] R. W. Cattrall and H. Freiser, “Coated wire ion-selective electrodes,” *Analytical Chemistry,* vol. 43, no. 13, pp. 1905-1906, 1971.

[36] B. P. Nikolskii and E. A. Materova, “Solid contact in membrane ion selective electrodes,” *Ion Selective Electrode Reviews,* vol. 7, pp. 3-39, 1985.

[37] H. H. Vandenvlekkert, B. Kloeck, D. Prongue, J. Berthoud, B. Hu, N. F. Derooij, E. Gilli and P. Decrousaz, “A pH-ISFET and integrated pH-pressure sensor with back side contacts,” *Sensors and Actuators,* vol. 14, pp. 165-176, 1988.

[38] M. Fibbioli, K. Bandyopadhyay, S. G. Liu, L. Echegoyen, O. Enger, F. Diederich, P. Buhlmann and E. Pretsch, “Redox active self assembled monolayers for solid contact polymeric membrane ion selective electrodes,” *Chemistry of Materials,* vol. 14, pp. 1721-1729, 2002.

[39] P. C. Hauser, D. W. L. Chiang and G. A. Wright, “A potassium ion selective electrode with valinomycin based poly (vinyl chloride) membrane and a poly (vinyl ferrocene) solid contact,” *Analytica Chimica Acta,* vol. 302, pp. 241-248, 1995.

[40] E. Lindner, V. V. Cosofret, S. Ufer, T. A. Johnson, R. B. Ash, H. T. Nagle, M. R. Neuman and R. P. Buck, “In vivo and in vitro testing of microelectronically fabricated planar sensors designed for applications in cardiology,” *Journal of Analytical Chemistry,* vol. 346, pp. 584-588, 1993.

[41] J. Bobacka, “Potential stability of all-solid-state ion-selective electrodes using conducting polymers and ion-to-electron transducers,” *Analytical Chemistry,* vol. 71, pp. 4932-4937, 1999.

[42] S. J. Dong, Z. H. Sun and Z. L. Lu, “A new kind of chemical sensor based on a conducting polymer film,” *Journal of the Chemical Society - Chemical Communications,* pp. 993-995, 1988.

[43] J. Bobacka, A. Ivaska and A. Lewenstam, “Potentiometric ion sensors based on conducting polymers,” *Electroanalysis,* vol. 15, pp. 366-374, 2003.

[44] J. Bobacka, Z. Q. Gao, A. Ivaska and A. Lewenstam, “Mechanism of ionic and redox sensitivity of p-type conducting polymers: Part 2 Experimental study of polypyrrole,” *Journal of Electroanalytical Chemistry,* vol. 368, pp. 33-41, 1994.

[45] A. Michalska and K. Maksymiuk, “The specific influence of hydrogen ions on poly (pyrrole) potentiometry,” *Electrochimica Acta,* vol. 44, pp. 2125-2129, 1999.

[46] A. Michalska and A. Lewenstam, “Potentiometric selectivity of p-doped polymer films,” *Analytica Chimica Acta,* vol. 406, pp. 159-169, 2000.

[47] A. Cadogan, Z. Q. Gao, A. Lewenstam, A. Ivaska and D. Diamond, “All solid state sodium selective electrode based on a calizarene ionophore in a poly (vinyl chloride) membrane with a polypyrrole solid contact,” *Analytical Chemistry,* vol. 64, pp. 2496-2501, 1992.

[48] J. Bobacka, M. Mccarrick, A. Lewenstam and A. Ivaska, “All solid state poly (vinyl chloride) membrane ion selective electrodes with poly (3-octylthiophene) solid internal contact,” *Analyst,* vol. 119, pp. 1985-1991, 1994.

[49] J. Bobacka, T. Alaviuhkola, V. Hietapelto, H. Koskinen, A. Lewenstam, M. Lamsa, J. Pursiainen and A. Inaska, “Solid contact ion selective electrodes for aromatic cations based on pi-coordinating soft carriers,” *Talanta,* vol. 58, pp. 341-349, 2002.

[50] J. Bobacka, T. Lindfors, M. Mccarrick, A. Ivaska and A. Lewenstam, “Single piece all solid state ion selective electrode,” *Analytical Chemistry,* vol. 67, pp. 3819-3823, 1995.

[51] T. Lindfors, P. Sjoberg, J. Bobacka, A. Lewenstam and A. Ivaska, “Characterization of a single piece all solid state lithium selective electrode based on soluble conducting polyaniline,” *Analytica Chimica Acta,* vol. 385, pp. 163-173, 1999.

[52] J. Migdalski, T. Blaz and A. Lewenstam, “Conducting polymer based ion selective electrodes,” *Analytica Chimica Acta,* vol. 322, pp. 141-149, 1996.

[53] F. Garnier, “Functionalized conducting polymers - Towards intelligent materials,” *Angewandte Chemie - International Edition in English,* vol. 28, pp. 513-517, 1989.

[54] H. K. Youssoufi, A. Yassar, S. Baiteche, M. Hmyene and F. Garnier, “Designing polypyrrole based sensors: Selective electrochemical cation in aza crown ethers,” *Synthetic Metals,* vol. 67, pp. 251-254, 1994.

[55] A. Michalska and K. Maksymiuk, “All plastic, disposable, low detection limit ion selective electrodes,” *Analytica Chimica Acta,* vol. 523, pp. 97-105, 2004.

[56] N.-H. Kwon, K.-S. Lee, M.-S. Won and Y.-B. Shim, “An all-solid-state reference electrode based on the layer-by-layer polymer coating,” *Analyst,* vol. 132, no. 9, pp. 906-912, 2007.

[57] R. W. Cattrall, D. M. Drew and I. C. Hamilton, “Some alkylphosphoric acid esters for use in coated wire calcium selective electrodes: Part I. Response characteristrics,” *Analytica Chimica Acta,* vol. 76, pp. 269-277, 1975.

[58] Y. F. Li and R. Y. Qian, “Stability of conducting polymers from electrochemical point of view,” *Synthetic Metals,* vol. 53, pp. 149-154, 1993.

[59] S. J. Dong, Z. S. Sun and Z. L. Lu, “Chloride chemical sensor based on an organic conducting polypyrrole polymer,” *Analyst,* vol. 113, pp. 1525-1528, 1988.

[60] K. Maksymiuk, J. Bobacka, A. Ivaska and A. Lewenstam, “Couple redox and pH potentiometric responses of electrodes coated with polypyrrole,” *Analytical Letters,* vol. 33, pp. 1339-1360, 2000.

[61] J. Bobacka, V. Vaananen, A. Lewenstam and A. Ivaska, “Influence of anionic addition of Hg2+ interfaces on Ag+-ISEs based on 2.2.2 p,p,p-cyclophane as neutral carrier,” *Talanta,*

vol. 63, pp. 135-138, 2004.

[62] M. Ocypa, A. Michalska and K. Maksymiuk, “Accumulation of Cu(II) cations in poly (3,4-ethylenedioxythiophene) films doped by hexacyanoferrate anions and its application in Cu2+ selective electrodes with PVC based membranes,” *Electrochimica Acta,* vol. 51, pp. 2298-2305, 2006.

[63] H. Shirakawa, E. J. Louis, A. G. Macdiarmid, C. K. Chiang and A. J. Heeger, “Synthesis of electrically conducting organic polymers: Halogen derivatives of polyacetylene (CH)x,” *Journal of the Chemical Society - Chemical Communications,* pp. 578-580, 1977.

[64] J. Heinze, “Electronically conducting polymers,” *Topics in Current Chemistry,* vol. 152, pp. 1-47, 1990.

[65] K. J. Kim, H. S. Song, J. D. Kim and J. K. Chon, “Mechanism of electropolymerization of pyrrole in acidic aqueous solutions,” *Bulletin of the Korean Chemical Society,* vol. 9, pp. 248-251, 1988.

[66] E. M. Genies, G. Bidan and A. F. Diaz, “Spectroelectrochemical study of polypyrrole films,” *Journal of Electroanalytical Chemistry,* vol. 149, pp. 101-113, 1983.

[67] S. Asavapiriyanont, G. K. Chandler, G. A. Gunawardena and D. Pletcher, “The electrodeposition of polypyrrole films from aqueous solutions,” *Journal of Electroanalytical Chemistry,* vol. 177, pp. 229-244, 1984.

[68] Y. J. Qiu and J. R. Reynolds, “Electrochemicaly initiated chain polymerization of pyrrole in aqueous media,” *Journal of Polymer Science Part A-Polymer Chemistry,* vol. 30, pp. 1315-1325, 1992.

[69] G. B. Street, “Polypyrrole: From powders to plastics,” in *Handbook of Conducting Polymers*, New York, Marcel Dekker, 1986.

[70] B. L. Groenendaal, F. Jonas, D. Freitag, H. Pielartzik and J. R. Reynolds, “Poly(3,4-ethylenedioxythiophene) and its derivatives: Past, present and future,” *Advanced Materials,* vol. 12, pp. 481-494, 2000.

[71] M. Dietrich, J. Heinze, G. Heywang and F. Jonas, “Electrochemical and spectroscopic characterization of polyalkylenesioxythiophenes,” *Journal of Electroanalytical Chemistry,* vol. 369, pp. 87-92, 1994.

[72] S. Kirchmeyer and K. Reuter, “Scientific importance, properties and growing applications of poly (3,4-ethylenedioxythiophene),” *Journal of Materials Chemistry,* vol. 15, pp. 2077-2088, 2005.

[73] L. Groenendaal, G. Zotti, P. H. Aubert, S. M. Waybright and J. R. Reynolds, “Electrochemistry of poly(3,4-alkylenedioxythiophene) studied by current sensing atomic force microscopy,” *Advanced Materials,* vol. 15, pp. 855-879, 2003.

[74] M. Vazquez, J. Bobacka, A. Ivaska and A. Lewenstam, “Influence of oxygen and carbon dioxide on the electrochemical stability of poly (3,4-ethylenedioxythiophene) used as ion to electron transducer in an all solid state ion selective electrodes,” *Sensors and*

Actuators B - Chemical, vol. 82, pp. 7-13, 2002.

[75] H. Xu, Y. Pan, Y. Wang, G. Li, Y. Chen and Y. Ye, "An all solid state screen printed carbon paste reference electrode based on poly(3,4-ethylenedioxythiophene) as a solid contact transducer," *Measurement Science and Technology,* vol. 23, no. 12, pp. 125101-125102, 2012.

[76] N. Sakmeche, S. Aeiyach, J. J. Aaron, M. Jouini, J. C. Lacroix and P. C. Lacaze, "Improvement of the electrosynthesis and physiochemical properties of poly (3,4-ethylenedioxythiophene) using sodium dodecyl sulfate micellar aqueous medium," *Langmuir,* vol. 15, pp. 2566-2574, 1999.

[77] J. Park, J. Kim and Y. Son, "Conducting polymer micro-tubules hosting electroactive species without guest modification," *Synthetic Metals,* vol. 156, pp. 714-720, 2006.

[78] D. H. Han, J. W. Kim and S. M. Park, "Electrochemistry of conducting polymers 38: Electrodeposited poly (3,4-ethylenethiophene) studied by current sensing atomic force microscopy," *Journal of Physical Chemistry B,* vol. 110, pp. 14874-14880, 2006.

[79] X. J. Wang and K. Y. Wong, "Effects of a base coating used for electropolymerisation of poly (3,4-ethylenedioxythiophene) on indium tin oxide electrode," *Thin Solid Films,* vol. 515, pp. 1573-1578, 2006.

[80] J. Y. Yang, K. Lipkin and D. C. Martin, "Electrochemical fabrication of conducting polymer poly (3,4-ethylenedioxythiophene) (PEDOT) nanofibrils on microfabricated neural prosthetic devices," *Journal of Biomaterials Science-Polymer Edition,* vol. 18, pp. 1075-1089, 2007.

[81] T. A. Skotheim, R. L. Elsenbaumer and J. R. Reynolds, Handbook of Conducting Polymers (2nd Ed.), New York: Marcel Dekker Inc, 1998.

[82] Y. Sulaiman and R. Kataky, "Effect of monomer modifications on the physical properties of electropolymerised PEDOT films," *Journal of the Electrochemicsl Society,* vol. 159, no. 2, pp. F1-F9, 2012.

[83] J. Roncali, "Synthetic principles for bandgap control in linear pi-conjugated systems," *Chemical Reviews,* vol. 97, pp. 137-205, 1997.

[84] H. Nam and G. S. Cha, Biosensors and their applications, New York: Kluwer Academic/Plenum, 2000.

[85] E. Pretsch, M. Badertscher, M. Welti, T. Maruizumi, W. E. Morf and W. Simon, "Design features of ionophores for ion selective electrodes," *Pure and Applied Chemistry,* vol. 60, no. 4, pp. 567-574, 1988.

[86] M. C. Rose and R. W. Henkens, "Stability of sodium and potassium complexes of valinomycin," *Biochimica et Biophysica Acta - General Subjects,* vol. 372, no. 2, pp. 426-435, 1974.

[87] T. J. Marrone and K. M. Merz, "Molecular recognition of potassium ions by the naturally occuring antibiotic ionophore nonactin," *Journal of the American Chemical Society,* vol.

114, no. 19, pp. 7542-7549, 1992.

[88] L. R. Junior, G. D. Neto, J. L. F. C. Lima and M. C. B. S. M. Monenegro, "Construction and evaluation of an ammonium tubular ion selective electrode with ionophore nonactin," *Quimica Nova,* vol. 19, no. 5, pp. 549-553, 1996.

[89] P. R. Albert and A. H. Tashjian, "Ionomycin acts as an ionophore to release TRH-regulated Ca2+ stores from GH4C1 cells," *American Journal of Physiology,* vol. 251, no. 6, pp. C887-C891, 1986.

[90] S. N. Graven, O. S. Estrada and H. A. Lardy, "Alkali metal cation release and respiratory inhibition induced by nigericin in rat liver mitochondria," *Proceedings of the National Academy of Sciences,* vol. 56, no. 2, pp. 654-658, 1966.

[91] M. Pinkerton and L. K. Steinrauf, "Molecular structure of monovalent metal cation complexes of monensin," *Journal of Molecular Biology,* vol. 49, no. 3, pp. 533-546, 1970.

[92] "SigmaAldrich," [Online]. Available: http://www.sigmaaldrich.com/united-kingdom.html. [Accessed 12 June 2013].

[93] A. Kuras and N. Gutmaniene, "Technique for producing a carbon fibre microelectrode with the fine recording tip," *Journal of Neuroscience Methods,* vol. 96, pp. 143-146, 2000.

[94] B. Comeau, Plasticizer alternatives for use in polymer membrane ion selective electrodes, PhD Thesis, Tufts University, 2008.

[95] D. Budai and Z. Molnar, "Novel carbon fiber microelectrodes for extracellular electrophysiology," *Acta Biologica Szegendiensis,* vol. 45, pp. 65-73, 2001.

[96] M. Huser, P. M. Gehrig, W. E. Morf, W. Simon, E. Lindner, J. Jeney, K. Toth and E. Pungor, "Membrane technology and dynamic response of ion selective liquid membrane electrodes," *Analytic Chemistry,* vol. 63, no. 14, pp. 1380-1386, 1991.

[97] G. Q. Shi, J. K. Xu and M. X. Fu, "Raman spectroscopic and electrochemical studies on the doping level changes of polythiophene films during their electrochemical growth processes," *Journal of Physical Chemistry B,* vol. 106, pp. 288-292, 2002.

[98] W. E. Morf, D. Ammann and W. Simon, "Elimination of the anion interference in neutral carrier cation selective membrane electrodes," *Chimia,* vol. 28, pp. 65-67, 1974.

[99] R. E. Gyurcsanyi and E. Lindner, "Spectroscopic method for the determination of the ionic site concentration in solvent polymeric membranes and membrane plasticizers," *Analytical Chemistry,* vol. 74, no. 16, pp. 4060-4068, 2002.

[100] B. Paczosa-Bator, J. Peltonen, J. Bobacka and A. Lewenstam, "Influence of morphology and topography on potentiometric response of magnesium and calcium sensitive PEDOT films doped with adenosine triphosphate (ATP)," *Analytica Chimica Acta,* vol. 555, pp. 118-127, 2006.

[101] S. J. Konopka and B. McDuffie, "Diffusion coefficients of ferri- and ferrocyanide ions in aqueous media, using twin-electrode thin-layer electrochemistry," *Analytical Chemistry,*

vol. 42, no. 14, pp. 1741-1746, 1970.

[102] MMI, [Online]. Available: http://www.molecular-machines.com/products/mmi_cellector_plus/technology_51. [Accessed 15 July 2013].

[103] S.-H. Wang, T. C. Chou and C. C. Liu, "Development of a solid state thick film calcium ion-selective electrode," *Sensors and Actuators B - Chemical,* vol. 96, no. 3, pp. 709-716, 2003.

[104] W. Qin, R. Liang, X. Fu, Q. Wang, T. Yin and W. Song, "Trace-level potentiometric detection in the presence of a high electrolyte background," *Analytical Chemistry,* vol. 84, pp. 10509-10512, 2012.

[105] A. R. L. Fraga, J. C. Quintana, G. L. Destri, N. Giamblanco, R. G. Toro and F. Punzo, "Polymeric membranes conditioning for sensors applications: mechanism and influence on analytes detection," *Journal of Solid State Electrochemistry,* vol. 16, pp. 901-909, 2012.

[106] E. Lindner and R. E. Gyurcsanyi, "Quality control criteria for solid-contact, solvent polymeric membrane ion-selective electrodes," *Journal of Solid State Electrochemistry,* vol. 13, pp. 51-68, 2009.

[107] E. Lindner and R. P. Buck, "Microfabricated potentiometric electrodes and their in vivo applications," *Analytical Chemistry,* vol. 72, no. 9, pp. 336A-345A, 2000.

[108] S. Joo and R. B. Brown, "Chemical sensors with integrated electronics," *Chemical Reviews,* vol. 108, no. 2, pp. 638-351, 2008.

4.0 CALIBRATION AND CHARACTERISATION OF THE MICROGRIPPER SENSOR DEVICE

This chapter focusses on testing the microgripper sensor devices. The devices are calibrated and characterised in controlled solutions; characterisation includes the determination of the detection limits, response times, selectivity coefficients, potential drift and hysteresis measurements.

There is a growing need for a sensor device that is produced via cost effective manufacturing and that can work without, or with minimal, calibration for analysis in minute volumes. Most research concentrates on developing single use planar ion selective electrodes (ISEs) to achieve this. Many research groups have developed multifunctional sensing devices for biological and chemical analysis [1] [2] [3]; point of care testing [4]; clinical and forensic analysis [5] [6] and molecular diagnosis and drug delivery [7] [8].

To be capable of *in vivo* monitoring the device needs to be sterilisable and all the parts of the sensor must be biocompatible; the sensors must also operate with excellent stability in that there must be negligible potential drift within the experiment's time frame.

4.1 Calibration

The calibration plot displays the ISE cell potential against the logarithm of the ionic activity of the analyte of interest. For historical reasons the measured potential is typically referred to as the electromotive force (EMF). It is important that, during calibration, constant ionic strength is maintained as the activity of the analyte, when determined from its concentration, is dependent on the ionic strength of the whole solution. A typical calibration plot is shown in Figure 4.1.

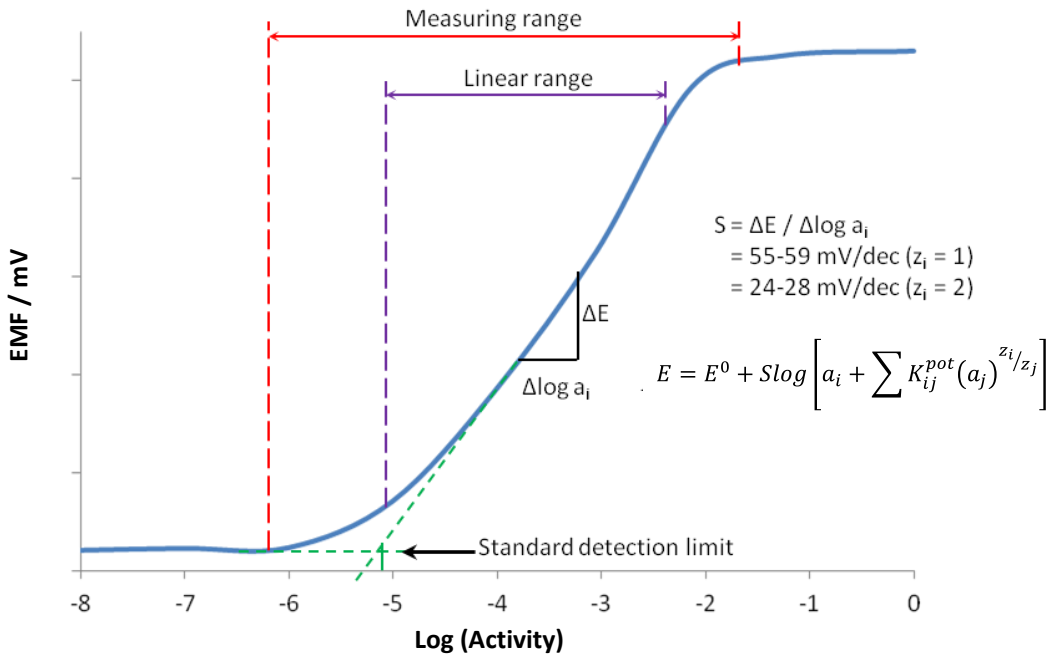

Figure 4.1 – Typical calibration plot of an ISE.

The linear range is defined as the part of the calibration curve where the data points do not deviate from linearity by more than 2 mV [9]. This is the useful working range of the ISE sensor as the linear relationship between the analyte concentration and EMF can be used to quantify the concentration of unknown solutions. The source of this limited working range for neutral and charged carrier based polymeric membranes is related to minor ionic fluxes across the membrane [10] [11]. The total measuring range includes the linear range plus the upper and lower curved portions. The upper curve occurs due to interference of the ISE response to the analyte of interest by the anions in the calibration solution. The lower curve occurs because the ISE response to the changing activity of the analyte of interest is altered by the presence of interfering ions in the calibration solution. With an increase in the interference of these interfering cations (or anions) with the ISM, the curve will begin at a higher (or lower) concentration. While unknown samples can be measured in this range, a highly accurate and repeatable calibration plot is required.

If the ISE is behaving ideally (i.e. the membrane fully discriminates the primary ion), the electrode response follows Nernstian behaviour. However, in reality, interfering ions

compete with the primary ion, and are extracted into the membrane. This means that the potential of the ion selective membrane (ISM) is governed by both the activity of the ion of interest and the interfering ion. This causes deviation from the expected Nernstian electrode response. The Nicolsky-Eisenman equation (Equation 4.1), a modification of the Nernst equation, accounts for the selectivity of the membrane and is a more accurate representation of the electrode behaviour.

$$E = E^0 + \frac{2.303RT}{z_i F} log\left[a_i + \sum K_{ij}^{pot}\left(a_j\right)^{z_i/z_j}\right]$$

Equation 4.1

where E is the measured EMF (V);

E^0 is the standard electrode potential (V);

R is the gas constant (J K^{-1} mol^{-1});

T is the temperature (K);

z_i and z_j is the valency of the ion of interest and the interfering ion respectively;

F is Faraday's constant (C mol^{-1});

a_i is the activity of the ion of interest;

K_{ij}^{pot} is the selectivity coefficient;

a_j is the activity of the interfering ion.

4.1.1 Flow Cell

A flow cell was specially designed around the L-shaped microgripper holder. This is shown in Figure 4.2. There is space underneath the microgripper to include a magnetic stirrer bar which, coupled with the offset liquid inlet and outlet, allows for effective mixing.

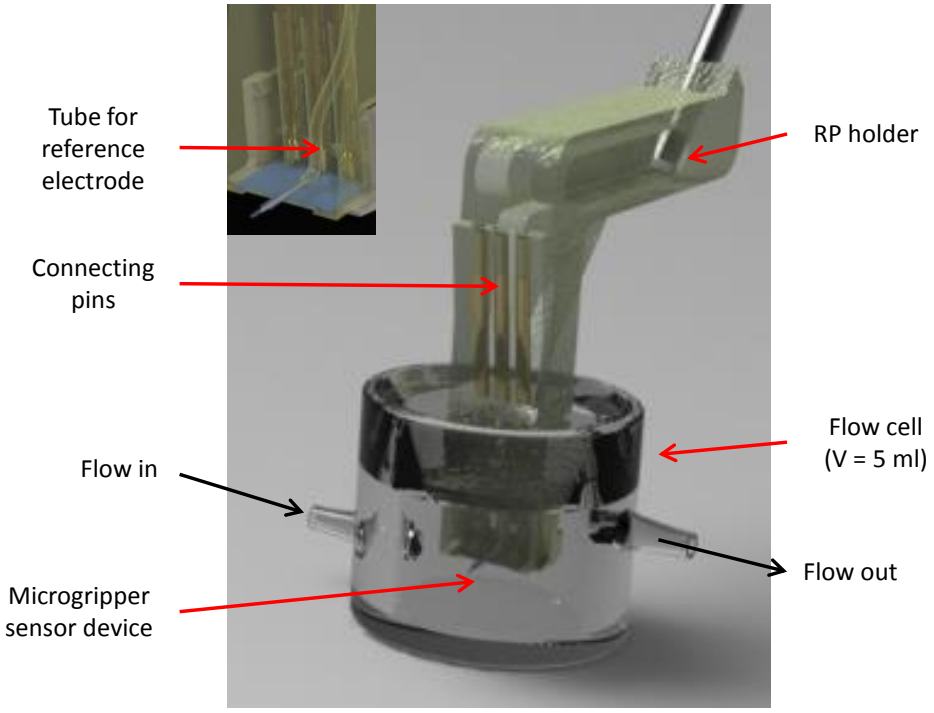

Figure 4.2 – Specially designed flow cell to incorporate L-shaped microgripper holder. Insert shows tubing within which the reference electrode was fed.

The flow cell is used in the set up of the constant dilution technique used to calibrate the ion selective electrodes (ISEs). An Aladdin syringe pump is connected to the flow cell within which the ISE and the solid silver-silver chloride reference electrode (RE) are contained. An Ivium potentiostat was used in potentiometry mode to record the voltage between the ISE and RE at set time intervals suitable for the investigation.

Starting with a solution containing the analyte of interest, A, at a concentration C_0 that is diluted by a solution that does not contain analyte A, the concentration of analyte A at any time point can be calculated as follows.

Assuming that in a well mixed cell the rate of accumulation = rate in – rate out + generation:

$$V\frac{dC}{dt} = 0 - qC + 0 = -qC$$

Equation 4.2

Rearranging Equation 4.2 gives:

$$\frac{dC}{C} = -\frac{q}{V}dt$$

Equation 4.3

Integrating Equation 4.3 gives:

$$ln\left(\frac{C}{C_0}\right) = -\frac{q}{V}(t - t_0)$$

Equation 4.4

Rearranging Equation 4.4 to calculate the concentration gives:

$$C = C_0 exp\left[-\frac{q}{V}(t - t_0)\right]$$

Equation 4.5

where C is the concentration of analyte A at time t (M);

C_0 is the initial concentration of analyte A (M);

t is the time (s);

t_0 is the time when dilution started (s);

q is the flow rate of the dilutent (mL s^{-1});

V is the volume of the flow cell (mL).

Equation 4.5 is used assuming that there is a constant volume within the flow cell and a constant flow rate of electrolyte through the flow cell. It is therefore important that the flow cell is completely sealed, as any leakage will affect both the volume and the flow rate parameters.

4.2 Characterisation

4.2.1 Detection Limit

The detection limit is defined as the concentration at which the extrapolated linear mid-range and final low concentration portions of the calibration plot cross, as indicated in Figure 4.1 [12]. The reliability of the detection limit determined via this method depends on the standard deviation of a single potential measurement, the number of data points in the

linear sections and the concentration range used. It is also important to remember that experimental conditions (such as composition of the solution, preconditioning of the ISEs, stirring rate and temperature) can affect the detection limit. These conditions should be stated when stating the detection limit for a specific device. Generally detection limits are in the order of 10^{-5} – 10^{-6} M for most ISEs unless specific modifications have been made (as mentioned previously) to enhance them.

4.2.2 Response Time

The response time is defined as the time which elapses between the instant when an ISE is brought into contact with the analyte and the first instant at which the slope of the EMF against time plot ($\Delta E/\Delta t$) becomes equal to a limiting value [12].

Another definition is that it is the time taken to achieve 95% of the change of potential when an ISE is placed into an analyte solution and it reaching its maximum potential. While this can underestimate response times with small potential spans, it is often more practical in non-static environments. As the microgripper sensor devices are being used to measure changes in analyte activity (i.e. a non-static system) this method is more relevant to this work.

4.2.3 Selectivity Coefficients

The selectivity coefficient defines the ability of an ISE to distinguish the analyte of interest from others, known as interfering ions [12]. The smaller the value of the selectivity coefficient the greater the electrode's preference is for the analyte of interest; in general a negative value indicates the preference of the ISE to the analyte of interest and a positive value indicates the preference of the ISE to the interfering ion. There are three main methods for determining the selectivity coefficient of an ISE: fixed interference method, separate solution method and matched potential method [13].

4.2.3.1 Fixed Interference Method

The fixed interference method's main advantage over the separate solution method is that it is deemed generally more accurate for a larger variety of systems, giving coefficients that translate fairly well to many observed selectivity performances. However, it cannot account for multiple ion-ion interactions, and so can be a poor match in performance for many physiological fluids that contain multiple ions (for example, serum and blood) [13] [14].

The selectivity coefficient is determined as follows. The EMF of a cell containing the ISE and a RE is measured for a solution containing a constant activity of interfering ion, a_B, and varying the activity of the analyte of interest, a_A. This can be done using the same constant dilution technique used to determine the calibration plot described previously, but where the analyte of interest is diluted at a constant rate by the interfering ion. In this case the initial concentration of the interfering ion should be the same as the analyte. The intersection of the extrapolated linear portions of this plot determine the limiting value of a_A used to calculate the selectivity coefficient from the Nickolsky-Eisenmann equation, as shown in Figure 4.3:

$$K_{A,B}^{pot} = \frac{a_A}{a_B^{\,z_A/z_B}}$$

Equation 4.6

where $K_{A,B}^{pot}$ is the selectivity coefficient;

a_A is the limiting activity of the analyte of interest;

a_B is the activity of the interfering ion;

z_A is the charge of the analyte of interest;

z_B is the charge of the interfering ion.

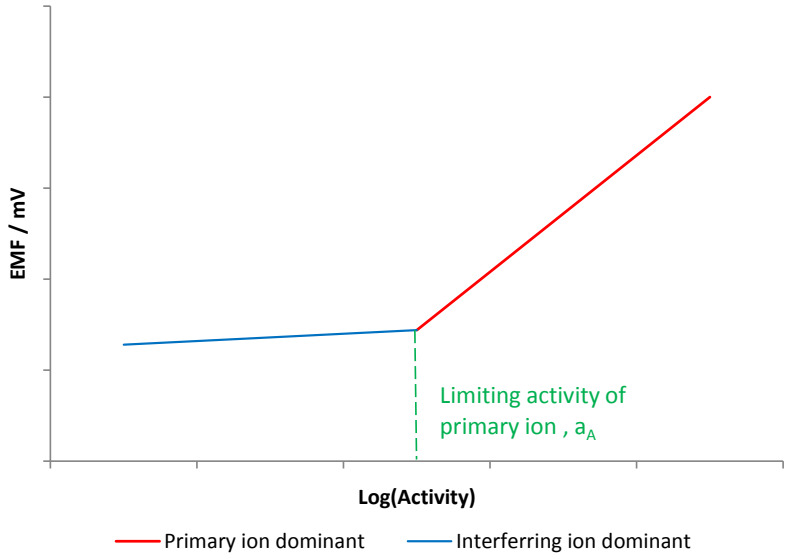

Figure 4.3 – Schematic of the plot for determining the selectivity coefficient using the fixed interference method.

The fixed interference method of determining the selectivity coefficient gives a dynamic selectivity coefficient value that is dependent on experimental conditions, such as the flow rate and cell geometry, though the data generated is generally accepted to be more accurate [9].

4.2.3.2 Matched Potential Method

This method does not depend on the Nicolsky-Eisenman equation; instead the selectivity coefficient is determined as the ratio of the activity of the primary and interfering ions that give the same EMF under identical conditions [15]. The selectivity coefficient is determined as follows. A solution of known activity of the primary ion is added to a reference solution of primary ions of known activity, and the corresponding change in potential is recorded. A solution of interfering ions is then added to a reference solution of primary ions of the same activity as previously until the corresponding change in potential equals that measured for the primary ion. The selectivity coefficient is then calculated using the following equation:

$$K_{A,B}^{pot} = \frac{(a_A^{'} - a_A)}{a_B}$$

Equation 4.7

where $K_{A,B}^{pot}$ is the selectivity coefficient;

a_A' is the activity of the primary ion in the reference solution;

a_A and a_B are the activities of the primary and interfering ions required to measure the same change in potential.

4.2.3.3 Separate Solution Method

The selectivity coefficient is determined as follows. The EMF of a cell containing the ISE and a RE is measured for two separate solutions. One containing the analyte of interest with activity a_A but no interfering ion; and the other containing the interfering ion of the same activity (i.e. $a_B = a_A$) but contains no analyte of interest. The selectivity coefficient is then calculated from the equation:

$$logK_{A,B}^{pot} = \frac{(E_B - E_A)z_A F}{2.303RT} + \left(1 - \frac{z_A}{z_B}\right) loga_A$$

Equation 4.8

where $K_{A,B}^{pot}$ is the selectivity coefficient;

E_A and E_B are the potentials of the analyte of interest and interfering ion respectively (V);

z_A and z_B are the valencies of the analyte of interest and interfering ion respectively;

F is Faradays constant (C mol^{-1});

R is the gas constant (J K^{-1} mol^{-1});

T is the temperature (K).

4.2.4 Potential Drift and Hysteresis

Potential drift is determined as the slow non-random change of EMF with time of an ISE in a solution of constant composition and temperature [12]. Most publications simply state

that an ISE with high stability is desirable. A specific value of what high potential stability relates to is seemingly dependent on the application in question. Long term measurements in implanted blood sensing devices indicate that high potential stability consists of a drift of less than 0.2 mV hr^{-1} [16].

Hysteresis is defined as the shift in EMF measured in a solution of a known concentration and that of a second measurement in the same solution after the ISE has been exposed to a solution of the same ion at a different concentration [12]. Hysteresis is generally in the direction of the concentration in which the ISE was previously exposed. Hysteresis is also referred to as electrode memory and is thought to be a kinetic process where the response is normally reversible when sufficient time is allowed for the system to return to its initial condition, as long as there is suitable bulk concentration of membrane components available.

4.3 Microgripper Ion Selective Electrode Sensor Characterisation

Concentration was converted into activity using the following equation:

$$a = \gamma C$$

Equation 4.9

where C is the concentration (M);

γ is the activity coefficient (M^{-1});

a is the activity of the analyte.

The activity coefficients, which adjust for the non ideality of the electrolye solutions, were calculated using the extended Debye-Hückel equation [17]:

$$log\gamma_{\pm} = \frac{-A|z_+z_-|\sqrt{I}}{1 + B\sqrt{I}} + CI$$

Equation 4.10

where γ is the activity coefficient;

$|z_+z_-|$ is the absolute product of valencies;

I is the ionic strength (M);

A is a constant (0.5108 at 298 K);

B and C are empirical parameters given in Table 4.1 [18].

Table 4.1 – Empirical parameters B and C for the electrolytes used in this study **[18]**.

Electrolyte	**Empirical Parameter**	
	B	C
NaCl	1.4255	0.02626
KCl	1.2796	0.00393
$CaCl_2$	1.5800	0.04570
$MgCl_2$	1.7309	0.05195

The ionic strength was calculated using the following equation:

$$I = \frac{1}{2}\sum c_i z_i^2$$

Equation 4.11

where I is the ionic strength (M);

c_i is the concentration of ion i (M);

z_i is the charge of ion i.

4.3.1 Experimental

All experiments were carried out at room temperature using chemicals obtained from Sigma Aldrich and were used without further purification. The ISE fabricated onto the microgripper device was used to record the potential against a solid silver|silver chloride reference electrode using an IVIUM potentiostat. The RE was attached onto the rapid prototyped (RP) holder to ensure that the distance between the electrodes remained constant throughout all experiments.

All ISE calibrations were done using the flow set up described in Section 4.1.1. Ca^{2+} ISE calibrations were done with 0.1 M $CaCl_2$ + 1 mM KCl solution. A 1 mM KCl solution was flowed through the system to dilute the concentration of calcium ions. A flow rate of 0.046 mL s^{-1} was

used for the multi-use device study, and 0.037 mL s^{-1} was used for the wafer comparison study. K^+ ISE calibrations were done with 0.1 M KCl + 1 mM NaCl solution, diluted with a 1 mM NaCl solution at a flow rate of 0.0146 mL s^{-1}. Na^+ ISE calibrations were done with 0.1 M NaCl + 1 mM KCl solution, diluted with 1 mM KCl solution at a flow rate of 0.046 mL s^{-1}. EMF measurements were recorded every 0.5 s using an IVIUM potentiostat.

The Ca^{2+} ISE potential drift measurements were done in a static solution of 0.01 M $CaCl_2$ using an unconditioned device, a conditioned device and a device that had already been used for calibration measurements (used device). EMF measurements were recorded every 60 s using an IVIUM potentiostat.

The Ca^{2+} ISE water layer tests were done with static solutions of 0.1 M $CaCl_2$ and 0.1 M KCl. First the microgripper sensor device and RE was placed into a solution of 0.1 M $CaCl_2$ and left for 5 hours. The solution was then changed for 0.1 M KCl and left for a further 9 hours. The solution was finally replaced by 0.1 M $CaCl_2$ and left for 5 hours. EMF measurements were recorded every 60 s using an IVIUM potentiostat.

All ISE hysteresis measurements were done with 0.1 and 1 mM solutions of the chloride salt of the analyte of interest. The potential was recorded in a static solution at a concentration of 0.1 M until it stabilises, then the solution was removed and replaced with a 1 mM one. Once the plot had restabilised, the solution was replaced with a fresh solution at a concentration of 0.1 M. EMF measurements were recorded every 60 s using an IVIUM potentiostat.

The Ca^{2+}, K^+ and Na^+ ISE response time experiments were carried out in a static background of 1 mM KCl, NaCl and KCl respectively. A 1 ml drop of 0.01 M solution of the analyte chloride salt was added onto the microgripper sensor and the resulting response recorded. EMF measurements were recorded every 0.1 s using an IVIUM potentiostat.

All selectivity studies were carried out using the fixed interference method using the flow cell set up described in Section 4.1.1. A 0.1 M solution of the chloride salt of the analyte of interest was diluted with a 0.1 M salt of the chloride salt of the interfering ion. For the Ca^{2+} ISE selectivity studies a flow rate of 0.046 mL s^{-1} was used; and for the K^+ and Na^+ ISEs a flow rate of 0.037 mL s^{-1} was used. EMF measurements were recorded every 0.5 s using an IVIUM potentiostat.

4.3.2 Ca^{2+} Ion Selective Electrodes

4.3.2.1 Calibration

Figure 4.4 shows the calibration plots of a single microgripper sensor device repeated several times over several days. The device was calibrated three times immediately after one another, and then left in 0.1 M $CaCl_2$ conditioning solution overnight before repeating. This was done for three consecutive days.

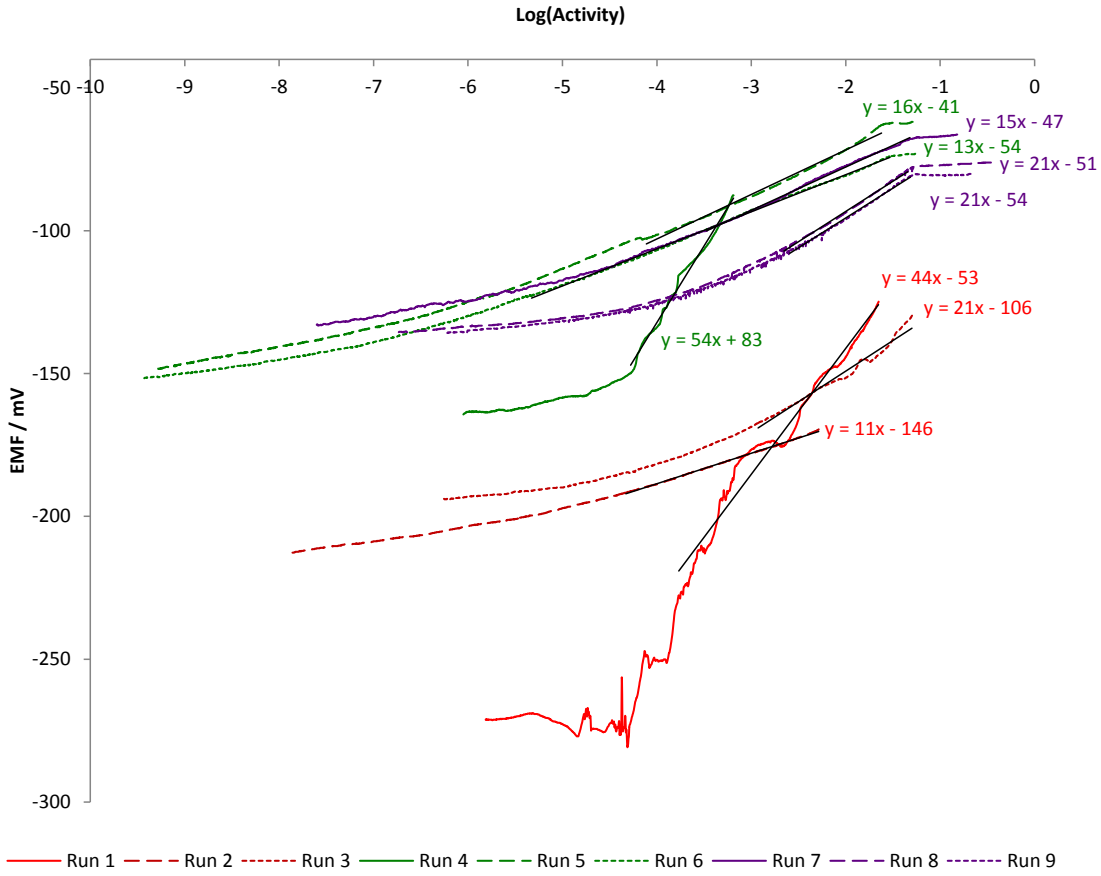

Figure 4.4 – Ca^{2+} ISE device multi use study (the black line on each trace indicates and in some cases exaggerates the linear portion).

It can clearly be seen from Figure 4.4 that the calibration response from the device changes dramatically with each use. Between runs 1, 2 and 3 (the calibration repeats done immediately after one another) a large decrease in the slop of the linear portion of the plot can be seen. This indicates the electrode is deviating further from ideal behaviour (ideal behaviour for a divalent ion is a slope of 29.5 mV per decade). Overnight conditioning seems to reverse the response near to its original behaviour, indicating that there is a dramatic loss of the Ca^{2+} ions during the calibration process, which are re-incorporated into the ISM during conditioning. A similar pattern is seen between the consecutive runs on day two (runs 4, 5 and 6) as for day one. By day three (run 7), however, even conditioning overnight does not yield a similar response as for the first run. Interestingly, it does seem that the device itself is more stable to loss of ions between the consecutive runs (runs 7, 8 and 9), as similar slope responses

are observed, even though the absolute potentials are quite different. A summary of this is given in Table 4.2.

It should be noted here that two of the runs (Run 1 and Run 4) gave greater than Nernstian slopes. This is likely due to a combination of factors. Firstly, that the ISM has a non-smooth surface; and secondly a complex ion-pair association occurring between the analyte and ionophore. It has been observed that the differing complex stabilities can give rise to super- or sub-Nernstian responses [19].

Table 4.2 – Ca^{2+} ISE device multi use study data.

		Run 1	**Run 2**	**Run 3**
Day one	Slope / mV/dec	44	10.7	21.4
(Red	Limit of detection / M	1.1×10^{-5}	1.3×10^{-5}	2.1×10^{-5}
traces)	EMF at 0.01 M / mV	-125.8	-167.9	-129.7
		Run 4	**Run 5**	**Run 6**
Day two	Slope / mV/dec	53.6	15.6	13
(Green	Limit of detection / M	4.0×10^{-5}	4.3×10^{-6}	4.7×10^{-7}
traces)	EMF at 0.01 M / mV	-	-62.9	-73.0
		Run 7	**Run 8**	**Run 9**
Day three	Slope / mV/dec	15.3	21.2	20.9
(Purple	Limit of detection / M	3.2×10^{-5}	2.5×10^{-4}	3.3×10^{-4}
traces)	EMF at 0.01 M / mV	-67.8	-76.6	-80.1

It is well known that small, planar sensors, like that of the microgripper sensors device, are quite delicate devices with fragile membranes of a few micrometres thickness, containing nanogram active components [20]. Delamination or perforation of membranes like this have been observed, which results in complete sensor loss. This is an unlikely scenario in the case of the data shown in Figure 4.4 as even the poorer electrode calibration plots still show near-Nernstian behaviour responses. It is also possible to get dissolution of the membrane components into the sample solution over time; this in turn then changes the ionic site:ionophore ratio, resulting in an observed loss in selectivity and sensitivity, increased membrane resistance, worse detection limits and increased noise. While a loss is selectivity

cannot be commented on at this juncture, a loss in sensitivity is definitely seen. Additionally, there is a general trend in worsening detection limits with each repeat, as seen in Table 4.2. Even conditioning the devices overnight does not fully retain their original detection limit. It is likely, therefore, that this general decline in electrode response with repetition is due to leaching of the membrane components during the calibration process.

Leaching has been observed in literature to be very significant when microfabricated electrodes are exposed to large solution volumes. Experimental evidence shows that less lipophilic salt derivatives, such as tetraphenyl borate ions (TPB^-), are rapidly lost from carrier-free PVC when first in contact with water [21]. It is unsurprising that this is the effect observed for the microgripper sensing device, even though tetrakis (4-chlorophenyl) borate ions ($TpClPB^-$) are used within the ISM, which are slightly more lipophilic than TPB^-. Additionally, it has been observed that adhesion strength between the sensing membrane and the solid support can deteriorate over time, once exposed to aqueous solutions [22], suggesting that, eventually, re-use of these devices would result in complete sensor loss.

However, calibration does not have to be done for each device. As microfabrication can produce identical sensors, calibration of a limited number of devices from a batch should be adequate to characterise the response function of the whole batch [16]. The MEMS fabrication of the microgripper device, and hence the electrode at the tip, yields an almost perfect replication of devices across each wafer. The only slight difference between these devices is the surface area of the electrode, due to the metal etching process. This slight difference in electrode surface area of each device means that the electropolymerisation of EDOT is not identical. The current magnitude of the PEDOT redox peak observed in the cyclic voltammogram of the electropolymerisation process is directly proportional to the concentration of PEDOT present on the electrode (as shown in Equation 4.12).

$$I_{ss} = 4nzFDCr$$

Equation 4.12

where n is the number of microelectrodes;

F is Faraday's constant (C mol^{-1});

D is the diffusion coefficient (m^2 s^{-1});

C is the concentration (M);

z is the ion valency;

r is the electrode radius (m).

Table 4.3, which summarises the responses of the different devices, records the steady state current for the PEDOT redox peak for each device. This shows that the changes in electrode surface area are small, as the steady state current (and hence the concentration of PEDOT deposited) only has a deviation of 12 %. It can therefore be concluded that the fabrication of the microgripper sensor device is identical up to the PEDOT deposition for all devices on a wafer.

The ISM deposition, however, is much more varied. Given the lack of automation of the drop-deposition technique, there is a large difference in the membrane surface area, thickness and morphology between devices. Any differences between devices are therefore likely to be due to the membrane.

Table 4.3 – 50 µm Ca^{2+} ISE comparison across a wafer study data.

	PEDOT CV steady state current / µA	**Slope / mV/dec**	**Limit of Detection / M**	**Potential at 0.1 M / mV**
Holder 2	0.13	18	6.7×10^{-5}	-129
Holder 3	0.11	15	1.4×10^{-5}	-182
Holder 4	0.10	12	2.4×10^{-6}	-80
Holder 5	0.10	11	4.6×10^{-6}	-106
Holder 6	0.12	16	8.7×10^{-6}	-153

Figure 4.5 shows the responses of 5 different devices from the same fabrication wafer, the data for which is summarised in Table 4.3 (it should be noted that a value for the potential

at 0.1 M is given here rather than at 0 M because the devices were conditioned in 0.1 M solutions and that the PEDOT steady state current was recorded during its deposition).

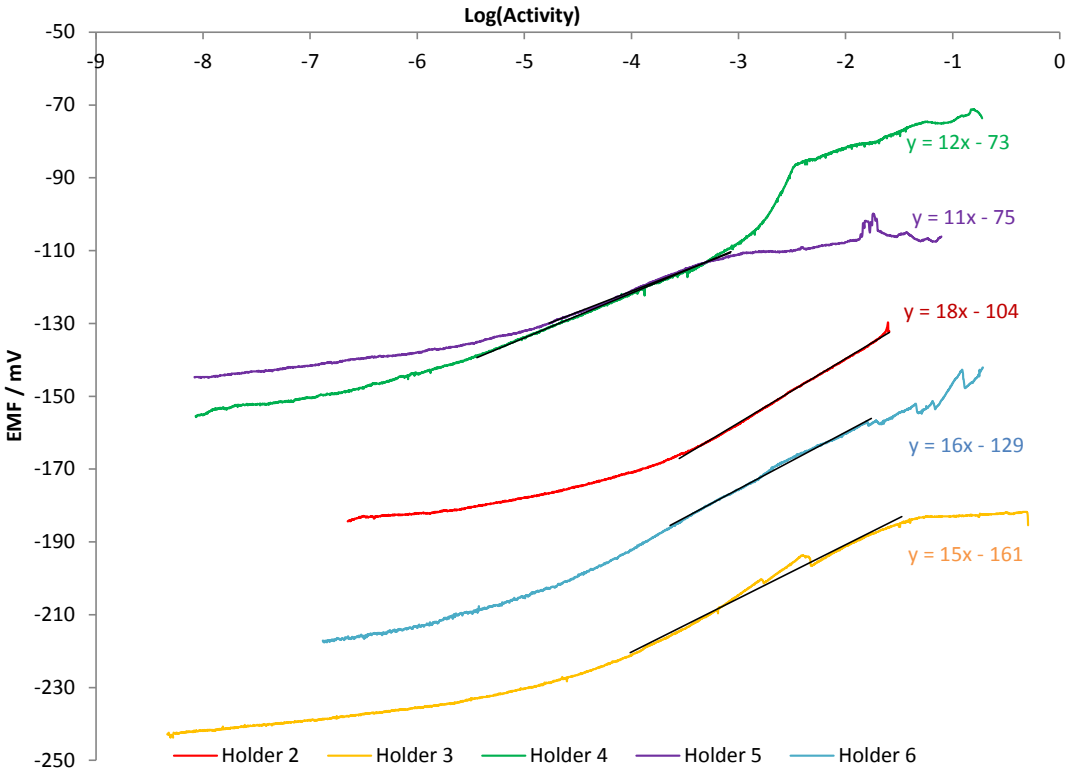

Figure 4.5 – 50 µm Ca^{2+} ISE comparison across a wafer study.

It can be seen from Figure 4.5 that the repeatability of the microgripper sensor devices is better for individual devices of the same fabrication wafer, than for the same device used more than once. Although the absolute EMF values vary between devices the slope response and detection limits for each device are similar within random experimental error (standard deviation).

The expected ideal slope response for a calcium ISE (a divalent ion) is 29.5 mV/dec at 298 K. The slope responses of the devices shown in Figure 4.5 show a sub-Nernstian response of 14 ± 4 mV/dec. Sub-Nernstian responses could be due to the non-smooth surface of the ISM, or more likely, when ion-pair association is taking place within the membrane [23]. The analyte ion does not always form a single type of complex with the ionophore within the membrane (as assumed for Nernstian behaviour); simultaneous formation of different

combinations with differing complex stabilities can give rise to super- or sub-Nernstian responses, depending on the complex formed [19]. The ISM components could be leaching from the device during conditioning, and hence varying the type of coordinating complexes at this stage. This would explain why a sub-Nernstian response is observed in this case when previous cases using the same composition observed ideal behaviour. Alternatively, the large deviation from Nernstian behaviour could relate to the more simplistic phase boundary model being implemented (Section 3.2.1.1), which assumes that the sensitivity of the sensor is time independent. While the complex model (Section 3.2.1.2) only has a small impact on the membrane potential, it has been used to demonstrate a link between poor selectivities and detection limits (and hence sensitivity) with an increase in surface concentration of the primary ion [24]. Given the planar dimensions of the microgripper sensor device, a high surface concentration of primary ion will be present, potentially explaining the very sub-Nernstian responses.

Another factor that could affect the microgripper sensor response is through an interaction between the device fabrication materials, including any contamination products occurring at the tip release stage, and the ISM. While these interactions, and hence resultant potentials, can be assumed to be constant, meaning that the phase boundary model still stands, their presence could explain the large deviance from ideal Nernstian behaviour. Specifically, the possible interactions with the SU8 building polymer and any complexed fluoride contamination from the XeF_2 silicon etch are a concern.

Additionally, incomplete coverage of the ISM should also be considered as breaks in the membrane would remove the selectivity of the device, and so the sensitivity would be defined by a mixture of mono- and divalent ions.

Data in Table 4.3 also indicates that there is a relationship between the PEDOT deposition thickness and the ISE slope response. Greater steady state currents observed in the

CV of the PEDOT deposition, and hence higher deposited PEDOT concentrations, relate to Nernstian slope response that is closer to ideal behaviour. This could mean that the thickness and morphology of the transducer layer is also contributing to the observed sub-Nernstian responses of the microgripper sensor devices.

The differences in absolute potential are likely to be a complex combination of both the PEDOT deposition and the ISM thickness, with additional factors such as surface morphology of all layers also playing a role. Potential stability of conducting polymer based sensors is often determined by spontaneous changes in the composition of the conducting polymer film. Additionally these potential instabilities could be due to the spontaneous formation of a water layer between the conducting polymer and the ISM [25]. With a thin water layer between the conducting polymer and the ISM, ASSISEs behave similarly to liquid ISEs but with an inadequate inner reference element (i.e. no reversible phase boundary potential). A water layer can also cause drift due to transport of small molecules, such as CO_2, O_2, NH_3, through the membrane changing the composition of the aqueous film.

It is widely accepted that the slope response of an ISE should remain constant, but that the EMF offset may drift between devices [16]. It is believed that this drifting offset indicates changes in the membrane due to: ion exchange processes occurring in the presence of high interfering ions in the sample; anion co-extraction in highly concentrated samples or in the presence of lipophilic anions; decomposition of the ionophore and/or added ionic sites; and leaching of membrane components into the sample solution.

The limit of detection (LOD) of the microgripper sensor devices varies slightly between devices on the same wafer, as seen in Table 4.3. This is likely due to the differing thickness of the ISM layer increasing its capacitive effect and affecting the ISE response time. Traditionally the LOD is directly dependent on the structure of the tetraphenylborate salt used (the more

lipophilic the salt the lower the LOD) [26] which, given the same solution composition of ISM is used for all devices, should not vary in this case.

The consistency of the electrode behaviour i.e. the magnitude of slope, (which was the same ± 4mV) means that one device on a wafer set can be calibrated and all others from that set assumed to have the same behaviour. Absolute potentials of the devices do vary, and so a normalisation point is needed. For example, if the potential at 10^{-2} M were known the y-intercept of the plot can be determined, so the absolute potentials for all concentrations within the linear region will be known. Concentration measurements outside the linear region cannot be determined via this method. Instead a measurement of how the potential changes from moving from one solution to another (hysteresis) can be used to shift the calibration slope accordingly.

4.3.2.2 Potential Drift and Conditioning Profiles

It is generally not considered important to measure and record how an ASSISE behaves during conditioning. However, for micro (and nano) ISE devices to be viable for use in analytical research laboratories and/or commercial devices with single use measurements in mind, this information is important to ensure performance characteristics are kept consistent [27].

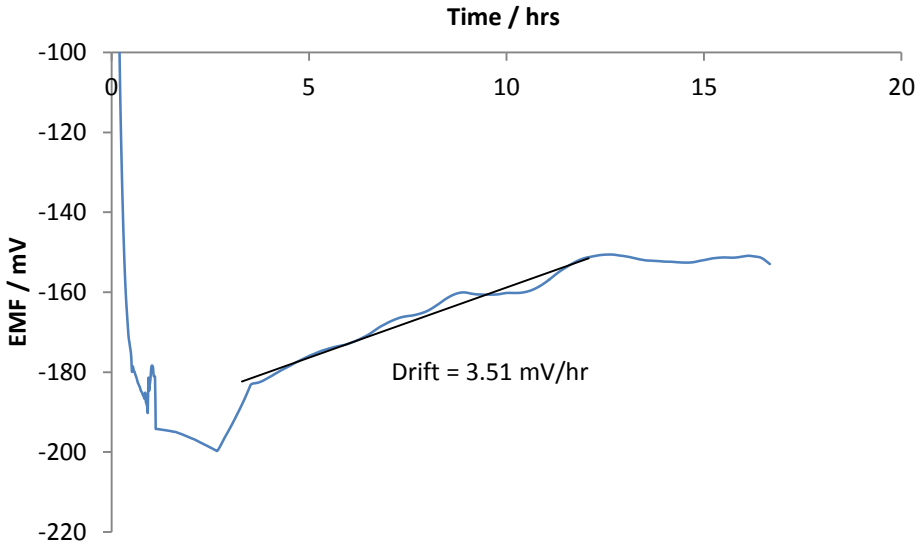

Figure 4.6 – Potential drift in a non-conditioned device.

Figure 4.6 shows the positive drift of a non-conditioned device as Ca^{2+} ions are taken into the membrane. The plot levels out after 12 hours, indicating that the ion concentrations have reached equilibrium. This means that the time required to fully condition the ISE should be at least this long. In the fabrication process of the ISE the devices are conditioned overnight, approximately 16 hours, which will yield fully conditioned devices. Large positive potential drifts (up to 100 – 150 mV) and/or an extensive time to reach a stable potential (up to 24 hours) can be indicative of the uptake of water across the membrane. The response shown in Figure 4.6 has a positive potential drift of 50 mV, with a stabilisation time of 12 hours indicating that no water layer is formed during conditioning.

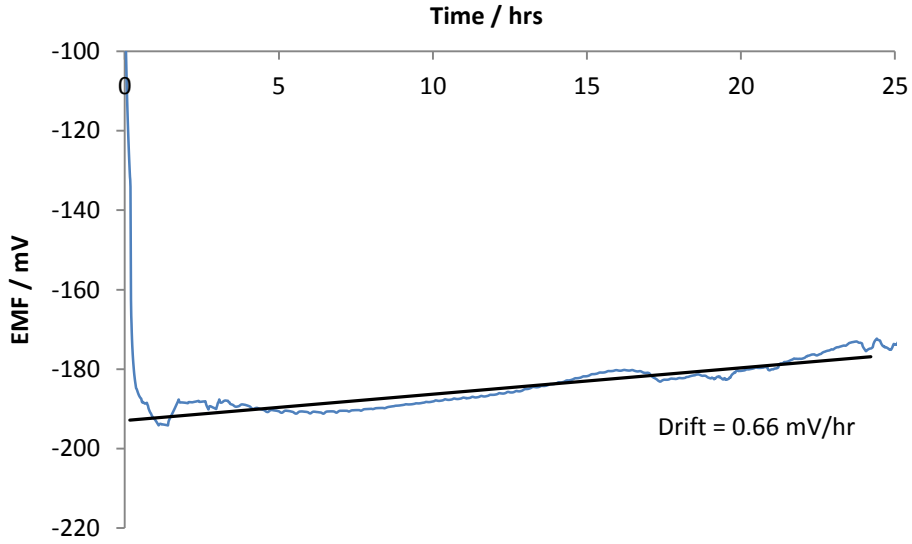

Figure 4.7 – Potential drift of a conditioned device.

The potential drift of a conditioned device (new device), shown in Figure 4.7, shows good stability (0.66 mV/hr), meaning that over the time frame of the cell experiments (several minutes) the internal boundary potentials of the ISE can be said to be stable, and therefore constant, and so quantitative analysis can be achieved. Implantable devices for blood analysis, which are described as having very high stability, must have a potential drift that is less that 0.2 mV/hr. The microgripper sensor devices have a drift comparable with this, indicating a high potential stability. Well defined phase boundary potentials are a requirement for long term stability [27], which is linked to reproducibility of the sensor response. It can therefore be said that the microgripper sensor device has a well defined phase boundary that is likely due to the excellent redox properties of PEDOT.

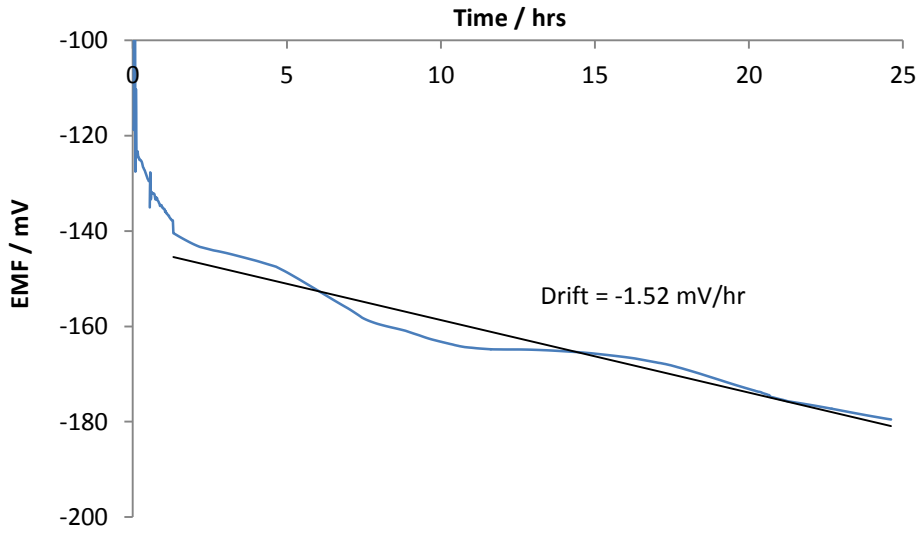

Figure 4.8 – Potential drift of a used device.

A used device (i.e. one that has undergone calibration in a standard solution) shows quite a large negative drift, indicative of ions being lost (via leaching) from the membrane. This is quite common for planar ASSISEs as the membrane is relatively thin and in complete contact with the solution (there is no bulk membrane for ion equilibration). Interferences due to the transport of small molecules, such as H_2O, CO_2 and O_2, across the membrane can also lead to unreliable sensor response, with drifting potentials. This again is a problem seen more frequently in ASSISEs. This means that the microgripper sensor device cannot be used for repeated long measurements. However, given the intended application is for sensing cellular ions where the study will only take several minutes, long term stability is not a necessary requirement. Potential drift experiments were carried out at room temperature, and so it is also interesting that in Figure 4.8 fluctuations in response due to the slight fluctuations in the laboratory temperature are observed (time stamped data was compared to the time monitored laboratory temperature data to clarify this). These temperature fluctuations can also be seen in Figure 4.6 and Figure 4.7, although not as clearly; similar effects have been seen by other groups [27] [28]. While the first use of the microgripper sensor devices shows excellent short term stability, and so temperature fluctuations are not a concern, it does raise

the issue of temperature control when using the calibration response of a separate device to quantify the response of another.

4.3.2.3 Water Layer

An unwanted, thin, aqueous layer can form between the CP and the ISM that can cause the ISE to behave non-ideally. Specifically the system can suffer from large potential drift; either positive if ions are added to the water layer, or negative if ions are lost. Additionally, sensitivity to changes in CO_2 can be increased, destabilising the CP|ISM interface and affecting the membrane potentials. ISE response is not the only thing that is affected; the adhesion strength between the ISM and the solid support can deteriorate over time once exposed to aqueous solutions, significantly reducing the lifetime of the sensor, as well as risking complete electrode failure.

The water layer can be formed by uptake of water molecules into the ISM; this effect has been observed in other PVC membrane based devices [29] [30]. There is no guarantee, however, that the water layer is not formed during the fabrication of the ASSISE. Although the CP layer is left overnight to dry, this is not done under vacuum or in a humidity controlled environment, and studies have shown that CP deposited from aqueous environments have a high likelihood of forming a water layer [31]. Additionally, traces of hygroscopic water are present as a contaminant in THF, which is used without alteration as the casting solvent for the deposition of the ISM, and could also contribute to the formation of a water layer.

A slow, asymptotic, positive potential drift observed during conditioning is indicative of water uptake into the ISM, which would form a layer between CP and ISM. Potential drift measurements can be misleading, and so an additional test involves submersion of the ISE into a concentrated solution of the primary ion (usually 0.1 M), then the interfering ion, and back to the primary ion. Any observed large positive drift is due to the presence of a water layer (around 100 Å thick [32]), and so small changes in ionic flux have a large impact on the

measured EMF. This test has to be run over several hours to ensure that equilibrium is reached with the primary ions in the sample solution and the internal water layer. This time is dependent on the thickness of the ISM as well as the diffusion coefficients of the mobile ions in the membrane.

Figure 4.9 shows the water layer test carried out on a PVC based Ca^{2+} ISE.

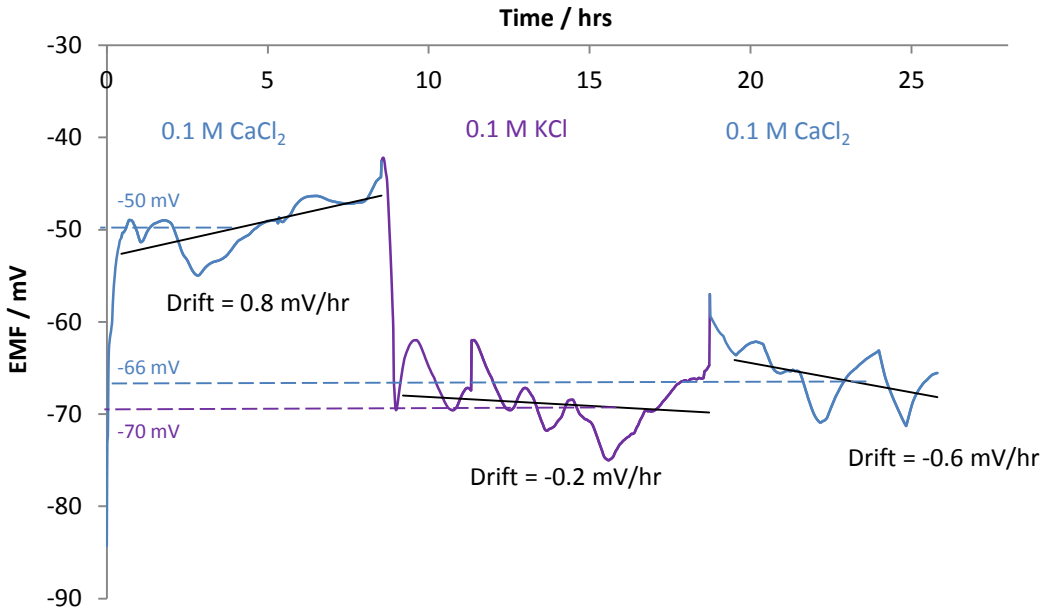

Figure 4.9 – Ca^{2+} ISE water layer test on a conditioned device.

Although the response plot for this device is quite noisy, the potential drift within each solution is minimal. There is, however, a large negative shift in potential (-16 mV) after submersion in an interfering ion solution and back to the $CaCl_2$. As a positive shift is indicative of a water layer, this negative shift is more likely due to a hysteresis like effect occurring when moving between solutions, as hysteresis occurs in the direction of the EMF of the lower concentration of the analyte of interest, which in this case is the KCl solution. Used devices, as shown in Figure 4.10, show a significantly worse response than new ones.

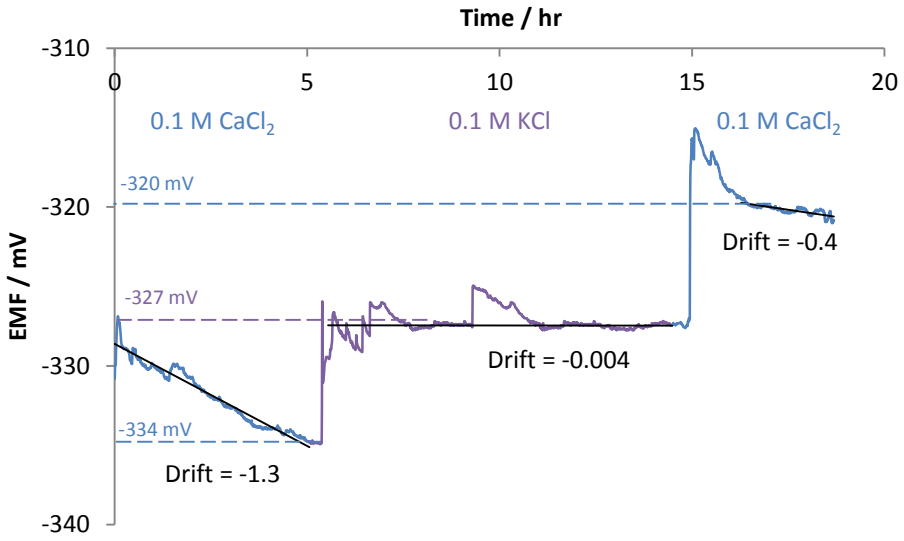

Figure 4.10 – Ca^{2+} ISE water layer test on a used device.

Figure 4.10 shows a large negative initial drift, indicative of a water layer, with a large positive shift of 14 mV on submerging in an interfering ion solution and back to the $CaCl_2$ also being observed. This means that on first use, membrane components are leached from the membrane, and as the device is re-submerged an osmotic gradient is formed, causing a flux of ions to be transported across the membrane, forming a water layer and destabilising the device.

4.3.2.4 Hysteresis

A measurement of the shift in potential of the microgripper sensor device when moved between solutions at different concentrations is an important parameter to consider, as it is needed to shift the non-linear portions of the calibration slope for the quantitative analysis of unknown samples. Figure 4.11 shows the response of a conditioned Ca^{2+}-ISE microgripper sensor device.

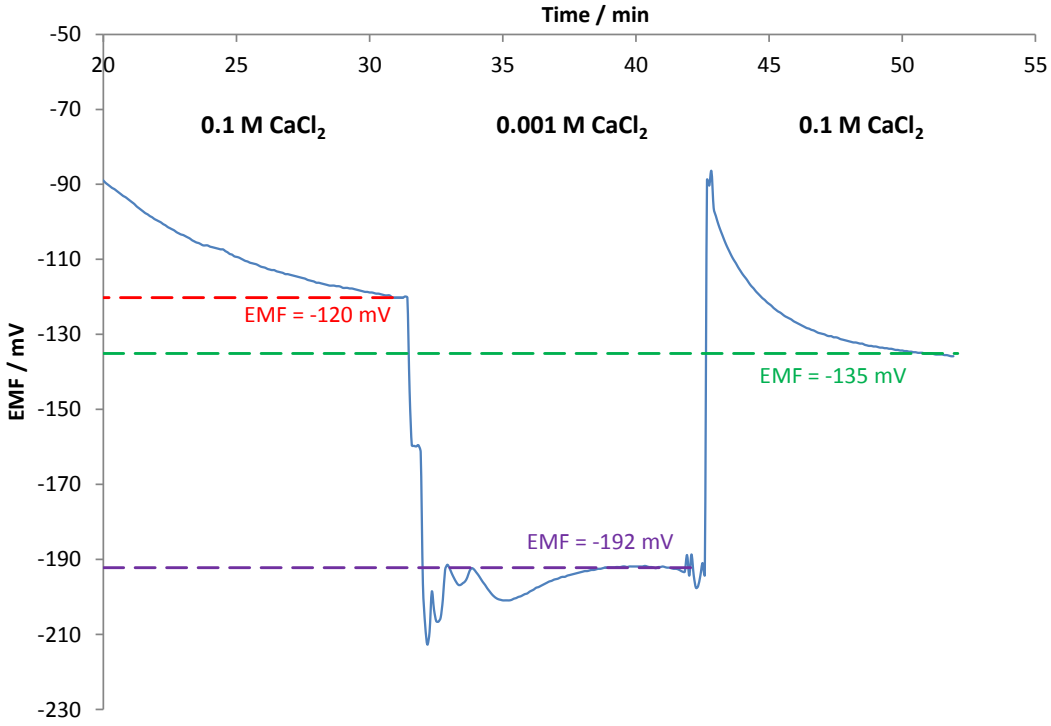

Figure 4.11 – Ca^{2+} ISE hysteresis study.

Ideally the output of the sensor will depend solely on the input parameter, and not on the previous history of the input. This, however, is not always the case. In Figure 4.11 it can be seen that there is a negative shift of 15 ± 1 mV in the measured stable potential, once submerged into an analyte solution at a lower concentration. The negative direction is to be expected as the systematic error is generally in the direction of the concentration in which the device is immersed, in this case a lower concentration, and so a negative shift is to be expected.

Given the one use nature of the microgripper sensor devices, measurements of ion activity in unknown samples must be done first to ensure high accuracy in the data collected. This means that the subsequent calibration data collected from samples of known concentrations need to be normalised as they will suffer from the hysteresis effect seen in Figure 4.11. To be able to normalise the absolute EMF potentials of one calibrated device on a wafer set with the others via a one point calibration measurement, it is therefore important

that all devices have a similar hysteresis value. The hysteresis test was repeated, and the corresponding plot is shown in Figure 4.12.

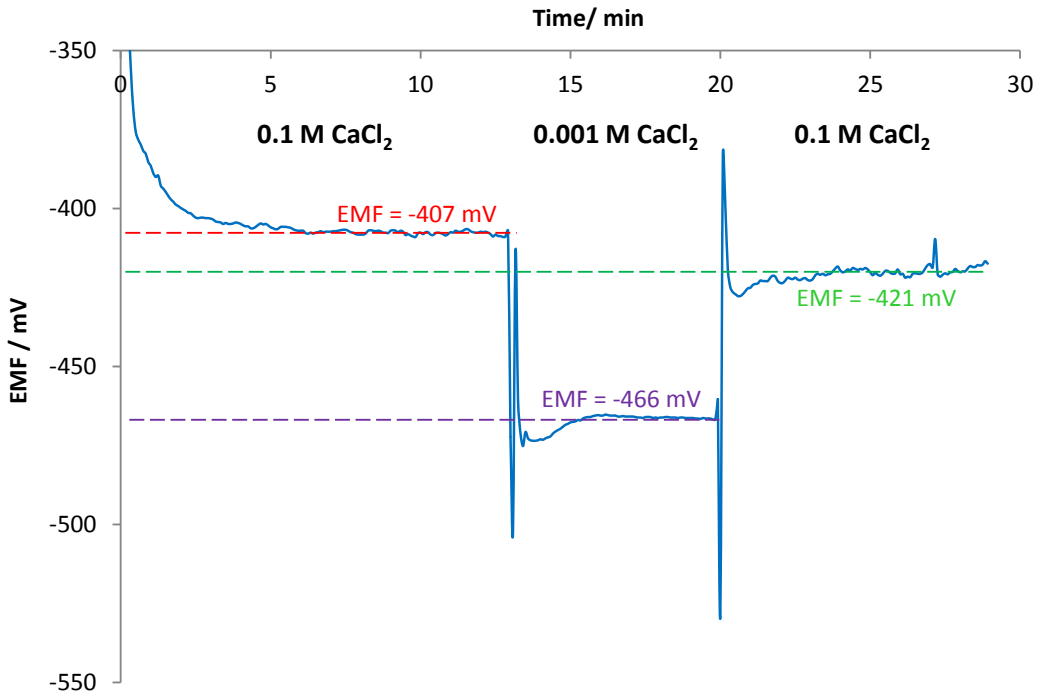

Figure 4.12 – Ca^{2+} ISE hysteresis repeat with a different device.

Again there is a negative shift, this time of 14 ± 1 mV, in the measured stable potential once it has been submerged into an analyte solution at a lower concentration. This is similar to that of the previous device, indicating that different devices from the same wafer set have a similar hysteresis value. It is therefore possible to quantitatively analyse unknown samples.

4.3.2.5 Response Time

The response time is defined as the time required to complete 95% of the change to the new value of EMF when the electrode is placed from one solution to another at a different concentration.

Figure 4.13 shows the plot of the response time of a Ca^{2+}-ISE reacting to a ten-fold increase in concentration. The study was undertaken in a static bulk solution; the higher concentration solution was added next to the electrode (so as to not perturb the solution on

the electrode), and so, as the ions diffused into the bulk solution, the ISE signal decayed as it was diluted. This method was chosen as it most closely related the real life situation of measuring ion efflux from cells. The Ca^{2+}-ISE took 6.7 ± 0.4 s to reach a peak concentration. This, however, is an underestimate of the true life time, which can be estimated from the hysteresis data as approximately 5 minutes (using the definition above). This time of 6.7 s, is more accurately the maximum time the device has to detect a change in concentration, as that concentration is diffusing from the point source. For reference, the diffusion coefficient of calcium ions in aqueous solutions at room temperature is 1.215 ± 0.022 $x10^{-9}$ m^2 s^{-1} [33]. The diffusion of ions across a cell membrane occurs over tens of seconds, meaning that the response time of the Ca^{2+} selective microgripper sensor device is limited, and an underestimation of the measured concentration could occur.

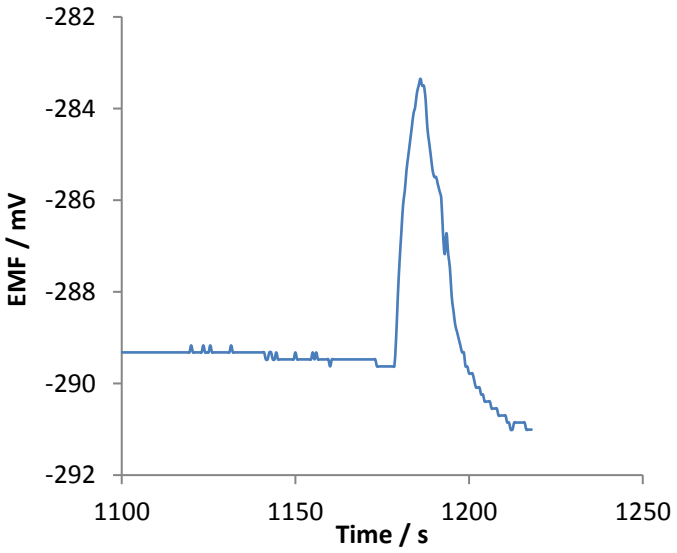

Figure 4.13 – Plot of the response of a Ca^{2+} ISE to a ten fold increase in concentration of CaCl.

4.3.2.6 Selectivity Studies

The ionophores used in ISE technology are not 100% selective to the ion of interest. Natural ionophores are generally highly selective towards one specific ion against those ions also found in its intended environment. Synthetic ionophores are specially designed for specific application areas, such as use in biological media or heavy metal sensing in aqueous

environments. Synthetic ionophores, therefore, often have a greater range of interfering ions that they are selective against, although some are much better than others. It is important to assess the selectivity of an ASSISE against all ions likely to be in the environment for which the device is intended for use.

The microgripper sensor device is intended for use to detect biological ions involved in cell communication; so for a Ca^{2+}-ISE the main interfering cations will be those also found in inter- and extra-cellular fluids, specifically K^+ and Na^+ ions.

The selectivity studies were done using the fixed interference method. Selectivity coefficients are usually quoted as the log value. If the value of $\log(K_{ij}^{pot})$ is positive, the selectivity coefficient is greater than 1, and the ISM has a higher affinity for the interfering ion than for the analyte. If the value of $\log(K_{ij}^{pot})$ is negative then the reverse is true. The more negative the value, the smaller the selectivity coefficient and the greater the affinity for the analyte over the interfering ion.

The values of $\log(K_{ij}^{pot})$ for the Ca^{2+}-ISE against the main interfering ions found in inter- and extra-cellular fluids are shown in Table 4.4.

Table 4.4 – Ca^{2+} ISE selectivity study summary table.

Interfering ion (0.1 / M)	**Log(Selectivity coefficient)**	**Log(Selectivity coefficient) from ref** [34]
KCl	-3.9	-3.7
$MgCl_2$	-1.4	-4.2
NaCl	-2.8	-3.6

Compared to other ISEs in the literature, these selectivity coefficients are good. A comprehensive review of many selectivity coefficients for many different ISM component variations can be found in reference [15]. T. Sokalski *et al.* [34] determined the selectivity coefficients via the separate solution method for several ions for the exact ISM composition

used in the fabrication of the Ca^{2+} selective microgripper sensor devices, and these results are also shown in Table 4.4. These values are comparable to those determined using the microgripper sensor device.

4.3.3 K^+ Ion Selective Electrodes

Water layer, potential drift and conditioning profiles were assumed to be similar for the K^+ selective microgripper sensor device as the fabrication of the ISE sensor device was identical; only the ionophore was changed. This change of ionophore means that the Nernstian response could be different (additionally as K^+ is a monovalent cation). Selectivity coefficients, response time and hysteresis are also important parameters to determine for the quantitative analysis of unknown samples.

4.3.3.1 Calibration

Figure 4.14 shows the calibration plot of a K^+ selective microgripper sensor device. The slope response was calculated as 29 ± 4 mV/dec, which is below that of the expected 59 mV/dec at 298 K for a monovalent ion. This sub-Nernstian response is again likely to be due to the coordination between the analyte and the ionophore within the membrane not forming a single type of complex due to leaching effects or any of the other factors discussed in Section 4.3.2.1.

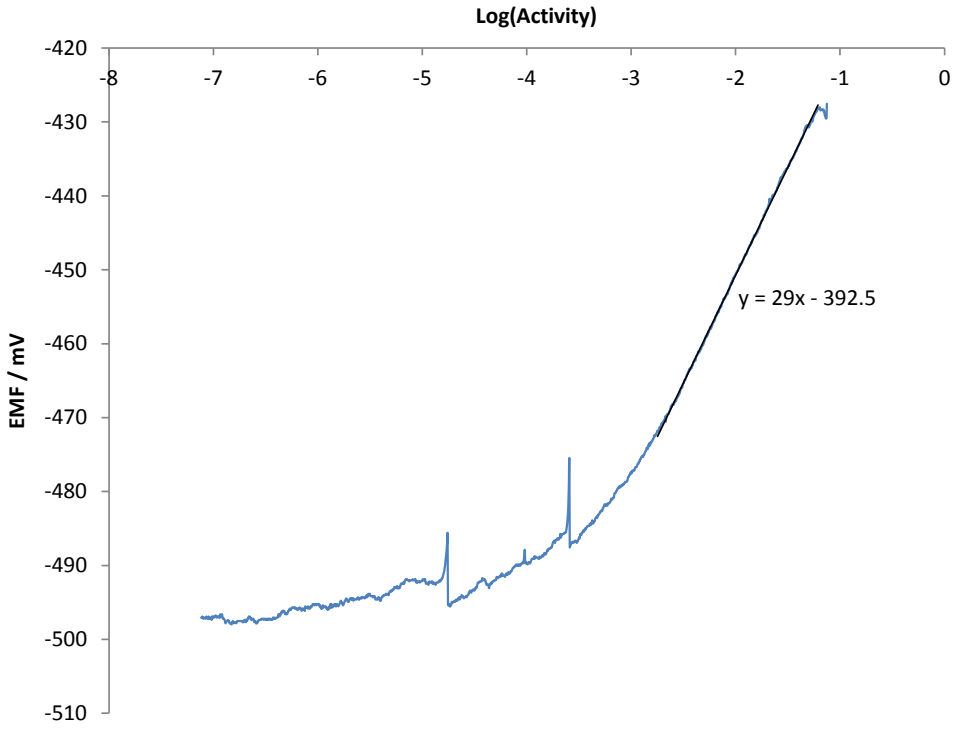

Figure 4.14 – K^+ ISE calibration plot.

The limit of detection was calculated as 2.4 x 10^{-4} M. This is slightly lower than that calculated for the Ca^{2+} devices. Given the fact that the LOD is directly dependent on the ionic active site used, which has not changed, this slight difference must be due to the differing thickness of the ISM layer. Figure 4.15 shows the SEM images of a range of difference ISM morphologies and thicknesses that have been fabricated and could affect the device's response. The precise mechanism by which this occurs is unknown, however similar effects have been seen by other groups [35] [36]. Specifically Figure 4.15(e) shows evidence of an air bubble being trapped between the PEDOT and the ISM as under the vacuum of the SEM the ISM has been perforated, this would have caused a very unstable electrode response as the PEDOT|ISM boundary potential would not have been stable. Additionally Figure 4.15(f) shows a thick membrane deposition, where the microgripper arms have been glued together by the ISM; while this would likely give a more stable response the operation of the microgripper is inhibited.

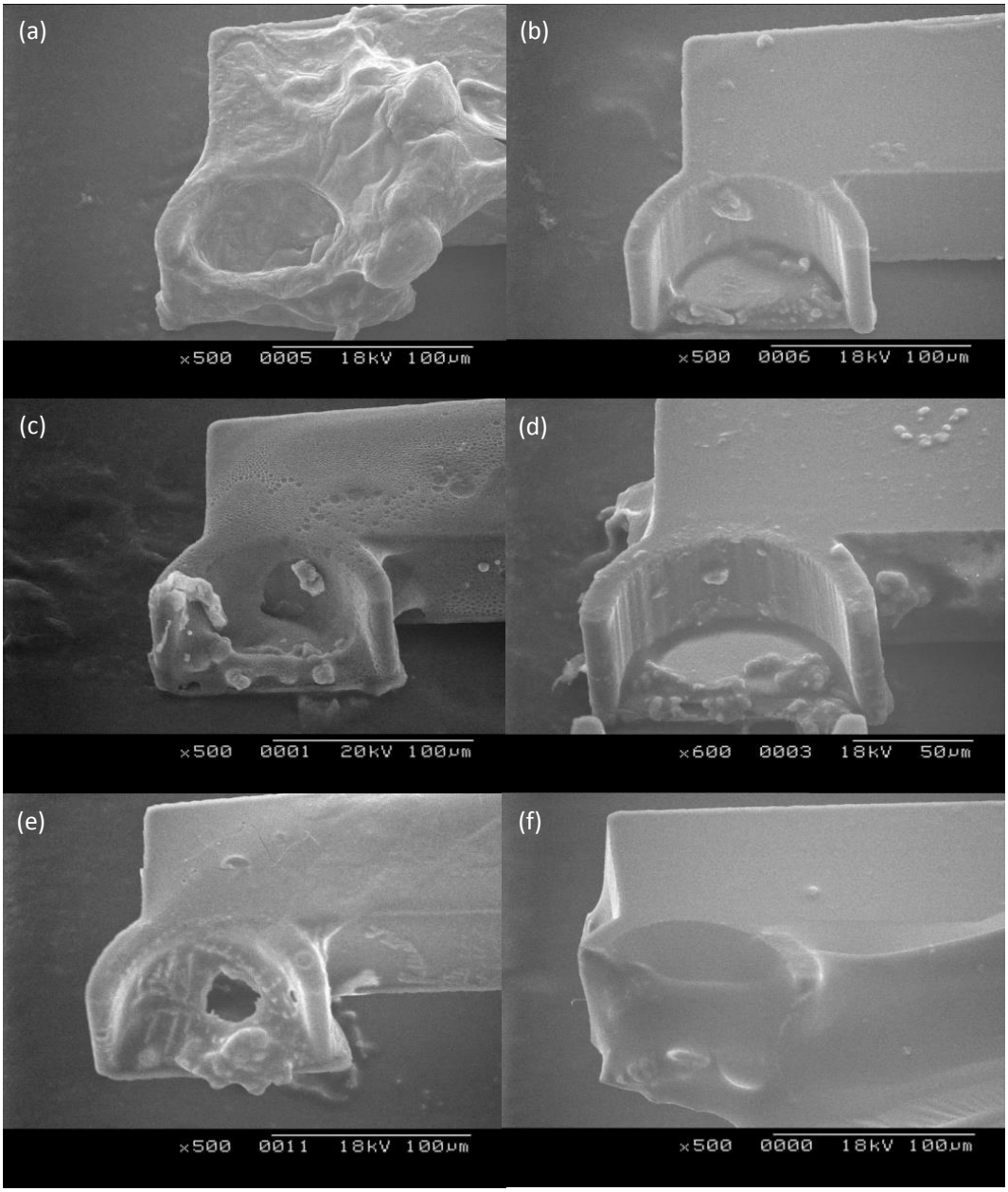

Figure 4.15 – SEM images of the different membrane morphologies and thicknesses for K^+-ISEs indicating the large inconsistencies with the membrane deposition, as well as highlighting (b – d) the lack of complete coverage of the membrane.

4.3.3.2 Selectivity Studies

The main ions found in the inter- and extra-cellular fluids, specifically Ca^{2+} and Na^+ ions, were used as the interfering ions in this study, carried out via the fixed interference method. The selectivity coefficients are shown in Table 4.5.

G. J. Moody *et al.* [37] determined selectivity coefficients via the separate solution method, using similar membrane components that were used in the fabrication of the

microgripper sensor device, with the only difference being the type of ionic active site used; bis(crown ether) was used rather than KTpClPB.

Table 4.5 – K^+ ISE selectivity study summary table.

Interfering ion (0.1 M)	**Log(Selectivity coefficient)**	**Log(Selectivity coefficient) from ref** [37]
NaCl	-1.8	-3.02
$CaCl_2$	-3.3	-3.96

The selectivity coefficient of the K^+ selective microgripper sensor device against Na^+ ions is worse than that described by Moody *et al.*; the device still shows good selectivity towards K^+ ions. However, in situations where the concentration of Na^+ ions is much greater than for K^+, the sensor response will be due to a combination of Na^+ and K^+ ion activity.

The selectivity coefficient of the K^+ selective microgripper sensor device against Ca^{2+} ions is comparable to that described by Moody *et al.* and it shows excellent selectivity towards K^+ ions.

4.3.3.3 Response Time

The response time is defined as the time required to complete 95% of the change to the new value of EMF when the electrode is placed from one solution to another at a different concentration.

Figure 4.16 shows the plot of the response time of a K^+-ISE reacting to a ten-fold increase in concentration. The study was undertaken in a static bulk solution, where the higher concentration solution was injected directly onto the electrode. As the ions diffused into the bulk solution, the ISE signal decayed as it was diluted. The K^+-ISE took 1.4 ± 0.1 s to reach a peak concentration. The t_{95} response time estimated from the hysteresis data is approximately 17 s (using the definition above). The diffusion of ions across a cell membrane occurs over tens

of seconds, meaning that the response time of the K^+ selective microgripper sensor device operates just within the tolerances for this application.

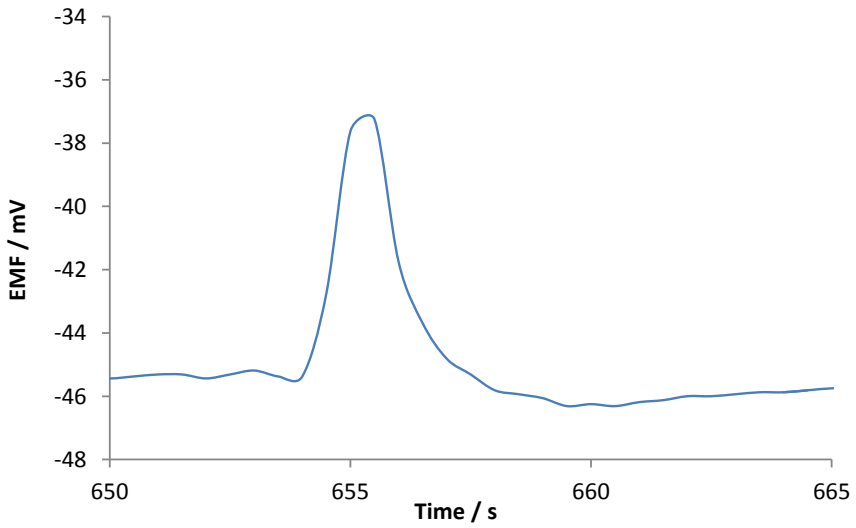

Figure 4.16 – Plot of the response of a K^+ ISE to a ten fold increase in concentration of KCl.

4.3.3.4 Hysteresis

To allow quantitative analysis to be performed, the measurement of the shift in potential of the microgripper sensor device when moved between solutions at different concentrations must be determined. Figure 4.17 shows the response of a conditioned K^+-ISE microgripper sensor device.

There is a negative shift of 4 ± 1 mV in the measured stable potential once submerged into an analyte solution at a lower concentration. This indicates a very high stability in the K^+ selective microgripper sensor devices compared to the Ca^{2+} counterparts.

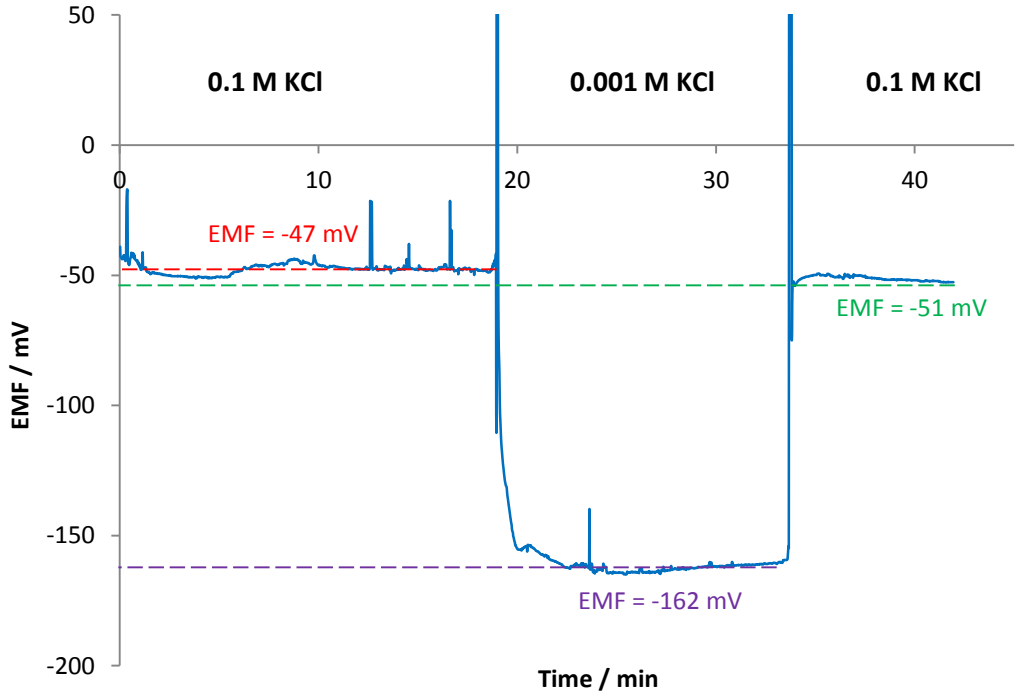

Figure 4.17 – K^+ ISE hysteresis.

4.3.4 Na^+ Ion Selective Electrodes

Again the water layer, potential drift and conditioning profiles can be assumed to be similar to those characterised for the Ca^{2+}-ISEs, as fabrication of the Na^+-ISE sensor devices was identical; only the ionophore was changed. The monovalent Nernstian response, selectivity coefficients, response time and hysteresis are therefore the important parameters to determine.

4.3.4.1 Calibration

Figure 4.18 shows the calibration plot of a Na^+ selective microgripper sensor device. The slope response was calculated as 32 ± 4 mV/dec, below that of the expected 59 mV/dec at 298 K for a monovalent ion. This sub-Nernstian response is again likely due to the coordination between the analyte and ionophore within the membrane not forming a single type of complex due to leaching effects or any of the other factors discussed in Section 4.3.2.1.

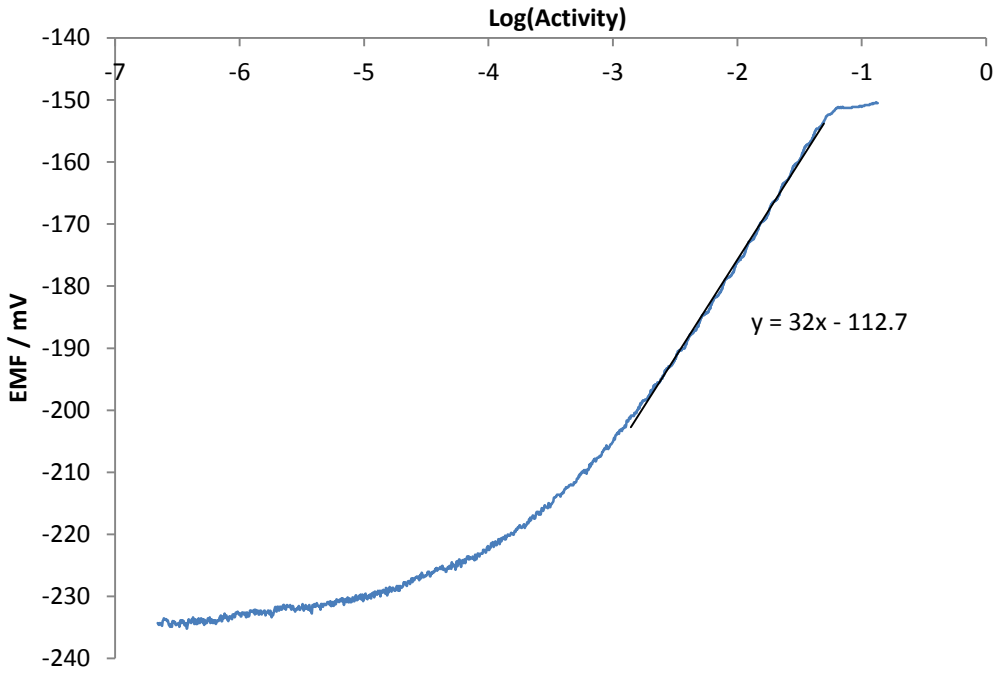

Figure 4.18 – Na^+ ISE calibration plot.

The limit of detection was calculated as 1.8 x 10^{-4} M. This is again slightly lower than that calculated for the Ca^{2+} devices, but is very similar to that for the K^+ devices. This indicates that the ionophore plays a role in the sensitivity of the device. Looking ahead to Section 4.3.4.2 shows that the log of the selectivity coefficient of the Na^+-ISE with K^+ as the interfering ion is -0.8. KCl is used as the background electrolyte during the calibration study, and so the reduced LOD is likely to be linked to the interference of K^+ ions. Comparing the LOD of the K^+-ISE device (2.4 x 10^{-4} M) and the log of the selectivity coefficient with Na^+ (-1.8) that was used as the background electrolyte, with the LOD of the Ca^{2+}-ISE devices (2.4 x 10^{-6}) and the log of the selectivity coefficient with K^+ (-3.9) that was used as the background electrolyte, a clear trend can be seen. The more susceptible the ISE is to the interfering ion used as the background electrolyte, the higher the LOD of that device is.

4.3.4.2 Selectivity Studies

The main ions found in the inter- and extra-cellular fluids, specifically Ca^{2+} and K^{+} ions, were used as the interfering ions in this study, carried out via the fixed interference method. The selectivity coefficients are shown in Table 4.6.

K. Cunningham *et al.* [38] determined the selectivity coefficients via the fixed interference method using similar membrane components that were used in the fabrication of the microgripper sensor device, with the only difference being the type of ionic active site used; p-tert-Butylcalix[4]arene was used rather than KTpClPB.

Table 4.6 – Na^{+} ISE selectivity study summary table.

Interfering ion (0.1 M)	**Log(Selectivity coefficient)**	**Log(Selectivity coefficient) from ref** [38]
KCl	-0.8	-1.5
$CaCl_2$	-1.2	-3.0

The selectivity coefficient with K^{+} as the interfering ion shows that the Na^{+} selective microgripper sensor device does show selectivity towards Na^{+} ions, but only in low concentrations of K^{+} ion. Comparing this to the selectivity coefficients determined by Cunningham *et al.*, indicates that this poor selectivity is most likely to be due to the ionophore used, as they too observed a poor selectivity.

The selectivity coefficient with Ca^{2+} as the interfering ion also shows poor preference for Na^{+} ions over Ca^{2+} ones. This is not comparable to that observed by Cunningham *et al.*

4.3.4.3 Response Time

The response time is defined as the time required to complete 95% of the change to the new value of EMF when the electrode is placed from one solution to another at a different concentration.

Figure 4.19 shows the plot of the response time of a Na^+-ISE reacting to a ten-fold increase in concentration. The study was undertaken in a static bulk solution; the higher concentration solution was injected directly onto the electrode, and as the ions diffused into the bulk solution, the ISE signal decayed as it was diluted. The Na^+-ISE took 2.6 ± 0.9 s to reach a peak concentration. The t_{95} response time estimated from the hysteresis data is approximately 3 minutes (using the definition above). The diffusion of ions across a cell membrane occurs over tens of seconds, meaning that the response time of the Na^+ selective microgripper sensor device will struggle to operate within the tolerances for this application.

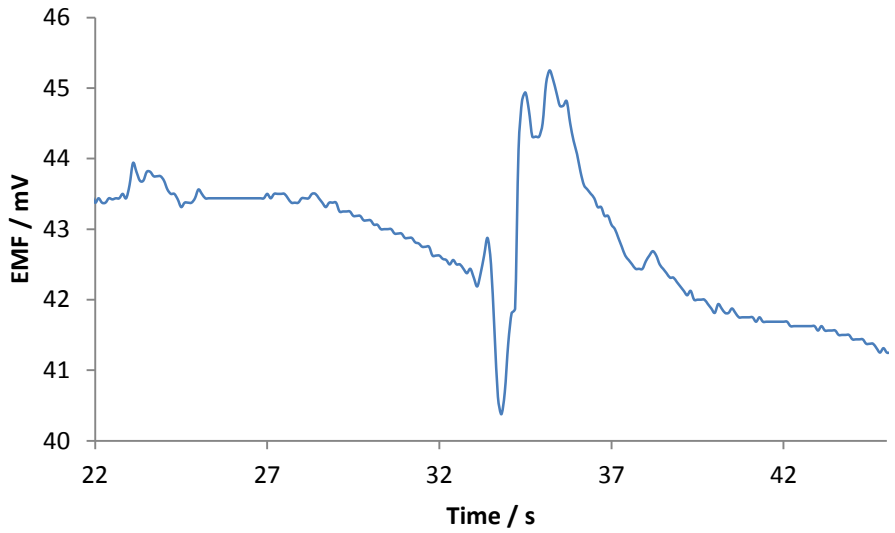

Figure 4.19 – Plot of the response of a Na^+ ISE to a ten fold increase in concentration of NaCl.

4.3.4.4 Hysteresis

To allow quantitative analysis to be performed the measurement of the shift in potential of the microgripper sensor device when moved between solutions at different concentrations must be determined. Figure 4.20 shows the response of a conditioned Na^+-ISE microgripper sensor device.

There is a negative shift of 23 ± 2 mV in the measured stable potential once submerged into an analyte solution at a lower concentration. This indicates the poor stability of the Na^+ selective microgripper sensor devices compared to the Ca^{2+} and K^+ counterparts.

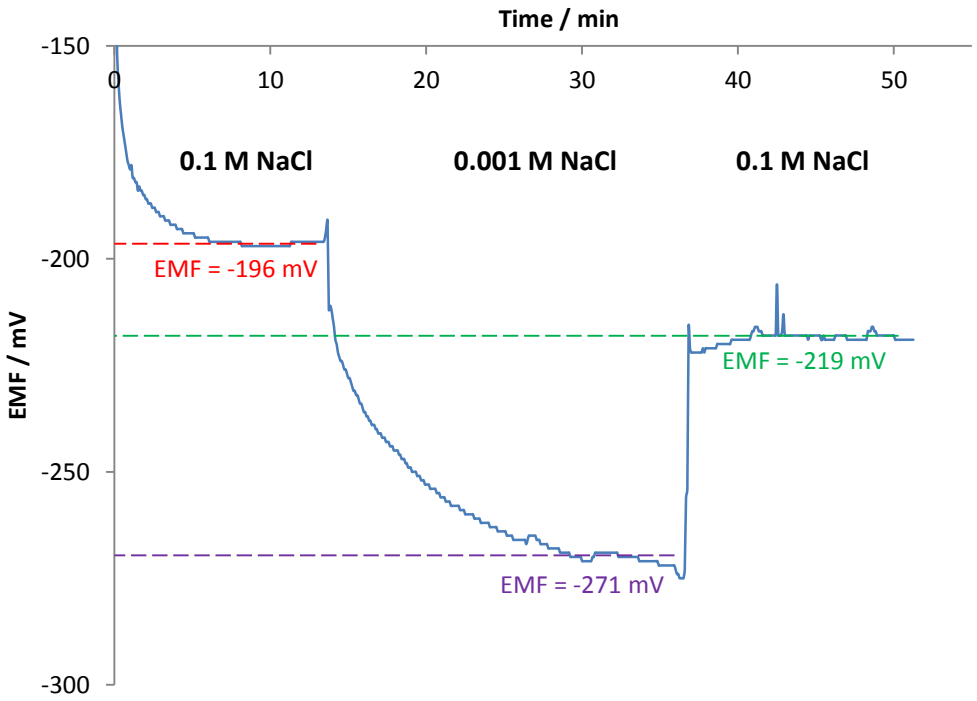

Figure 4.20 – Na^+ ISE hysteresis.

4.4 Chapter Summary

This chapter focused on the calibration characterisation of the microgripper sensor devices. Before it can conclusively be said that a device has performance characteristics that can rival those of the liquid contact macro ion selective electrode certain quality control and testing criteria must be matched. Specifically these include investigation into the detection limits, response times, selectivity coefficients (in this case done via the fixed interference method), and stability (such as drifts in potential, hysteresis and a test for the presence of a water layer) of the devices.

The main investigation into the calibration behaviour of the microgripper sensor devices was done using Ca^{2+} devices in a flow cell system. It was observed that the multiple use of these devices was not possible as there was a great loss of membrane components (leaching) between runs, causing a destabilisation in the device response. This was also indicative of the formation of a water layer on used devices, possibly due to the delamination of the ISM. The single use of devices from a wafer batch was possible due to the MEMS

technologies that were used to fabricate the devices resulted in near identical processing. The only difference during the fabrication process was in the etching of the gold electrode. This difference occurred due to the differing grain structures formed when electroplating and results in differing active surface areas of the gold electrode. This could be monitored during the electrodeposition of PEDOT, using cyclic voltammetry, as the steady state current is proportional to the PEDOT concentration. Comparison of the steady state currents reached during the PEDOT deposition illustrated that the differences for devices across the same wafer were only slight. The deposition of the ISM, however, was not controllable, which caused changes in the ISM morphology and thickness. This was observed to mainly affect the absolute EMF. The linear range, electrode response and limit of detection were all very similar between different devices on the same fabrication wafer.

The Ca^{2+} ISE microgripper sensor devices had a sub-Nernstian response of 14 ± 3 mV/dec compared to the 29 mV/dec expected for divalent ions at 298 K. The sub-Nernstian response was likely due to the coordination between the analyte and the ionophore not having a single type of complex due to leaching effects, or due to a failing in the phase boundary potential model, the presence of a large surface concentration of the primary ion due to the planar device dimensions, or any interactions between the devices fabrication materials and the ISM. The detection limit for the Ca^{2+} ISE microgripper sensor device was $2 \pm 3 \times 10^{-5}$ M, which was not low enough to sense 0.002 mM changes in cellular Ca^{2+} ion movement out of a stressed cell. It was also observed that the ionophore plays a role in the sensitivity of device, as the better the selectivity coefficient against a specific interfering ion, the better the limit of detection in a background solution of that ion.

Potential drift studies indicated that to fully condition the membrane took 12 hours. This meant that the 16 plus hours that the devices were condition during the fabrication process was sufficient. It was observed that conditioned devices had good stability,

0.66 mV hr^{-1}, however, used devices had a much poorer stability, -1.52 mV hr^{-1}, and were much more sensitive to slight changes in external temperature. This indicated that there was a loss of sensitivity of the device that was likely due to the leaching of membrane components.

The water layer tests of a conditioned device showed a negative (-16 mV) shift in potential, and little potential drift during the experimental time frame. This was not indicative of the formation of a water layer. In used devices, however, the observed positive shift (14 mV) and a large negative potential drift of -1.3 mV hr^{-1} was indicative of the formation of a water layer. This further implies that the multiple use of the microgripper sensor devices was not feasible.

The hysteresis of the Ca^{2+} ISE microgripper sensor devices was a small and quantifiable shift (14 ± 1 mV) allowing normalisation of a device response from a calibration standard from the same wafer batch, once the EMF at a known concentration is known. This meant that quantitative analysis could be undertaken.

The response time for the Ca^{2+} ISE microgripper sensor device occurred over several seconds (6.7 ± 0.4 s), which also included the diffusion time to the electrode. This was suitable for the monitoring of intercellular ion movement, which occurs over tens of seconds.

The selectivity coefficients against K^+, Mg^{2+} and Na^+ as the interfering ions, which are common ions in the extracellular fluid, were good (-3.9, -1.4 and -2.8 respectively) and were comparable with that seen in literature.

The K^+ ISE microgripper sensor devices were also characterised. The calibration responses also showed a sub-Nernstian response of 29 ± 4 mV/dec, compared to the 59 mV/dec at 298 K expected for a monovalent ion. The limit of detection was characterised as 2.4 ± 2 x 10^{-4} M, which was sensitive enough to quantify the 139 mM changes in cellular K^+ ions. The selectivity coefficients with Na^+ and Ca^{2+} as the interfering ions were average (-1.8)

and good (-3.3) respectively. Log $K_{K,Ca}$ was comparable to that from literature, whereas log $K_{K,Na}$ was not. The response times were excellent (1.4 ± 0.1 s), as was the hysteresis (4 ± 1 mV shift), which was indicative of a highly stable device.

The Na^+ ISE microgripper sensor devices were also characterised. The calibration responses also showed a sub-Nernstian response of 32 ± 4 mV/dec compared to the 59 mV/dec at 298 K expected for a monovalent ion. The limit of detection was characterised as 1.8 ± 2 x 10^{-4} M, which was sensitive enough to monitor the 5 mM changes in Na^+ cellular ion concentrations. The selectivity coefficients with K^+ and Ca^{2+} as the interfering ions were both poor (-0.8 and -1.2 respectively). However, K^+ selectivity coefficients were similar to that seen in literature. The response times were good, 2.6 ± 0.9 s, whereas the hysteresis was poor (23 ± 2 mV shift) although repeatable. This was indicative of the instability of the Na^+ devices.

All the characterisation data for the three different microgripper sensor devices is summarised in Table 4.7.

Table 4.7 – Summary table of characterisation of the different microgripper sensor devices.

Device	**Ca^{2+}-ISE**	**K^+-ISE**	**Na^+-ISE**
Sensitivity / mV/dec	14 ± 4	29 ± 4	32 ± 4
Limit of detection / M	2 ± 3 x 10^{-5}	2 ± 2 x 10^{-4}	2 ± 2 x 10^{-4}
Potential drift / mV hr^{-1}	0.66 (conditioned) -1.52 (used)	-	-
Water layer formation	NO (conditioned) -16 mV shift, -0.8 mV hr^{-1} drift YES (used) 14 mV shift, -1.3 mV hr^{-1} drift	-	-
Hysteresis / mV	14 ± 1	4 ± 1	23 ± 2
Response time / s	300	17	180
Selectivity coefficients	log $K_{Ca,K}$ = -3.9 log $K_{Ca,Na}$ = -2.8 log $K_{Ca,Mg}$ = -1.4	log $K_{K,Na}$ = -1.8 log $K_{K,Ca}$ = -3.3	log $K_{Na,K}$ = -0.8 log $K_{Na,Ca}$ = -1.2

Overall the characterisation of the Ca^{2+} ISE microgripper device indicated a good, stable device. However, the limit of detection of these devices implied that the sensitivity was not great enough to detect changes in intercellular calcium ions. The K^{+} ISE microgripper devices had excellent sensitivity and selectivity, whereas the Na^{+} ISE microgripper devices had selectivity issues with respect to potassium ions, which given the high concentration of potassium ions in cellular fluids could cause an interference issue with the ability of these devices to sense sodium.

4.5 References

[1] D. J. Beebe, G. A. Mensing and G. M. Walker, "Physics and applications of microfluidics in biology," *Annual Review of Biomedical Engineering,* vol. 4, pp. 261-286, 2002.

[2] W. T. Liu, L. Zhu, Q. W. Qin, Q. Zhang, H. H. Feng and S. Ang, "Microfluidic device as a new platform for immunifluorescent detection of viruses," *Lab on Chip,* vol. 5, no. 11, pp. 1327-1330, 2005.

[3] C. F. Lin, G. B. Lee, C. H. Wang, H. H. Lee, W. Y. Liao and T. C. Chou, "Microfluidic pH sensing chips integrated with pneumatic fluid control devices," *Biosensors and Bioelectronics,* vol. 21, no. 8, pp. 1468-1475, 2006.

[4] A. J. Tudos, G. A. J. Besselink and R. B. M. Schasfoort, "Trends in miniaturized total analysis systems for point of care testing in clinical chemistry," *Lab on Chip,* vol. 1, no. 2, pp. 83-95, 2001.

[5] E. Verpoorte, "Microfluidic chips for clinical and forensic analysis," *Electrophoresis,* vol. 23, no. 5, pp. 677-712, 2002.

[6] A. Bange, H. B. Halsall and W. R. Heineman, "Microfluidic immunosensors systems," *Biosensors and Bioelectronics,* vol. 20, no. 12, pp. 2488-2503, 2005.

[7] Y. Huang, E. L. Mather, J. L. Bell and M. Madou, "MEMS based sample preparation for molecular diagnostics," *Analytical and Bioanalytical Chemistry,* vol. 372, no. 1, pp. 49-65, 2002.

[8] A. S. Rudolph and J. Reasor, "Cell and tissue based technologies for environmental detection and medical diagnostics," *Biosensors and Bioelectronics,* vol. 16, no. 7-8, pp. 429-431, 2001.

[9] C. C. Rundle, A Beginners Guide to Ion-Selective Electrode Measurements, London: Nico2000 Ltd, 2000.

[10] T. Sokalski, A. Ceresa, T. Zwickl and E. Pretsch, "Large improvement of the lower detection limit of ion selective polymer membrane electrodes," *Journal of the American Chemical*

Society, vol. 119, no. 46, pp. 11347-11348, 1997.

[11] S. Mathison and E. Bakker, "Effect of transmembrane electrolyte diffusion on the detection limit of carrier based potentiometric ion sensors," *Analytical Chemistry,* vol. 70, no. 2, pp. 303-309, 1998.

[12] R. P. Buck and E. Lindner, "Recomendation for nomenclature of ion selective electrodes," *Pure and Applied Chemsitry,* vol. 66, no. 12, pp. 2527-2536, 1994.

[13] E. Bakker, E. Pretsch and P. Buhlmann, "Selectivity of potentiometric ion sensors," *Analytical Chemistry,* vol. 72, pp. 1127-1133, 2000.

[14] Y. Umezawa , K. Umezawa and H. Sato, "Selectivity coefficients for ion-selective electrodes: Recommended methods for reporting K values," *International Union of Pure and Applied Chemistry,* vol. 67, no. 3, pp. 507-518, 1995.

[15] Y. Umezawa, P. Buhlmann, K. Umezawa, K. Tohda and S. Amemiya, "Potentiometric selectivity coefficients of ion-selective electrodes Part I. Inorganic cations," *Pure Applied Chemistry,* vol. 72, no. 10, pp. 1851-2082, 2000.

[16] E. Lindner and Y. Umezawa, "Performance evaluation criteria for preparation and measurement of macro and microfabricated ion selective electrodes," *Pure and Applied Chemistry,* vol. 80, no. 1, pp. 85-104, 2008.

[17] J. N. Butler, Ionic Equilibrium: Solubility and pH calculations, New York: Wiley, 1998.

[18] Y. Sulaiman, Characterisation of PEDOT and its derivatives in electrochemical sensing applications, PhD Thesis: Durham University, 2011.

[19] M. Miyake, L. D. Chen, G. Pozzi and P. Buhlmann, "Ion-selective electrodes with unusual response functions: Simultaneous formation of ionophore-primary ion complexes with different stoichiometries," *Analytical Chemistry,* vol. 84, pp. 1104-1111, 2012.

[20] O. Dinten, U. E. Spichiger, N. Chaniotakis, P. Gehrig, B. Rusterholtz, W. E. Morf and W. Simon, "Lifetime of neutral carrier based liquid membranes in aqueous samples and blood and the lipophilicity of membrane components," *Analytical Chemistry,* vol. 63, no. 6, pp. 596-603, 1991.

[21] E. Bakker and E. Pretsch, "Lipophilicity of tetraphenyl borate derivatives as anionic sites in neutral carrier based solvent polymeric membranes and lifetime of corresponding ion selective electrochemical and optical sensors," *Analytica Chimica Acta,* vol. 309, no. 1-3, pp. 7-17, 1995.

[22] E. Lindner, V. V. Cosofret, S. Ufer, R. P. Buck, R. P. Kusy, R. B. Ash and H. T. Nagle, "Flexible (Kapton based) microsensor arrays for high stability for cardiovascular applications," *Journal of the Chemical Society - Faraday Transactions,* vol. 89, no. 2, pp. 361-367, 1993.

[23] P. L. H. M. Cobben, R. M. Egberink, J. G. Bomer, P. Bergveld and D. N. Reinhoudt, "Chemically modified field effect transistors: the effect of ion-pair association on the membrane potentials," *Journal of Electroanalytical Chemistry,* vol. 368, pp. 193-208, 1994.

[24] A. Hulanicki, T. Sokalski and A. Lewenstam, “Side-effects in measurements of selectivity coefficients of solid state ion selective electrodes,” *Mikrochimica Acta,* vol. 3, no. 1-6, pp. 119-129, 1988.

[25] M. Fibbioli, W. E. Morf, M. Badertscher, N. F. de Rooij and E. Pretsch, “Potential drifts of solid contacted ion selective electrodes due to zero current ion fluxes through the sensors membrane,” *Electroanalysis,* vol. 12, no. 16, pp. 1286-1292, 2000.

[26] G. H. Zhang, T. Imato, Y. Asano, T. Sonoda, H. Kobayashi and N. Ishibashi, “Vitamin B1 sensitive poly (vinyl chloride) membrane electrode based on hydrophobic tetraphenylborate derivatives and their application,” *Analytical Chemistry,* vol. 62, no. 15, pp. 1644-1648, 1990.

[27] E. Lindner and R. E. Gyurcsanyi, “Quality control criteria for solid-contact, solvent polymeric membrane ion-selective electrodes,” *Journal of Solid State Electrochemistry,* vol. 13, pp. 51-68, 2009.

[28] F. Phillips, K. Kaczor, N. Gandhi, B. D. Pendley, R. K. Danish, M. R. Neuman, B. Toth, V. Horvath and E. Lindner, “Measurement of sodium ion concentration in undiluted urine with cation-selective polymeric membrane electrodes after the removal of interfering compounds,” *Talanta,* vol. 74, no. 2, pp. 255-264, 2007.

[29] Z. Li, X. Z. Li, S. Petrovic and D. J. Harrison, “Dual-sorption model of water uptake in poly(vinyl chloride)-based ion-selective membranes: Experimental water concentration and transport parameters,” *Analytical Chemistry,* vol. 68, no. 10, pp. 1717-1725, 1996.

[30] T. Zwickl, B. Schneider, E. Lindner and E. Pretsch, “Chromoionophore-mediated imaging of water transport in ion-selective membranes,” *Analytical Sciences,* vol. 14, no. 1, pp. 57-61, 1998.

[31] J. Sutter, E. Lindner, R. E. Gyurcsanyi and E. Pretsch, “A polypyrrole-based solid-contact Pb(2+)-selective PVC-membrane electrode with a nanomolar detection limit,” *Analytical and Bioanalytical Chemistry,* vol. 380, no. 1, pp. 7-14, 2004.

[32] R. DeMarco, J. P. Veder, G. Clarke, A. Nelson, K. Prince, E. Pretsch and E. Bakker, “Evidence of a water layer in solid-contact polymeric ion sensors,” *Physical Chemistry Chemical Physics,* vol. 10, no. 1, pp. 73-76, 2008.

[33] A. C. F. Ribeiro, M. C. F. Barros, A. S. N. Teles, A. J. M. Valente, V. M. M. Lobo, A. J. F. N. Sobral and M. A. Esteso, “Diffusion coefficients and electrical conductivities for calcium chloride aqueous solutions at 298.18 K and 310.15 K,” *Electrochimica Acta,* vol. 54, pp. 192-196, 2008.

[34] T. Sokalski, M. Maj-Zurawska and A. Hulanicki, “Determination of true selectivity coefficients of neutral carrier calcium selective electrodes,” *Mikrochimica Acta,* vol. 1, no. 5-6, pp. 285-291, 19991.

[35] S. H. Wang, T. C. Chou and C. C. Liu, “Development of a solid-state thick film calcium ion-selective electrode,” *Sensors and Actuators B-Chemical,* vol. 96, no. 3, pp. 709-716, 2003.

[36] B. Paczosa-Bator, J. Peltonen, J. Bobacka and A. Lewenstam, “Influence of morphology and topography on potentiometric response of magnesium and calcium sensitive PEDOT films

doped with adenosine triphosphate (ATP)," *Analytica Chimica Acta,* vol. 555, no. 1, pp. 118-127, 2006.

[37] G. J. Moody, B. B. Saad and J. D. R. Thomas, "Studies on bis(crown ether) based ion-selective electrodes for the potentiometric determination of sodium and potassium serum," *Analyst,* vol. 114, no. 1, pp. 15-20, 1989.

[38] K. Cunningham, G. Svehla, S. J. Harris and M. A. McKervey, "Sodium-selective membrane-electrode based on p-tert-butycalix[4]arene methoxyethylester," *Analyst,* vol. 118, no. 4, pp. 341-345, 1993.

5.0 CELL TESTING

This chapter focusses on the testing of the microgripper sensor in the real life environment for which it was designed. Here the device is used to manipulate mouse oocytes and electrochemically monitor the efflux of potassium, sodium and calcium ions upon mechanical stressing, all in a background of cell media. Here it will be shown that the K^+ ISE microgripper sensor devices are capable of monitoring changes in potassium ion concentration released from the cell. However, monitoring ion concentration changes with the Na^+ and Ca^{2+} ISE microgripper sensor devices is more challenging due to interference and sensitivity restrictions respectively.

5.1 Cell Signalling Sensing

There are three classical technologies that are used to monitor ion activity and/or concentrations across a cell membrane; these are radiolabelled tracers [1], ion sensitive fluorescent dye indicators [2] [3] and ISEs [4] [5]. ISEs are advantageous over the other methods as numerous ISEs can be used to monitor a single cell at the same time, without their output signals interfering with each other. Additionally, ISEs can monitor ion activity at specific locations, such as the cell surface or cyctoplasm [6]. They are, however, limited, as ISMs are not perfectly selective and in vivo measurements can only be realistically achieved on large cells; typically xenopus oocytes are used, which have diameters of around 1 mm.

Carbon fibre based electrodes were first used to monitor cell signalling in the early 1980s. However, these generally use amperometric methods (not the potentiometric method discussed in this project) for signal detection [7] [8]. The advantages of using carbon fibres were their biocompatibility, they had reasonable working life times, were small (fibre diameters are typically 5 μm) and so tissue damage minimised, and were very resistant to strain so could be placed firmly against the cell without breaking [9]. These carbon fibre

electrodes were further developed by placing the carbon fibre into a glass capillary with a tapered end, usually bevelled to 45° [10]. Epoxy was used to ensure there was a tight seal between the carbon fibre and the glass capillary. These carbon fibre electrodes usually have diameters of 5 – 10 µm, which was important, as the signal to noise ratio improves when the electrode size is similar in size to the detection area. However, electrodes with larger diameters were also useful, as they could detect a greater number of electrochemical events due to the increased spatial and temporal resolution [11] [12]. The carbon fibre could be coated with Nafion, a perfluorinated cation exchange polymer, to significantly reduce any anion interference; however, this was observed in the detection of dopamine in anaesthetised rat brains to reduce the response times, and hence temporal resolution was lost [13] [14]. Further developments have included increasing the flexibility and rigidity of the glass enclosed carbon fibre electrodes by encasing them in a polymer instead. Orwar, Weber and colleagues electrodeposited a negative photoresist onto a carbon fibre and controllably exposed a specific area of the carbon fibre by varying the fabrication parameters of the photoresist [15]. These polymer encased carbon fibre electrodes were then used in tightly configured arrays, increasing the spatial and temporal resolution of the sensor array [16].

ISE have been successfully used to measure steady and dynamic changes in extracellular ion concentration at the surface of single cells and tissue [5]; however, these studies have been carried out in proximity of the cell (2 µm from cell) and so diffusion modelling was used to calculate the expelled concentration. A more recent study has used 1 µm diameter glass pipette ISEs to monitor intracellular ion concentrations [6]. This, however, is an invasive and destructive technique, and not useful for monitoring live cell behaviour.

A common method of monitoring cell signalling is done via patch clamping, which is used specifically to measure ion currents across biological membranes. Patch clamping involves electrically isolating a patch of the cell membrane from the external solution by

pressing an extremely fine pipette, which has been filled with a suitable electrolyte, tightly against the cell membrane and applying suction. Under these conditions the pipette and cell membrane are usually less than 1 nm apart and the seal resistance is more than 10 GΩ, which is important as a high electrical resistance reduces the measured current noise. Patch clamping was first used by Neher and Sakmann in 1976 to resolve currents through single acetylcholine-activated channels in frog skeletal muscle [17].

For patch clamping to work effectively the surface of the cell membrane must be enzymatically cleaned and free of extracellular matrix and connective tissue; cells in tissue cultures are preferred. It is also important that all solutions used are free of dust and macromolecules, such as components of serum, and the pipettes used must have a clean, usually fire polished, tip and must be very small. Loose patch clamping uses large diameter pipettes (10 μm) to gain information over a large area, usually as a measurement of the distribution of ionic channels over a cell membrane.

Sometimes it is necessary to do patch clamping in cell-free mode. In this case the investigation is done with ripped-off patches that can either be inside out or outside out. Inside out patches are made by pulling the membrane patch off the cell into the bath solution. Outside out patches are made by applying suction to destroy the membrane and then pulling it away from the cell. The membrane then re-seals to give a patch whose intracellular face is in contact with the pipette solution. The two methods of producing patches are shown schematically in Figure 5.1.

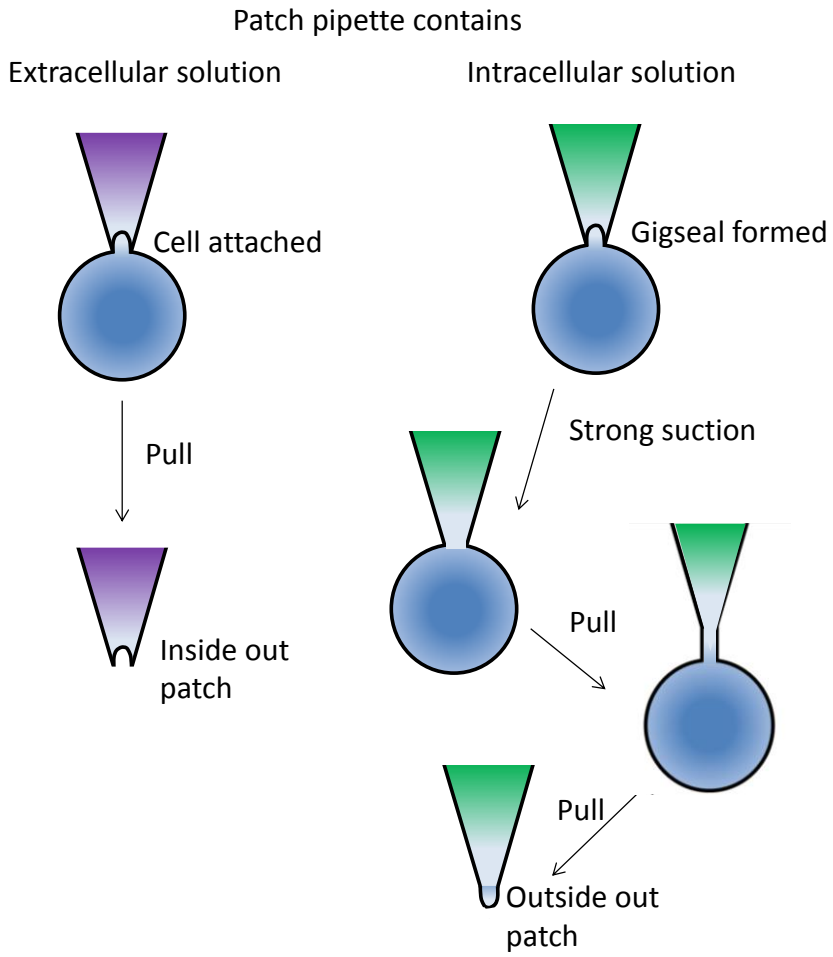

Figure 5.1 – Schematic illustrating inside out and outside out patches.

5.1.1 Cell Communication

Cell signalling is essential for cell survival, as every cell needs to monitor the environment and respond appropriately to any external stimuli, both in time and space. Cells are enclosed within a lipophilic plasma membrane that acts as a formidable barrier to be crossed. Hydrophobic molecules, such as steroid hormones, can simply diffuse across this cell membrane; however, hydrophilic molecules, such as ions, need more elaborate mechanisms to cross, as a large amount of energy is required to put a charged species inside a lipid bilayer that has a low dielectric constant [18].

Cells communicate through electrical and chemical signals. Electrical signalling is very fast (less that 2 ms) but requires the cells to be coupled together, i.e. they are in direct contact

with each other. This is known as juxtacrine signalling and is found mainly in excitable systems such as heart and brain cells. Chemical signalling is much more complex and can occur over short distances (paracrine signalling) or large distances (endocrine signalling) [19].

Cell signalling (or signal transduction) occurs via the following process. First, there is a detection of a stimulus. This is followed by the transfer of a signal to the cytoplastic side of the cell membrane. Transmission of this signal to the effector down a signalling pathway occurs next (the most common method being phosphorylation, by kinases, or dephosphorylation, by phosphatases). Finally a cell response is triggered. This is shown schematically in Figure 5.2. Cell signalling can occur between cells of a single organism, as well as between two different organisms. For example, in mammals early embryo cells exchange signals with uterus cells.

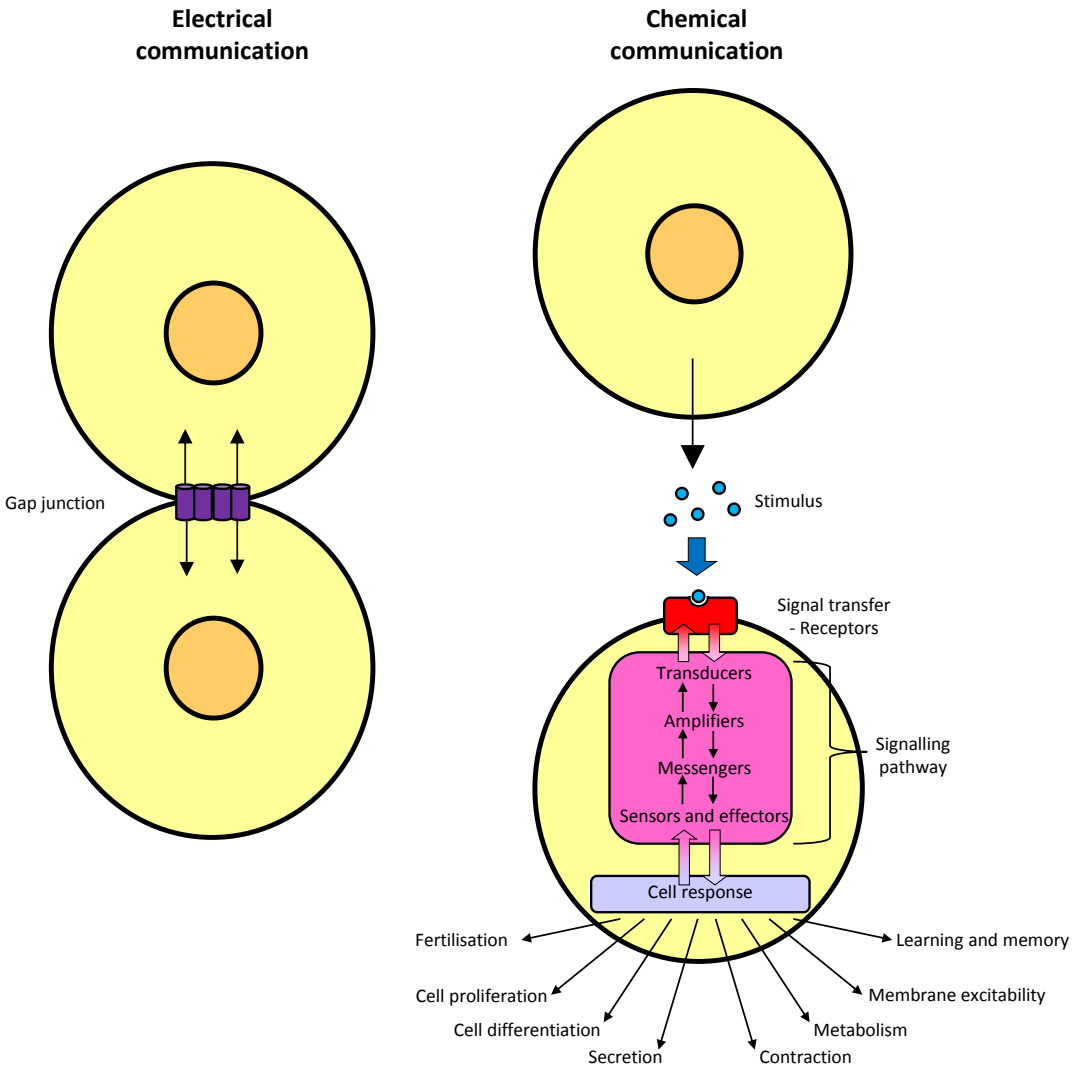

Figure 5.2 – Schematic representation of the general process of cell signalling, adapted from [20].

The microgripper sensor device is intended for use in monitoring the intra and inter cellular ions involved in chemical communication. The main cell membrane receptors involved with interactions with extracellular ligands or ions are ion channels.

Ion channels have two main signalling functions: (1) to generate second messengers; and (2) to function as effectors by responding to such messengers. They are mainly centred around Ca^{2+} signalling pathways, such as the Ca^{2+} entry channels and internal Ca^{2+} release channels.

There are also a large number of K^+ channels, such as voltage dependent K^+ channels, which regulate the membrane potential and excitability; inward rectifier K^+ channels, such as

G protein-gated inward rectifier K^+ (GIRK) channels and ATP-sensitive K^+ channels; and two-pore domain K^+ channels that are responsible for the large background K^+ current [21].

When ion channels are activated, the ions are driven by the electrochemical gradient and move from the inside to the outside of the cell, or vice versa. Ion channel activation occurs via agonist-operated channels (AOCs), which use a ligand as a messenger; or voltage-operated channels (VOCs) that are generally found in excitable cells to control fast cellular processes such as muscle contraction and neurotransmitter release at synaptic endings [22] [23]. Other channel types include thermosensors and mechanosensitive channels (stretch activated channels) [24] [25]. The three main types of ion channels (ligand gated, voltage gated and mechanically gated) are shown schematically in Figure 5.3.

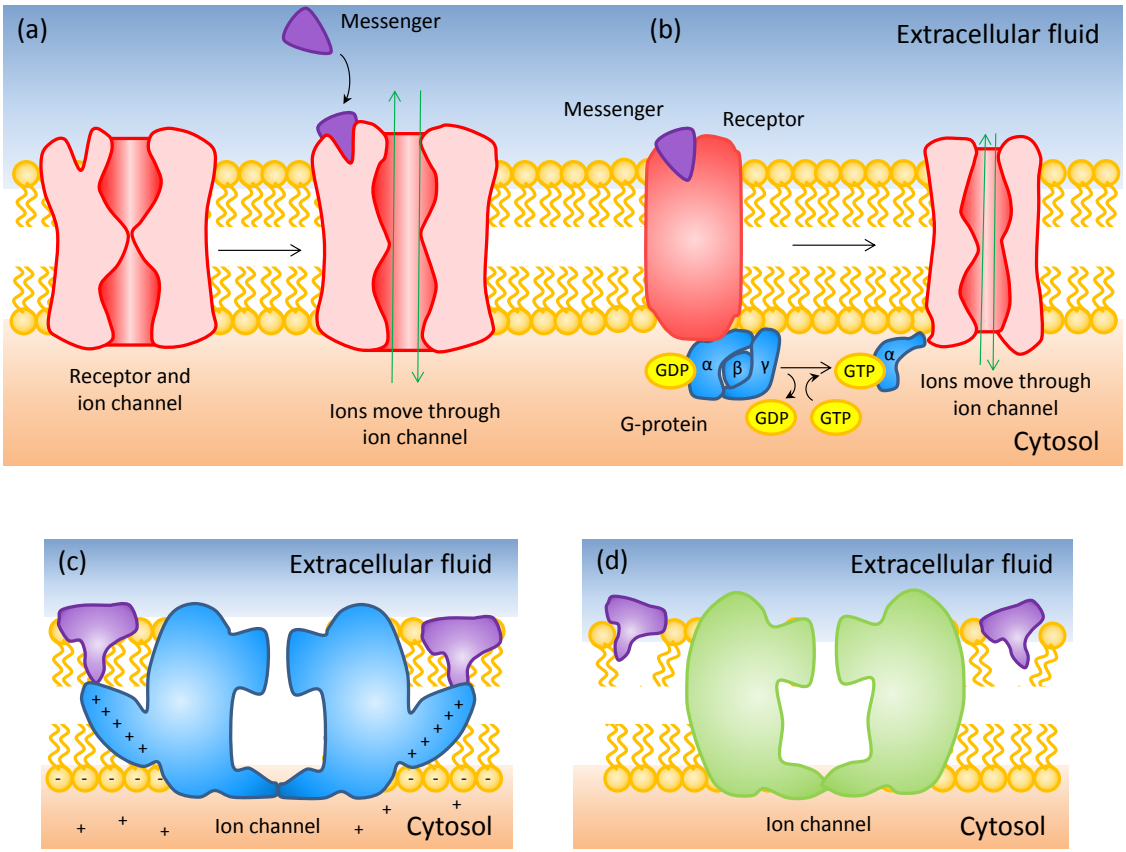

Figure 5.3 – Schematic showing (a) fast ligand gated, (b) slow ligand gated, (c) voltage gated and (d) mechanically gated ion channels.

Fast ligand-gated channels (Figure 5.3(a)) are proteins that function as both receptor and ion channel. The binding of an appropriate messenger opens the ion channel and allows ions to enter or leave the cell, which can then go on to trigger a range of different signalling effects. Slow ligand-gated channels (Figure 5.3(b)) are regulated by a G-protein, which is a molecular switch. When these proteins are bound to guanosine triphosphate (GTP) they are in the 'on' state, so ions can flow through the channel, and when they are bound to guanosine diphosphate (GDP) they are in the 'off' state. A messenger molecule will bind to a G-protein coupled receptor, activating the G-protein. This in turn activates a cascade of different signalling events that 'switch on' the ion channel.

Voltage gated ion channels (Figure 5.3(c)) are activated by changes in the electrical potential (which is dependent on cell type; for example, nerve cells have a resting potential of -60 mV) near the channel. These channels tend to be ion-specific, as the pore through the channel is a specific size, though similarly sized ions with similar charges may travel through the same channel. Voltage gated ion channels are made up of three parts: the voltage sensor, the pore (or conducting pathway), and the gate. In the resting state the membrane is negative on the inside and positive charges reside inside the cell (shown in Figure 5.3(c)); this is known as hyperpolarisation of the membrane. When a potential is applied over the cell membrane, depolarisation of the internal side of the membrane occurs and the positive charges within the cell are driven outwards. The associated electromagnetic field affects the voltage sensor proteins attached to the channel. These voltage sensor proteins, which can either be helical, tubular or paddle shaped, move, and induce a conformational change in the channel that opens up the pore. The movement of ions through the channel generates a transient electrical current (known as the gating current), which depolarises the outside of the cell membrane, and closes the channel [26].

Mechanically gated ion channels (Figure 5.3(d)) open their pores in response to mechanical deformation. These stretch activated ion channels are known as mechanotransducers as they transduce the mechanical stimuli into a biochemical or electrical signal. There are two accepted models by which these channels are opened: the prokaryotic model, where the channels open directly in response to a force on the membrane; and mammalian hair cell model, where a tether bound to both the channel and the extracellular matrix or cytoskeleton is displaced. Once opened, internal and external ions will move across the cell membrane due to osmotic forces.

Given the microgripper sensor device mechanically stresses the cell, the signalling response will likely be dominated by the mechanically gated channels.

5.2 Cell Handling

Cell handling is traditionally done using vacuum pipettes. Denudation pipettes suck the cell into a capillary (with surrounding media), and then the whole unit is moved and the cell expelled from the capillary when repositioned. This work uses the microgripper technology, as discussed in Chapter 2. Figure 5.4 shows a 60 µm mouse oocyte with both technologies.

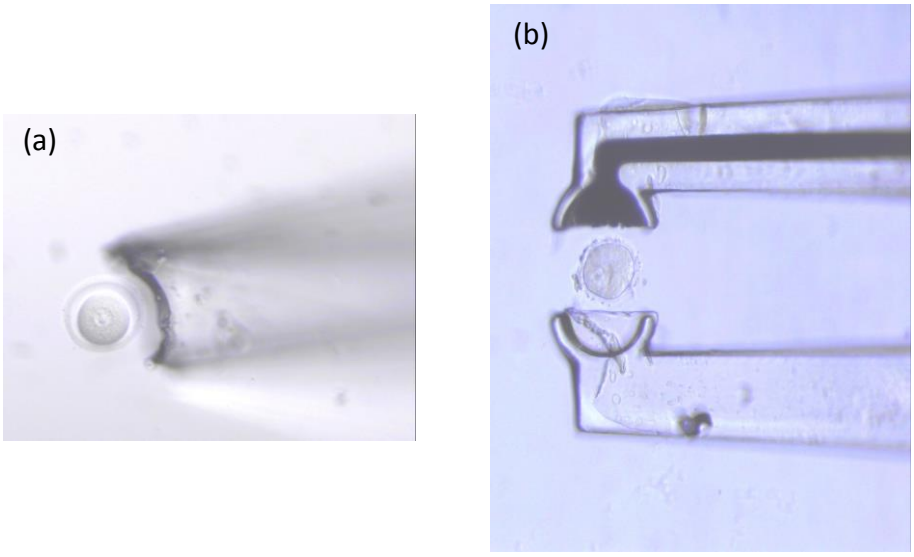

Figure 5.4 – Microscope images of a mouse oocyte with (a) a suction capillary and (b) the microgripper sensor device.

When using the microgripper to manipulate the cells, it was generally found to be easier to catch cells as the microgripper arms are in same focal plane as the cells, whereas the pipette only has the tip in the focal plane. Even with an external manipulator it was quite easy to catch the pipette on the microscope slide, causing it to break, whereas the arms of the microgripper could flex. Additionally, cells are quite sticky, and so can get stuck in the capillary, which only has a finite volume of media to wash them out. Large denudation pipettes that are used with a bulb and holder are better as they use greater volumes of media, but handling can still be a problem.

The microgripper works effectively to move a cell or other small particle around. Figure 5.5 shows the ease of moving a 30 μm particle in the x, y plane. Movement in the z plane, however, is more difficult, as the SU8 polymer that the microgripper cantilevers are fabricated from have a large flex to them, and are also prone to electrostatic charging. This means that the arms of the microgripper bend as they pass through the meniscus of the manipulation fluid. When released from the meniscus the microgripper arms spring back to their resting state which, when manipulating an object, can cause the object to be flung from the tip of the microgripper and be lost. This is not a problem when operating the microgripper outside of a liquid environment. However, for the application of cell handling, an aqueous environment is required to maintain cell health. With the scoop-like arrangement of the microgripper tips it is possible to remove an object from a small droplet of solution simply by dragging it through the side of the droplet, but this requires a large working area.

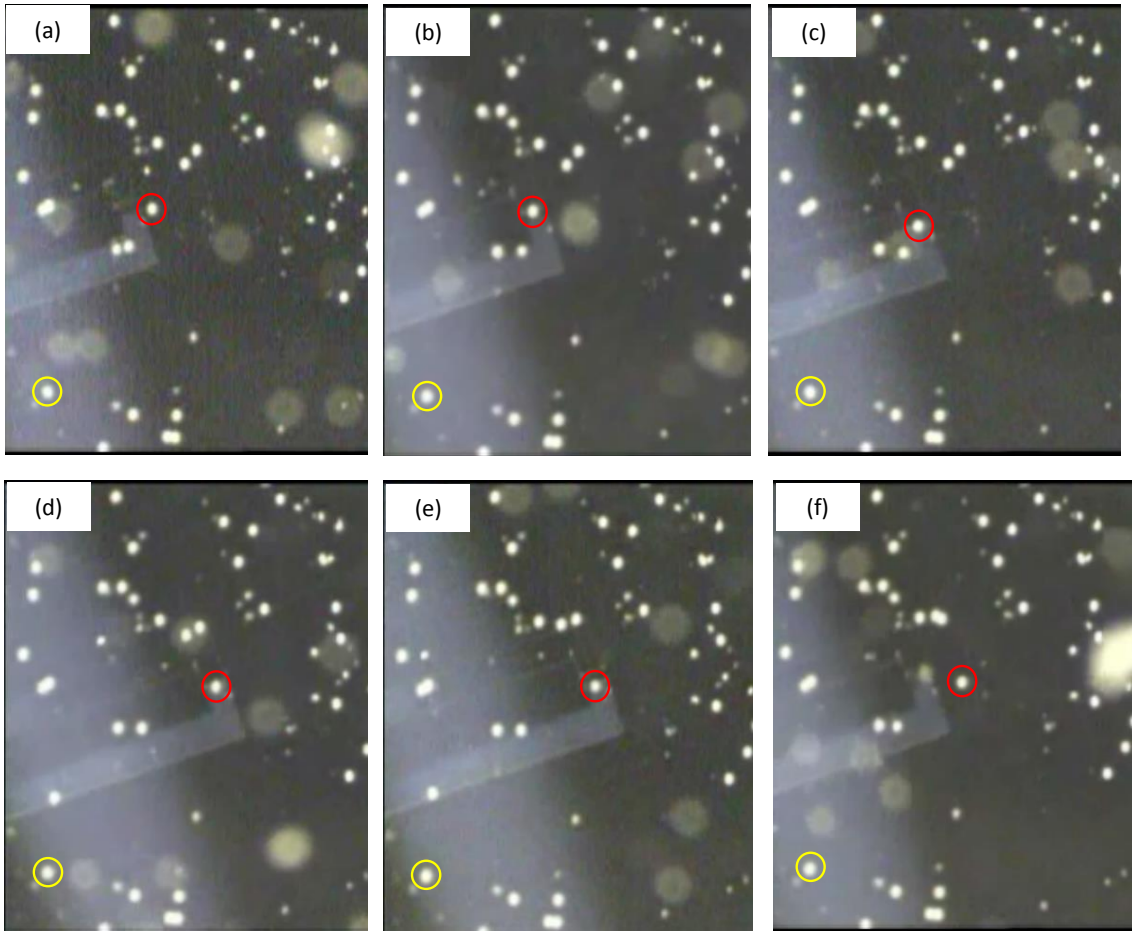

Figure 5.5 – Stills taken from a video showing the manipulation of a 30 µm particle using the microgripper. (a) Approach; (b) capture; (c) movement down; (d) movement right; (e) release; and (f) withdrawal. The red circle highlights the manipulated particle and the yellow circle is a static reference point. The arms of the microgripper are optically transparent, and hence look faded in the images.

5.3 Actuation Interference

During the sensing of changes in specific ion activities of biological ion from a manipulated cell, it is necessary to simultaneously operate both the microgripper actuators and use the ISE as an electrode in potentiometry. When under DC control, it was observed that when a current flows through the actuators, an interference signal was formed in the potentiostat response, shown in Figure 5.6.

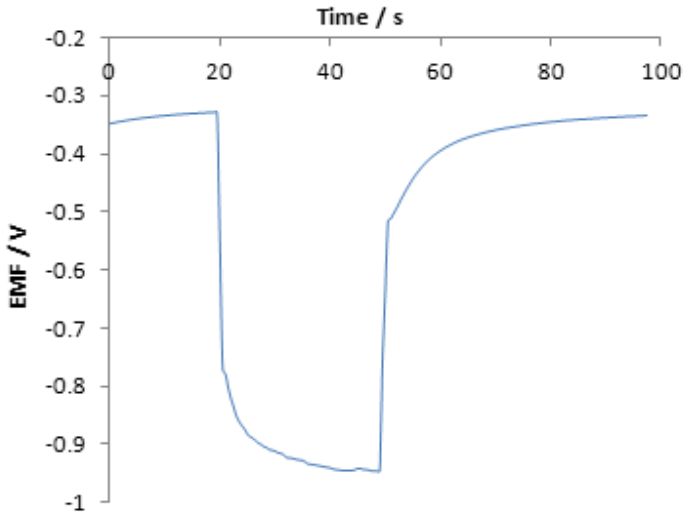

Figure 5.6 – DC actuation interference.

This occurs because, when actuated under DC control, a potential drop relative to ground occurs across the actuators. When the microgripper arms are placed in the highly conductive electrolyte solution the arm becomes a capacitor, with the actuator and solution being the conductive plates and the SU8 being the insulator. The ions within the solution are attracted to the build up of charge in the actuator, causing a drop in the recorded potential between the ISE and the RE on the potentiostat. This is shown schematically in Figure 5.7.

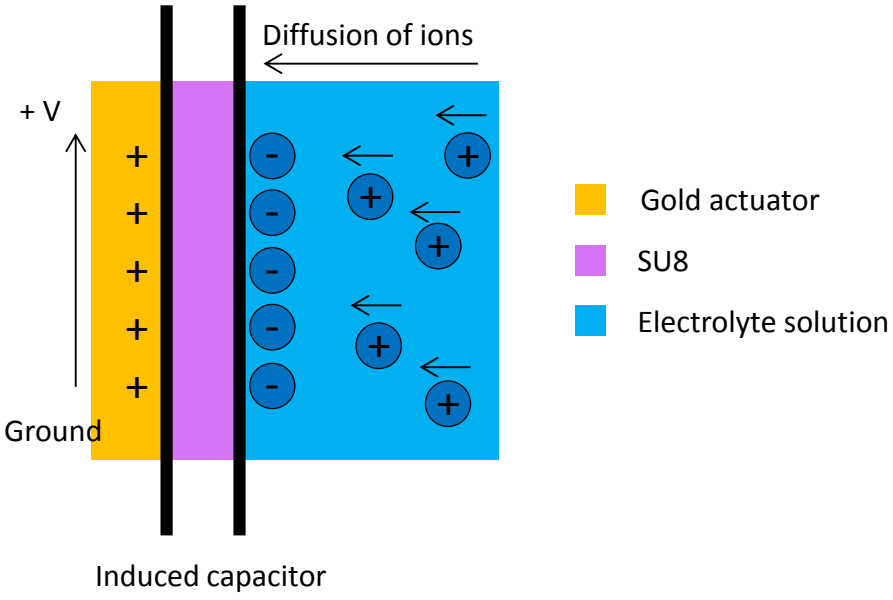

Figure 5.7 – Schematic of the actuator – ISE coupled system under DC control.

Given that the actuators operate via resistive heating of the metal elements, they can also be operated under AC control. When actuated under AC control, if the frequency is high enough so that the electrons cycle faster than the ions can diffuse, no capacitor is formed between the actuator and electrolytic solution, which means the measured potentiometric signal remains stable. Figure 5.8 shows the ISE response upon AC actuation.

At a very low frequency (1 Hz), seen at t = 17 s in Figure 5.8(a), a fluctuating signal is observed. At this frequency the induced capacitor plate within the electrode is switching between positive and negative, and the ions in solution are responding to that change, causing a cycled positive peak and then negative drop in the measured ISE potential.

At low frequencies (100 Hz – 100 kHz), shown in Figure 5.8(b), a drop in potential is generally observed. Even though the actuator potential is cycled about zero, only a negative change in measured potential is observed. This is due to two effects: (1) the potentiostat is sampling every 0.1 s so the signal is undergoing an aliasing like effect (where the signal is discretely sampled at a rate that is insufficient to capture the changes in the signal); and (2) the response time of the ISE device and the time for the ions to diffuse are too slow to fully respond to the cycling of the electrons, so a voltage average signal is observed. This means that, in general, the system behaves like that seen in DC actuation. Occasionally, however, positive peaks are seen, though these are more diffuse peaks, which could be due to the fact that as the ion diffusion takes longer, the averaging of the negative ion effects has a greater effect.

No interference peak is seen at higher frequencies (1 MHz), as shown in Figure 5.8(b), as the frequency is faster than the ions can diffuse and so there is no induced capacitor, meaning that the ions in solution are not affected.

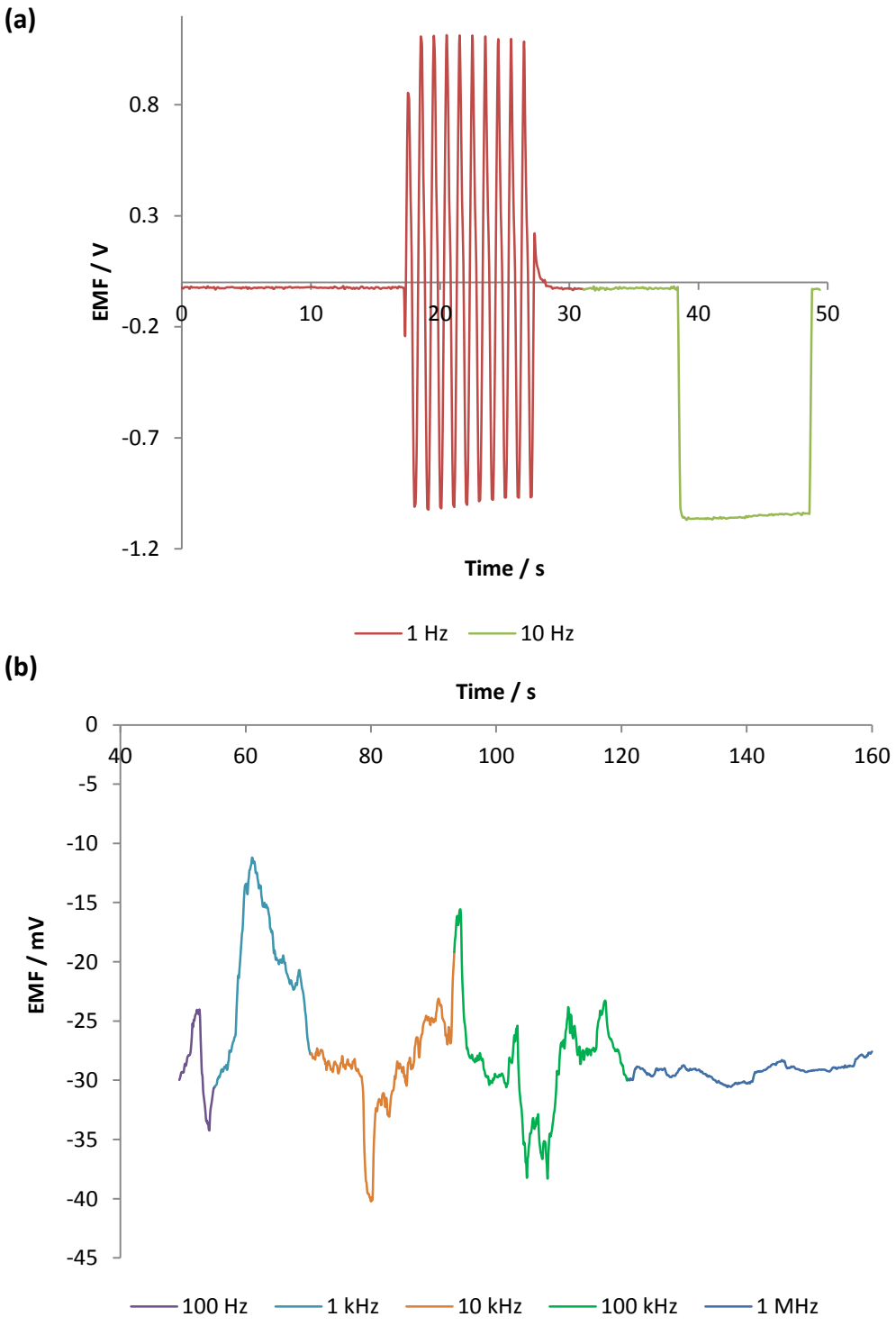

Figure 5.8 – AC actuation interference.

Although the distance between the actuators and the ISE is 1.5 mm, which is a large distance for ions to diffuse or be attracted by the charge layer formed at the actuators, during the ISM deposition process the membrane is usually thinly deposited onto the extended arms and actuators of the microgripper. Hence the interference signal is likely to occur at the

actuators. This signal is then passed down the extended arm to the microgripper tip. It should be noted, therefore, that the formation of this capacitive layer causes a drop (or increase depending on the polarity of the metal) in potential in the solution, which is detected by the ISM deposited on the actuators and extended arms of the microgripper and recorded as an artefact signal response.

Another possible reason for this observed interference is the connection of the circuits through the grounding loop as the DC or AC current source and the potentiostat are both connected to mains ground. Simply removing one or both of these circuits from the mains circuit removes this link. The response plot of the isolated circuits is shown in Figure 5.9.

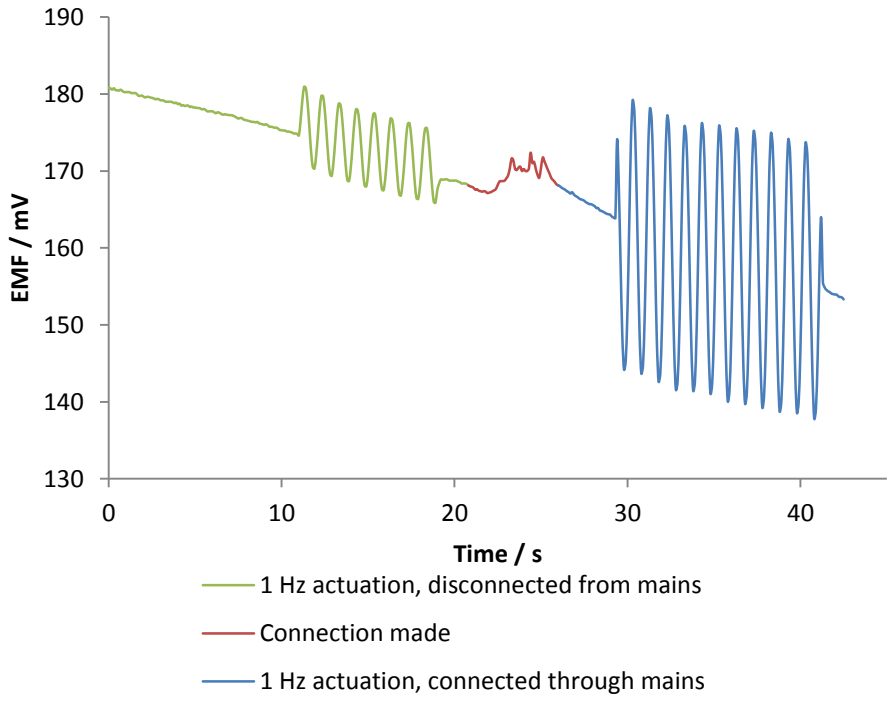

Figure 5.9 – Response plot of an AC interference of two isolated circuits.

It can clearly be seen that the magnitude of the interference signal is reduced on isolating the circuits, but the effect is not removed, indicating that a grounding link is not the cause of the interference signal, but does enhance the problem.

If the interference signal is indeed a capacitive effect, then increasing the thickness of the insulator layer, i.e. the SU8, will effectively increase the distance between the capacitor plates. From Coulombs law (Equation 5.1), the force between two capacitive plates can be derived (Equation 5.2).

$$F = \frac{1}{4\pi\varepsilon_0}\frac{q_1 q_2}{r^2}$$

Equation 5.1

where F is the electric force (N);

ε_0 is the electric constant (F m^{-1});

q_1 and q_2 are the point charges (C);

r is the distance between the two charges (m).

$$F = \frac{\varepsilon_0 A V^2}{2r^2}$$

Equation 5.2

where A is the area (m^2)

V is the potential drop between the plates (V)

r is the distance between the two plates (m)

While the actuator-electrolytic solution capacitor model cannot be accurately modelled using the force between two capacitor plates, as the actuator dimensions closer resemble that of an asymmetrical coaxial wire, the relationship between the force and the distance between the actuators and the ions in solution (i.e. the insulating SU8 thickness) still stands. As the electric force is inversely proportional to the distance squared, as the distance is increased, the force felt by the ions in solution will be significantly reduced. This means that the maximum frequency at which an interference signal is observed, and the magnitude of that interference signal will be reduced.

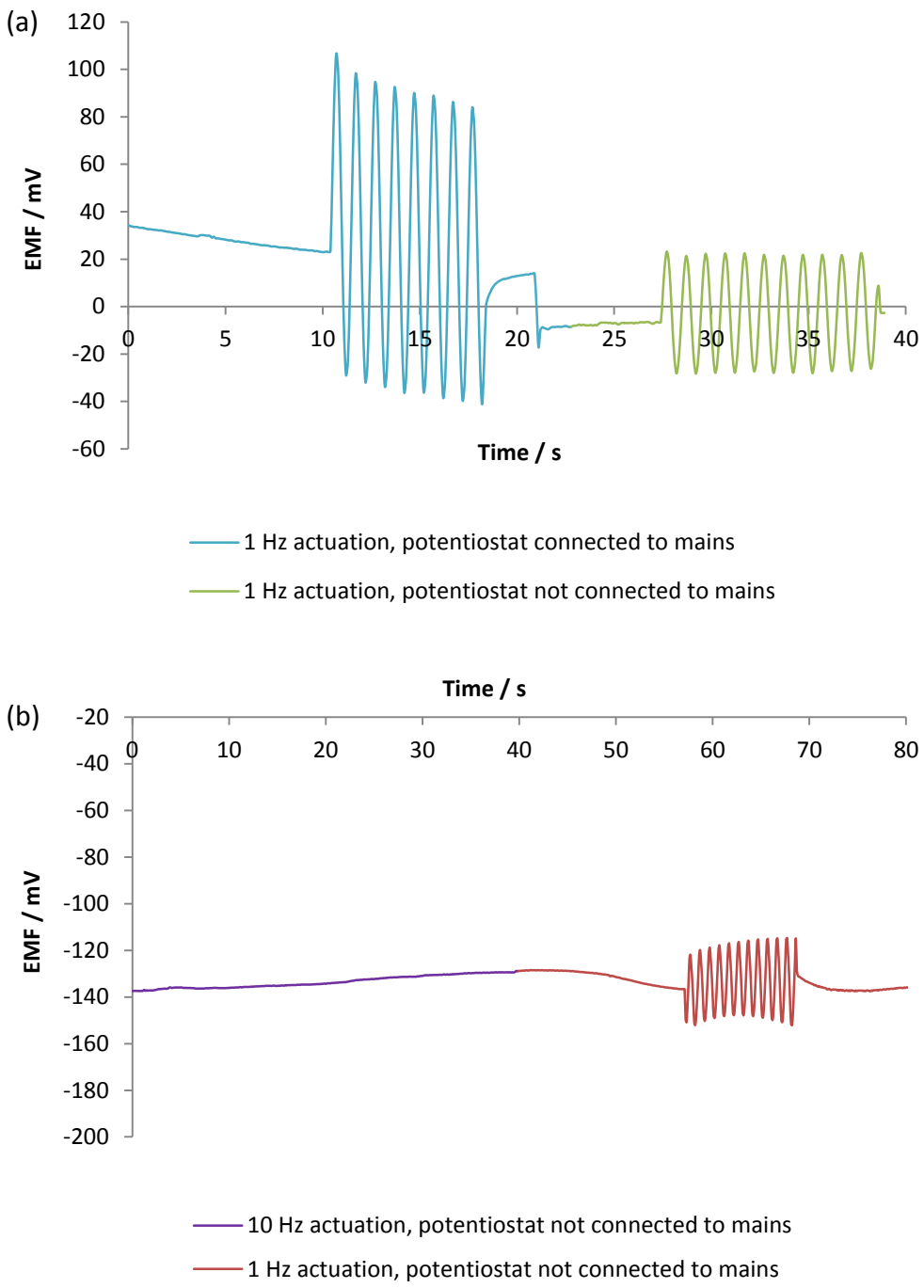

Figure 5.10 – Response plot of AC interference in DI water of a system (a) connected to and isolated from mains and (b) isolated from mains with increased insulator thickness (approx. 25 times thicker).

The thickness of the insulating layer was achieved by painting a layer of positive photoresist (SPR-350) onto the underside of the actuators and letting it dry overnight. This gave an insulator thickness (on the underside) of approximately 50 µm compared to the usual 1.7 µm. Figure 5.10 shows the interference response of a Na^+ ISE in DI water with the different experimental parameters for comparison. It can clearly be seen that increasing the thickness of

the insulator polymer significantly affects the interference response observed. The signal magnitude is further reduced compared to the circuits that are isolated from mains. Additionally, the frequency at which the signal is no longer observed is significantly lowered from 1 MHz to 10 Hz. These details are summarised in Table 5.1.

Table 5.1 – Summary of the observed AC interference signals.

Connected to mains	Insulator thickness / µm	Magnitude of interference signal / mV	Frequency at which signal not observed / Hz
Yes	1.7	130	$1x10^6$
No	1.7	50	$1x10^6$
No	~ 50	35	10

The reduction in the magnitude of the interference is not as great as expected for the large increase in insulator thickness; this is likely due to the restrictions in the simplicity of the model, as the effects on the system due to the ISE have not been considered. There is a large reduction in the maximum frequency at which the signal is not observed, this is directly related to the large reduction in the force and is the dominant effect.

Although the exact mechanism by which the interference occurs is not fully understood, it is likely to be a capacitive effect caused by the activation of the actuators. This causes an electronic change in the solution due to the local diffusion of ions, which is recorded by the potentiostat. There are two methods by which this interference can be removed: (1) by increasing the SU8 layer, to increase the distance between the actuator and the solution; and (2) by operating the actuators at a greater frequency that the ions can diffuse. Due to the restrictions of the fabrication process, increasing the SU8 layer is not feasible, and so controlling the actuator temperature using AC cycling at a frequency greater than the ions can diffuse is the best method to eliminate this interference effect. This allows the microgripper sensor device to be used to monitor changes in ion activity in a solution, as intended.

Additionally all cell experiments should be carried out with the potentiostat and AC current source isolated from mains.

5.4 Experimental

Mouse oocytes, a female immature ovum or egg cell, were the cells used in the sensing experiments. They are rich in cytoplasm that contains the intracellular fluid, the content of which is given in Table 5.2 [27]. Additionally their size (around 60 μm) is within the range that the microgripper tip diameters can be fabricated.

Table 5.2 – Average chemical content in mammalian intracellular fluid.

Ion	Concentration / mM
Potassium	139 – 141
Sodium	12 – 14
Chloride	4
Bicarbonate	10 – 12
Amino acids (in proteins)	128
Magnesium	0.8
Calcium	<0.0002

The plasma membrane of the mouse oocyte is surrounded by the zona pellucida, which is composed of three which is composed of three sulphated glycoproteins [28] [29]. It plays an important role in the fertilisation fertilisation process as it helps bind the spermatozoa. The zona is present in all mammalian oocytes, and does not oocytes, and does not seem to hinder the ability of the oocyte to communicate, indicating that the zona should the zona should not inhibit the movement of ions in and out of the cell, although it could reduce their measured reduce their measured concentration. The zona can be removed by placing the cell in an acidic lysing solution lysing solution known as Acid Tyrode's solution [30], the components of which are shown in

Table 5.3, for 2 – 20 minutes until the zona has dissolved.

Table 5.3 – Chemical components of Acid Tyrode's solution at pH 6.5.

Chemical	Concentration / g L^{-1}
NaCl	8.00
KCl	0.20
$CaCl_2$	0.20
$MgCl_2$	0.10
NaH_2PO_4	0.05
$NaHCO_3$	1.00
Glucose	1.00

Mouse oocytes were obtained from the Centre for Life in Newcastle. These were extracted by researchers in the institution on the day experiments were undertaken, then collected and transported to the research facility in Durham University.

Cells will stay alive for several hours at 37 °C in M2 media, which allowed them to be transported from the Centre of Life in Newcastle. Cells were placed in a sealed eppendorf tube, which in turn was placed into a thermos flask containing water at 37 °C. The thermos flask retained the temperature of the water ± 0.5 °C for several hours; within that needed for travel between Newcastle and Durham (40 min). On arrival, the cells needed to be sorted into those that were healthy and those that were degraded. Figure 5.11 shows the various stages of cell degradation. Healthy cells were kept in an incubator at 37 °C until used; all other cells were disposed of safely.

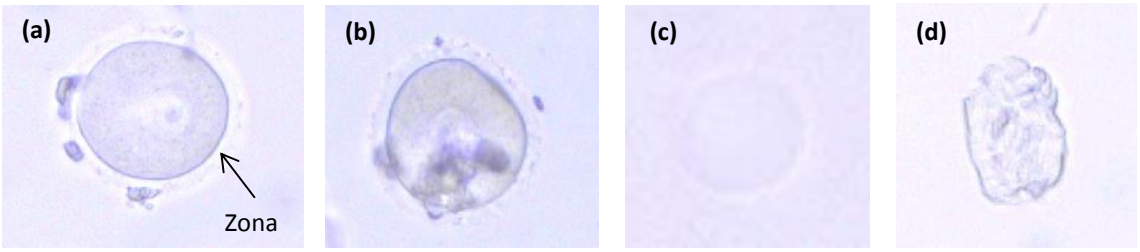

Figure 5.11 – Microscope images of mouse oocytes in various stages of degradation: (a) healthy; (b) yellowing; (c) dissolving and (d) degraded.

All experiments were carried out in M2 media, obtained from Sigma Aldrich, at 37 °C. Acid Tyrode's solution used to remove the zona was purchased from Sigma Aldrich and stored at -20 °C until required.

5.4.1 Stability of the Microgripper Sensor Devices in M2 Media

Although potential drift characterisation has been done for the Ca^{2+} ISE microgripper sensor device, this was in a solution containing a single analyte. The stability of each type of sensor was therefore tested in M2 media, the components of which are shown in Table 5.4, to record the stability of the ISE sensor devices when in contact with a range of interfering ions. During the stability experiments conditioned ISE microgripper sensor devices were placed in M2 media for several hours. The ionic strength of the M2 medium was 3.2×10^{-2} M [31].

Table 5.4 – Chemical components of M2 media [32].

Component	Mass in 1 L / g
Calcium chloride . $2H_2O$	0.25137
Magnesium sulphate (anhydrous)	0.1649
Potassium chloride	0.35635
Potassium phosphate, monobasic	0.162
Sodium bicarbonate	0.35
Sodium chloride	5.53193
Albumin, Bovine Fraction V	4.0
D-Glucose	1.0
HEPES . Na	5.42726
Phenol red . Na	0.0106
Pyruvic acid . Na	0.0363
DL-Lactic acid . Na	2.95

Figure 5.12 shows response of the K^+ ISE device when left in M2 media for 3 hours. A potential drift of 2.0 mV hr^{-1} was observed indicating a moderately stable device, although with some temperature fluctuations. These temperature fluctuations further indicate the importance of temperature control. This potential drift is acceptable over a short time frame, but is far from the high stability range of 0.2 mV hr^{-1}. This poorer observed stability is mainly due to the interference of the other ions (and molecules) present in the M2 media.

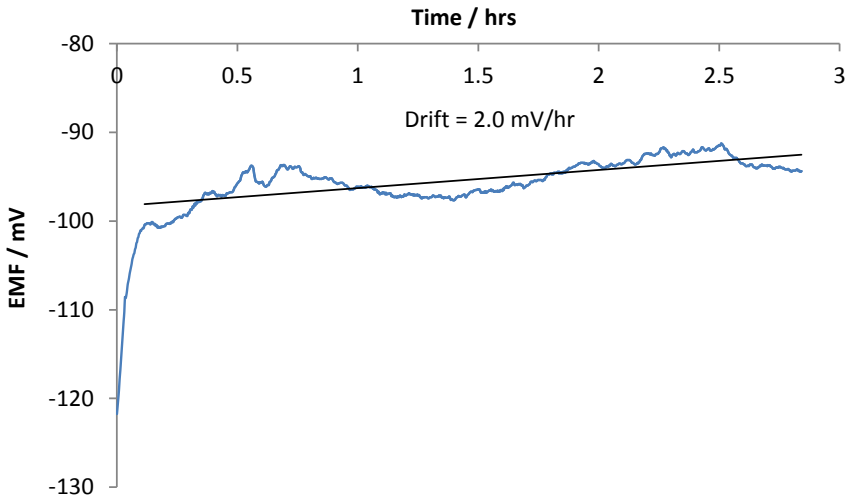

Figure 5.12 – Scan of a K^+ ISE in M2 media.

Figure 5.13 shows the potential drift of the Na^+ ISE microgripper sensor device. Fewer temperature fluctuations are observed, but that is likely to be due to better temperature control of the environment rather than the greater stability of the device. The potential drift of 3.8 mV hr^{-1} is greater than that of the K^+ device, which is to be expected when looking at the selectivity coefficients ($logK_{K,Na}$ = -0.8, $logK_{K,Ca}$ = -1.2). The Na^+ device is more susceptible to interference by the other ions in the M2 media giving rise to a greater potential drift. Looking closely, Figure 5.13 has a similar electrode response to the conditioning profiles seen in Section 4.3.2.2 (Figure 4.6), indicative of the Na^+ ISE incorporating the interfering ions into the membrane.

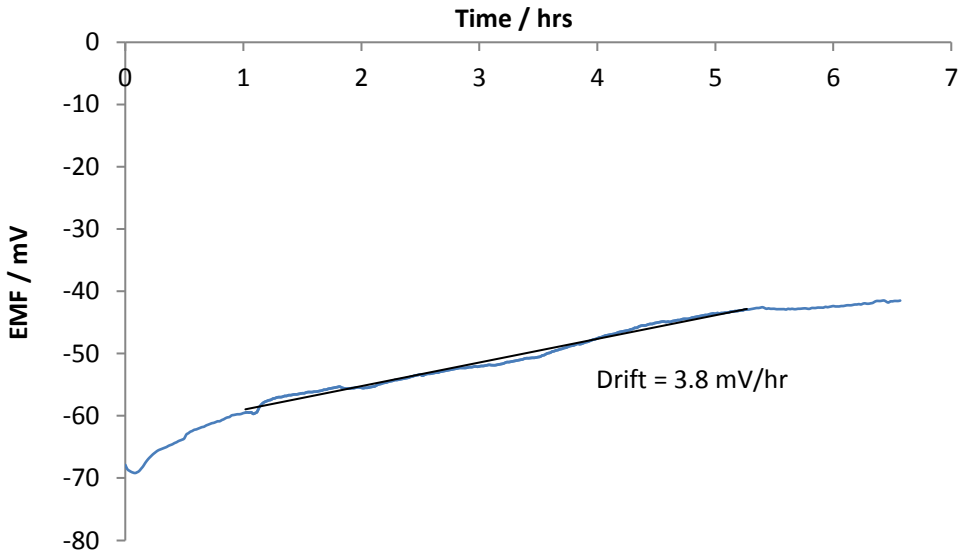

Figure 5.13 – Scan of a Na^{+} ISE in M2 media.

Figure 5.14 shows the potential drift of the Ca^{2+} ISE microgripper sensor device. Interestingly this plot shows two response domains. An initial large negative drift of -10 mV hr^{-1} is observed over the first 10 hours, followed by a more stable negative drift of -0.5 mV hr^{-1} for the subsequent 10 hours. This indicates that during the first 10 hours there is significant loss of calcium from the ISM into the M2 media. This is followed by a more stable drift, but a more noisy response, indicative of an ISE with ill-defined boundary potentials. The stability coefficient with Mg^{2+} as the interfering ion ($\log K_{Ca,Mg}$ = -1.4), the main competitive ion for the calcium ionophore due to the similar size and charge, implies only a slight preference of the ionophore for Ca^{2+} over Mg^{2+}. Magnesium, therefore, is likely to be the main ion that causes the instability in the calcium ISM.

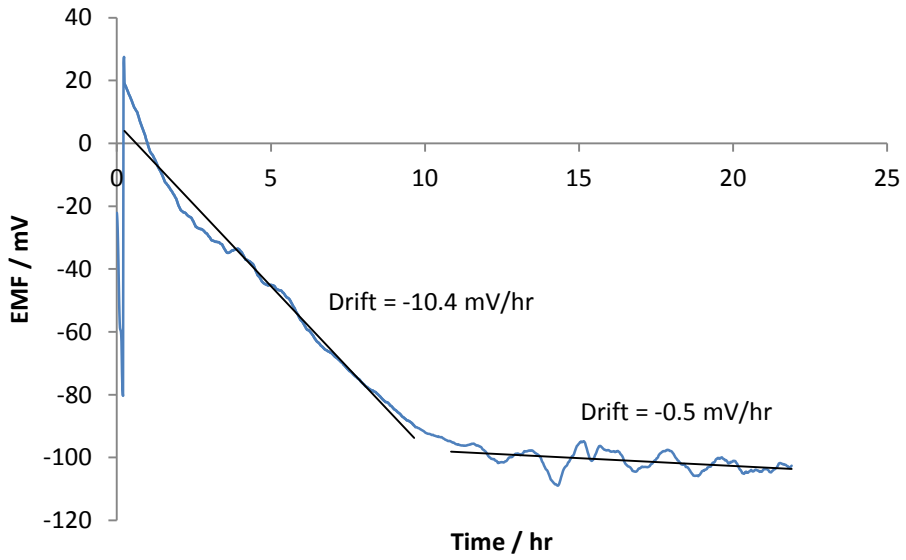

Figure 5.14 – Scan of a Ca^{2+} ISE in M2 media.

5.5 Extracellular Ion Sensing

One device from a wafer set was calibrated and the behaviour of the electrode of all devices fabricated from the same wafer set was assumed to be the same within the linear range, as determined in Section 4.3.2.1, from Figure 4.5.

Normalisation of the calibration plot, i.e. the translation of the calibration plot in the y axis, to the correct EMF values for the specific device used, was done during the experiment as the stable background reading obtained in the M2 media gave the EMF value for the electrode behaviour at the concentration of the ion of interest within the M2 media, which was accurately known.

For reference, the summary of the characterisation behaviour of each type of microgripper sensor device can be found in Table 4.7.

5.5.1 K^+ Sensing

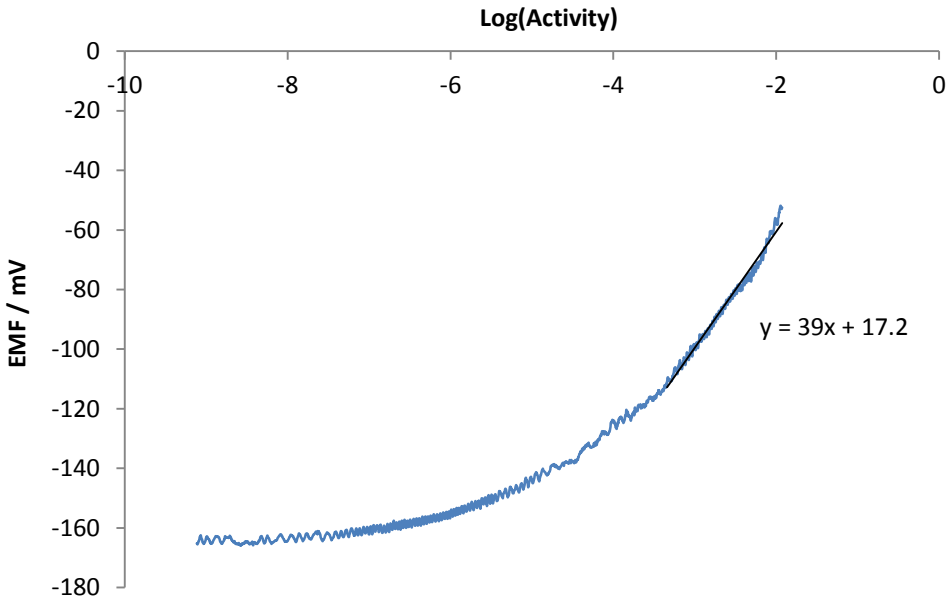

Figure 5.15 – Calibration standard used for the K^+ ISE device done in a background of M2 media.

Figure 5.15 shows the calibration plot for the wafer batch used in the cell sensing experiments. A sub-Nernstian response is still observed, and with a detection limit of 3.3 x 10^{-5} M the device should be able to quantify changes in K^+ concentration from ion movement in and out of the cell.

Figure 5.16 shows a mouse oocyte being mechanically stressed and Figure 5.17 shows the resulting potentiometric response from the K^+ ISE.

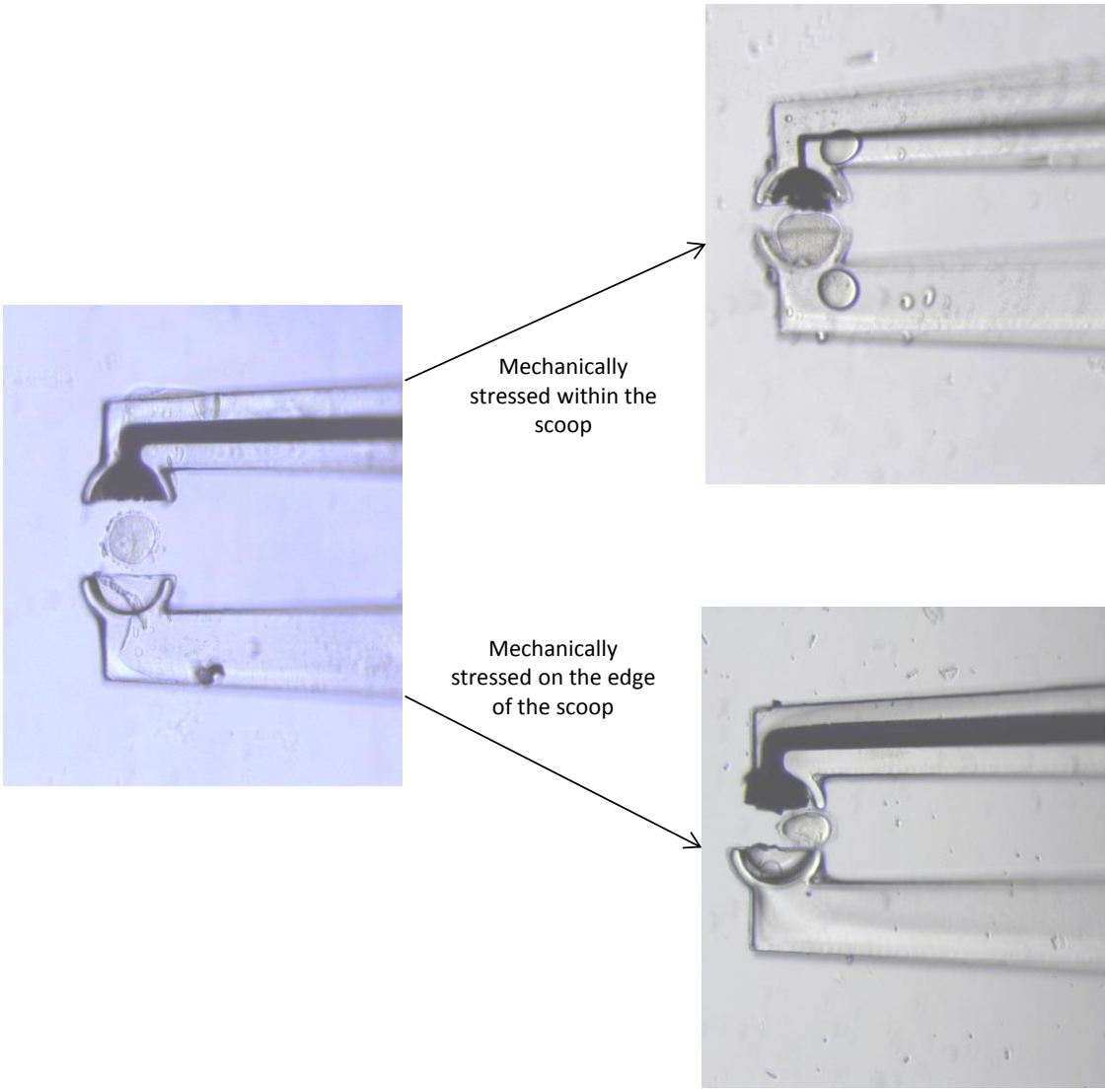

Figure 5.16 – Microscope images of a 60 µm mouse oocyte being mechanically stressed.

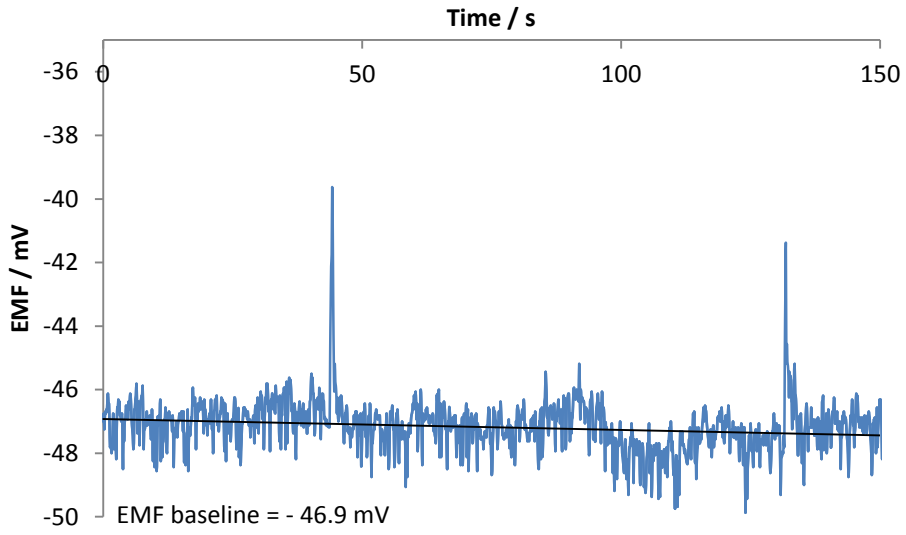

Figure 5.17 – K^+ ISE response from mechanical stressing of a mouse oocyte using the microgripper sensor device actuated at 10 MHz. The two peaks result from actuation with the cell on the edge of the scoop and within the scoop respectively.

The concentration of K^+ in M2 media is 6.0 mM. It is possible to use the stable base line in Figure 5.17 as the calibration point; at this concentration the EMF is -47.1 mV. The calibration plot in Figure 5.15 can therefore be normalised within the linear region, so that at a log(Activity) of -2.2 the EMF is -47.1 mV. This is shown in Figure 5.18.

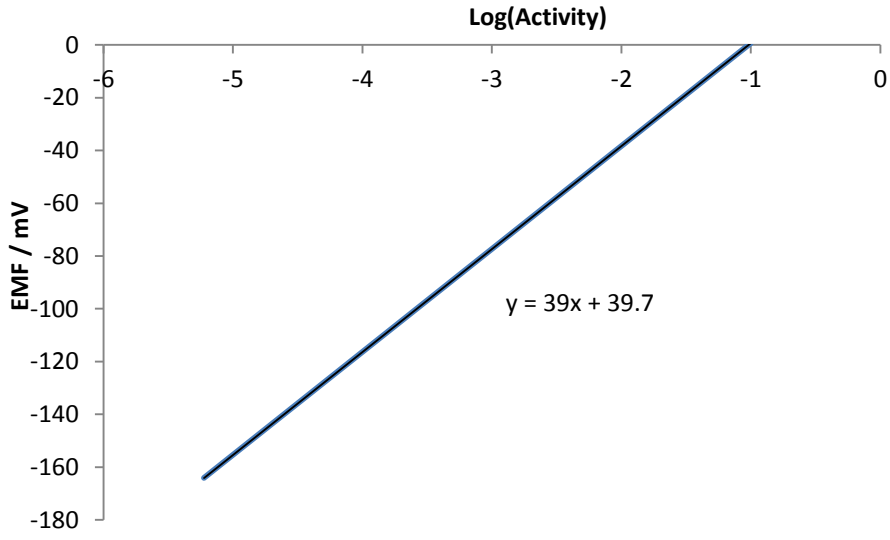

Figure 5.18 – Normalised K^+ calibration plot for the linear region.

The first peak at 44 s in Figure 5.17, which is during full actuation so the cell is under maximum mechanical stress, yields a peak EMF of -39.6 mV. Using the normalised calibration plot, this relates to a concentration of 9 ± 3 mM being expelled by the cell.

The second peak at 132 s in Figure 5.17, which is during half actuation so the cell is under less than maximum mechanical stress, yield a peak EMF of -41.4 mV. Using the normalised calibration plot, this relates to a concentration of 8 ± 3 mM being expelled by the cell.

Measurements were taken with five different devices, with varying applied actuation voltages (applied stress) and under different cell conditions. The quantified data is shown in Table 5.5.

Table 5.5 – K^+ ion concentrations expelled from the mouse oocyte at different applied voltages of actuation.

Device	**V_{app} / V**	**EMF / ± 0.2 mV**	**Concentration expelled / ± 3 mM**
1 (Cell 1)	(Burst)	-32.4	6
1 (Cell 2)	(Burst)	-84.1	12
2 (shown in Figure 5.17)	(Edge of scoop)	-39.6	9
	(Within scoop)	-41.1	8
3	7	-17.2	9
	8	-16.0	10
	9	-18.8	9
4	5	-41.4	10
	7	-39.6	11
	9	-38.2	12
5 (Cell 1 – zona)	10	-145.4	6
(shown in Figure 5.21(a))	10	-145.7	7
5 (Cell 2 – no zona)	10	-167.4	6
(shown in Figure 5.21(b))	10	-168.4	7

It should be noted that while the same actuation voltages yield similar arm deflection, and hence the change is the distance between the tips of the microgripper is the similar ± 1 %,

the stress felt by the cell may be different. This is because when the ISM is deposited into the scoop of the microgripper tip, the volume that is filled differs greatly, meaning that the surface area in contact with the cell is different, and therefore the force felt by that cell will be different. Additionally, different cells vary slightly in size (range of 50 – 70 µm), as well as assorted batches of cells being different, as they have numerous characteristics, such as expression concentrations of critical ions and pattern response to a given stimulus [33]. This makes comparisons between the different devices difficult.

Comparing the results from device 1 to the other devices, the measured expelled concentrations are similar to those for all other devices. The expelled concentration of potassium ions of the burst cell, however, is much lower than the intracellular potassium ion concentration of 139 mM. This could be due to the cellular proteins blocking the interface of the ISM, causing any signal to be reduced. Another possibility is that the concentration of free, unbound ions within the cell is much lower than the total specific ion concentration.

EMF measurements were recorded with an increase in force for devices 2 and 3. Conversely with device 4 the EMF was measured as the force was reduced; this was done to reduce ageing effects in the system.

From Table 5.5, data collected from devices 2, 3 and 4 shows that increasing the stress applied to the cell, i.e. as V_{app} increases, increases the EMF value. It should be noted the EMF for device 3, actuation with V_{app} = 9 V does not fit into this trend. This would indicate that there is a small increase in K^+ ion concentration expelled on an increase in applied stress. However, although this trend is observed in the quantified concentration measurements, the magnitude of that change cannot be conclusively determined since it is smaller than the systematic error. This error is due to the limitation of the calibration procedure (where the calibration of one device is applied to all others for that wafer set). The large variance in the slope response between the different devices generates this high systematic error.

In devices 3 and 4 applied actuation voltages below 7 and 5 V respectively gave no discernible signal. It was observed that at voltages of 5 and 4 V respectively, the microgripper tips were in contact with the cell surface. This lack of signal could indicate that the cell stress signalling mechanism occurs via a switch on response. However, the unknown relationship between the cell stress and applied voltage/stress cannot be determined. It is also possible that at these lower stresses the signal response is not detected due to the signal being below the detection limit of the device. While in the calibration solutions, where the concentration of K^+ is much higher than the background electrolyte used, the detection limit is recorded as 3.3 x 10^{-5} M. However, when in the M2 media, which contains a high background of interfering ions, specifically 98 mM of Na^+ ions, this detection limit will be slightly higher. Especially given that the selectivity coefficient of the K^+ ISE microgripper sensor device against Na^+ ions (-1.8), is good but not excellent.

Another consideration is that the physical contact of the cell with the ISM of the ISE gives an artefact response. This was checked using inert particles to mimic the interaction of the cell with the ISM. Figure 5.19 shows the manipulation of an inert 60 μm polystyrene bead.

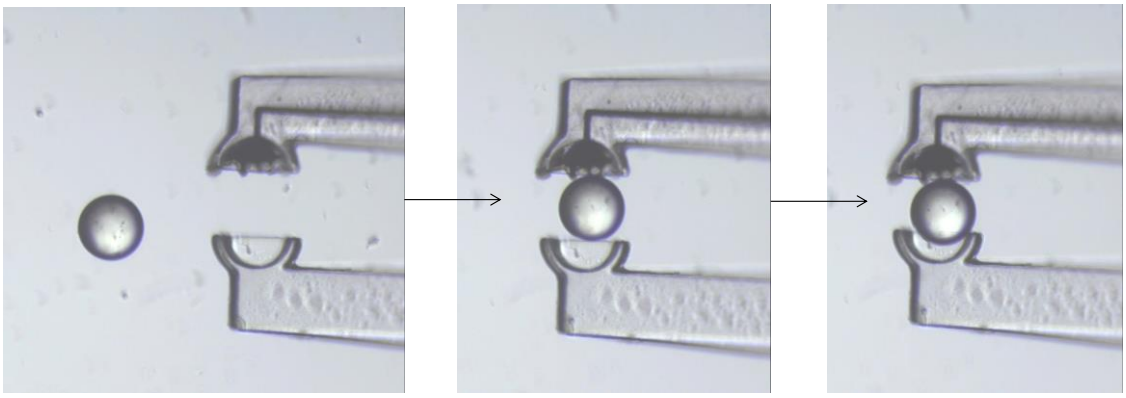

Figure 5.19 – Microscope images showing the microgripper sensor device gripping a 60 μm polystyrene bead.

The resulting potentiometric response is shown in Figure 5.20. It can clearly been seen that there is no response when an object is in contact with the ISM, meaning that any signal recorded when mechanically stressing a cell is due to a change in the local ion concentration.

There are a few dips at 12.6, 30.6, 41.5 and 52.3 s that are due to the actuation interference discussed earlier, but no positive signals as observed in Figure 5.17.

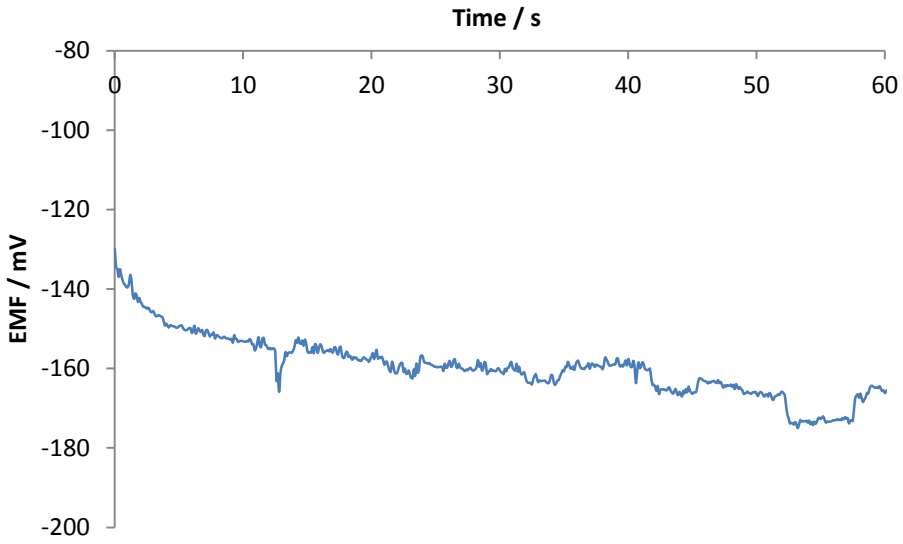

Figure 5.20 – K^+ ISE response from mechanical stressing of an inert particle using the microgripper sensor device actuated at 10 MHz.

These experiments were performed with cells that still had their zona in place. This could have reduced the concentration of the ions expelled, which would reduce the EMF response. Comparing the potentiometric response when mechanically stressing a cell with and without the zona present (Figure 5.21) and quantitatively analysing the peak heights, gives an expelled K^+ ion concentration of 6 $\pm$ 3 mM for peak 1, 7 $\pm$ 3 mM for peak 2, 6 $\pm$ 3 mM for peak 3, and 7 $\pm$ 3 mM for peak 4. Again due to the high error in the quantification method it cannot be conclusively said how or if the presence of the zona is affecting the concentration of potassium sensed from expulsion by the cell. It should be noted that these results were obtained from a different wafer batch and a different calibration plot was used accordingly. This could explain the slightly lower concentrations recorded compared to those shown in Figure 5.17.

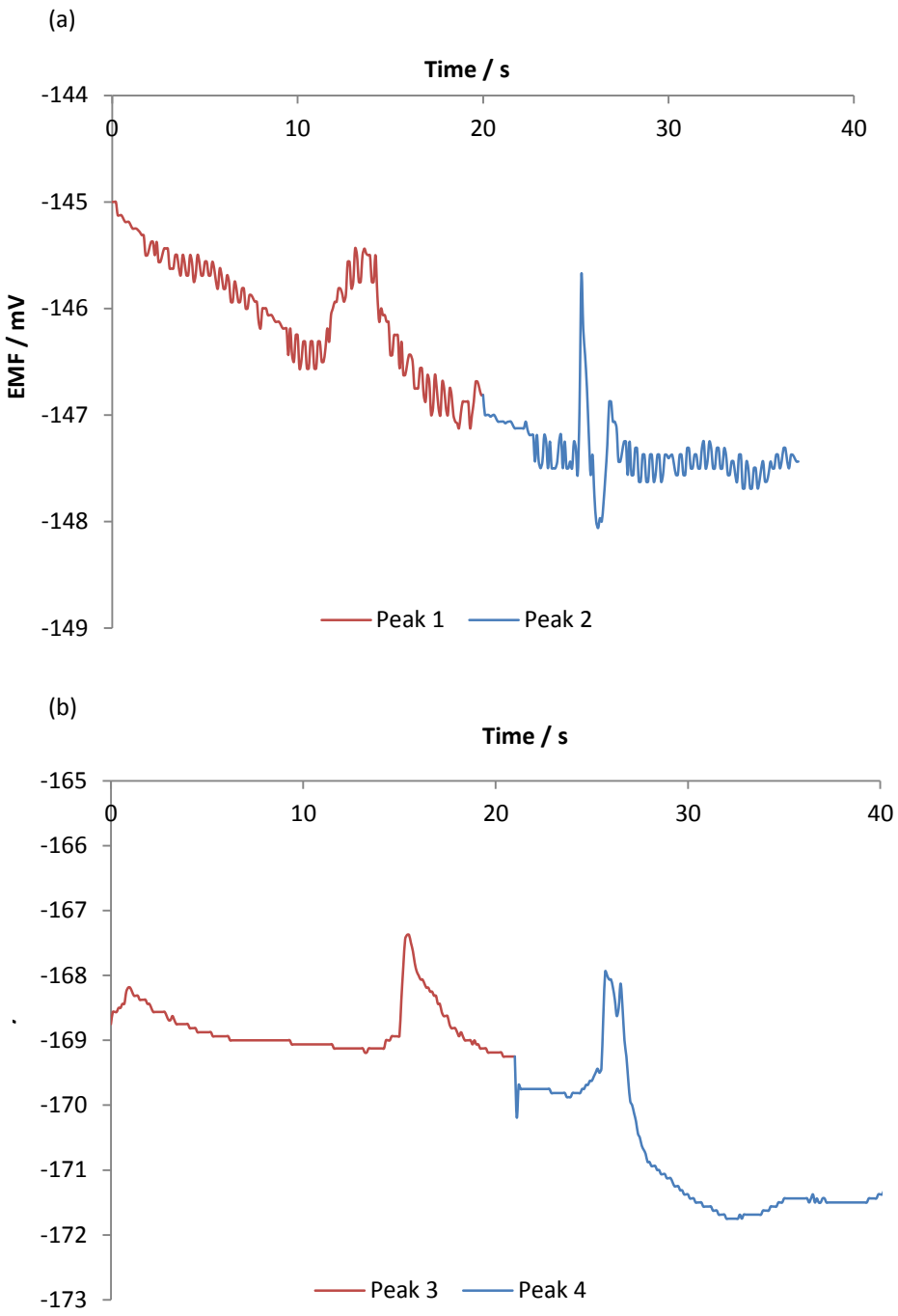

Figure 5.21 – K^+ ISE response from mechanical stressing of a mouse oocyte (a) with zona and (b) without zona using the micrograpper sensor device actuated at 10 MHz.

5.5.2 Na^+ Sensing

Figure 5.22 shows the calibration plot for the wafer batch used in the cell sensing experiments. A sub-Nernstian response is still observed, and with a detection limit of 2.6 x 10^{-4} M the device should be able to quantify changes in Na^+ concentration from ion movement in and out of the cell.

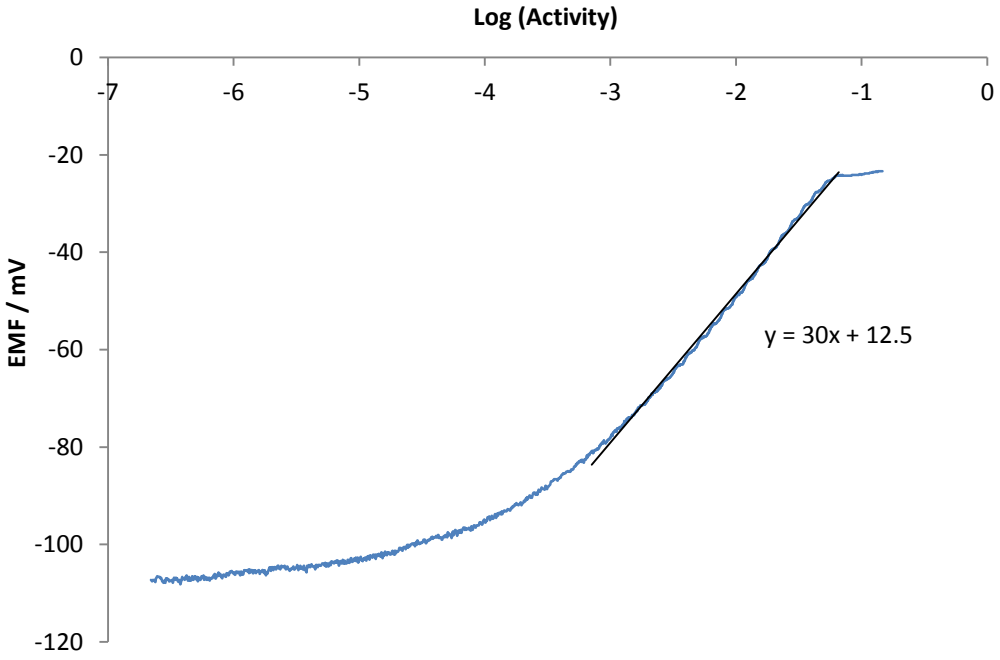

Figure 5.22 – Calibration standard use for the Na^+ ISE device done in a background of M2 media.

There are two main types of signal, and these are shown in Figure 5.23.

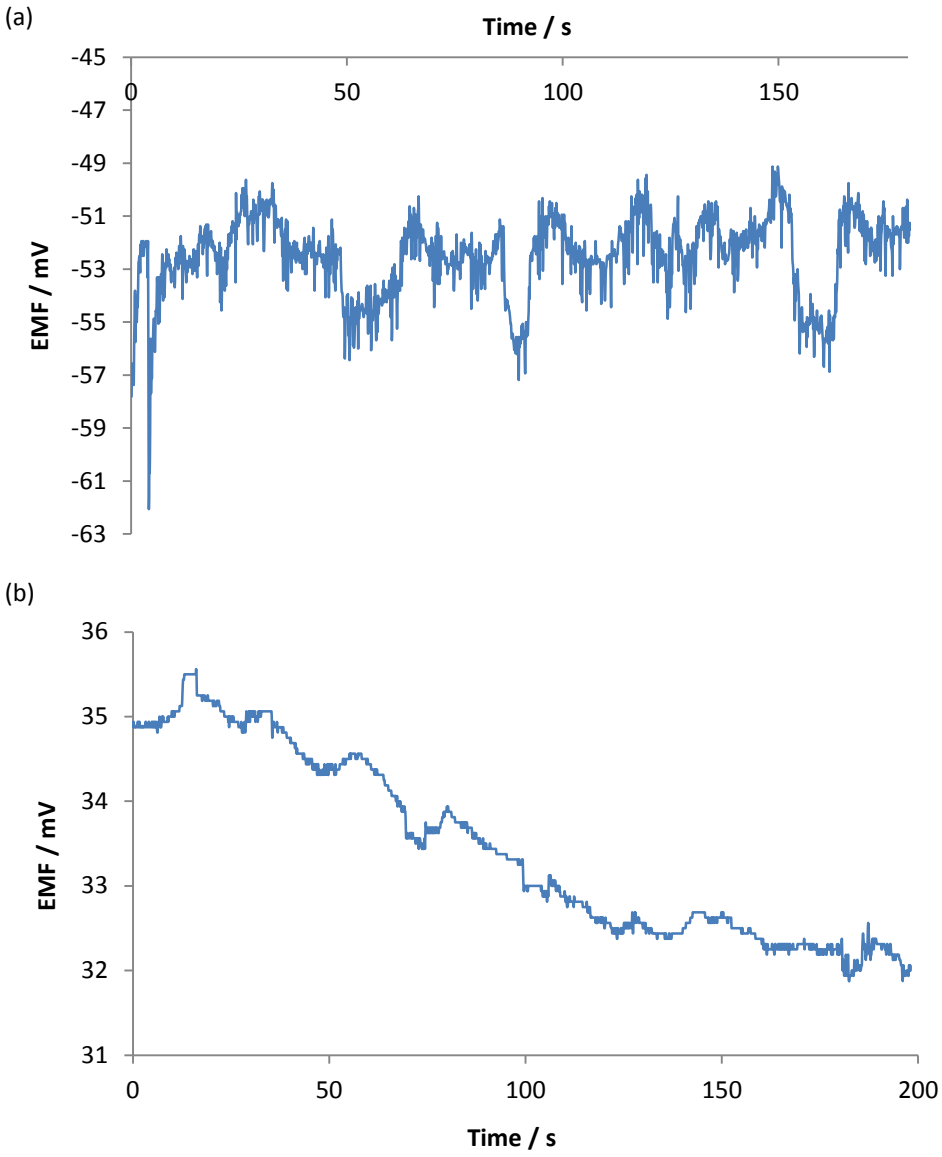

Figure 5.23 – Two different Na^+ ISE responses from mechanical stressing of mouse oocyte using the microgripper sensor device actuated at 10 MHz.

Figure 5.23(a) gives a response that is mainly noise, although slight dips are observed at 45, 80 and 153 s that could be loss of Na^+ ions from the M2 media. When mechanically stressing a cell the mechanically gated ion channels are opened and ions move across the membrane, driven by their concentration gradient. The concentration of Na^+ ions inside the intracellular fluid is 12 mM, compared to 98 mM in the M2 media, so the net movement of ions is from the outside to the inside of the cell. It is difficult to determine whether the dips are due to the actuation interference or a signal response due to Na^+ ion movement into the cell.

Using the base line, which is at the concentration of Na^+ in the M2 media (98 mM), as the calibration point, the EMF is -52.0 mV. The calibration plot in Figure 5.22 can be normalised within the linear region, so that at a log(Activity) of -1.0 the EMF is -52.0 mV. This is shown in Figure 5.24.

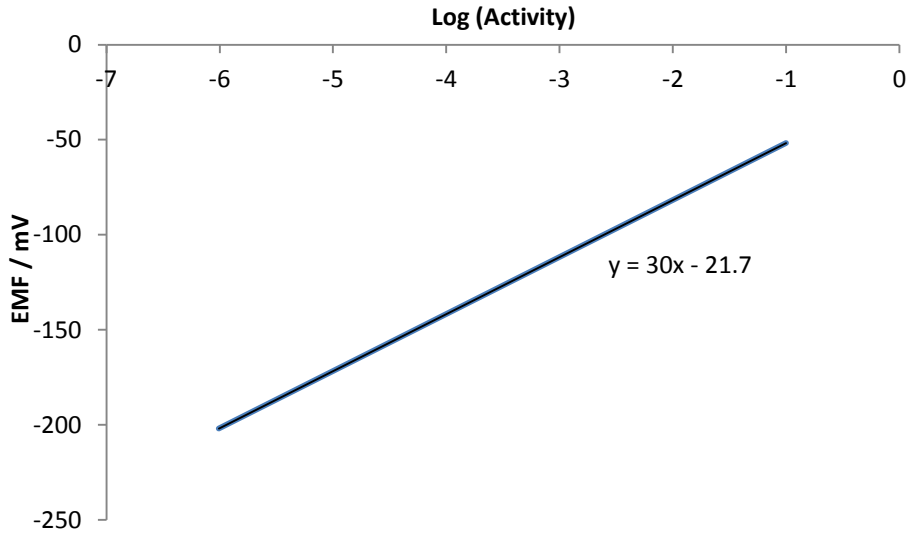

Figure 5.24 – Normalised Na^+ calibration plot for the linear region.

In Figure 5.23(a), the Na^+ ISE microgripper sensor device was actuated without the cell at 110 s, where there is no dip observed. However, quantifying the dips using the normalised calibration plot (Figure 5.24) gives a loss of Na^+ ions of 80 ± 4 mM, which is unrealistically high. Additionally it is observed that the signal response is very noisy, indicative of the interference of the ISM by competitive ions, and so the dips could just be due to this interference destabilising the membrane rather then local changes in sodium ion concentration.

Figure 5.23(b) again illustrates an unstable membrane response as there is a large negative potential drift of -0.03 mV s^{-1} (equivalent to -94 mV hr^{-1} for comparison with potential drift of the Na^+ ISE microgripper sensor device in M2 media shown in Figure 5.13), which is indicative of the leaching of membrane components from the ISM and competitive ion interference. Additionally, analysis of the peaks observed at 5, 49, 79, and 130 s indicates an increase in Na^+ ion activity of 100 ± 4 mM, which given the sodium concentration in the

intracellular fluid is 12 mM, is impossible (the normalised calibration plot used is not shown). Given that the selectivity coefficient of the sodium membrane with potassium ions as the interfering ions ($logK_{Na,K}$ = -0.8) does not show a high affinity of the membrane for sodium ions when in the presence of potassium ion, it is likely, therefore, that these observed peaks are due to the Na^+ ISE microgripper sensor device detecting changes in potassium ion concentration instead of sodium.

Figure 5.25 shows the repeat potentiometric response of the Na^+ ISE microgripper sensor device, again indicating the interference of potassium ions with the sodium membrane.

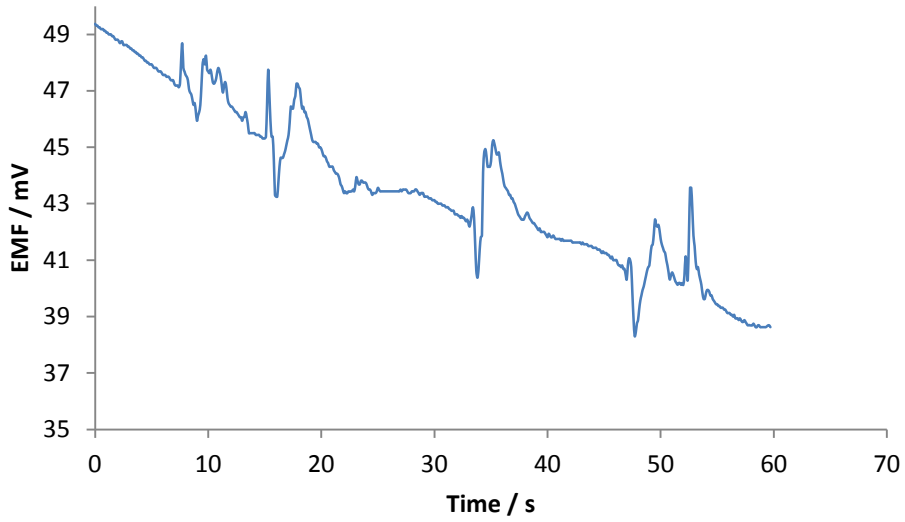

Figure 5.25 – Na^+ ISE response indicating K^+ ion interference.

Table 5.6 summaries the peaks observed in Figure 5.25. Again, when the peaks are quantified using the calibration standard from the Na^+ ISE microgripper device the determined concentrations are well above the maximum concentration of Na^+ ions that could have left the cell. Interestingly, if the calibration plot from the Na^+ ISE microgripper sensor device in a pure solution of potassium ions is used to quantify the peaks observed in Figure 5.25, the concentration values determined are similar to those observed when the K^+ ISE microgripper sensor device is used to determine changes in K^+ ion concentration on mechanically stressing the cell, shown in Section 5.5.1.

Table 5.6 – Summary table of the peak analysis from the Na^+ ISE microgripper device responses from Figure 5.25.

Time peak occurs / s	Analysed as Na^+ ISE / mM	Analysed as K^+ ISE / mM
5	100	6
50	112	7
80	114	7
130	119	7

5.5.3 Ca^{2+} Sensing

The detection limits of the Ca^{2+} ISE microgripper sensor devices are at best 2 x 10^{-5} M, which given the calcium ion concentration in the intracellular fluid is less than 0.0002 mM is beyond the limit that the devices can detect. As mechanically stressing the cell opens the mechanically gated ion channels, Ca^{2+} ions will move from high to low concentration. The concentration of Ca^{2+} in the M2 media is 2.3 mM, which is within the detection limit of the devices, but is very low.

The potentiometric ISE responses from mechanically stressing a mouse oocyte with the Ca^{2+} ISE microgripper sensor devices gave only a background response with no discernible peaks or dips within the noise level. Given that the potential drift observed when the Ca^{2+} ISE microgripper sensor device was places in M2 media was large, indicative of a high membrane component leaching and competitive ion interference, the high noise level in the potentiometric signal response is not surprising.

5.6 Chapter Summary

The first part of this chapter gave an overview of some of the main competitive techniques that have been used to monitor cell signalling in cells; these included patch clamping and carbon fibre electrodes. Carbon fibre electrodes have been used since the 1980s due to their excellent biocompatiblity, good lifetimes, and their small diameters that minimises cell tissue damage. Carbon fibres have been fabricated into ISEs that have been used to measure steady and dynamic changes in extracellular ion concentration. However, these are

usually performed in proximity of the cell (around 2 μm) so diffusion modelling had to be used to accurately quantify ion activity at the cell membrane. ISEs have also been used to monitor intracellular ion concentrations by piercing the cell membrane, although this technique was very invasive and destructive and so was not suitable to monitor live cell signalling. Patch clamping was a common technique for cell signal monitoring, with different connotations on the technique being used depending on the type of signal (electrical or chemical) being monitored. However, patch clamping techniques required an incredible clean environment to work effectively; this included the surface of the cell being enzymatically cleaned and free of extracellular matrix, dust and serum. This was not realistically achievable in real life environments, so patch clamping techniques were generally restricted to lab based analysis.

The second part of this chapter discussed the different types of cell signalling, which were classed as either electronic or chemical. This project concentrated on the chemical signalling type, which occurred via the following scheme. First stimulus was detected, followed by the transfer of a signal to the cytoplastic side of cell (through the cell membrane). This signal was then transmitted through the cell, finally triggering a cell response. The microgripper sensor device was intended for use in monitoring the ionic signal transfer from the outside to the inside of the cell (or vice versa). The transfer of chemical signals across the cell membrane usually occurs via cell receptors, the most common of which were ion channels. There were many different types of ion channels that can be grouped into voltage gated, ligand (or agnostic) gated and mechanically gated. As the microgripper was used to mechanically stress the cell the likely ion channel types of interest were those that were mechanically gated.

The next part of this chapter focused on the comparison of the microgripper sensor device with the denudation vacuum pipettes (the main competitive manipulation technique used). It was observed that when using the microgripper it was easier to catch cells and

particles as they were in the same focal plane as that object being manipulated. It was also observed that it was much easier to break the vacuum pipette, whereas the microgripper device was much more robust as the arms could flex quite substantially. An addition problem with the vacuum pipettes that is not observed when using the microgripper device was that due to their sticky nature, cells could get stuck inside the capillary.

The microgripper sensor device worked effectively at manipulating cells and particles, with particles as small as 30 μm being successfully manipulated. However, the flex in the microgripper arms made movement in the z direction through a liquid-air interface more challenging than with the vacuum pipettes. It was still possible to remove cells and particles from droplets via movement through the liquid-air interface in the x or y direction.

This chapter then went on to discuss the interference observed when the potentiometry of the ISE and the electrothermal actuation was done simultaneously. When activating the actuators under DC control a capacitive layer was created, with the gold of the actuator and the electrolytic solution being the two conducting plates, and the SU8 polymer as the insulator. When operating the actuators under AC control, at a high enough frequency (1 MHz or greater), the electrons in the gold cycled faster than the ions in the electrolytic solution could diffuse, and so a capacitive plate was not formed and the interference signal was not observed. Although the ion selective electrode was 1.5 mm from the actuators, the method of ion selective membrane deposition meant that the whole of the microgripper was coated in ISM, significantly reducing the distance over which the ions had to diffuse to several microns.

The stability of all the microgripper sensor devices in M2 media (the media in which the cell investigations were conducted) was good over short time frames (several minutes). However, over several hours they showed evidence that in a mixed ionic system there was significant interference by other ions in the system, which indicated that ionic interference

caused a stability problem within the microgripper sensor devices. Specifically the stability of the K^+ ISE microgripper sensor device was 2 mV hr^{-1}, which was by far the most stable compared to the other devices. The Na^+ ISE microgripper sensor device had a stability of 3.8 mV hr^{-1}, which when the selectivity coefficients of the Na^+ ISM with the main interfering ions in the M2 media were considered, indicated that the Na^+ ISE microgripper sensor devices were more susceptible to interference by these ions. The Ca^{2+} ISE microgripper sensor device had a large initial drift of -10 mV hr^{-1}, followed by more stable drift of -0.5 mV hr^{-1}, which was again indicative of the instability of the Ca^{2+} devices.

The last part of this chapter concentrated on the signal response from mechanically stimulated mouse oocytes recorded using the ISE microgripper sensor devices. Inert 60 µm polystyrene beads were used to determine whether there was any interference from the physical contact of the bead (or cell) with the ISM. It was observed that a stable background was produced with no discernible signal response from physical contact.

Sensing K^+ ion movement from a mechanically stressed mouse oocyte using the K^+ ISE microgripper sensor devices gave a good response, with an increased in K^+ ion concentration upon mechanically stressing of the cell. These signals are summarised inTable 5.5.

This was a reasonable response given that the maximum concentration of K^+ ions in the intracellular fluid of a cell is 139 mM. It was observed that the presence of the zona around the cell membrane had no effect on the signal response, indicating that the transfer of K^+ ions through the zona was not impaired. Differences in the cell response from varying the level of mechanical stress were shown to have an increase in EMF (and hence concentration) with increasing stress. However, due to the large systematic error in the concentration analysis, the magnitude of this change is unknown. Initial studies also indicated that stress signalling occurred via a switch on mechanism as no signals were observed at low stress levels, i.e. when the microgripper was just in touch with the cell.

Sensing Na^+ ion movement from a mechanically stressed mouse oocyte using the Na^+ ISE microgripper sensor devices gave either a noisy signal where it was impossible to resolve any signal response, or a signal response that was dominated by the sensing of K^+ interfering ions. This was unsurprising given that the selectivity coefficients for the Na^+ ISE microgripper sensor device indicate that this device is much more susceptible to these interfering ions.

Sensing Ca^{2+} ion movement from a mechanically stressed mouse oocyte using the Ca^{2+} ISE microgripper sensor devices gave no response as the limit of detection for these devices was not great enough to detect the 0.0002 mM Ca^{2+} ion concentration found in the intercellular fluid.

5.7 References

[1] D. Markovich, "Expression cloning and radiotracer uptakes in Xenopus Laevis oocytes," *Nature Protocols,* vol. 3, no. 12, pp. 1975-1980, 2008.

[2] R. Y. Tsien, "Fluorescent indicators of ion concentration," *Methods in Cell Biology,* vol. 30, pp. 127-156, 1989.

[3] Y. Umezawa, "Genetically coded optical probes for imaging cellular signaling pathways," *Biosensors and Bioelectronics,* vol. 20, pp. 2504-2511, 2005.

[4] B. Reid and M. Zhao, "Ion-selective self-referencing probes for measuring specific ion

flux," *Communicative and Integrative Biology,* vol. 4, no. 5, pp. 524-527, 2011.

[5] M. A. Messerli, E. D. Corson and P. J. Smith, "Measuring extracellular ion gradients from single channels with ion-selective microelectrodes," *Biophysical Journal: Biophysical Letters,* vol. 92, no. 7, pp. L52-L54, 2007.

[6] S. -K. Lee, W. F. Boron and M. D. Parker, "Monitoring ion activities in and around cells using ion-selective liquid-membrane microelectrodes," *Sensors,* vol. 13, pp. 984-1003, 2013.

[7] M. A. Dayton, A. G. Ewing and R. M. Wightman, "Evaluation of amphetamine-induced in vivo electrochemical response," *European Journal of Pharmacology,* vol. 75, pp. 141-144, 1981.

[8] F. Gonon, M. Buda, R. Cespuglio, M. Jouvet and J. F. Pujol, "In vivo electrochemical detection of catechols in the neostraitum of anaesthetized rats: dopamine or DOPAC?," *Nature,* vol. 286, pp. 902-904, 1980.

[9] K. L. Adams, M. Puchades and A. G. Ewing, "In vitro electrochemistry of biological systems," *Annual Review of Analytical Chemistry,* vol. 1, pp. 329-355, 2008.

[10] K. T. Kawagoe, J. B. Zimmerman and R. M. Wightman, "Principles of voltammetry and microelectrode surface states," *Journal of Neuroscience Methods,* vol. 48, pp. 225-240, 1993.

[11] E. R. Travis and R. M. Wightman, "Spatio-temporal resolution of exocytosis from individual cells," *Annual Review of Biophysics and Biomolecular Structure,* vol. 27, pp. 77-103, 1998.

[12] P. S. Cahill, Q. D. Walker, J. M. Finnegan, G. E. Mickelson, E. R. Travis and R. M. Wightman, "Microelectrodes for the measurement of catecholamines in biological systems," *Analytical Chemistry,* vol. 68, no. 3, pp. 180-186, 1996.

[13] G. A. Gerhardt, A. F. Oke, G. Nagy, B. Moghaddam and R. N. Adams, "Nafion-coated electrodes with high selectivity for CNS electrochemistry," *Brain Research,* vol. 290, no. 2, pp. 390-395, 1984.

[14] E. W. Kristensen, W. G. Kuhr and R. M. Wightman, "Temporal characterization of perfluorinated ion exchange coated microvoltammetric electrodes for in vivo use," *Analytical Chemistry,* vol. 59, pp. 1752-1757, 1987.

[15] B. A. Lambie, O. Orwar and S. G. Weber, "Controlling the electrochemically active area of carbon fibre microelectrodes by the electrodeposition and selective removal of an insulating photoresist," *Analytical Chemistry,* vol. 78, no. 5, pp. 165-171, 2006.

[16] A. Hermans and R. M. Wightman, "Conical tungsten tips as substrates for the preparation of ultramicroelectrodes," *Langmuir,* vol. 22, pp. 10348-10353, 2006.

[17] E. Neher and B. Sakmann, "Single-channel currents recorded from membrane of denervated frog muscle fibres," *Nature,* vol. 260, pp. 799-802, 1976.

[18] A. Parsegian, “Energy of an ion crossing a low dielectric membrane: Solutions to four relevant electrostatic problems,” *Nature,* vol. 221, pp. 844-846, 1969.

[19] O. H. Petersen, “Ca2+ signalling and Ca2+ activated ion channels in exocrine acinar cells,” *Cell Calcium,* vol. 38, no. 3-4, pp. 171-200, 2005.

[20] M. J. Berridge, “Cell Signalling Biology: Module 1 Introduction,” BJ Signal, [Online]. Available: www.biochemj.org/csb/001/csb001.pdf. [Accessed 22 April 2013].

[21] M. Berridge, “Cell Signalling Biology: Module 3 Ion Channels,” BJ Signal, [Online]. Available: www.cellsignallingbiology.org/csb/003/csb003.pdf. [Accessed 22nd April 2013].

[22] I. Bezprozvanny, P. Zhong, R. H. Scheller and R. W. Tsien, “Molecular determinants of the functional interaction between syntaxin and N-type Ca2+ channel gating,” *Proceedings of the Natioinal Academy of Sciences of the United States of America,* vol. 97, no. 25, pp. 13943-13948, 2000.

[23] S. Q. Wang, L. S. Song, E. G. Lakatta and H. Cheng, “Ca2+ signalling between single L-type Ca2+ channels and ryanodine receptors in heart cells,” *Nature,* vol. 410, pp. 592-596, 2001.

[24] A. P. Christensen and D. P. Corey, “TRP channels in mechanosensation: direct or indirect activation,” *Nature Reviews Neuroscience,* vol. 8, pp. 510-521, 2007.

[25] S. Sukharev and D. P. Corey, “Mechanosensitive channels: multiplicity of families and gating paridigms,” *Science Signalling STKE,* no. 219, p. re4, 2004.

[26] F. Bezanilla, “Voltage-gated ion channels,” *IEEE Transactions on Nanobioscience,* vol. 4, no. 1, pp. 34-48, 2005.

[27] H. Lodish, A. Berk, L. Zipursky, P. Matsudaira, D. Baltimore and J. Darnell, Molecular Cell Biology 4th Ed., New York: W. H. Freeman, 2000.

[28] E. S. Boja, T. Hoodbhoy, H. M. Fales and J. Dean, “Structural characterization of native mouse zona pellucida proteins using mass spectrometry,” *Journal of Biological Chemistry,* vol. 278, pp. 34189-34202, 2003.

[29] L. Han, M. Monne, H. Okumura, T. Schwend, A. L. Cherry, D. Flot, T. Matsuda and L. Jovine, “Insights into egg coat assembly and egg-sperm interaction from the x-ray structure of full-length ZP3,” *Cell,* vol. 143, no. 3, pp. 404-415, 2010.

[30] H. C. Zeringue, M. B. Wheeler and D. J. Beebe, “A microfluidic method for removal of the zona pellucida from mammalian embryos,” *Lab on Chip,* vol. 5, no. 1, pp. 108-110, 2004.

[31] R. Cruz, I. Lazaro, I. Gonzalez and M. Monroy, “Acid disssolution influences bacterial attachment and oxidation of arsenopyrite,” *Minerals Engineering,* vol. 18, pp. 1024-1031, 2005.

[32] Sigma-Aldrich, “Product Information M2 Medium,” [Online]. Available: http://www.sigmaaldrich.com/etc/medialib/docs/Sigma/Product_Information_Sheet/1/m7167pis.Par.0001.File.tmp/m7167pis.pdf. [Accessed 08 May 2013].

[33] C. E. Sims and N. L. Allbritton, “Analysis of single mammalian cells on-chip,” *Lap on Chip,* vol. 7, pp. 423-440, 2007.

6.0 CONCLUSION

The aim of this project was to design, fabricate, characterise and test a potentiometric ion selective electrode situated at the tip of a specially designed electrothermally actuated microgripper. This microgripper sensor device was intended for use in the application of detecting, in real time, movement of keys ions involved in intercellular communication, specifically potassium, sodium and calcium, from a mechanically stressed single cell. The cells used in this study were mouse oocytes.

6.1 Improvements to the Microgripper Fabrication Process

Initial work concentrated on improving the microgripper fabrication first proposed by Dr Belen Solano [1] and expanding the design to accommodate use with a much wider range of object types, including the design that enabled the handling of the significantly smaller cells that were essential for the successful proof of concept work described in Chapter 5. Improvements to the fabrication processes focussed on optimising the process flow for the main building material, SU8, which was vital to ensure that delamination problems and cantilever bending effects were substantially reduced. The previous processing flow used could not be followed due to a change in SU8 formulation. The expansion of the microgripper design concentrated on increasing the functionalisation of the microgripper device by incorporating a gold electrode at the microgripper tip, a fundamental requirement for the subsequent development of the sensor capabilities; the miniaturisation of the device's dimensions with respect to the tip separation distance, an essential requirement for the manipulation of the cells intended for use in this study; and the development of the microgripper tip shape, an important consideration when widening the type of manipulated objects to ensure minimal deformation of that object.

The previous microgrippers were designed for the manipulation of large cells, specifically those with diameters in the 100 – 150 µm range. The mouse oocytes used for testing the microgripper sensor device were around 60 µm diameter. It was intended that this microgripper sensor device could be used to detect ionic movement from a large range of plant and animal cells, which fall within the range of 10 – 100 µm and 10 – 30 µm respectively. To miniaturise the microgripper device, care had to be taken when considering the effects of adhesion between the layers and the feature definition of the device, both of which related to the thin film stress of the individual layers deposited during the microgripper fabrication. It was also important that, during fabrication, good vertical sidewall profiles were maintained, which became increasingly challenging as the aspect ratio was increased (i.e. as the microgripper tip separation was reduced).

A range of microgrippers with tip separation dimensions between 10 – 100 µm were successfully fabricated. Additionally, several shape connotations of the microgripper tips were fabricated. These included flat, square, recessed curve, curved, pestle and mortar and scoop tips. The tip shape used for the fabrication of microgripper sensor devices was the scoop tips as it gave the needed support for the ISE components.

An additional fabrication step was also included compared to the original design that increased the functionality of the microgripper device. A gold electrode was fabricated at the microgripper tip, which was electroplated to achieve the desired thickness and roughness required for the subsequent assembly of the ISE element.

The fabrication of the microgripper delivered a high yield (95%) of operational devices that were identical within error. The SU8 tip dimensions were the same ± 1% and the actuation resistances, which related directly to the operation powers required to achieve full closure of the microgripper tips, only varied by ± 2%.

A rapid prototype (RP) holder was designed to house the microgripper and allowed it to be easily integrated into the external handling systems used throughout this project. A holder clip housed the microgripper chip that was diced from the wafer after the microgripper tip release. This simply clipped onto an L-shaped RP holder, making a good connection between the bond pads on the chip and the pogo pins connected to the external actuation operation circuit. The holder clip was set at an angle of 10° to ensure that the microgripper tips could come into contact with the surface of the cell container during manipulation, while ensuring that the whole RP device was still free to move.

6.2 Development and Characterisation of the Sensor Element

The second stage of this project was to transform the bare gold electrode at the tip of the microgripper device into a potentiometric ion sensor. This was integral to achieve the aims of the thesis, specifically monitoring, in real time, the movement of key biological ions involved in intercellular communication. The application of all solid state ion selective electrode (ASSISE) based technology to the electrode residing at the tip of the microgripper was utilised to achieve this. For this work to be successful, careful selection of appropriate materials had to be made to ensure the excellent sensitivity, selectivity and stability of the microgripper sensor device, as well as significant development and refinement of the fabrication process to guarantee sensor response repeatability and therefore high device stability. Extensive characterisation of the microgripper sensor device was undertaken to ensure operational specifications, specifically device sensitivity, selectivity, reproducibility, temporal resolution and stability, were achieved to the highest standard. This was essential to ensure that the microgripper sensor device was competitive compared to similar tools used in the monitoring of ion movement from live cells.

The electroactive area of the bare gold electrode was determined, using chronoamperometry, as 1800 ± 20 μm^2, which, combined with the fact that all the dimensions

of the electrode are in the micron scale, meant that the electrode behaved as a microelectrode. This was verified using cyclic voltammetry, which gave a sigmoidal shape and an independence of the steady state current with the scan rate, both indicative of a microelectrode.

The ASSISEs were fabricated via two steps: deposition of the conducting polymer (CP) transducer onto the bare gold electrical contact; followed by the deposition of the ion selective membrane (ISM) onto the CP.

Poly(3,4-ethylenedioxythiophene) (PEDOT) was the CP of choice due to its high stability, conductivity, good environmental stability, and low oxidation potential. Additionally, the oxygen electron donor in position 3 and 4 on the 6 carbon ring made it possible to carry out the electrochemical polymerisation in an aqueous environment. Sodium polystyrene sulphonate (NaPSS) was used as the dopant to aid the aqueous solubility of EDOT and to act as a charge-balance in the resulting polymer film.

PEDOT was electrochemically deposited onto the electrode at the tip of the microgripper using cyclic voltammetry. It was observed that there was a need to carefully control the concentration of EDOT and the scan rate to ensure that over deposition and reaction of the EDOT radicals with the uncapped SU8 polymer chains did not occur.

The small volumes (0.5 – 1 µl) of the ISM solution were drop cast, using THF as the casting solvent, onto the electrode using the CellEctor. The tip of a 30 µm diameter capillary that contained the ISM solution was placed into the scoop of the microgripper tip and the ISM solution expelled.

The PEDOT deposition thickness was the same ± 8%, however the membrane deposition varied widely between devices. Membrane depositions where the microgripper tips were not fused together (the membrane was too thick), or where no ruptures in the film were

observed (the membrane was too thin) were considered successful. The ISM thickness in devices with successful membrane deposition varied by approximately ± 30%, but the surface morphologies varied widely – in fact no two were the same.

Before it could conclusively be stated that the microgripper sensor devices had performance characteristics that could rival those of the liquid contact macro ion selective electrodes, certain quality control and testing criteria had to be matched. IUPAC definitions of ISE characterisations were used throughout the project to maintain consistency and to enable comparable data to that presented in literature. The main investigations into the characterisation of the microgripper sensor devices were done using the Ca^{2+} ISE devices.

Initial studies concluded that the microgripper sensor devices were not suitable for multiple use due to the great loss in membrane components (leaching) that caused a destabilisation in the device response between repeated runs. However, the batch processing of the microgripper devices that used MEMS technology yielded near identical processing, allowing all microgripper sensor devices from a wafer set to be calibrated from one device. There were only slight differences in the PEDOT deposition thickness, which did not greatly affect the microgripper sensor device response. However, the difference in ISM deposition meant that the absolute electromotive force (EMF) observed varied drastically between each device. This meant that the linear portion of the calibration plot needed to be translated in the y-direction for each individual device before quantitative analysis could be conducted.

All the characterisation data for the three different microgripper sensor devices is summarised in Table 6.1.

Table 6.1 – Summary table of characterisation of the different microgripper sensor devices.

Device	**Ca^{2+}-ISE**	**K^+-ISE**	**Na^+-ISE**
Sensitivity / mV/dec	14 ± 3	29 ± 4	32 ± 4
Limit of detection / M	$2 \pm 3 \times 10^{-5}$	$2 \pm 2 \times 10^{-4}$	$2 \pm 2 \times 10^{-4}$
Potential drift in analyte / mV hr^{-1}	0.66 (conditioned) -1.52 (used)	-	-
Potential drift in M2 media / mV hr^{-1}	-10.4 (first 10 hrs) -0.5 (subsequent 10 hrs)	2.0	3.8
Water layer formation	NO (conditioned) -16 mV shift, -0.8 mV hr^{-1} drift YES (used) 14 mV shift, -1.3 mV hr^{-1} drift	-	-
Hysteresis / mV	14 ± 1	4 ± 1	23 ± 2
Response time / s	300	17	180
Selectivity coefficients	$\log K_{Ca,K} = -3.9$ $\log K_{Ca,Na} = -2.8$ $\log K_{Ca,Mg} = -1.4$	$\log K_{K,Na} = -1.8$ $\log K_{K,Ca} = -3.3$	$\log K_{Na,K} = -0.8$ $\log K_{Na,Ca} = -1.2$

While the characterisations of the K^+ ISE devices met the specifications for the use in monitoring K^+ ion movement between cells, the Na^+ ISE devices were susceptible to interferences from competitive ions in the M2 media, and the Ca^{2+} had too poor detection limits. As a general comparison with conventional liquid and ASSISEs, these microgripper sensor devices had an insufficient long term stability of the ISM, were more susceptible to interferences from competitive ions in the sample, had a relatively large drift over long time frames, were difficult to accurately calibrate, were at risk to bio-fouling due to the environmental conditions in which the experiments were carried out, and the detection limits could be lower. However, the relatively good solution characterisation responses of the microgripper sensor devices meant they could be used in the real life application for which the device was intended. Despite this, improvements could be made to the ISM cocktail and ISE fabrication route to develop these characteristics further.

Furthermore it should be noted, with biological applications in mind, leaching of the membrane components could cause biocompatibility and/or toxicity issues. This could be

limited by the use of membranes based on polyacrylate or perfluorocarbons. Specifically, because of certain properties of the latter, such as chemical stability and the decreased affinity to proteins and lipids, perfluorocarbons may offer significant benefits in terms of development of biocompatible and more rugged membranes.

6.3 Monitoring Ion Movement from Single Cells: Proof of Concept Experiments

The final section of this project concentrated on assessing the ability of the microgripper sensor device to monitor the movement of intracellular ions from a single cell; the designed application of the device and the overall aim of this work. The ease of manipulation of mouse oocytes and the successful sensing of ion movement out of that cell revealed that the use of the microgripper sensor device in this field is extremely promising.

The microgripper sensor devices worked effectively at moving cells around and were capable of manipulating particles as small as 30 µm. Vacuum denudation pipettes are the main competitive technique currently used in industry and research labs and it was observed that the microgripper was capable of manipulating cells as well, if not better, than their pipette counterparts.

Stable background measurements of the signal response from mechanically stressing an inert 60 µm polystyrene bead determined that there were no interference signals from the physical contact of the bead, and therefore the cell, with the ISM.

The K^+ ISE microgripper sensor device gave a good response, with an observed increase in K^+ ion concentration with increasing applied mechanical stress upon the mouse oocyte. It was possible to discern that the zona pellicuda surrounding the cell had no effect on the signal response, indicating that the transfer of K^+ ions through the zona was unimpaired. It was not possible, however, to quantify the magnitude of the increase in concentration that

occurred when the level of mechanical stimulation was increased due to the high systematic error.

The preliminary theory from the data collected using the K^+ ISE microgripper sensor devices was that stress signalling occurred via a switch on mechanism and the EMF measurements indicated that once activated there was a small increase in K^+ ion concentration efflux with increasing stress.

The Na^+ ISE microgripper sensor devices either gave very noisy signals where it was impossible to resolve any signal response from the movement of Na^+ ions in and out of the cell, or a signal response that was dominated by the sensing of K^+ interfering ions. The selectivity coefficient of the Na^+ ISM with K^+ as the interfering ion (-0.8) indicated that the Na^+ ISM only had a slight preference for Na^+ ion over K^+ ones, which made this device very susceptible to the interference by K^+ ions.

Due to the limited detection limit of the Ca^{2+} ISE microgripper sensor devices it was impossible to discern and signal response from mechanically stressing a mouse oocyte that only contains 0.0002 mM of Ca^{2+} ions in the intercellular fluid.

In summary, the microgripper sensor devices have a great potential in being able to monitor, in real time, the movement of ions due to signalling from mechanical stimuli. Improvements to the fabrication process, specifically the ISM deposition, would allow a more accurate calibration process to be undertaken, which would reduce the systematic error in the system, and the K^+ ISE devices to resolve the magnitude of the signal responses from different magnitudes of mechanical stimuli. Greater improvements to the ISM cocktail for the Na^+ and Ca^{2+} devices are needed to improve the interference and detection limit restrictions respectively. This is required before the Na^+ and Ca^{2+} ISE devices will have characteristics that are competitive to those techniques already being used in this area.

6.4 Future Work

Initial development of the microgripper sensor devices can be separated into two main sections. Firstly, changes to the ISM cocktail should be made to improve the measured sensitivity, selectivity and stability. Secondly, a redesign of the microgripper device itself should be done to improve the ISE fabrication consistency, and hence reduce the systematic error within the device calibration process. Altering the device design will also allow improvements to the device stability and sensitivity to be made.

The ionophore is the main contributor to the selectively of an ISM. Substantial research has been done on the analysis of natural ionophores, as well as into the development of many different synthetic ones. Umezawa *et al.* compiled an extensive list of inorganic cation selective ionophores that have been used in the literature [2]. The K^+ and Ca^{2+} ISE microgripper sensor devices had good selectivities, and so exchanging the ionophore in their case is not necessary. However, the Na^+ ISE microgripper sensor devices suffered from interference by K^+ ions so an ionophore with greater selectivity against K^+ ions is desirable. Yamamoto *et al.* [3] claim $\log K_{Na,K}$ values of -3.15, -3.2 and -3.5 for Na^+ ionophores 28, 29 and 30 respectively (the structures of which are shown in Figure 6.1). The membranes used in these studies were also PVC based membranes that contained oNPOE and KTpClPB, like that used in the microgripper sensor device membrane cocktails.

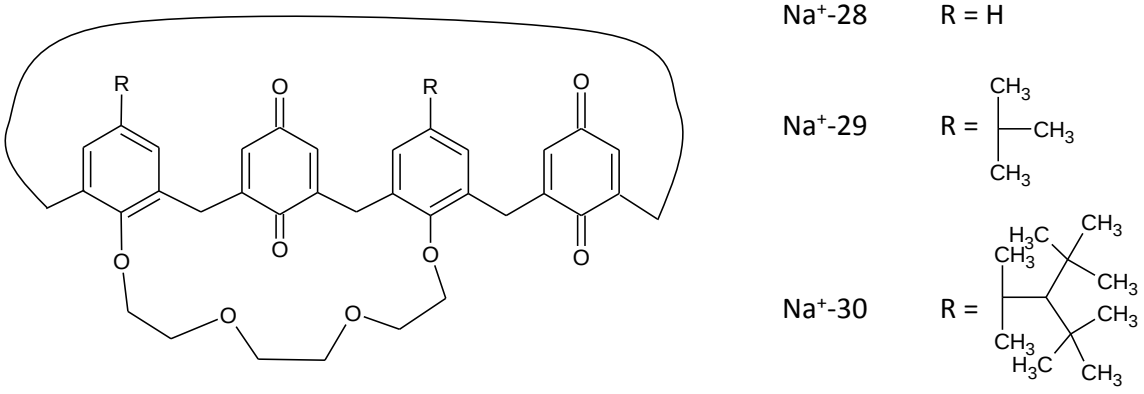

Figure 6.1 – Chemical structure of ionophores Na^+-28, 29 and 30.

It should also be noted that the mole ratio of the ionophore to ionic site in the ISM also affects the selectivity [4]. For example, a change in the ionophore : ionic site ratio of 1:77 to 1:64 showed an improvement in the $\log K_{Na,K}$ values from -2.2 to -2.59 [5] [6] when sodium ionophore X and KTpClPB are used.

The Ca^{2+} ISE microgripper sensor devices suffered from limited sensitivity, which has been linked to minor ionic fluxes across the membrane [7]. In liquid ISEs it has been observed that the most efficient way of improving the detection limit is to establish a concentration gradient across the membrane that opposes the primary ion leaching from the membrane [8]. However, this is not possible in ASSISEs. Szigeti *et al.* [9] published a summary of ten different approaches for improving the lower detection limit of polymeric membrane ISEs. These included applying a bias voltage across the membrane, increasing the membrane thickness, suppressing ion fluxes in the membrane by using high viscosity sensing membranes or co-polymers [10], incorporating a complexing agent into the conducting polymer [11] and lowering the plasticiser concentration in the membrane [9].

All the ion selective microgripper sensor devices suffered from stability limitations, specifically in solutions that have high ionic strength and multiple interfering ions. The drifting offset is known to be due to changes in the ISM composition, which is linked to:

(i) ion-exchange processes in the presence of high interfering ions;

(ii) anion co-extraction in highly concentrated samples, or in the presence of highly lipophilic anions;

(iii) decomposition of the ionophore and/or ionic active sites in the membrane;

(iv) leaching of the membrane components.

The first effect is reduced by improving the selectivity of the membrane against all interfering ions (as discussed previously). Decomposition is linked to membrane aging, which can be improved by ensuring that completely inert, light and moisture sensitive components

are used. The extraction and leaching issues are the most likely cause of the instability in the ISE microgripper sensor devices as these effects are very significant for microfabricated devices exposed to large volumes. Additionally, in ASSISEs based on conducting polymer solid contacts, potential instability has been observed due to spontaneous changes in the conducting polymer film. Altering the structure of the tetraphenyl borate salt used has been shown to improve the leaching effect, and hence detection limit, with more lipophilic derivatives showing significant reduction in the loss of membrane components [12]. The plasticisers and polymer matrix of the ISM also have an effect, for example, complete KTpClPB extraction from a PVC/oNPOE system can occur in 1 – 2 hours [13].

While investigation into appropriate ISM cocktail mixes to optimise the ISE characteristic performance is important, developments into the reduction of the high systematic error in the calibration process need to be achieved in order for real-time ion movement measurements to be made in real-life environments. This systematic error occurs due to the differences in the devices that occur during the fabrication process. The most dominatent step is the drop-casting of the ISM, which results in a range of different membrane thicknesses and morphologies. Three potential fabrication designs could be realised.

The electrode fabricated at the tip of the microgripper could be recessing into the SU8, creating a cavity within which the ASSISE fabrication process could be applied. This is shown schematically in Figure 6.2. This could potentially be quite challenging as the cavity dimension would restrict the PEDOT deposition process, as slow scan rates would be required to allow diffusion of the analytes in and out of the cavity, which would risk the EDOT radicals reacting with the SU8 polymer chains. Additionally, the active surface area of the microelectrode would be significantly reduced (around 50 μm^2), which would make the electrochemical signals more susceptible to experimental and environmental noise. The ISM deposition into a small cavity

would also be quite challenging. Specialist equipment that could deposit fL (10^{-15} L) of ISM accurately into a cavity, without trapping any air, would be required.

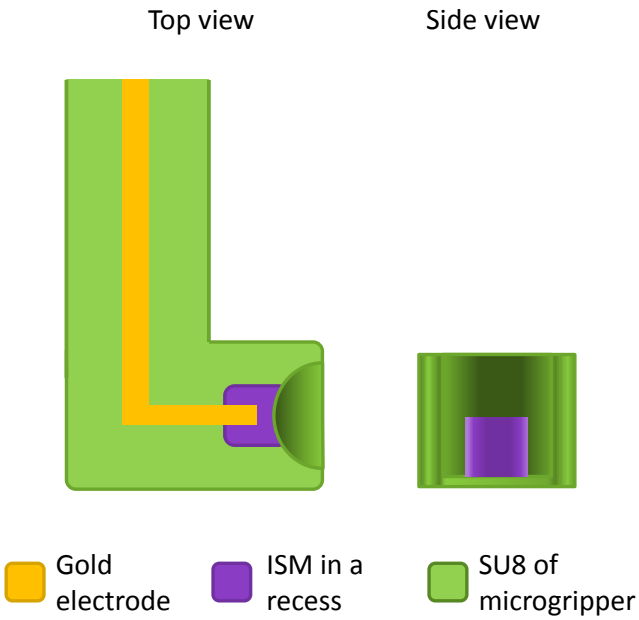

Figure 6.2 – Schematic representation of the recessed ISE microgripper design

An alternative design would be to incorporate a microfluidic channel down the arm of the microgripper that could be converted into an ASSISE similar to those seen in the double barrel electrodes that contain both the ISE and the reference electrode (RE) in a single glass tip. These double barrel electrodes have already been successfully used to detect signalling responses from sheep cardiac Purkinje fibres [14] and insect Malpighian tubule cells [15]. Given the excellent support properties that SU8 has, creating a microchannel within the SU8 arm would be possible using sacrificial layers. Using microchannels would allow investigation into both ASSISEs and liquid ISEs. Carbon fibres that have been pre-coated with PEDOT could be fed down the microchannel and then the channel could be filled with the ISM. The challenge would be to completely fill the length of the microchannel effectively. Backfilling the channel (from the tip) would be the most efficient way of achieving this, though doing so without coating the external surface of the microgripper could be difficult. If the ISM is

backfilled into the channel, the rest of the channel could be filled with an internal filling solution, enabling a liquid ISE to be fabricated, this is shown schematically in Figure 6.3.

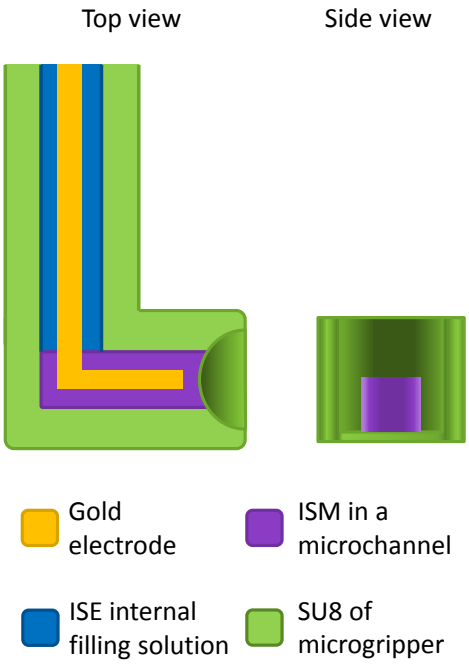

Figure 6.3 – Schematic representation of the microfluidic ISE microgripper design.

The final design is to separate the technologies into two separate units, and so can be fabricated individually. The units can then be assembled into the microgripper sensor device as a final step. This would allow independent optimisation of the technologies and would eliminate any interference problems. However, great care would have to be taken with the assembly of the two units to ensure that any measurements were done in contact with the cell and not at proximity.

With each of these designs, the membrane deposition method needs to be improved. Additionally, good adhesion between the conducting polymer and ISM is needed. This can be improved by changing the conducting polymer used to a more hydrophobic one. For example, poly(3-octylthiophene) (POT) has been shown to have excellent adhesion properties [16] [17]. However, the deposition method has to be via solvent casting as the high charge density that

occurs during electropolymerisation of POT has been shown to have a detrimental effect on ASSISE performance [10].

Once the performance characteristics and fabrication route have been optimised it would be interesting to monitor different types of cells. This project has shown that it is possible to fabricate devices with tip separation distances down to 10 µm. Assuming that it is possible to apply the ISE technology onto a device that small, the microgripper sensor device should be able to monitor ion movement from a large range of cell types.

The sensor system could then be further expanded so a single microgripper sensor device is capable of detecting the movement of a range of different ions. This would utilise the fabrication of an array like system that is used in micro-total analysis systems [18]. The sensor type itself could be broadened to include specific hormone or DNA sensing. Additionally, other electrochemical techniques, such as chronoamperometry, could be utilised.

Alternative functionalities of the microgripper could also be explored. Research into applying strain gauges using piezoelectric resistors to the microgripper, or adding the ability of the microgripper to remove small samples from the tips and/or break up cell aggregates using piezoelectric agitators or electromagnetic impulse devices respectively have the potential to yield interesting results. Additionally, by fabricating electrodes down both arms of the microgripper it is possible to perform cytolysis and electroporation of single cells.

6.5 References

[1] B. Solano, A microgripper for single cell manipulation, PhD thesis, Durham University, 2008.

[2] Y. Umezawa, P. Buhlmann, K. Umezawa, K. Tohda and S. Amemiya, "Potentiometric selectivity coefficients of ion-selective electrodes. Part I. Inorganic cations (Technical Report)," *International Union of Pure and Applied Chemistry,* vol. 72, no. 10, pp. 1851-2082, 2000.

[3] H. Yamamoto, K. Ueda, H. Suenaga, T. Sakaki and S. Shinkai, "Exploitation of Na+ selective electrodes for protein solutions from crown-bridged calix[4]quinones," *Chemistry Letters,*

no. 1, pp. 39-40, 1996.

[4] R. E. Gyurcsanyi and E. Lindner, “Spectroscopic method for the determination of the ionic site concentration in solvent polymeric membranes and membrane plasticizers,” *Analytical Chemistry,* vol. 74, no. 16, pp. 4060-4068, 2002.

[5] A. M. Cadogan, D. Diamond, M. R. Smyth, M. Deasy, M. A. McKervey and S. J. Harris, “Sodium-selective polymeric membrane electrodes based on calix[4]arene ionophores,” *Analyst,* vol. 114, no. 12, pp. 1551-1554, 1989.

[6] M. Telting-Diaz, F. Regan, D. Diamond and M. R. Smyth, “Comparison of a calizarene-based ion-selective electrode with 2 automated analyzers for the clinical determination of sodium in blood-plasma,” *Journal of Pharmaceutical and Biomedical Analysis,* vol. 8, no. 8-12, pp. 695-700, 1990.

[7] S. Mathison and E. Bakker, “Effect of transmembrane electrolyte diffusion on the detection limit of carrier-based potentiometric ion sensors,” *Analytical Chemistry,* vol. 70, no. 2, pp. 303-309, 1998.

[8] T. Sokalski, A. Ceresa, T. Zwickl and E. Pretsch, “Large improvement of the lower detection limit of ion-selective polymer membrane electrodes,” *Journal of the American Chemical Society,* vol. 119, no. 46, pp. 11347-11348, 1997.

[9] Z. Szigeti, T. Vigassy, E. Bakker and E. Pretsch, “Approaches to improving the lower detection limit of polymeric membrane ion-selective electrodes,” *Electroanalysis,* vol. 18, no. 13-14, pp. 1254-1265, 2006.

[10] J. Sutter, A. Radu, S. Peper, E. Bakker and E. Pretsch, “Solid-contact polymeric membrane electrodes with detection limits in the subnanomolar range,” *Analytica Chimica Acta,* vol. 523, no. 1, pp. 53-59, 2004.

[11] A. Konopka, T. Sokalski, A. Michalska, A. Lewenstam and M. Maj-Zurwska, “Factors affecting the potentiometric response of all-solid-state solvent polymeric membrane calcium-selective electrodes for low-level measurements,” *Analytical Chemistry,* vol. 76, no. 21, pp. 6410-6418, 2004.

[12] E. Bakker and E. Pretsch, “Lipophilicity of tetraphenylborate derivatives as anionic sites in neutral carrier-based solvent polymeric membranes and lifetime of corresponding ion-selective electrochemical and optical sensors,” *Analytica Chimica Acta,* vol. 309, no. 1-3, pp. 7-17, 1995.

[13] M. Telting-Diaz and E. Bakker, “Effect of lipophilic ion-exchanger leaching on the detection limit of carrier-based ion-selective electrodes,” *Analytical Chemistry,* vol. 73, no. 22, pp. 5582-5589, 2001.

[14] S. O. Semb, B. Amundsen and O. M. Sejersted, “A new improved way of making double-barrelled ion-selective micro-electrodes,” *Acta Physiologica Scandinavica,* vol. 161, no. 1, pp. 1-5, 1997.

[15] J. P. Ianowski, R. J. Christensen and M. J. O'Donnell, “Intracellular ion activities in Malpighian tubule cells of Rhodnius prolixus: Evaluation of Na+-K+2Cl- cotransport across the basolateral membrane,” *Journal of Experimental Biology,* vol. 205, pp. 1645-1655,

2002.

[16] J. Boback, M. McCarrick, A. Lewenstam and A. Ivaska, “All-solid-state poly(vinyl chloride) membrane ion-selective electrodes with poly(3-octylthiophene) solid internal contact,” *Anaalyst,* vol. 119, no. 9, pp. 1985-1991, 1994.

[17] B. Paciorek, P. D. van der Wal, N. E. de Rooij and M. Maj-Zurawska, “Optimization of the composition of interfaces in miniature planar chloride electrodes,” *Electroanalysis,* vol. 15, no. 15-16, pp. 1314-1318, 2003.

[18] R. D. Johnson, V. G. Gavalas, S. Daunert and L. G. Bachas, “Microfluidic ion-sensing devices,” *Analytical Chimica Acta,* vol. 613, pp. 20-30, 2008.

[19] W. Simon, E. Pretsch, D. Ammann, W. E. Morf, M. Guggi, R. Bissig and M. Kessler, “Recent developments in field of ion selective electrodes,” *Pure and Applied Chemistry,* vol. 44, no. 3, pp. 613-626, 1975.

[20] K. Y. Chumbimuni-Torres, N. Rubinova, A. Radu, L. T. Kubota and E. Bakker, “Solid contact potentiometric sensors for trace level measurements,” *Analytical Chemistry,* vol. 78, no. 4, pp. 1318-1322, 2006.

[21] S. -K. Lee, W. F. Boron and M. D. Parker, “Monitoring ion activities in and around cells using ion-selective liquid-membrane microelectrodes,” *Sensors,* vol. 13, pp. 984-1003, 2013.